



# City Research Online

## City, University of London Institutional Repository

---

**Citation:** Crowther, David Neville (1986). The hot ductility of steels. (Unpublished Doctoral thesis, The City University)

This is the accepted version of the paper.

This version of the publication may differ from the final published version.

---

**Permanent repository link:** <https://openaccess.city.ac.uk/id/eprint/19368/>

**Link to published version:**

**Copyright:** City Research Online aims to make research outputs of City, University of London available to a wider audience. Copyright and Moral Rights remain with the author(s) and/or copyright holders. URLs from City Research Online may be freely distributed and linked to.

**Reuse:** Copies of full items can be used for personal research or study, educational, or not-for-profit purposes without prior permission or charge. Provided that the authors, title and full bibliographic details are credited, a hyperlink and/or URL is given for the original metadata page and the content is not changed in any way.

THE HOT DUCTILITY OF STEELS

David Neville Crowther

Submitted for the Degree of PhD

The City University  
Department of Mechanical Engineering

June 1986

## CONTENTS

LIST OF TABLES	1
LIST OF FIGURES	2
ACKNOWLEDGEMENTS	10
DECLARATION	11
ABSTRACT	12
LIST OF SYMBOLS	13
<u>CHAPTER 1</u> INTRODUCTION	15
<u>CHAPTER 2</u> LITERATURE SURVEY	18
2.1 Introduction	19
2.2 Transverse Cracking in Continuously Cast Slab	
2.2.1 Observations of transverse cracks	20
2.2.2 Mechanics of the slab straightening process	20
2.2.3 The influence of process variables on transverse cracking	21
2.3 High Temperature Strength and Structure	
2.3.1 General	24
2.3.2 Dynamic Recovery	25
2.3.3. Dynamic Recrystallization	26
2.4 Interaction Between High Temperature Cracking and Softening Processes	
2.4.1 High temperature crack nucleation and growth	30
2.4.2 Influence of dynamic recovery on hot ductility	31
2.4.3 Influence of dynamic recrystallization on hot ductility	32
2.5 The Influence of Strain Rate on Hot Ductility	
2.5.1 General	35
2.5.2 The influence of strain rate on hot ductility above 1200°C	35
2.5.3 Influence of strain rate on hot ductility from 1200 to 1000°C	36
2.5.4 The influence of strain rate on hot ductility below 1000°C	36
2.6 The Influence of Grain Size on Hot Ductility	38
2.7 The Influence of Inclusions on Hot Ductility	41
2.8 The Influence of Phase Transformation and Duplex Structure on the Hot Ductility of Steels.	
2.8.1 Phase transformation	44
2.8.2 Duplex structure	44

2.9	The Influence of Composition on the Hot Ductility of Steels	
2.9.1	Nb	47
2.9.2	Al	51
2.9.3	Ti	54
2.9.4	V	56
2.9.5	S and Mn:S ratio	57
2.9.6	C	60
2.9.7	Other Elements	62
<u>CHAPTER 3</u> EXPERIMENTAL TECHNIQUES		64
3.1	Introduction	65
3.2	Hot Tensile Test	
3.2.1	Gleeble tests	68
3.2.2	Instron tests	68
3.2.3	Induction heating tests	69
3.3	Carbon Extraction Replica Preparation and Examination	71
<u>CHAPTER 4</u> THE INFLUENCE OF C CONTENT ON THE HOT DUCTILITY OF PLAIN C-Mn STEELS		73
4.1	Introduction	74
4.2	Experimental	75
4.3	Results	
4.3.1	Hot tensile tests	77
4.3.2	Metallography	78
4.3.3	Dilatometry	82
4.4	Discussion	83
4.5	Conclusions	88
<u>CHAPTER 5</u> THE INFLUENCE OF GRAIN SIZE ON THE HOT DUCTILITY OF C-Mn STEELS		
5.1	Introduction	90
5.2	Experimental	92
5.3	Results	
5.3.1	Metallography	94
5.3.2	Hot ductility	94
5.3.3	Fractography	95
5.4	Discussion	97
5.5	Conclusions	102
<u>CHAPTER 6</u> THE INFLUENCE OF GRAIN SIZE ON THE HOT DUCTILITY OF MICRO-ALLOYED STEELS		103
6.1	Introduction	104
6.2	Experimental	105

6.3	Results	
6.3.1	Hot tensile tests and metallography	107
6.3.2	Determination of solution temperatures	110
6.4	Discussion	112
6.5	Conclusions	116
<u>CHAPTER 7</u>	THE INFLUENCE OF STATIC AND DYNAMIC PRECIPITATES ON HOT DUCTILITY	118
7.1	Introduction	119
7.2	Experimental	122
7.3	Results	
7.3.1	Hot tensile tests	124
7.3.2	Metallography	124
7.3.3	Static precipitation of NbCN	126
7.4	Discussion	127
7.5	Conclusions	130
<u>CHAPTER 8</u>	THE INFLUENCE OF TEMPERATURE OSCILLATIONS DURING COOLING ON THE HOT DUCTILITY OF A C-Mn-Nb-Al STEEL.	131
8.1	Introduction	132
8.2	Experimental	134
8.3	Results	
8.3.1	Hot tensile tests	136
8.3.2	Metallography	137
8.4	Discussion	139
8.5	Conclusions	143
<u>CHAPTER 9</u>	THE HOT DUCTILITY OF A DIRECTLY CAST C-Mn-Nb-Al STEEL	144
9.1	Introduction	145
9.2	Experimental	146
9.3	Results	
9.3.1	Hot ductility tests	148
9.3.2	Metallography	148
9.4	Discussion	151
9.5	Conclusions	155
<u>CHAPTER 10</u>	THE HOT DUCTILITY OF MICRO-ALLOYED STEEL HEATED DIRECTLY TO TEST TEMPERATURE	156
10.1	Introduction	157
10.2	Experimental	159

10.3	Results	
10.3.1	Hot strength	161
10.3.2	Hot ductility	162
10.3.3	Metallography	164
10.3.4	Dilatometry and transformation data	165
10.4	Discussion	
10.4.1	Hot strength	167
10.4.2	Hot ductility	168
10.4.3	The influence of strain rate on hot ductility	172
10.5	Conclusions	174
<u>CHAPTER 11</u> SUMMARY AND RECOMMENDATIONS FOR FUTURE WORK		175
11.1	Introduction	176
11.2	Summary	177
11.2.1	Low ductility failure; $\alpha + \gamma$ region	177
11.2.2	Low ductility failure; $\gamma$ region	178
11.3	Recommendations for the Reduction of Transverse Cracking	181
11.4	Recommendations for Future Work	183
Appendices		
A1	Nickel Coating of Samples	185
A2	Recent Publications	188
A3	Publications	191
REFERENCES		194

## LIST OF TABLES

- 2.1 Possible softening processes associated with hot deformation (from Sellars and Tegart, 1972)
- 4.1 Compositions of the steels examined.
- 4.2 Transformation temperatures determined by dilatometry, metallography, and by the method of Andrews (1965)
- 4.3 Influence of C content in C-Mn steels on the activation energy for deformation,  $Q$ , and stress exponent,  $n$ .
- 5.1 Compositions of the steels examined.
- 5.2 Variation of austenite grain size with reheating temperature.
  
- 6.1 Compositions of the steels examined.
- 8.1 Compositions of the steels examined.
- 9.1 Composition of the steel examined.
- 9.2 Results of EDAX micro-analysis of sulphides and surrounding matrix.
- 10.1 Compositions of the steels examined.
- 10.2 Comparison of activation energy,  $Q$ , and stress exponent,  $n$ , of present work with previous studies.
- 10.3 Precipitate types and sizes present at test temperatures of 850 and 1050°C.
- 10.4 Transformation data,  $A_e$  temperatures calculated using the equation of Andrews (1965),  $A_c$  temperatures determined by dilatometry.

## LIST OF FIGURES

- 1.1 Percentage of total steel output produced by continuous casting, by region.
- 2.1 Cold machine scarfed slab showing transverse cracking.
- 2.2 Slab which had been partially rolled showing severe transverse edge cracking.
- 2.3 Profile of Gary slab caster.
- 2.4 Straightening of continuously cast slab (After Lankford, 1972)
- 2.5 Temperature oscillations in continuously cast slab (after Tomono, 1977)
- 2.6 Schematic models showing the formation of wedge cracks due to grain boundary sliding. The arrows indicate a sliding boundary and the sense of translation (After Chang and Grant, 1956)
- 2.7 Mechanism for void formation at grain boundary ledge. (After Gifkins, 1959)
- 2.8 Influence of strain rate on the hot ductility of a C-Mn-Nb-Al steel. (After Mintz and Arrowsmith, 1979)
- 2.9 Variation of relative plasticity of sulphide inclusions with deformation temperature and oxygen content. (After Charles, 1980)
- 2.10 Variation of ductility with temperature and grain size for Magnox A.180. (From Evans, 1969)
- 2.11 Variation of ductility with temperature and grain size for a Cr-Mn-N austenitic steel, showing decrease in ductility at fine grain sizes. (From Kutumba Rao et al, 1975)
- 2.12 Hot ductility of irons tested in hot torsion. (From Robbins et al, 1961)
- 2.13 Influence of Nb on the transverse cracking of continuously cast slabs. (From Mintz and Arrowsmith, 1979)
- 2.14 Influence of Nb on the hot ductility of C-Mn-Nb-Al steels. (After Mintz and Arrowsmith, 1979)
- 2.15 Influence of Al on the hot ductility of C-Mn-Nb-Al steels. (After Mintz and Arrowsmith, 1979)
- 3.1 Schematic illustration of variation of strain rate at point of fracture with total elongation of test piece.
- 3.2 Gleeble test piece.
- 3.3 Instron test piece.

- 3.4 Schematic illustration of Instron high temperature testing equipment.
- 3.5 Schematic illustration of induction heating equipment for high temperature tensile testing.
- 3.6 Induction test piece.
- 3.7 Temperature distribution in Induction test piece at three different temperatures.
- 3.8 Comparison of reduction in area values from different testing equipment, tests performed under identical conditions.
- 3.9 Extraction of precipitates using single stage carbon replicas.
- 4.1 Variation of reduction in area with test temperature for steels 1 - 6.
- 4.2 Variation of reduction in area with C content at 900 and 600°C
- 4.3 Variation of peak stress with test temperatures for steels 1 - 6.
- 4.4 Variation in peak stress with C content at 900 and 600°C
- 4.5 Influence of C content on austenite grain size at 1330°C.
- 4.6 Grain boundary ferrite and side plate formation in .10%C steel, tested at 600°C.
- 4.7 Hot ductility, transformation and fracture data for the 0.10%C steel.
- 4.8 Hot ductility, transformation and fracture data for the 0.19% steel.
- 4.9 Hot ductility, transformation and fracture data for the 0.28%C steel.
- 4.10 Hot ductility, transformation and fracture data for the 0.35%C steel.
- 4.11 Optical micrograph showing point of fracture of the 0.19%C steel tested at 600°C. (R of A 90%)
- 4.12 Micrographs illustrating grain boundary crack formation in the 0.19%C steel tested at 650°C (R of A 43%)
- 4.13 Micrograph showing point of fracture of the 0,19%C steel tested at 650°C.
- 4.14 Detail of grain boundary crack formation in the 0.19%C steel tested at 650°C.
- 4.15 Crack formation in the 0.35%C steel tested at 850°C.

- 4.16 Low temperature ductile rupture (LTDR) fracture mode, showing void formation at second phase particles. 0.04%C steel, tested at 550°C.
- 4.17 Intergranular micro void coalescence (IMC) fracture mode, showing void formation on grain facets. 0.10%C steel tested at 775°C.
- 4.18 Intergranular decohesion (ID) fracture mode, showing relatively smooth grain facets, some with wavy ridges. 0.35%C steel tested at 750°C.
- 4.19 High temperature ductile rupture (HTDR) fracture mode, showing large voids on fracture surface. 0.04%C steel tested at 900°C.
- 4.20 Hot ductility, transformation and fracture data for the 0.04%C steel.
- 4.21 Hot ductility, transformation and fracture data for the 0.65%C steel.
- 4.22 Comparison of present hot ductility results with previous work.
- 4.23 Variation of peak stress,  $\sigma_p$ , with absolute temperature, T, at different strain rates for the 0.19%C steel.
- 4.24 Variation of peak stress,  $\sigma_p$ , with absolute temperature, T, at different strain rates for the 0.65%C steel.
- 4.25 Plot of strain rate,  $\dot{\epsilon}$ , against  $1/T$ , where T is the absolute temperature, for the 0.19%C steel.
- 4.26 Plot of strain rate,  $\dot{\epsilon}$ , against  $1/T$ , where T is the absolute temperature, for the 0.65%C steel.
- 4.27 Plot of  $\ln \dot{\epsilon}$  against  $\ln \sigma_p$  for the 0.19%C steel.
- 4.28 Plot of  $\ln \dot{\epsilon}$  against  $\ln \sigma_p$  for the 0.65%C steel.
- 4.29 Variation of activation energy for deformation with C content.
- 4.30 Sample elongation at peak stress for the 0.19%C steel, and for the 0.65%C steel, at different temperature and strain rates.
- 5.1 Ferrite volume fraction after quenching small samples of varying initial grain size from various temperatures, 0.19%C steel.
- 5.2 Hot ductility curves for the 0.19%C steel after reheating to various temperatures to produce grain sizes in the range 70 - 210  $\mu\text{m}$  prior to testing. Also included are the Gleeble test results of chapter 4.
- 5.3 Hot ductility curves for the 0.65%C steel after reheating to various temperatures to produce grain sizes in the range 50 - 300  $\mu\text{m}$  prior to testing.

- 5.4 Intergranular fracture showing microvoids on grain facets, grain size 290  $\mu\text{m}$ , test temperature 750°C.
- 5.5 Form of grain boundary ferrite in 290  $\mu\text{m}$  grain size steel, prior to testing at 750°C.
- 5.6 Form of grain boundary ferrite in 70  $\mu\text{m}$  grain size steel, prior to testing at 750°C.
- 5.7 Hot ductility curves for the .19%C steel following heating to 925°C and cooling at either 10°C/min. or 15°C/min. to test temperature.
- 5.8 Minimum reduction of area values in the temperature range 700 - 1000°C plotted against grain size.
- 5.9 Hot ductility curve for the .19%C steel after normalising and heating directly to test temperature.
- 6.1 Influence of reheating temperature on the austenite grain size of the C-Mn, C-Mn-Al, C-Mn-V-Al, and C-Mn-Nb-Al steels.
- 6.2 Reduction of area values following tensile testing at 850°C after reheating to various temperatures for C-Mn, C-Mn-Al, C-Mn-V-Al and C-Mn-Nb-Al steels.
- 6.3 Variation of reduction in area values with austenite grain size.
- 6.4 Load-elongation curves for the C-Mn-Al steel
- 6.5 Load-elongation curves for the C-Mn-V-Al steel
- 6.6 Load elongation curves for the C-Mn-Nb-Al steel
- 6.7 Extent of fracture mode for each steel.
- 6.8 Example of ID fracture mode in C-Mn-Nb-Al steel after reheating to 1330°C and testing at 850°C.
- 6.9 Example of HTDR fracture mode in C-Mn-Nb-Al steel after reheating to 1100°C and testing at 850°C.
- 6.10 NbCN precipitates extracted from fracture surface of C-Mn-Nb-Al steel after reheating to 1330°C
- 6.11 C-Mn-Al steel heated directly to 850°C, showing grain boundary precipitation of AlN.
- 6.12 C-Mn-Al steel reheated to 1000°C, tested at 850°C with associated X-ray spectrum.
- 6.13 Precipitation in C-Mn-V-Al steel heated to 850°C and tested, showing VCN and AlN precipitation and associated X-ray spectra.
- 6.14 Precipitation in C-Mn-V-Al steel after reheating to 1050°C and testing at 850°C.

- 6.15 Precipitation in C-Mn-Nb-Al steel heated to 850°C and tested, showing AlN and NbCN precipitation.
- 6.16 Precipitation in C-Mn-Nb-Al steel heated to 1100°C prior to testing at 850°C, and associated X-ray spectrum.
- 6.17 Precipitation in C-Mn-Nb-Al steel heated to 1330°C prior to testing at 850°C.
- 6.18 Hardness of samples of the C-Mn-Nb-Al steel and C-Mn-V-Al steel reheated to various temperatures, and quenched and tempered.
- 7.1 Influence of holding time prior to testing on peak stress and hot ductility of the C-Mn-Nb-Al steel tested at 950°C.
- 7.2 Influence of holding time prior to testing on peak stress and hot ductility of the C-Mn-Al steel tested at 850°C.
- 7.3 Influence of holding time prior to testing on peak stress and hot ductility of the C-Mn-V-Al steel tested at 850°C.
- 7.4 Stress-elongation curves for the C-Mn-Nb-Al steel held at 950°C for various times prior to testing.
- 7.5 Stress elongation curves for the C-Mn-Al steel held at 850°C for various times prior to testing.
- 7.6 Stress elongation curves for the C-Mn-V-Al steel held at 850°C for various times prior to testing.
- 7.7 NbCN precipitation in C-Mn-Nb-Al steel after holding for a) 1 s b) 7200 s and c) 21000 s prior to testing at 950°C
- 7.8 Precipitate size distributions in C-Mn-Nb-Al steel after holding for a) 1 s b) 7200 s and c) 21000 s prior to testing at 950°C.
- 7.9 Precipitation in C-Mn-V-Al steel after holding for a) 1 s and b) 21000 s prior to testing at 850°C
- 7.10 Precipitate size distributions in C-Mn-V-Al steel after holding for a) 1s and b) 21000 s prior to testing at 850°C.
- 7.11 Hardness of the C-Mn-Nb-Al steel following quenching and tempering after holding for various times at 950°C.
- 8.1 Schematic illustration of cooling patterns from solution temperatures.
- 8.2a Actual cooling curves for cooling pattern 2, test temperatures 870 and 1050°C.
- 8.3 Hot ductility curves for each cooling pattern, occurrence of dynamic recrystallization indicated by shaded regions.
- 8.4 Representative load-elongation curves for cooling pattern 1.
- 8.5 Representative load-elongation curves for cooling pattern 2.

- 8.6 Representative load-elongation curves for cooling pattern 3.
- 8.7 Precipitation in steels tested at 870°C after a) cooling pattern 1 and b) cooling pattern 3.
- 8.8 Precipitation in steels tested at 970°C after a) cooling pattern 1 and b) cooling pattern 3.
- 8.9 Precipitation in steels tested at 1050°C after a) cooling pattern 1 and b) cooling pattern 3.
- 8.10 Precipitation in continuously cast C-Mn-Nb-Al slab a) surface b) centre.
- 9.1 Induction heating equipment for the high temperature tensile testing of 'directly cast' samples.
- 9.2 Variation of reduction in area with test temperature for samples in 'as cast', 're-heated' and 're-heated Gleeble' samples.
- 9.3 High temperature ductile rupture fracture mode, from 'as cast' samples fractured at 950°C.
- 9.4 Intergranular microvoid coalescence fracture mode, from 'as cast' sample fractured at 950°C.
- 9.5 Interdendritic failure in 'as cast' sample fractured at 950°C, showing rows of sulphide inclusions
- 9.6 Sulphide and NbCN precipitation at grain boundaries in 'reheated' sample tested at 950°C.
- 9.7 Sulphide precipitation after reheating to 1200°C prior to cooling to 950°C.
- 9.8 Precipitation in 'reheated' sample tested at 950°C. N.B. precipitate free zones.
- 9.9 Precipitation in 'as cast' sample tested at 950°C.
- 9.10 Coarse NbCN extracted from 'as cast' sample tested at 950°C, with associated X-ray spectrum.
- 9.11 Precipitation in 'reheated Gleeble' sample tested at 950°C.
- 10.1 Variation of peak stress with test temperature for six steels heated directly to test temperature.
- 10.2 Variation of peak stress with temperature and strain rate for the C-Mn steel.
- 10.3 Variation of peak stress with temperature and strain rate for the C-Mn-Al steel.
- 10.4 Variation of peak stress with temperature and strain rate for the C-Mn-Nb-Al steel.

- 10.5 Plot of  $\ln \dot{\epsilon}$  against  $I/T$  at constant  $\sigma_p$  for the C-Mn steel.
- 10.6 Plot of  $\ln \dot{\epsilon}$  against  $I/T$  at constant  $\sigma_p$  for the C-Mn-Al steel.
- 10.7 Plot of  $\ln \dot{\epsilon}$  against  $I/T$  at constant  $\sigma_p$  for the C-Mn-Nb-Al steel.
- 10.8 Plot of  $\ln \dot{\epsilon}$  against  $\ln \sigma_p$  at constant temperatures for the C-Mn steel.
- 10.9 Plot of  $\ln \dot{\epsilon}$  against  $\ln \sigma_p$  at constant temperatures for the C-Mn-Al steel.
- 10.10 Plot of  $\ln \dot{\epsilon}$  against  $\ln \sigma_p$  at constant temperatures for the C-Mn-Nb-Al steel.
- 10.11 Representative load-elongation curves at various temperatures and strain rates.
- 10.12 Hot ductility curves for all size steels at  $\dot{\epsilon} = 3 \times 10^{-3} \text{ s}^{-1}$ , occurrence of dynamic recrystallization indicated by shaded regions.
- 10.13 Influence of strain rate on the hot ductility of C-Mn steel, occurrence of dynamic recrystallization indicated by shaded regions.
- 10.14 Influence of strain rate on the hot ductility of C-Mn-Al steel, occurrence of dynamic recrystallization indicated by shaded regions.
- 10.15 Influence of strain rate on the hot ductility of C-Mn-Nb-Al steel, occurrence of dynamic recrystallization indicated by shaded regions.
- 10.16 Variation of austenite grain size with temperature.
- 10.17 Fracture surface of C-Mn-Nb-Al fractured at 850°C using a strain rate of  $3 \times 10^{-3} \text{ s}^{-1}$
- 10.18 AlN precipitation in C-Mn-Al steel tested at 850°C using a strain rate of  $3 \times 10^{-3} \text{ s}^{-1}$
- 10.19 AlN precipitation in C-Mn-Al steel tested at 1050°C using a strain rate of  $3 \times 10^{-3} \text{ s}^{-1}$ , with associated X-ray spectrum.
- 10.20 AlN precipitation in C-Mn-Al-Ca steel tested at 850°C using a strain rate of  $3 \times 10^{-3} \text{ s}^{-1}$ .
- 10.21 AlN precipitation in C-Mn-Al-Ca steel tested at 1050°C using a strain rate of  $3 \times 10^{-3} \text{ s}^{-1}$ .
- 10.22 Precipitation in C-Mn-Ti-Al steel tested at 850°C using a strain rate of  $3 \times 10^{-3} \text{ s}^{-1}$
- 10.23 Precipitation in C-Mn-Ti-Al steel tested at 1050°C using a strain rate of  $3 \times 10^{-3} \text{ s}^{-1}$ , and the associated X-ray spectrum.
- 10.24 Precipitation in C-Mn-V-Al steel tested at 850°C using a

- 10.24 Precipitation in C-Mn-V-Al steel tested at 850°C using a strain rate of  $3 \times 10^{-3} \text{ s}^{-1}$
- 10.25 Precipitation in C-Mn-V-Al steel tested at 1050°C using a strain rate of  $3 \times 10^{-3} \text{ s}^{-1}$ , and associated X-ray spectra.
- 10.26 Precipitation in C-Mn-Nb-Al steel tested at 850°C using a strain rate of  $3 \times 10^{-3} \text{ s}^{-1}$
- 10.27 Precipitation in C-Mn-Nb-Al steel tested at 1050°C using a strain rate of  $3 \times 10^{-3} \text{ s}^{-1}$ , with associated X-ray.
- 10.28 Section through C-Mn steel fractured at 850°C using a strain rate of  $3 \times 10^{-3} \text{ s}^{-1}$  (A coarse ferrite/pearlite aggregate was produced prior to testing by heating to 1200°C and furnace cooling.
- 11.1 Schematic illustration of variation of fracture strain ( $\epsilon_f$ ) and strain for the nucleation of dynamic recrystallization, ( $\epsilon_c$ ) with temperature.
- 11.2 Schematic illustration of variation of  $\epsilon_c$  and  $\epsilon_f$  with temperature and strain rate.
- 11.3 Schematic illustration of variation of  $\epsilon_c$  and  $\epsilon_f$  with temperature and precipitation, assuming a sufficient volume fraction of 'fine' precipitates to increase  $\epsilon_c$ .
- 11.4 Schematic illustration of variation of  $\epsilon_c$  and  $\epsilon_f$  with temperature and grain size.

## ACKNOWLEDGEMENTS

Thanks are due to Professor G.T. Done for the provision of laboratory facilities, and to the staff of the Department of Mechanical Engineering for their help, and Mr. R. Vipond in particular.

I am especially indebted to my supervisor Dr. B. Mintz for his help and encouragement during my three years of study. Thanks are also due to BSC Swinden Laboratories, in particular to Dr. R.C. Cochrane, for supplying the steels and the use of their Gleeble testing and dilatometer facilities. Also, the help of Dr. J. Wilcox, BSC Scottish Labs., is much appreciated.

I am especially grateful to Mrs. B. Wynne for typing this manuscript, and also to my parents for their help in the preparation of the thesis.

Finally, the financial assistance of the SERC is acknowledged.

DECLARATION

I grant powers of discretion to the University Librarian to allow this thesis to be copied in whole or in part without further reference to me. This permission covers only single copies made for study purposes, subject to normal conditions of acknowledgement.

## ABSTRACT

Hot tensile tests have been performed on a variety of plain carbon and micro-alloyed steels, in order to determine the influence of such factors as phase transformation, grain size and precipitation on hot ductility. The  $\gamma$ - $\alpha$  phase transformation has been shown to produce a significant ductility trough in the high temperature tensile behaviour of plain C steels, and factors which alter the  $A_3$  temperature, such as cooling rate and C content, have been shown to produce a change in the temperature at which the ductility trough occurs. This ductility trough is due to strain concentration in the ferrite films surrounding the grains, leading to intergranular failure. It has also been shown that an increase in grain size can increase the depth and width of this ductility trough. For plain C steels with a C content of 0.35% or above, and for some micro-alloyed steels, a ductility trough may also be present in the single phase austenite region. For the plain C steel, this is believed to be due to the increase in activation energy for deformation associated with increasing C contents. In micro-alloyed steels, the trough is due to the retardation of dynamic recrystallization associated with the presence of fine carbide and/or nitride precipitates, which allows intergranular cracks to develop. The depth and width of this ductility trough is primarily dependent on the size and amount of precipitates present, although it has been shown that grain size has a secondary effect. In C-Mn-Nb-Al steels, factors which tend to reduce hot ductility by reducing precipitate size and/or increasing the amount of precipitate present include the reheating of tensile samples cast 'in-situ', the introduction of temperature oscillations during cooling from solution temperature, and the presence of large amounts of 'dynamic' precipitates formed during tensile testing. In C-Mn-V-Al steels, 'dynamic' precipitates do not have such an adverse effect. Strain rate was also shown to have an important influence on hot ductility, and decreasing strain rates have been shown to reduce hot ductility in both plain carbon and micro-alloyed steels.

## LIST OF SYMBOLS

a	numerical constant
A	numerical constant
A <sub>0</sub>	initial cross sectional area
A <sub>f</sub>	final cross sectional area
b	numerical constant
B	numerical constant
C	length of inclusion minor axis
d	length of inclusion major axis
d <sub>a</sub>	grain diameter
d <sub>0</sub>	initial grain size
d <sub>r</sub>	dynamically recrystallized grain size
d <sub>s</sub>	subgrain diameter
d <sub>i</sub>	precipitate of diameter d <sub>i</sub>
D	numerical constant
D <sub>m</sub>	mean precipitate diameter
D <sub>s</sub>	self diffusivity
K <sub>c</sub>	numerical constant
K <sub>s</sub>	numerical constant
L	gauge length during continuously cast slab straightening
m	numerical constant
M	grain boundary mobility
n	stress exponent
N	numerical constant
N <sub>c</sub>	number of crack nuclei per unit area
N <sub>si</sub>	number of precipitates per unit area of diameter d <sub>i</sub>
N <sub>vi</sub>	number of precipitates per unit volume of diameter d <sub>i</sub>
p	numerical constant
P	driving force for grain boundary migration
q	numerical constant
Q	activation energy for deformation
R	universal gas constant
R	bending radius for straightening of continuously cast slab
R <sub>v</sub>	'ductility'
S	number of active slip systems
t	slab thickness
T	absolute temperature
T <sub>c</sub>	temperature at which $\epsilon_c = \epsilon_f$
T <sub>h</sub>	homologous temperature
v	grain boundary migration velocity
V	continuous casting speed
Z	Zener-Holloman parameter
$\alpha$	numerical constant
$\alpha$	ferrite
$\gamma$	austenite
$\delta$	solidified skin thickness in continuously cast slab
$\Delta$	tangent point to first bending roll
$\dot{\epsilon}$	strain rate
$\epsilon_c$	critical strain for the nucleation of dynamic recrystallization
$\epsilon_{gb}$	grain boundary strain
$\epsilon_p$	strain at peak stress
$\epsilon_s$	surface strain at continuously cast slab
$\epsilon_t$	total strain
$\nu$	Poisson's ratio
$\sigma$	stress
$\sigma_f$	flow stress
$\sigma_c$	numerical constant
$\epsilon_f$	fracture strain

$\sigma_p$  peak stress  
 $\tau_c$  critical shear stress for wedge crack nucleation  
 $\nu_r$  inclusion relative plasticity  
 $\psi_r$  reduction in area

CHAPTER 1

INTRODUCTION

In recent years, the amount of steel produced by the continuous casting route has increased dramatically, as shown in Fig. 1.1. As with any other casting process, continuous casting can lead to the formation of a wide variety of defects in the solidified slab. (Brimacombe and Sorimachi, 1977) Therefore, as the tonnage of steel produced by continuous casting increases it becomes more important to gain an understanding of the formation of these defects, in order to prevent their occurrence.

One such defect is known as transverse cracking, described in section 2.2. These cracks are particularly deleterious, since they form at the slab surface, and hence cannot weld up during subsequent rolling. In some cases, the cracking can be so severe that an entire slab must be scrapped. These problems have resulted in intensive study of transverse cracking over the last decade, and these studies have shown that particular grades of steel are especially susceptible to this form of cracking. For example, experience at BSC Ravenscraig Works has shown that BS 4360: grade 50D steels are particularly prone to cracking. These steels contain small additions of Nb and Al and after hot rolling and normalising, the resulting fine grained, ferrite-pearlite structure is particularly suited for offshore applications. To gain a better understanding of the transverse cracking phenomenon, hot tensile tests have been performed using thermal cycles and strain rates designed to simulate the continuous cracking process (see chapter 2). These studies have related low ductility failures in hot tensile tests to the occurrence of transverse cracking in continuously cast slabs. Factors identified as being responsible for low reduction of area failures during hot tensile testing include the austenite to ferrite transformation, and the precipitation of carbides and/or nitrides. It is intended in this study to investigate further these aspects.

The influence of grain size on creep ductility has been extensively studied, but there appear to be few reports in the literature relating grain size to hot tensile test ductility, and to transverse cracking. Therefore it was also decided to investigate the influence of grain size on the hot ductility of plain carbon and micro-alloyed steels.

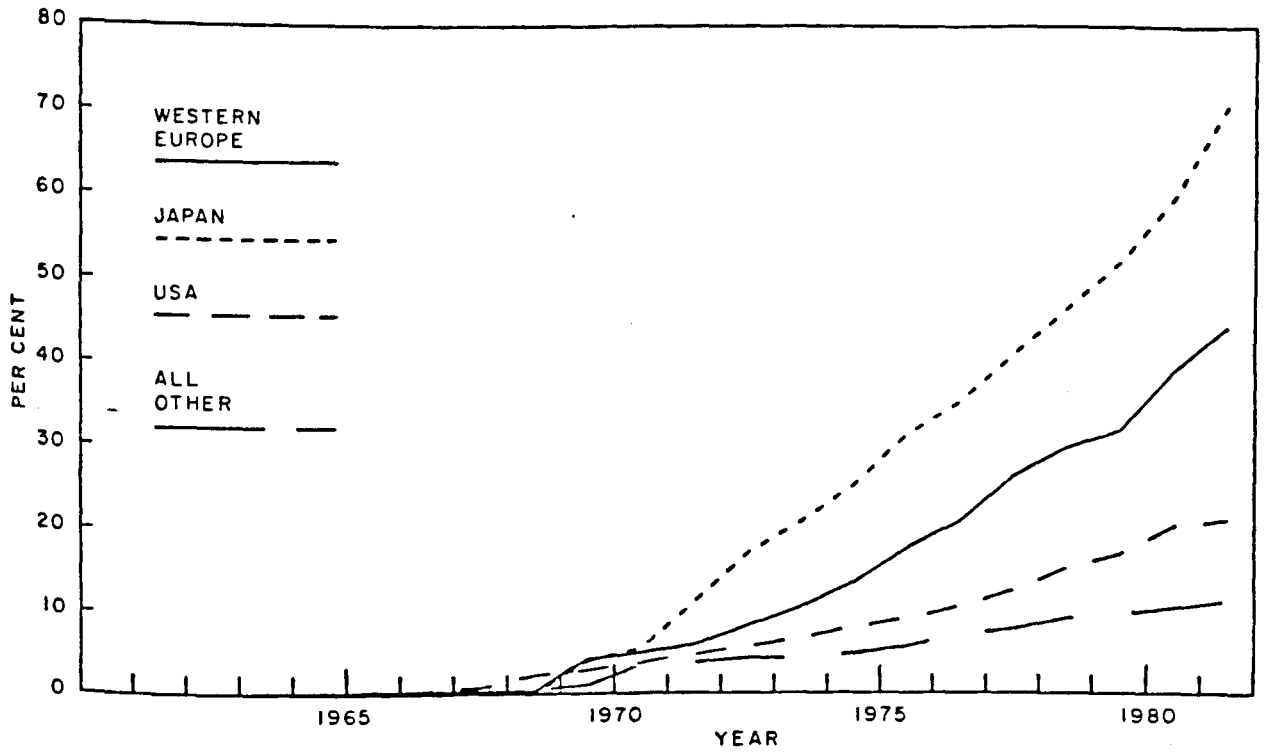


Fig. 1.1 Percentage of total steel output produced by continuous casting, by region.

CHAPTER 2

Literature Survey

## 2.1 INTRODUCTION

Much of the previous work on hot ductility has concentrated on either high strain rate deformation aimed at simulating rolling or forging operation, or has involved creep tests resulting in very low strain rates. The continuously cast slab straightening operation is carried out at strain rates in the range  $10^{-3}$  -  $10^{-4}$  s<sup>-1</sup>, as described in subsequent sections, and there is less information available on strength, structure and ductility at high temperatures for these immediate strain rates. It is intended in this chapter to briefly review the literature describing high temperature strength and structure, and particularly ductility. Special attention will be paid to examinations using intermediate strain rates and steels with small additions of such elements as Nb, Al, V and Ti.

## 2.2 TRANSVERSE CRACKING IN CONTINUOUSLY CAST SLAB

### 2.2.1 Observations of transverse cracks

Transverse cracks in continuously cast slabs are often difficult to see on the original slab surface, and a control scarf pass is required to reveal them. (Figs. 2.1 and 2.2. courtesy of B.S.C.). They appear at the base of the ripples on the slab surface left by the oscillation of the mould (oscillation marks). It is believed that these oscillation marks act as stress concentrators, and hence promote crack formation. The crack width is approximately 0.2 mm and crack depth varies from 1 to 15 mm. (Brimacombe and Sorimachi, 1977). It is believed that the cracks form in the mould, and propagate during the straightening process. (Schmidt and Josefsson, 1974; Mercer and Mcpherson, 1979). In addition, Schmidt and Josefsson have shown that the cracks propagate along the austenite grain boundaries, and that coarse grained regions are particularly prone to cracking. A variety of particles have been identified on the crack surfaces, including AlN (Mori, 1974; Cochrane, 1982) and MnS, NbCN and various oxides. (Cochrane, 1982)

The incidence of transverse cracking is dependent on many factors, which can be classed as either process variables (including such factors as secondary cooling patterns and mould oscillation frequency) or compositional variations. Process variables will be discussed in section 2.2.3 and the influence of composition on transverse cracking in section 2.9.

### 2.2.2 Mechanics of the slab straightening process

Transverse cracks propagate during the slab straightening process, and several estimates have been made to determine the surface strain and strain rate experienced by the slab during the straightening process. Fig. 2.3 shows the profile of a typical slab caster. Following Lankford (1972), Fig. 2.4 illustrates the surface strain and strain rate developed during the straightening process. These strains may

be the greatest to which the slab is subjected during the continuous casting operation. The surface strain,  $\epsilon_S$ , due to bending is given approximately by

$$\epsilon_S = t/2R \dots\dots\dots 2.1$$

where  $t$  is the slab thickness, and  $R$  the bending radius. For typical  $R$  values of 9.8 m, and a slab thickness of 229 mm, a surface strain of 1.2% is expected.

The strain rate is less well defined, due to the uncertainty in the gauge length necessary to develop the full bending strain. Lankford has given three values for this gauge length,  $L$  (Fig. 2.4): the distance from a tangent point to the first bending rolls ( $\Delta$ ), a distance equal to the skin thickness ( $\delta$ ), or a distance equal to the slab thickness, ( $t$ ). The strain rate,  $\dot{\epsilon}$ , is then given by:-

$$\dot{\epsilon} = \epsilon_S V/L \dots\dots\dots 2.2$$

where  $V$  is the casting speed. For a typical casting speed of 0.9 m/min. and suitable values for  $L$ , the surface strain rate is in the range  $0.2 \times 10^{-3} - 3.0 \times 10^{-3} \text{ S}^{-1}$ . Similar results for surface strain and strain rate have been calculated by Bernard et al (1978). It should be noted that these calculations are approximate, and deal with the deformation of the slab as a whole. Locally, at the bottom of the oscillation works, for example, different values may be obtained for  $\epsilon_S$  and  $\dot{\epsilon}$ .

### 2.2.3 The influence of process variables on transverse cracking

In section 2.9, results will be reported which show that when micro-alloyed steels are tested at strain rates in the range  $10^{-4} - 10^{-3} \text{ S}^{-1}$  at high temperature, they can show a loss of ductility in the temperature range 600 - 1,000°C. These conditions are close to those experienced during the straightening operation in which transverse cracks propagate, and so attempts have been made to alter the slab surface temperature by adjusting the secondary cooling pattern.

'Soft' cooling patterns aim to produce a slab surface temperature above the low ductility region, whilst 'hard' cooling patterns try to produce slab temperatures below the low ductility region.

Mercer and Mcpherson (1979) have reported that 'soft' cooling patterns, using reduced amounts of cooling water, resulted in an increase in slab surface temperature, and a reduction in the incidence of transverse cracking. Offerman et al (1981) have also reported reduced cracking using soft cooling patterns.

Birat et al (1981) have discussed the limitations of the soft cooling pattern. They pointed out that the high temperature extent of the ductility trough is more composition dependent than the low temperature extent. Straightening temperatures therefore, either have to be adjusted for a particular composition, or kept at temperatures high enough to avoid the ductility trough of the steel with composition showing the broadest ductility trough. Additionally, there are strict limitations which must be put on casting speed if the soft cooling pattern is adopted: a rapid casting speed can result in incomplete solidification at the straightener, whilst a casting speed which is too slow can produce a straightening temperature close to the ductility trough.

These limitations led Birat et al (1981) to develop a cooling pattern which reduced surface temperature at the straightener to 700°C, and this produced a decrease in the frequency of transverse cracking. Similar 'hard' cooling patterns have been used successfully by Nozaki et al (1978), and by Schmidt and Josefsson (1974). The latter authors attributed the reduction in cracking to the elimination of the coarse austenite grains with which they had previously associated transverse cracking.

However, the 'hard' cooling pattern also had disadvantages, as noted by Offerman et al (1981). Although such cooling patterns reduce

the slab surface temperature to below 700°C, at some point below the slab surface, the temperature can be high enough to place it in the low ductility region, leading to the formation of subsurface transverse cracks. Cooling uniformity is more difficult to achieve using the 'hard' cooling pattern. For example, clogged spray nozzles can produce localised bands at the surface which are at an elevated temperature, and cracking can then occur along these bands. The impingement of cooling sprays can also lead to oscillations in the slab temperature near the slab surface (Fig. 2.5). The thermal stresses set up by this effect are in themselves enough to form cracks (Tomono, 1977). In addition, thermal cycling below the  $A_{r3}$  temperature can increase the rate of AlN precipitation (Nozaki et al, 1978), and hence reduce hot ductility. Offerman et al (1981) have also demonstrated this effect. Thus the introduction of a more uniform cooling pattern which eliminates these temperature oscillations has been shown to reduce transverse cracking. (Nozaki et al, 1978; Coleman and Wilcox, 1985)

Mould oscillation frequency can also effect transverse cracking and experience at the BSC Ravenscraig plant has shown than an increase in mould oscillation frequency led to a significant reduction in plate rejection levels, presumably by reducing the stress concentration effect of the oscillation marks (Mercer and Mcpherson, 1979).

## 2.3 HIGH TEMPERATURE STRENGTH AND STRUCTURE

### 2.3.1 General

During hot deformation, work hardening and dynamic restoration processes are occurring simultaneously, and it is the balance between these processes that determines the hot strength. The operative dynamic restorative process is dependent on strain and alloy type, and the behaviour of different metals and alloys is summarised in Table 2.1.

Hot strength is strongly influenced by temperature and strain rate, and Sellars and Tegart (1966) have shown that hot working data can be correlated using the relationship developed from creep studies:-

$$\dot{\epsilon} = A (\sinh \alpha \sigma)^n \exp (-Q/RT) \dots 2.3$$

where  $\dot{\epsilon}$  is the strain rate,  $\sigma$  stress (either peak or steady state), T the absolute temperature, R the universal gas constant, A,  $\alpha$  and n temperature independent constants, and Q an activation energy.

Equation 2.3 can also be expressed in terms of Z, the Zener-Holloman parameter, where

$$Z = \dot{\epsilon} \exp (Q/RT) \dots 2.4$$

so that 2.3 can be written as

$$Z = A (\sinh \alpha \sigma)^n \dots 2.5$$

This relationship has been successfully applied for a number of alloys, including plain carbon steels (Tegart, 1968), and micro-alloyed steels (Sankar et al, 1979) in the austenitic state. The value of Q may remain constant over a wide range of strain rates, but in some cases different values are obtained for creep and hot working conditions (Jonas et al, 1969).

In the former case, Q is equal to the activation energy for self diffusion, and is indicative that the rate controlling softening process is dynamic recovery over a wide range of strain rates. In the latter case, the higher activation energy for hot working is taken to be due to the operation of dynamic recrystallization.

during hot working. Steels in the austenitic state belong to this second group.

### 2.3.2 Dynamic recovery

This softening process operates at all strains for metals in group A, but only at small strains for group B metals. The microstructural evidence for dynamic recovery has been reviewed by Jonas et al (1969). This work has shown that the grains of the original microstructure become elongated in the direction of hot working, and appear fibrous. This distortion of grain boundaries is accompanied by subgrain formation. For  $\alpha$  iron, it has been shown that the subgrains assume their final size by strains of 0.2 to 0.3 for strain rates of 0.05 to 1.5  $S^{-1}$  (Glover and Sellars, 1973). After their formation, subgrain size and mis-orientation, and dislocation density between the sub-boundaries, remain constant. A situation is reached in which dislocation generation and annihilation rates are equal, and the strain hardening rate is then reduced to zero.

For group A metals, the subgrains are narrow and well defined, whereas for group B metals, the subgrains are highly tangled, leading to higher levels of stored energy for these metals. The subgrains remain equiaxed even at large strains for both group A and group B metals, and it is thought that this occurs by the process of re-polygonization, that is the repeated destruction and subsequent re-formation of new sub-boundaries in such a manner as to keep their spacing and dislocation density constant. The mean subgrain size is increased by increasing temperature and decreasing strain rate, and is related to the Zener-Holloman parameter, Z, by:-

$$d_s^{-1} = a + b \log Z \dots\dots 2.6$$

where  $d_s$  is the mean subgrain diameter, and a and b constants (McQueen et al, 1967). A correlation has also been observed by many workers between flow stress and subgrain size. The most general

relationship is of the form:-

$$\sigma_f = \sigma_0 + kd_s^{-m} \dots\dots 2.7$$

where  $\sigma_f$  is the flow stress, and  $\sigma_0$ ; k and m constants. Jonas et al (1969) have reviewed the literature for Al alloys of varying purity, and determined that for such alloys, m was 1.5. Other values of m are 1 for Fe-Cr and Fe-Ni alloys. (Redfern and Sellars, 1969).

As described previously, substructure differs between group A and group B metals, and this is thought to be due to differences in stacking fault energy between the two groups; group A metals have a high stacking fault energy, whilst group B metals have a low stacking fault energy. These differences mean that thermally activated cross slip in group B metals is difficult, and hence substructure cannot develop to the extent observed in group A metals. In general, solid solution alloying additions to pure metals reduce stacking fault energy, and hence makes dynamic recovery more difficult, and as a consequence, flow stress is increased. Subgrain size may either decrease (Zr -Sn alloys), increase (Al-Mg alloys) or remain constant (Fe-Si) alloys, with increasing alloying additions. (McQueen and Jonas, 1975)

Metals containing stable second phase particles develop substructure more rapidly than an equivalent particle free alloy, and these particles finally stabilize the sub structure. Subgrain diameter can be reduced to the order of interparticle spacing. If the second phase particle is less stable, particle coarsening and coalescence can occur. This process is great accelerated by hot deformation, as sub-boundaries act as paths for diffusion at higher rates than the lattice. This process can lead to a decrease in the flow stress during hot deformation.

### 2.3.3 Dynamic recrystallization

After undergoing a limited amount of dynamic recovery group B

metals can undergo dynamic recrystallization, if sufficiently large strains are reached. The limited dynamic recovery occurring in these metals means that the sub structure is poorly developed, with tangled sub grains having high stored energy levels. These high levels of stored energy in group B metals are considered essential to obtain the differences in stored energy levels required to nucleate dynamic recrystallization.

Nucleation of dynamic recrystallization occurs at existing grain boundaries at lower strain rates. (Luton and Sellars, 1969; Roberts et al, 1979). The poorly developed sub-boundaries pin sections of the original grain boundaries, which bulge out and migrate due to the strain energy difference across the boundary. At higher strain rates recrystallization nuclei throughout each grain have been observed. (McQueen and Bergesson, 1972).

As the new grains grow the metal, and hence the new grains, continue to be deformed. At low strain rates, the stored energy gradient between the centre of the new grain and the advancing boundary is low, and so the driving force for dynamic recrystallization is not significantly effected by deformation. Recrystallization proceeds to completion, with the centre of each grain having a higher dislocation density than the edge. As deformation continues, the stored energy within the recrystallized grains increases until the critical level for recrystallization is reached. At this stage, the flow stress falls as recrystallization proceeds again, and the repetition of this process leads to the cyclic flow curves observed for low strain rate deformation in group B alloys. (Sellars and Tegart, 1966).

For high strain rate deformation, the stored energy behind the migrating boundary is high, and hence the driving force for grain boundary migration is reduced. Before recrystallization is complete, the stored energy levels in the centres of the recrystallized grains

reaches the critical level for nucleation and the cycle repeats itself. This process leads to the steady state flow stress observed during hot deformation at higher strain rates.

Nucleation of dynamic recrystallization occurs at a critical strain level,  $\epsilon_c$ , which is less than the strain at peak stress,  $\epsilon_p$ , as measured from the flow curve. According to Rossard (1973),  $\epsilon_c$  is given approximately by:-

$$\epsilon_c = 0.83 \epsilon_p \quad \dots\dots 2.8$$

$\epsilon_c$  increases as the initial grain size,  $d_o$ , increases (Roberts et al, 1979; Sellars, 1980; Ruibal et al, 1984), and as Z increases. (McQueen and Jonas, 1975, Sellars, 1980). Sellars has shown that for steels, a relationship of the form:-

$$\epsilon_p = B d_o^{\frac{1}{2}} Z^p \quad \dots\dots 2.9$$

exists, when B and p are constants, and p is in the range 0.125 to 0.175. At very low stresses,  $\epsilon_c$  may decrease with increasing Z. (Luton and Sellars, 1969). This complex variation of  $\epsilon_c$  with Z is not fully understood. It is thought that at very low stresses, the low dislocation density requires large strains to provide the necessary stored energy for dynamic recrystallization. At higher stresses, the increase in  $\epsilon_c$  with increasing Z may be due to the need for an increase in stored energy with increasing strain rate to provide the necessary driving force for dynamic recrystallization to proceed.

Dynamically recrystallized grain size,  $d_r$ , is determined by the flow stress,  $\sigma_f$ , and is independent of temperature.  $\sigma_f$  and  $d_r$  are related by:-

$$\sigma_f = N d_r^{-q} \quad \dots\dots\dots 2.10$$

where N and q are constants - q falls in the range 0.7 - 1.0, depending on composition and purity. (McQueen and Jonas, 1975). Solid solution alloying reduces the rate of dynamic recovery, and hence might be expected to promote dynamic recrystallization; however,

the rate of grain boundary migration is also reduced by alloying additions and this reduces the rate of dynamic recrystallization. For some alloys, this reduction in the rate of dynamic recrystallization can lead to the formation of a ductility trough.

The elements Nb and to a lesser extent V, are particularly effective in retarding dynamic recrystallization. The technical importance of this phenomenon for the production of controlled rolled microalloyed steels has meant that the subject has been investigated extensively. Recent investigations (le Bon et al, 1975; Sekine and Maruyama, 1976; Weiss and Jonas, 1979; Ouchi and Okita, 1982) have all shown that increasing Nb additions increase  $\epsilon_p$ . Weiss and Jonas have shown that this effect is due to solute drag on grain boundaries at high strain rates, and to the dynamic precipitation of fine NbCN at slower strain rates, which reduce grain boundary migration rates. The nucleation of dynamic recrystallization can be delayed until the dynamic precipitation of NbCN is complete, leading to the characteristic 'reverse knee' form of the RTT diagram for Nb containing steels.

Similar studies on the influence of V on dynamic recrystallization by Akben et al (1981) have shown that V in solution retards dynamic recrystallization, though not to as great an extent as Nb. Dynamic precipitation of VN also increase  $\epsilon_p$ .

## 2.4 INTERACTION BETWEEN HIGH TEMPERATURE CRACKING AND SOFTENING PROCESSES

### 2.4.1 High temperature intergranular crack nucleation and growth

It has now been known for many years that under appropriate conditions of stress and temperatures, intergranular failure can occur during creep and during hot workability tests. As described in section 2.2.1, transverse cracks propagate along austenite grain boundaries. Therefore, the factors which influence high temperature intergranular crack nucleation and growth will be discussed briefly. This subject has been covered extensively by Evans (1984), who deals with the subject in greater depth than it is possible to here. Traditionally, intergranular creep defects have been classified as either 'grain edge' or 'r type' (r for rounded) or as 'grain corner' or 'w type' (w for wedge cavities). Both types of cavity require grain boundary sliding to nucleate the cavity. The models proposed for the nucleation of 'w type' cracks are illustrated in Fig. 2.6. Calculations have been made to estimate the critical stress required to nucleate a wedge crack, the simpler models assuming no matrix relaxation, whilst more complex models consider the role of thermal activation in reducing the values of the local concentrated stress. Stroh (1955), using no matrix relaxation, estimated the critical shear stress for wedge crack nucleation,  $\tau_c$  as:-

$$\tau_c = \left[ \frac{K_s \mu \gamma_f}{(1 - \nu) d_g} \right]^{\frac{1}{2}} \quad \dots\dots\dots 2.11$$

where  $\nu$  is Poisson's ratio,  $\gamma_f$  is the fracture energy,  $K_s$  a constant,  $d_g$  the grain diameter and  $\mu$  the shear modulus. Other more sophisticated treatments have shown that wedge crack nucleation requires sliding rates greater than  $10^{-9} \text{ ms}^{-1}$  (Evans, 1984).

Generally, steady state sliding rates are less than  $10^{-10} \text{ ms}^{-1}$  would indicate that nucleation only occurs under high, transient rates of sliding.

'r' type cavities also require grain boundary sliding for cavity nucleation, and one possible mechanism for their formation was proposed by Gifkins (1956), and is illustrated in Fig. 2.7. In this mechanism, ledges produced by the impingement of slip bands with the grain boundary could lead to the formation of cavities as grain boundary sliding proceeded.

Another possible source of stress concentrators at grain boundaries are grain boundary particles. If the stress concentration at such particles is produced by grain boundary sliding alone, the slip distance corresponds to the interparticle spacing, and large applied stresses are required for particle fracture or particle-matrix decohesion. However, for the case of the intra granular slip impingement against a grain boundary particle, much smaller applied stresses are required for particle fracture, as slip distances are much greater. In alloys which develop particle free zones (PFZ) adjacent to the grain boundary, particle fracture is much more likely, as a large fraction of the specimen strain is concentrated in the PFZ.

It should be noted that the critical stresses required for the nucleation of 'r' type cavities are much lower than those required for 'w' type cavity nucleation, and so 'r' type cavity formation is favoured by low stress, high temperature creep tests, or low strain rate hot workability tests.

Many mechanisms have been proposed to describe the growth of 'r' type cavities, and they can be classified as either cavity growth by deformation mechanisms, or cavity growth by vacancy diffusion mechanisms. The subject is complex, and is dealt with in detail by Evans (1984)

#### 2.4.2. Influence of dynamic recovery on hot ductility

As discussed in 2.4.1, low ductility failures at high temperature can be intergranular in nature, and intergranular cracks are

nucleated by grain boundary sliding. In creep tests, it has been observed that with increasing stress, crack nucleation sites change from grain boundary ledges and particles to triple points. Materials in which dynamic recovery occurs readily (Group A alloys, Table 2.1) have low flow stresses and flow readily at triple points to relieve stress concentrations, and thus diminish the initiation of 'w' type cracks. In addition, metals which are susceptible to dynamic recovery may form 'scalloped' grain boundaries (McQueen and Jones, 1975), which diminishes grain boundary sliding, and hence reduces intergranular crack nucleation. In such metals, ductility increases with increasing temperature, because the stress relieving processes are more sensitive to temperature than those promoting crack nucleation. (Gittins, 1970) However, in group B metals, the rate of dynamic recovery is low and ductility may decrease with increasing temperature in the lower part of the high temperature range, because of increases in the amount of grain boundary sliding. (White and Rossard, 1968)

In general, solid solution alloying tends to reduce ductility. This is partly because the smaller subgrains often formed in these materials are not as effective in producing 'scalloped' grain boundaries, so that grain boundary sliding is not impeded to the same extent. The scalloping is also reduced by the retarding effect solutes exert on grain boundary migration. In addition, the decreased ease of dynamic recovery associated with alloying raises the flow stress considerably, which is instrumental in nucleating and opening up cracks.

#### 2.4.3. Influence of dynamic recrystallization on hot ductility

Metals which undergo limited dynamic recovery often show a minimum in ductility in a temperature range close to the hot working range. This minimum in ductility is associated with intergranular failure. This occurs because the limited dynamic recovery gives rise to high

flow stresses and work hardening rates, preventing the accommodation by lattice deformation of the stresses built up at triple points or grain boundary particles. As the temperature is increased beyond that of the ductility minimum, dynamic recrystallization is observed. The introduction of new grains isolates the cracks already formed from the grain boundaries, thus inhibiting crack propagation. Further crack growth occurs by the 'capture' of a moving grain boundary for a sufficient time for vacancy diffusion and applied tensile stress to lengthen the crack before the boundary breaks away. New cracks may also form in the boundaries of the recrystallized grains. Thus under these conditions, grain boundary migration rate may be the process controlling crack propagation.

This increase in ductility associated with the onset of dynamic recrystallization has been reported for a wide range of group B metals: in Inconel 600 (Dieter et al, 1968), Fe-25%Ni (White and Rossard, 1968), in a range of Fe-Ni alloys, (Evans and Jones, 1976), in cupro-nickels (Evans and Jones, 1978), and austenitic stainless steels. (Bywater and Gladman, 1976; Norstrom, 1977; Ouchi and Okita, 1982). In all these studies, high ductility failures were associated with dynamic recrystallisation. The high temperature failure of austenitic irons of varying purities has been studied by Wray (1975). Austenitic iron undergoes limited dynamic recovery and displays a temperature range in which ductility is low. However, Wray showed that at temperatures less than 1000°C electrolytic iron deformed using a strain rate of  $2.8 \times 10^{-5} \text{ S}^{-1}$ , although undergoing dynamic recrystallisation, failed in an intergranular manner with low ductility.

Studies on the hot deformation of Nb micro-alloyed steels show a ductility trough within which dynamic recrystallisation does not occur, due to the retardation of recrystallization associated with

Nb additions. (le Bon et al, 1975; Sekine and Maruyama, 1976; Weiss and Jonas, 1979) Bernard et al (1978) used these recrystallization arguments to explain the occurrence of the ductility trough in Nb micro-alloyed steels. However, for micro-alloyed steels, results have been reported which have shown that their complex hot ductility behaviour cannot be explained by dynamic recrystallization arguments alone. Ouchi and Matsumoto (1982) studied the influence of strain rate on the hot ductility of micro-alloyed steels. Their results showed that the temperature of minimum hot ductility did not change with strain rate. They pointed out that since the critical strain for nucleation of dynamic recrystallization decreased with decreasing strain rate, tests performed at low strain rates might be expected to have a narrower ductility trough, due to an earlier onset of dynamic recrystallization. Wilcox and Honeycombe (1984) showed that the hot ductility of a C-Mn-Nb steel began to increase rapidly with increasing temperature before the onset of dynamic recrystallization. They concluded that in C-Mn-Nb steels, the precipitation of NbCN, rather than dynamic recrystallization, was the most important factor controlling hot ductility. However, in C-Mn-Al and C-Mn-Nb-Al steels, Wilcox and Honeycombe showed that ductility improved when a strain sufficient to nucleate dynamic recrystallization could be applied before fracture.

## 2.5 THE INFLUENCE OF STRAIN RATE ON HOT DUCTILITY

### 2.5.1 General

During laboratory simulations of hot working processes, the strain rate is chosen to approximate that experienced during the hot working process. In many alloys, the strain rate has a profound influence on fracture strain. (Sellars and Tegart, 1972; Evans and Jones, 1976). Several hot ductility studies of irons and steels have included investigations into the strain rate dependence of hot ductility (White and Rossard, 1968; Wagenaar, 1968; Vodopivec, 1978; Sanker et al, 1979), and all have shown an increase in hot ductility with increasing strain rate. However, these tests were performed to simulate hot working processes such as rolling and forging, and were carried out at strain rates in the range  $0.1 - 10 \text{ S}^{-1}$ .

Of particular relevance to the continuous casting process are those studies conducted above  $700^\circ\text{C}$  in the strain rate range  $10^{-4} - 10^{-3} \text{ S}^{-1}$ , as these are believed to be the conditions experienced during the continuously cast slab straightening process (section 2.2.2). For irons and steels tested under these conditions, the influence of strain rate on hot ductility is temperature and composition dependant, and three temperature regimes may be defined:- from the solidus temperature to  $1200^\circ\text{C}$ ; from  $1200^\circ\text{C}$  to  $1000^\circ\text{C}$ ; and below  $1000^\circ\text{C}$ .

### 2.5.2 The influence of strain rate on hot ductility above $1200^\circ\text{C}$

Suzuki et al (1982) investigated the influence of strain rate on hot ductility in this temperature range for a high purity electrolytic iron, and for a 0.4%C steel. They found hot ductility and strain rate to be independent for strain rates in the range  $5 \times 10^{-3} - 20 \text{ S}^{-1}$ . This behaviour has been related to the fracture made for steels tested near their melting points.

Several workers (Weinberg, 1979; Rogberg, 1983) have reported

fracture near the melting point to be due to incipient melting at grain boundaries and/or dendrite interfaces, and thus strain rate would be expected to have no influence on fracture processes in this temperature range.

### 2.5.3 Influence of strain rate on hot ductility from 1200°C to 1000°C

In this temperature range, low ductility failures have been observed for steels which have undergone a 'sensitizing' treatment, typically involving reheating above 1200°C, and which also have a low (<40) Mn:S ratio (see section 2.9.5). Conflicting results have been reported for the influence of strain rate in this temperature range. Lankford (1972) has reported no influence of strain rate on the hot ductility of a range of plain carbon steels, whilst Suzuki et al (1982) have reported an increase in ductility with decreasing strain rate between  $5 \times 10^{-3}$  and  $20 \text{ s}^{-1}$  for a plain carbon steel. They have explained their results as being due to the coarsening of (Fe, Mn)S and (Fe, Mn)O intergranular precipitates occurring during the long test times at slow strain rates, which reduces the embrittling effect of these precipitates. Yasumoto et al (1985) have also reported an increase in hot ductility as the strain rate is reduced from  $2.3 \text{ s}^{-1}$  to  $0.01 \text{ s}^{-1}$  in a range of C-Mn-Al steels with Mn:S ratios in the range 10-25.

### 2.5.4 The influence of strain rate on hot ductility below 1000°C

Investigations by Wray (1975) on pure irons, and by Carlsson (1964), Bernard et al (1978), Mintz and Arrowsmith (1979), Ouchi and Matsumoto (1982), Suzuki et al (1982), Wilcox (1982), and Maehara and Ohmori (1984) on plain carbon and micro-alloyed steels have all shown a decrease in hot ductility with decreasing strain rate (Fig. 2.8). In addition, some investigators (Mintz and Arrowsmith, 1979; Maehara and Ohmori 1984) have reported a

broadening of the ductility trough with decreasing strain rate. These results can be explained by the fact that an increase in strain rate leads to a decrease in the ratio  $\epsilon_{g.b.} / \epsilon_t$ , where  $\epsilon_{g.b.}$  is the grain boundary strain, and  $\epsilon_t$  the total strain (Ouchi and Matsumoto, 1982). In addition, an increasing strain rate will produce an increase in the grain boundary migration velocity,  $v$ , through the equation of Lucke and Stuwe (1963):

$$v = M (C, T) P (C, \dot{\epsilon}, T) \dots\dots\dots 2.12$$

where  $M$  is the grain boundary mobility and includes terms describing the influence of composition  $C$ , and temperature,  $T$ , and  $P$  is the driving force for grain boundary migration. As pointed out by Evans and Jones (1976) and Mintz and Arrowsmith (1979), a rapidly migrating grain boundary will isolate grain boundary cracks, inhibiting their propagation and thus improving ductility.

## 2.6 THE INFLUENCE OF GRAIN SIZE ON HOT DUCTILITY

As described in section 2.4, high temperature fracture can occur in an intergranular manner under appropriate strain rates, and the influence of grain size on hot ductility has been the subject of many studies. The majority of these investigations have used the creep test, and a wide range of metals and alloys have been examined, including copper (Fleck et al, 1970), alpha brass (Taplin and Whittaker, 1963), Magnox A180 (Evans, 1969), austenitic steels (Bywater and Gladman, 1976; Katumba Rao et al, 1975) and a low alloy steel (Reynolds and Gladman, 1980). The majority of these studies have shown that creep ductility decreases continuously with increasing grain size (Fig. 2.10).

In his study of magnox A180, Evans (1969) showed that increasing grain size led to an increase in the rate of grain boundary sliding. He therefore, attributed the decrease in ductility with increasing grain size as being due to the increased sliding rate producing an increased grain boundary cavity growth rate. However, it is now believed that creep ductility, when intergranular fracture occurs, is controlled by the final stages of fracture, rather than the nucleation and early stages of growth of grain boundary cavities (Fleck et al, 1970; Kutumbo Rao et al, 1975). In the later stages of crack growth, a propagating grain boundary crack must grow through triple points, and it seems likely that the ease of propagation of a crack through a triple point, and the number of triple points encountered, will be an important fact in determining creep ductility. Thus a coarse grained material, with fewer triple points than a fine grained material will be more susceptible to intergranular cracking. It has also been pointed out that the crack aspect ratio will influence the ease of crack propagation through triple points. (Fleck et al, 1970). In coarse grained material, crack aspect ratio and hence stress concentration at the

crack tip, will be high, allowing such cracks to readily grow through triple points. The reverse is true for fine grained materials.

Although the majority of investigations on the influence of grain size on hot ductility have shown that ductility decreases with increasing grain size, Fleck et al (1970) in their investigation of copper, and Kutumba Rao et al (1975) in their investigation of a Cr-Mn-N austenitic steel, have shown that at fine grain sizes, creep ductility can decrease with decreasing grain size (Fig. 2.11) Garofalo (1968) attempted to account for both the increase and decrease in creep ductility with continually increasing grain size by using the equation:-

$$\psi_r = \frac{1}{D \lambda dg} (1/\pi N_c)^{\frac{1}{2}} \dots\dots\dots 2.13$$

Where  $\psi_r$  is the reduction in area at fracture, D a constant,  $\lambda$  the fraction of deformation due to grain boundary sliding, dg is the grain diameter, and  $N_c$  is the average number of crack nuclei per unit area that lead to fracture. This equation predicts a decrease in creep ductility with increasing d if  $N_c$  and  $\lambda$  remain constant. Decreasing ductility with decreasing grain size will occur if  $N_c$  and  $\lambda$  increase rapidly at small grain sizes, compensating for the decrease in dg. However, equation 2.12 was derived assuming that intergranular cavity growth occurs by grain boundary sliding, and therefore cannot be generally applicable. For example, in the work of Kutumba Rao et al (1975), the angular distribution of cavities indicated that cavity growth had occurred predominantly by vacancy diffusion processes, and so equation 2.12 is not applicable to this situation. Kutumba Rao et al have attributed their results to the presence of abnormally large grains in an otherwise fine grained specimen, the abnormally large grains controlling the fracture process.

There appear to be few reports in the literature examining the influence of grain size on the hot ductility of micro-alloyed steels. Carlsson (1964) in a study of the hot ductility of Al killed steels at temperatures in the range 700 - 1100°C, reported no influence of austenite grain size on hot ductility. More recently, Ouchi and Matsumoto (1982) showed that the hot ductility of both C-Mn-Al and C-Mn-Nb-Al steels was independent of austenite grain size in the range 300 - 1000  $\mu\text{m}$ , when tested at 900°C.

Grain size appears to be an important factor in the transverse cracking phenomenon. Schmidt and Josefsson (1974) have observed that transverse cracks are associated with coarse austenite grains, and that this cracking is reduced when coarse grained structures are eliminated by the use of a suitable secondary cooling pattern.

The... on which of the... will produce a... will... which of the above... is dependent on the deformation... of the inclusion, and the strength of the matrix... is not usually described in terms... the ratio of true strain... strain developed in the matrix. The... Malkiewicz and Rudnik (1961)...

$$\frac{\ln (d/c)}{3 \ln (2c/a)}$$

where  $a$  and  $c$  are the lengths of the minor and major axes of the

## 2.7 THE INFLUENCE OF INCLUSIONS ON HOT DUCTILITY

It is well known that non metallic inclusions have an extremely detrimental effect on hot ductility, and can be a major cause of defects during hot working. (Cottingham, 1968; Nicholson et al, 1968; Smith et al, 1972; Sellars and Tegart, 1972; Gittins, 1977; Charles, 1980). The influence of inclusions on hot ductility is often apparent in hot workability tests, and for example Robbins et al (1961) have shown that in hot torsion tests of irons of varying purity, ductility decreases as inclusion volume fraction increases. The inclusions act as fracture sites, and during hot workings, as described by Sellars and Tegart, three situations can be envisaged:-

- a. the inclusion fractures.
- b. the inclusion will deform plastically, maintaining continuity with the matrix.
- c. decohesion of the inclusion matrix interface will occur.

The size of the cavity formed will be dependant on which of the three processes described above occurs. Case a will produce a cavity of similar size to the inclusion, whilst case c will produce a cavity smaller than the inclusion. Which of the above three processes actually occurs is dependant on the deformation behaviour of the inclusion, and the strength of the matrix inclusion interface.

Inclusion deformation behaviour is now usually described in terms of their relative plasticities, i.e. the ratio of true strain developed in the inclusion to true strain developed in the matrix.

The relative plasticity,  $\nu_r$ , is given by Malkiewicz and Rudnik (1963) as:-

$$\nu_r = \frac{2 \ln (d/c)}{3 \ln (A_0/A_1)} \dots\dots\dots 2.14$$

where c and d are the lengths of the minor and major axes of the

deformed inclusion (initially assumed spherical), and  $A_0$  and  $A_1$ , the initial and final ingot cross section respectively. Gove and Charles (1974) have shown that the inclusion hardness,  $H_i$ , and the matrix hardness,  $H_m$ , can be related to  $\nu_r$  by:-

$$\nu_r = 2 - H_i/H_m \dots\dots\dots 2.15$$

The principle factors controlling  $\nu_r$  are deformation temperature and inclusion composition. Inclusion composition controls the inclusion liquids temperature and hardness, whilst the hot working temperature effects the flow stress of the matrix. The influence of temperature and composition on  $\nu_r$  are illustrated for sulphide inclusions in steel in Fig. 2.9. The influence of inclusion size on relative plasticity is unclear, but some workers have reported that  $\nu_r$  increases with increasing inclusion size. (Segal and Charles, 1977).

The relative plasticity of inclusions can influence hot ductility during hot working processes. Low values of  $\nu_r$  are undesirable during rolling, as voids have been shown to nucleate preferentially on inclusions with low  $\nu_r$  values. (Kießling, 1968; Maunder and Charles, 1980). Also, in hot working processes where tensile forces are present, such as the production of seamless tube by piercing, defects are associated with less deformable oxide type inclusions, sulphide inclusions being less harmful. (Nicholson, 1968).

Although the influence of inclusion size on relative plasticity is uncertain, it has been shown that large inclusions have a more detrimental effect on hot workability than smaller inclusions, (Klevebring et al, 1975; Coward et al, 1977; Charles, 1980) and nucleate voids preferentially. Waudby (1979) has reviewed the subject, and concludes that non deforming inclusions in steels above 2-3  $\mu\text{m}$  in diameter will nucleate voids.

The roles of inclusions in the transverse cracking of

continuously cast slabs is uncertain, but any effect is likely to be small, as transverse cracks occur at small strains, ( - 2%), whereas much larger strains are generally required to nucleate voids at inclusions.

## 2.8 THE INFLUENCE OF PHASE TRANSFORMATION AND DUPLEX STRUCTURE ON THE HOT DUCTILITY OF STEELS

### 2.8.1 Phase Transformation

Several studies have been performed using the hot torsion test to investigate the hot ductility of irons (Robbins et al, 1961; Reynold and Tegart, 1962; Keane et al, 1968; Wagenaar, 1968).

The results of these studies all show similar trends, irrespective of strain rate or purity; a ductility drop is associated with the ferrite to austenite transformation and by the extrapolation of the hot ductility curves, it is evident that austenite is less ductile than ferrite at the same temperature (Fig. 2.12). Robbins et al proposed that the inferior ductility of austenite was due to two factors: firstly, the self diffusivity of Fe is greater in ferrite than in austenite, and secondly, austenite has only 12 active slip systems, as opposed to 48 for ferrite. They attempted to relate self diffusivity,  $D_s$ , and the number of active slip systems,  $S$ , to ductility,  $R_v$ , using a relation of the form:

$$R_v = S D_s^{\frac{1}{2}} f(x) \dots\dots\dots 2.16$$

where  $f(x)$  is a function of factors such as purity and the amount of grain boundary sliding. However, the later work of Reynolds and Tegart showed that the initial success of 2.16 was fortuitous.

### 2.8.2. Duplex Structure

The presence of a duplex structure in an alloy normally leads to reduced ductility, as for example in the stainless steel investigated by Kobayashi et al (1980). The ductility of duplex phase alloys is dependent on the volume fraction of each phase, their distribution and their relative ductilities. For example, Muller (1967) has shown that hot ductility is a minimum for duplex stainless steels with approximately 30%  $\delta$  ferrite, since interphase cracking is particularly severe for this composition. McQueen and Jonas (1975) have suggested that the decrease in the hot

ductility of duplex stainless steels associated with increasing  $\delta$  ferrite volume fractions is due to the inhibition of dynamic recrystallization in the  $\gamma$  phase by restricting grain boundary mobility. Investigations into the hot torsional ductility of irons revealed low ductility failures caused by the presence of an extended ( $\alpha + \gamma$ ) region, owing to impurities present in the irons (Robbins et al, 1961; Reynolds and Tegart, 1962; Keane et al, 1968). Reynolds and Tegart observed in the two phase region, fracture generally occurred in the ferrite, although in some cases, cracking was observed at large inclusions or the ferrite-austenite interface.

More recently, hot tensile tests have been performed on plain carbon and micro-alloyed steels to determine whether the ductility loss associated with the two phase region is responsible for transverse cracking in continuously cast slabs. Some of these tests have produced conflicting results. Bernard et al (1978) observed that after solution treatment, the austenite to ferrite transformation lead to an improvement in hot ductility for a range of C-Mn-Al and C-Mn-Nb-Al steels. Wilcox and Honeycombe(1984) reported little influence of transformation on the hot ductility of C-Mn, C-Mn-Al and C-Mn-Nb-Al steels. In contrast, other authors have reported ductility troughs apparently associated with the two phase region for C-Mn and C-Mn-Al steels (Mintz and Arrowsmith, 1979; Yamanaka et al, 1980; Wray, 1981, Suzuki et al, 1982). In these steels, fracture has been observed to occur within the pro-eutectoid ferrite at precipitates and inclusions. In accord with this idea, Yamanaka et al showed that by increasing the Al content of a C-Mn-Al, and hence increasing the volume fraction of AlN precipitator within the pro-eutecoid ferrite, ductility was reduced. For C-Mn-Nb-Al and some C-Mn-Al steels, it is believed that the phase trans-

formation is of secondary importance in controlling hot ductility, as the loss of ductility associated with AlN and NbCN precipitation is dominant. (Ouchi and Matsumoto, 1982; Ohmori; and Maehara, 1984).

## 2.9 THE INFLUENCE OF COMPOSITION ON THE HOT DUCTILITY OF STEELS

### 2.9.1 Nb

The adverse effect of Nb on the hot ductility of steels first became evident when Nb additions were made to heavy forgings and castings to achieve grain refinement (Kazinczy, 1965; Vodopivec, 1975). Hannerz et al (1968) identified extensive precipitation of NbC in these heavy castings, and attributed ingot cracking to intergranular embrittlement due to NbC and MnS precipitation at austenite grain boundaries.

In more recent years, it has been shown that Nb micro-alloyed steels can be particularly prone to transverse cracking during the continuous casting process (Brimacombe and Sorimachi, 1977). Mintz and Arrowsmith (1979) have shown that Nb levels strongly effect the cracking of continuously cast slabs, distressed casts increasing from 0 to 30% as Nb levels increased from 0.008 to 0.025 wt. % (Fig. 2.13).

This relationship between transverse cracking and Nb content has led to numerous investigations into the hot ductility of micro-alloyed steels, using hot tensile tests at strain rates and temperatures designed to simulate the continuously cast slab straightening process (Hasebe, 1972; Schnabel et al, 1976; Bernard et al, 1978; Mintz and Arrowsmith, 1979; Ouchi and Matsumoto, 1982; Maehara and Ohmori, 1984). These investigations have all shown that Nb additions to C-Mn and C-Mn-Al steels produce an extended ductility trough, the depth and width of which increases with increasing Nb levels (Fig. 2.14). This ductility trough has been shown to extend over the temperature range 700 - 1000°C, the temperature range over which the straightening of continuously cast slab occurs.

Fractographic studies have revealed that at temperatures above and below the ductility trough, the fracture mode is transgranular

rupture (Wilcox and Honeycombe, 1984). Low ductility failures are associated with failure at austenite grain boundaries when the steel is fully austenitic, and fracture within this pro-eutectoid ferrite films when the steel is in the two phase region (Ouchi and Matsumoto, 1982; Maehara and Ohmori, 1984). In the two phase region, the fracture mode is intergranular micro void co-alescence. Ouchi and Matsumoto showed that hot ductility increased with increasing ferrite thickness, and they concluded that since composition had little influence on hot ductility in the two phase region, ferrite thickness was the most important factor controlling hot ductility in this region.

In the low temperature austenite region, Ouchi and Matsumoto reported intergranular fracture characterized by a wavy pattern on the grain facets. However, Mintz and Arrowsmith, and Maehara and Ohmori have observed the micro-void coalescence mode of fracture in the single phase austenite region, and Maehara and Ohmori have suggested that these micro voids are formed by decohesion of the NbCN-matrix interface.

Observations of precipitates of NbCN on fracture surfaces are few, due to the small size of the precipitates, which is often below SEM resolution limits. Wilcox (1982), although not examining grain boundary precipitates from fractured samples, used a hydrogen embrittlement technique to expose austenite grain boundaries, and used carbon extraction replicas to examine precipitation. Wilcox was able to show that using suitable thermal cycles, NbCN precipitates were present at austenite grain boundaries prior to deformation. Ouchi and Matsumoto used the carbon extraction replica technique to identify fine (20 nm) NbCN precipitates, which were found to be present on the fracture surfaces of steels which had failed in an intergranular manner. An examination by Cochrane (1982) of subsurface cracks in continuously cast slabs of Nb micro-

alloyed steels revealed a fracture surface characterized by micro voids containing MnS (50 - 70%), AlN (23 - 33%), oxide inclusions (3 - 14%), but only 1 - 3% were NbCN.

Bernard et al (1978) attributed the ductility trough in Nb containing steels as being due to the retardation of dynamic recrystallization associated with Nb additions (see section 2.3.3.). He proposed that fracture in these steels occurred before the critical strain for the nucleation of dynamic recrystallization was reached, and supported this argument with metallographic evidence of coarse, un-recrystallized austenite grains in low ductility tests. Wilcox and Honeycombe (1984) have confirmed this explanation of the ductility trough for C-MN-Nb-Al steels, for which a good correlation exists between the onset of dynamic recrystallization (as determined from stress-strain curves), and the recovery of ductility. However, for a C-Mn-Nb steel, Wilcox and Honeycombe showed that precipitation of NbCN, rather than dynamic recrystallization was the dominant factor controlling hot ductility. Mintz and Arrowsmith (1979) proposed the more general argument that poor ductilities were associated with low grain boundary mobilities due to the precipitation of NbCN. They showed that hot ductility increased with increasing change in austenite grain size relative to the solution treated grain size.

In accord with this idea, Mintz and Arrowsmith showed that decreasing precipitate size reduced hot ductility, since, for a given volume fraction, fine precipitates reduce grain boundary mobility more than coarse precipitates for a given volume fraction. (Gladman and Pickering, 1967). To support this idea, they showed that increasing the cooling rate from the solution temperature reduced hot ductility by refining the size of the NbCN precipitates.

The prime importance of precipitation in controlling hot ductility of Nb micro-alloyed steels was further emphasized by Ouchi and Matsumoto (1982), who used a variety of thermal cycles to alter the precipitate distribution, and hence hot ductility. As well as influencing hot ductility by reducing grain boundary mobility, it has been suggested that the extensive matrix precipitation of NbCN sometimes observed in Nb micro-alloyed steels concentrates strain at the grain boundaries, hence promoting intergranular fracture and low ductility (Bernard et al, 1978; Wilcox and Honeycombe, 1984; Maehara and Ohmori, 1984). It is well known that deformation accelerates the precipitation of NbCN in austenite, and that this dynamic precipitation is finer than the equivalent static precipitates at the same temperature (Weiss and Jonas, 1980). This led Mintz and Arrowsmith to propose that dynamic precipitation of NbCN would have a greater detrimental effect on hot ductility than static precipitation. However, Ouchi and Matsumoto were of the opinion that as it is likely that the most important nucleation sites for dynamic precipitates are on dislocations and sub-boundaries within the matrix, dynamic precipitates would have little influence on grain boundary mobility. Wilcox and Honeycombe in their study of C-Mn-Nb and C-Mn-Nb-Al steels concluded that dynamic precipitation of NbCN, both intergranular and transgranular, had a greater detrimental effect on hot ductility than precipitates present before the start of deformation.

## 2.9.2 Al

In the late fifties, the phenomenon of ingot panel cracking of plain carbon and low alloy steels treated with aluminium for grain size control first became apparent (Desai, 1959; Biggs, 1959). It was shown that cracks occur internally and propagate to the surface as a result of thermal stresses set up during the cooling of the ingot. The cracks follow the ferrite networks at the prior austenite grain boundaries, which implies that they occur at a temperature below that at which the ferrite is formed. It was also shown that basic electric arc steels were more prone to panel cracking than basic O.H. steels, and the defect was rarely experienced in the case of the acid O.H. process. In addition a significant relationship was found between the incidence of cracking, and the Al content of the steel, the incidence increasing as the Al content increased. Intergranular cracking of ingots was later shown to be associated with the precipitation of AlN at the austenite grain boundaries (Woodfine and Quarrell, 1960; Wright and Quarrell, 1962). In a later investigation of the hot workability of as cast structures, Harding et al (1977) also attributed poor ductilities to AlN precipitation.

As well as ingot cracking, forging difficulties were sometimes experienced with certain low alloy steels containing Al (Erasmus, 1964). Forging break up was due to intergranular failure caused by AlN precipitation. Low alloy steels containing Ni were particularly susceptible to this form of defect, as Ni raised the solution temperature of AlN. This can lead to AlN being present at the forging temperature, promoting intergranular failure. A more recent study by Ericson (1977) has confirmed that ingot panel cracking can be due to the precipitation of AlN in pro-eutectoid ferrite networks.

Carlsson (1964) demonstrated that AlN can also lead to high

temperature, intergranular failure in wrought as opposed to cast, structures, when hot tensile tests are performed at sufficiently low strain rates. Furthermore, as the strain rate is decreased, the hot ductility is found to decrease, leading to the formation of a ductility trough in the temperature range 800 - 1000°C, when the steel is fully austenitic.

More recent studies have confirmed this work, and shown that increasing Al levels in C-Mn-Al steels decrease hot ductility (Funnell and Davies, 1978; Vodopivec, 1973; Bernard et al, 1978; Ouchi and Matsumoto, 1982). As in cast structures, it is AlN that is responsible for the ductility loss, and for a given AlN volume fraction, smaller AlN precipitates are more detrimental to hot ductility (Vodopivec, 1978; Funnell and Davies, 1978). Funnell and Davies have explained this effect as being due to grain boundary pinning at lower strain rates, and to the retardation of dynamic recrystallization at higher strain rates. Wilcox and Honeycombe (1984) have shown a close correlation between the onset of dynamic recrystallization and the hot ductility of a C-Mn-Al steel - ductility improved rapidly when a strain sufficient to nucleate dynamic recrystallization could be applied before fracture.

Precipitation of AlN occurs slowly after solution treatment, but the rate is increased by the application of strain (Vodopivec, 1973). It has been shown by Vodopivec (1978) and Wilcox (1982) that static AlN precipitates, as opposed to dynamic, are more detrimental to hot ductility.

The slow rate of AlN precipitation after solution treatment means that under appropriate cooling conditions, Al has little influence on hot ductility. Mintz et al (1980) showed that Al additions to a C-Mn steel made no difference to hot ductility when the steels

were cooled at 60°C/min. after solution treatment. This cooling rate was sufficient to suppress AlN precipitation.

Al additions have a severe detrimental effect on the hot ductility of C-Mn-Nb steels, as shown in Fig. 2. 15 (Mintz and Arrowsmith, 1979). This effect is due to the refinement of Nb(CN) precipitates, which leads to a reduction in grain boundary mobility, rather than increased AlN precipitation. In fact, AlN precipitation was only observed in these steels for soluble Al levels > 0.07%, using a 60°C/min. cooling rate. Mintz and Arrowsmith proposed that this refinement of Nb (CN) was due to an increase in the driving force for Nb (CN) precipitation with increasing Al levels.

### 2.9.3. Ti

Desai (1959) and Biggs (1959) showed that ingot panel cracking in Al grain refined steels could be reduced by the partial replacement of Al with Ti. Woodfine and Quarrell (1960) obtained similar results, and also showed that Ti additions reduced the amount of AlN precipitation at the austenite grain boundaries. A later investigation by Ericson (1977) concluded that the amount of pro eutectoid ferrite in castings was an important factor in determining their ductility and that the retardation of the austenite to ferrite transformation associated with Ti additions improved ductility. In addition, Ericson showed that TiN, which formed in preference to AlN, was precipitated uniformly throughout the steel, whereas AlN tended to precipitate at austenite grain boundaries leading to low ductility intergranular failures. In addition to reducing ingot cracking, Ti additions have been shown to have beneficial effects on hot ductility during high temperature mechanical testing. Stone and Murray (1965) and Harris and Barnard (1968) have reported that Ti additions to low alloy steels improve their creep ductility. Mintz et al (1980) investigated the influence of Ti on the hot ductility of micro-alloyed steels using hot tensile tests and a cooling rate from solution temperature of 60°C/min., to approximate that experienced during continuous casting. They noted an improvement in the hot ductility of C-Mn-Al steels with Ti additions. However, these results could not be explained by the preferential formation of TiN as opposed to AlN, since the rapid cooling rate employed suppressed the precipitation of AlN. They attributed the observed improvement of ductility to the fine austenite grain size produced by the stable TiN precipitates.

Although Ti additions have improved the hot ductility of C-Mn-Al steels, they have been less successful in improving the hot

ductility of C-Mn-Nb-Al steels, since grain boundary precipitates of NbCN are still formed. (Mintz and Arrowsmith, 1980) Ouchi and Matsumoto (1982) also investigated the hot ductility of C-Mn-Nb-Al steels with Ti additions, under similar cooling conditions to those used by Mintz and Arrowsmith. Ductility was improved by the addition of 0.018 Wt.% Ti and this was attributed to the grain refining effect of TiN precipitates, and also to the reduction of N available to form NbCN. Coleman and Wilcox (1985) have reported a reduction in transverse cracking which is associated with Ti additions, and have attributed this to a reduction in AlN precipitation. However, Ti additions cannot always be made to Nb grades to be used in the as rolled or normalised conditions, since strength and toughness are impaired.

Although in some cases, partial replacement of Al by Ti will improve hot ductility, this is not always the case. As pointed out by Funnell and Davies (1978), only thermal cycles which produce coarse evenly distributed TiN particles which are less effective in pinning grain boundaries can be expected to improve hot ductility. When they used a thermal cycle producing fine TiN precipitates which pinned austenite grain boundaries, low ductility failures were observed.

#### 2.9.4 V

Harris and Barnard (1968) reported that hot cracking of certain low alloy steels containing 0.3%V was due to the precipitation of VN at austenite grain boundaries. These precipitates were thought to act as crack nucleation sites, and to inhibit dynamic recrystallization. Later investigations by Hasebe et al (1972), Mintz and Arrowsmith (1980) and Coleman and Wilcox (1985) using hot tensile tests in the temperature range 650 - 1050°C showed that V additions to C-Mn steels deepened (Hasebe et al) or broadened (Mintz and Arrowsmith, Coleman and Wilcox) the ductility trough normally associated with the austenite to ferrite transformation in C-Mn steels. These results indicate that V has a slight detrimental effect on the hot ductility of steels, although far less severe than that associated with Nb. Coleman and Wilcox showed that the slight detrimental effect of V can be reduced by the addition of Al. They explained these results by the decrease in intragranular VN precipitation, due to the preferential formation of AlN. This produces a reduction in matrix hardening by VN, and hence a more uniform strain distribution between matrix and grain boundary.

Gittins and Muller (1974) investigated the strength and ductility of C-Mn steels with V additions, using a hot impact test producing a strain rate of  $5S^{-1}$ . They showed that over the temperature range 850-1200°C, V additions of up to 0.07% had little effect on either strength or ductility.

### 2.9.5 S and Mn:S ratio

It has been believed for many years that the hot shortness exhibited by some steels in the temperature range 900 - 1150°C is due to the presence of the low melting point compound FeS, which forms liquid films at the austenite grain boundaries (Kiessling, 1968). To prevent FeS formation a theoretical Mn:S ratio of 1.7 is required, although in practice much higher ratios are commonly used. The optimum Mn:S ratio necessary to prevent hot shortness in low S and high S steels has been the subject of a review by Mintz (1973), which concluded that for both low and high S steels, hot workability is markedly reduced below Mn:S ratios of 2-3. However, the optimum Mn:S ratio varies for high S and low S steels: for low S steels, the optimum ratio appears to be in the range 15-30. For high S steels, this optimum ratio appears to be lower, in the region of 4.

S itself is also detrimental to hot workability, even when the Mn:S ratio is sufficiently high to prevent FeS formation (Bellot and Gantois, 1978). High S steels have a larger volume fraction of MnS inclusions which can reduce hot workability, as discussed in section 2.7. S also has a marked detrimental effect on hot ductility near the solidus temperature (Sopher, 1958), and this is believed to be due to the presence of liquid films in the inter dendritic regions which do not freeze until temperatures well below the solidus are reached (Brimacombe and Sorimachi, 1977).

The hot tensile testing below 1200°C of C-Mn and C-Mn-Al steels with Mn:S ratios below 60 has revealed that after certain thermal cycles, low ductility intergranular failures can occur (Lankford, 1972; Wilber et al, 1975; Suzuki et al, 1982; Yasumoto et al, 1985). The loss of ductility during cooling below 1200°C is strongly

dependent on the Mn:S ratio and thermal history of the steel. The effect of thermal history is complex, but it can be said that hot ductility is decreased with increasing cooling rate, increased solution temperature, and decreased isothermal holding time at the test temperature. Matsubara (1966) has attributed the loss of ductility to matrix hardening of austenite by the precipitation of sulphides, an explanation which is supported by the high temperature strength measurements of Yasumoto et al. Lankford has proposed that low ductility failures result from the precipitation of liquid droplets of FeS at austenite grain boundaries, which then form easy paths for crack propagation. Weinberg (1979) has proposed that reheating causes local melting of solute rich pockets which subsequently spread along the grain boundaries, leading to brittle intergranular failure at the lower test temperature. Suzuki et al (1982) have identified sulphides and oxides on intergranular fracture surfaces, whilst Yasumoto et al have shown using C extraction replicas, that intergranular failures are associated with extensive grain boundary and matrix precipitation of (Mn, Fe)S.

It is unlikely that this form of high temperature embrittlement influences the transverse cracking of micro-alloyed continuously cast slabs, as these grades of steels typically have Mn:S ratio greater than 70, a composition which is not susceptible to this form of cracking (Weinberg; 1979).

Mintz (1979) simulated the continuous casting of a C-Mn-Nb-Al steel using a Gleeble machine, and has shown that S levels in the range 0.001 to 0.022 Wt.% have no influence on hot ductility in the temperature range 750 to 1000°C. This implies that S has no influence on transverse cracking, although S may be important in crack formation near the solidus temperature. Despite this apparent lack of influence of S on hot ductility, Coleman and

Wilcox (1985) have reported that MnS particles act as cavity nucleation sites during transverse cracking, and that the removal of MnS particles from grain boundaries by rare earth treatment reduces transverse cracking.

### 2.9.6 C

Investigations into the influence of C content on the hot ductility of steels have concentrated on two temperature regimes - between 500 and 1,200°C, or ductility near the melting point.

Hot ductility tests near the melting point have shown that brittle failure can occur at temperatures approximately 30°C lower than the solidus temperature. (Weinberg, 1979). This behaviour has been attributed to incipient grain boundary melting. Increasing C content, by lowering the solidus temperature, lowers the temperature at which this form of brittle failure can occur. Morozenskii et al (1965) have found that at temperatures just below the solidus, fracture strain is at a minimum for steels with C contents in the range 0.17 to 0.20%C. This effect may exacerbate cracking during continuous casting. For example, Brimacombe and Sorimachi (1977) have reported an increase in longitudinal mid face cracks for steels with C levels around 0.12%. In the lower temperature regime, Robbins et al (1967) examined the influence of C contents between 0.1 and 1.1% on hot workability using a hot torsion test. Below the  $A_1$  temperature, hot ductility is first increased by small additions of C, then decreased at C levels above 0.1%. They attributed this behaviour to the decrease in ferrite grain size associated with C contents of less than 0.1%. Above the  $A_3$  temperature, ductility increased with increasing C content. Robbins et al proposed that these results could be explained by the increased self diffusion rate of iron in austenite with increasing C content. However, later work by Gittins et al (1971) showed that a stronger correlation was found between O content and ductility than C content and ductility. Gittins et al therefore attributed the increase in ductility with increasing C content as being due to the decrease in volume fraction of oxide inclusions associated with higher C contents. The previous investigations were performed

using high strain rate hot torsion tests, and it appears that there have been few investigations into the influence of C on hot ductility at intermediate strain rates. Ouchi and Matsumoto (1982) investigated the influence of C on the hot ductility of a micro-alloyed steel in the temperature range 600 - 1000°C. For C contents in the range 0.081 to 0.20%, no change in hot ductility was observed. An extensive investigation by Wray (1984) covered steels with C contents in the range 0.007 to 1.89%C. Severe embrittlement of the hyper-eutectoid was observed in the pearlite and cementite, and austenite and cementite region of the phase diagram.

### 2.9.7 Other Elements

P It is well known that during solidification, P segregates strongly between growing dendrites, and it has been shown that high P levels can lead to internal cracks in continuously cast slabs (Fujii et al, 1975; Brimacombe and Sorimachi, 1977) Fractography of internal cracks formed near the solidus temperature has revealed smooth fracture surfaces, which is often indicative of the presence of a liquid film at the time of crack formation. In accordance with this picture, it has been shown that P drastically reduces strength and ductility near the solidus temperature (Sopher, 1958). Thus increasing P levels can lead to increased cracking in steels at temperatures from 1340°C to the solidus temperature.

The influence of P on the formation of transverse cracks, which propagate at much lower temperatures, is less certain. Mintz and Arrowsmith (1979) have reported a slight beneficial effect of increasing P levels on the hot ductility of C-Mn-Nb-Al steels. They have suggested that this is due to P atoms reducing the nucleation of NbCN at grain boundaries, by occupying NbCN nucleation sites. However, Ouchi and Matsumoto (1982) have reported that P levels between 0.004% and 0.026% have no influence on the hot ductility of C-Mn-Nb-Al steels.

O O effects the hot ductility of steels mainly through its influence on the amount and composition of oxide inclusions (Gittins, 1977).

In general, inclusions have a strong detrimental effect on hot ductility, as discussed in section 2.6, thus increasing O content reduces hot ductility by increasing the volume fraction of oxide inclusions. In addition, O may increase the relative plasticity of sulphide inclusions (Smith et al, 1972) which may decrease hot ductility, as described in section 2.6.

Zr Desai (1959) reported that the partial replacement of Al with

Zr was ineffective in reducing panel cracking in ingots. Woodfine and Quarrell (1960) also confirmed that in Al killed castings, Zr additions did not prevent cracking. However, Coleman and Wilcox (1985) have reported that Zr additions to C-Mn-Nb-Al steels improve hot ductility, in tensile tests due to a reduction in AlN precipitation.

Ca, Ce, La (Sopher, 1958) reported that additions of misch metal (Ce 45-50%, La 30%, 20 - 25% other rare earths) additions to C-Mn steels improved hot ductility near the melting point. This was attributed to the reduced S levels associated with increasing misch metal additions, and also to the formation of rare earth sulphides, with high melting points. Coleman and Wilcox (1985) have reported that Ca or Ce additions can produce crack free continuously cast slab, due to the removal of sulphides from austenite grain boundaries as the rare earth sulphides solidify in the melt.

N Mintz and Arrowsmith (1980) and Ouchi and Matsumoto (1982) showed that increasing N level in C-Mn-Nb-Al steels produce a small reduction in hot ductility. Ouchi and Matsumoto attribute this effect to the formation of Nb CO.85 in low N steels, as opposed to Nb CO.6 NO.25 in steels with N >0.005%. They proposed that Nb CO.6 NO. 25 precipitates more rapidly in austenite than Nb CO.85, leading to larger volume fractions of precipitate in the higher N steels. Ouchi and Matsumoto also showed that increasing N levels produced a slight reduction in the hot ductility of C-Mn-Al steels.

Te Bellot and Gantois (1978) have shown that steels with Mn:Te of less than 4.2 show poor hot ductility, due to the formation of iron telluride compounds with low melting points, leading to cracking of the hot shortness type.

Group	Example	Dynamic	Static
A	Al, $\gamma$ -Fe, ferritic alloys	Recovery (all strains)	Recovery followed by re-crystallization
B	Cu, Ni, $\gamma$ -Fe, austenitic alloys	Recovery (small strains)  Re-crystallization (large strains)	Very limited recovery, followed by re-crystallization

Table 2.1 Possible softening processes associated with hot deformation (from Sellars & Tegart, 1972)



Fig.2.1 Cold machine scarfed slab showing transverse cracking.



Fig.2.2 Slab which had been partially rolled showing severe transverse edge cracking.

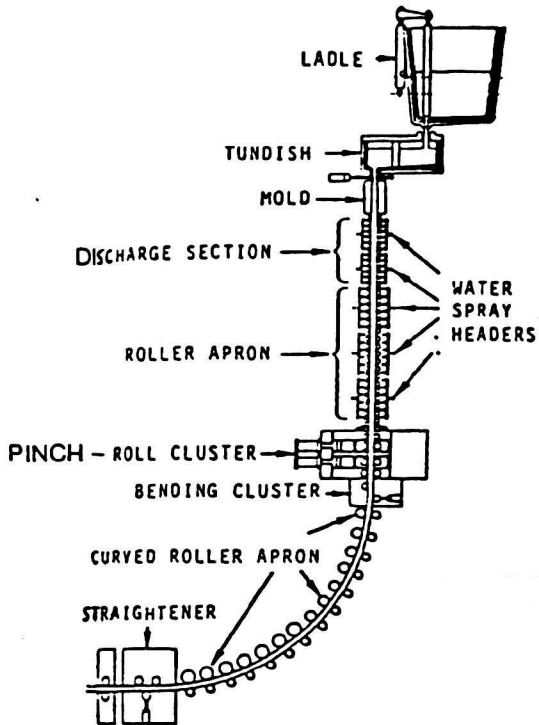


Fig. 2.3 Profile of Gary Slab Caster

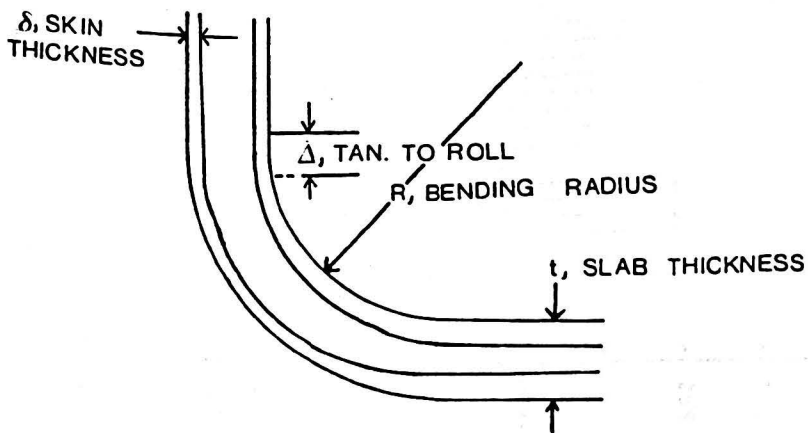


Fig. 2.4 Straightening of Continuously Cast Slab (Aster Lankford, 1972)

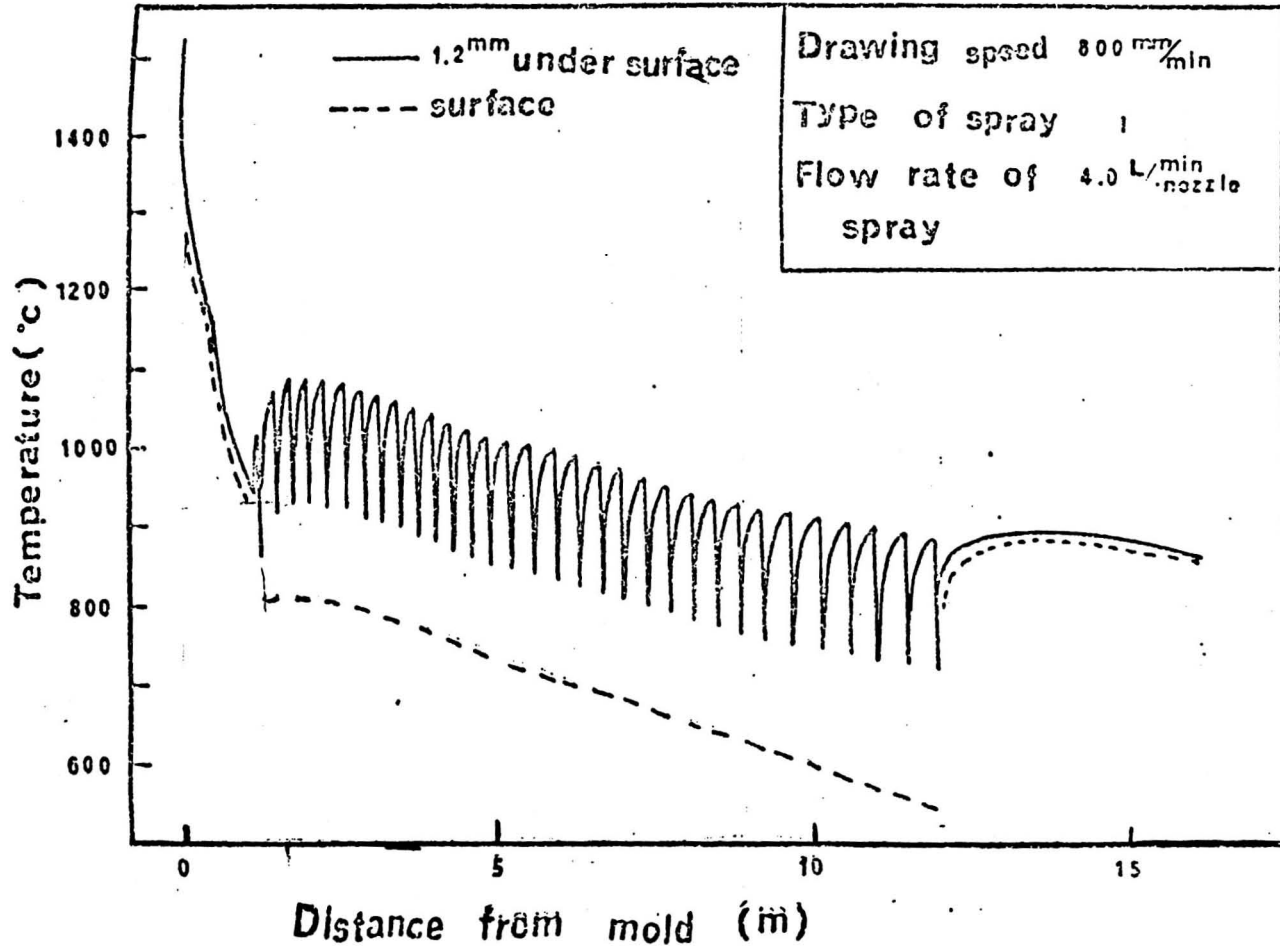


Fig. 2.5 Temperature oscillation in surface of continuously cast slab, from Tomono (1973)

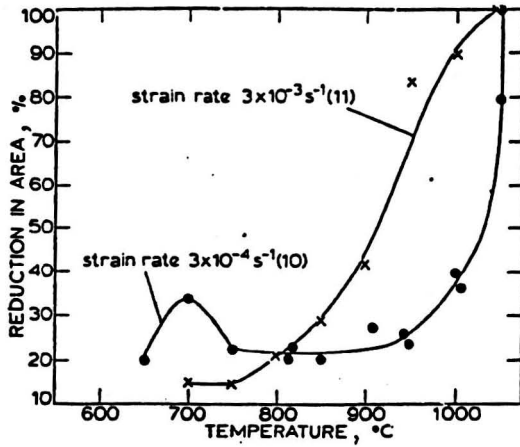


Fig. 2.8 Influence of strain rate on the hot ductility of a C-Mn-Nb-Al steel. (After Mintz and Arrowsmith 1979)

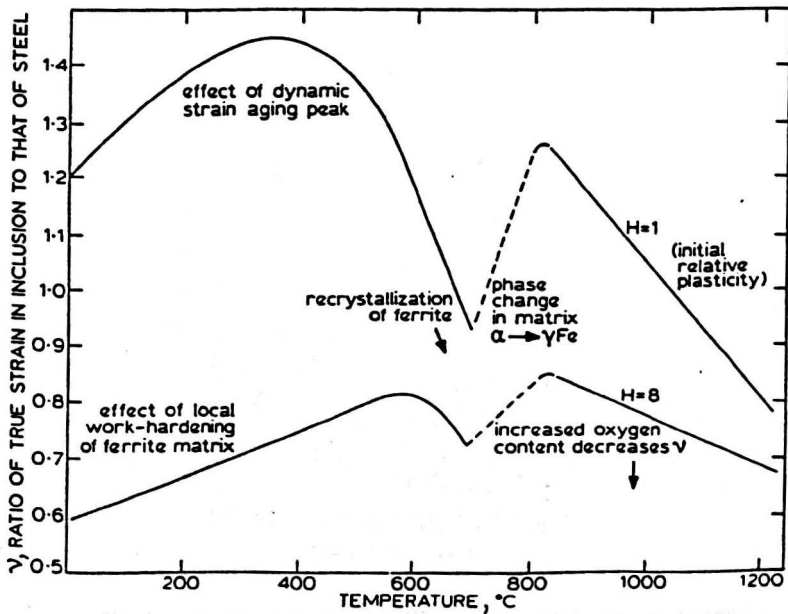


Fig. 2.9 Variation of relative plasticity of sulphide inclusions with deformation temperature and oxygen content. (After Charles, 1980)

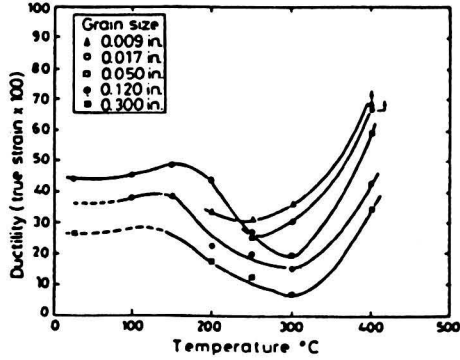


Fig. 2.10 Variation of ductility with temperature and grain size for Magnox A.180. (From Evans, 1969)

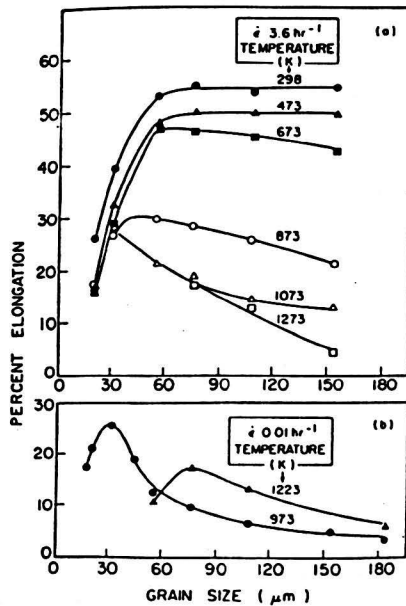


Fig. 2.11 Variation of ductility with temperature and grain size for a Cr-Mn-N Austenitic steel, showing decrease in ductility at fine grain sizes. (From Kutumba-RaO et al, 1975)

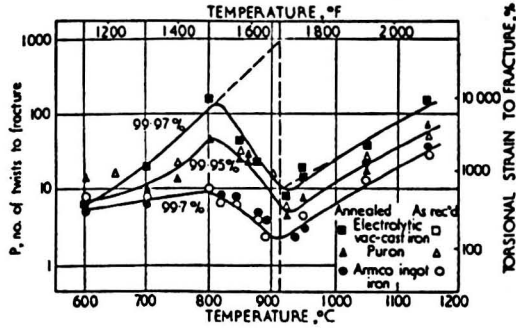


Fig. 2.12 Hot ductility of irons tested in hot torsion. (From Robbins et al, 1961)

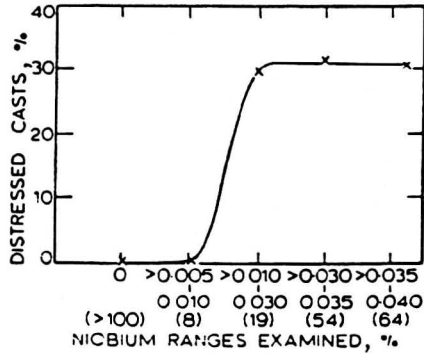


Fig. 2.13 Influence of Nb on the transverse cracking of continuously cast slabs. (From Mintz and Arrowsmith, 1979)

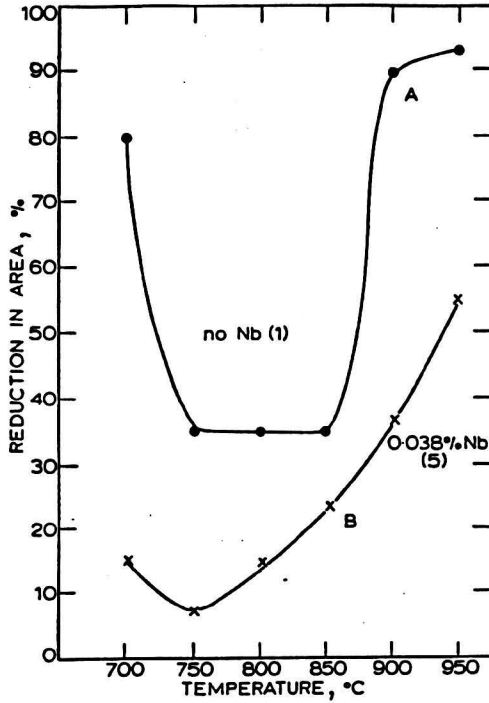


Fig. 2.14 Influence of Nb on the hot ductility of C-Mn-Nb-Al Steels. (After Mintz and Arrowsmith, 1979)

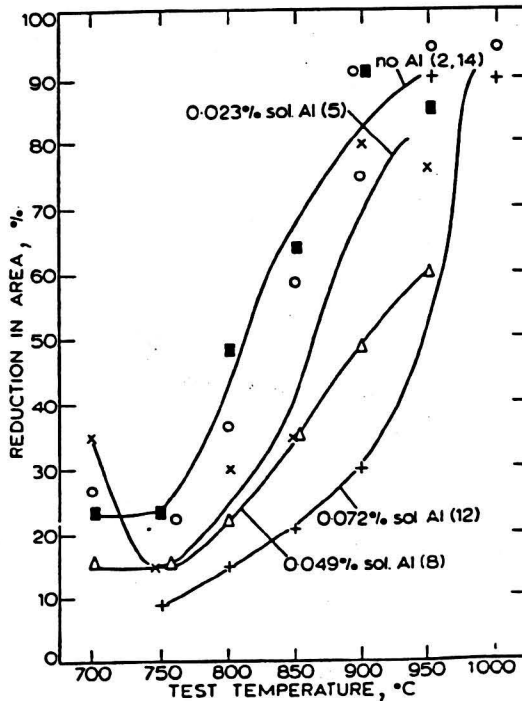


Fig. 2.15 Influence of Al on the hot ductility of C-Mn-Nb-Al steels. (After Mintz and Arrowsmith, 1979)

## CHAPTER 3

### Experimental Techniques

### 3.1 INTRODUCTION

High temperature mechanical tests can be divided into two classes: creep tests, in which stress is the independent variable and strain rate the dependent variable; and hot workability tests in which strain rate is the independent variable and stress the dependent variable. Creep tests generally study materials behaviour in the temperature range  $0.4 - 0.7 T_h$ , where  $T_h$  is the homologous temperature, and stresses which produce strain rates of less than  $10^{-3} \text{ s}^{-1}$ . The hot workability test is designed to simulate a particular hot working process, and so such tests cover an extremely wide range of temperatures and strain rates.

The information generally required from a hot workability test are hot strength measurements, and some indication of the plastic flow and fracture behaviour of the material at high temperature. Previous studies into the transverse cracking of continuously cast slabs have concentrated on examining the fracture process, and have reported the variation of fracture strain with temperature, composition and strain rate.

Many tests have been used to determine ductility under hot working conditions, but the only ones capable of providing quantitative information on fracture behaviour are the torsion test, impact test and tensile test. The first two of these tests have been used to simulate hot rolling processes, for which it is necessary to apply high strain rates and large strains. The tensile test is not suitable for such work, because of the difficulty in obtaining high strain rates, and in applying large strains before sample necking begins. However, the hot tensile test has proved very popular in the study of transverse cracking, since such cracks form at strains of between 1 and 2% (section 2.2.2), a strain usually below the value required for sample necking.

Ductilities from the hot tensile test can be measured by a) the amount of uniform elongation, b) the total elongation at fracture, or c) the reduction in area at the point of fracture. Uniform elongation can be a useful measure of fracture strain if little or no necking has occurred, as sometimes happens with brittle, intergranular fractures. However, it is not a suitable parameter for comparing the wide range of ductility levels which occur when the test temperature is varied over a wide range. Total elongation at fracture comprises components of uniform elongation, and elongation due to necking. The values of these two components are a complex function of test temperature, strain rate, composition and microstructure. This makes comparison of total elongation measurements over, for example, a wide range of temperatures, difficult, since at different temperatures, identical elongation measurements may be made from samples having very different fracture geometries, and hence different fracture strains. Reduction in area measurements provide quantitative information on fracture strain at the point of fracture, irrespective of sample fracture geometries. This fracture strain,  $\epsilon_f$ , is related to the initial cross sectional area,  $A_0$ , and final cross sectional area,  $A_f$ , by:-

$$\epsilon_f = \ln (A_0/A_f) \dots\dots\dots 3.1$$

Thus reduction in area is suitable for the comparison of ductility over a wide range of temperatures, and is the parameter used in the present study. The experimental details of the measurement of reduction in area are given in section 3.2.4.

One of the principal disadvantages of the simple tensile test is that of the difficulty in maintaining a constant true strain rate as straining proceeds. As straining proceeds in a tensile test using a constant cross head speed, true strain rate at the point of fracture initially falls, as the sample elongates uniformly,

but rises rapidly as heterogeneous deformation commences, and most of the strain is concentrated in the neck. (Fig. 3.1) Since flow stress and fracture strain are generally strain rate dependent, this is potentially a serious short coming of the tensile test in the study of hot ductility. Methods for maintaining constant true strain rates have been developed, as discussed in detail by Moore (1968), but these can be complex and expensive. However, hot ductility is relatively insensitive to changes in strain rate, often requiring a change in strain rate of a factor of 10 to produce noticeable changes in ductility. (Suzuki et al, 1982) Since the changes in strain rate as straining proceeds, are usually less than this, tensile tests using constant crosshead speeds have proved adequate for the study of hot ductility. Another potential disadvantage of the tensile test is the hydrostatic stress state set up in a necked sample. Such stress states can have a strong effect on increasing the rate of growth and coalescence of voids nucleated at inclusions within the specimen, an effect not present under the original hot working conditions when such a hydrostatic stress state is not present.

Despite these potential drawbacks, the simple hot tensile test using a constant cross head speed has proved quite adequate for hot ductility studies aimed at simulating the continuous casting process.

In the present study, hot tensile tests using constant cross head speeds have been used. Three different hot tensile tests were used, and are described and compared in section 3.2. The metallographic techniques used to study precipitation are described in section 3.3.

## 3.2 HOT TENSILE TESTS

### 3.2.1 Gleeble Test

The Gleeble machine has proved a popular method of investigating hot ductility, and has been used by Bernard et al (1978), Mintz and Co-workers, Ouchi and Matsumoto (1982) and Suzuki et al (1982). In their investigation, Mintz and Arrowsmith (1979) concluded that laboratory hot tensile tests performed using a Gleeble machine could be used to predict the transverse cracking behaviour of continuously cast slabs.

The Gleeble equipment of the BSC Swinden Laboratories was used to perform the tests detailed in chapter 4. The Gleeble test specimen, having a diameter of 6.35 mm and gauge length of 165 mm is shown in Fig. 3.2. Heating is by electrical resistance, which produces a uniform temperature in a region approximately 1 cm in length. The tests were performed in an argon atmosphere, and the initial strain rate used was  $3 \times 10^{-3} \text{ s}^{-1}$ . Mintz and Arrowsmith (1979) have given an indication of the repeatability of the Gleeble test by performing 6 identical hot tensile tests. They reported that the standard deviation about the mean reduction in area of 36% was  $\pm 3\%$ .

### 3.2.2 Instron Tests

The second piece of tensile test equipment used was an Instron model 1026 equipped with a split platinum wound furnace, illustrated in Fig. 3.4. The tensile samples, having diameter 5.04 mm and gauge length 25.4 are shown in Fig. 3.3. Temperature control was by means of a Pt v Pt 13% Rh thermocouple connected to a purpose built Isoheat temperature controller unit, capable of maintaining fixed heating and cooling rates. Thermocouples were attached to a dummy sample, and this showed that the temperature controller unit reading was 10°C higher than the actual sample surface temperature, and that the temperature difference along the sample

gauge length was less than 5°C. Test temperatures were taken to be the sample surface temperature, i.e. 10°C less than temperature controller reading. Tests were conducted in a flowing argon atmosphere, and the samples were also nickel plated, as described in Appendix 1, to prevent decarburization. This procedure restricted the decarburized layer to a thickness of 0.1 mm. Tensile tests were performed using constant cross head speeds in the range  $0.75 \text{ mm s}^{-1}$  to  $7.5 \times 10^{-3} \text{ mms}^{-1}$ . An indication of the scatter on the results was obtained by repeating five tensile tests. The standard deviation about the mean reduction in area of 55% was  $\pm 4\%$ .

### 3.2.3 Induction heating tests

To enable rapid changes in sample temperature, and also to enable specimens to be cast 'in situ', tensile testing equipment using induction heating, was employed. The equipment is shown schematically in Fig. 3.5. Test samples having diameter 7.9 mm and gauge length 80 mm, are shown in Fig. 3.6. Sample temperature was monitored using a Pt v Pt 13% Rh thermocouple at the sample centre. The induction coil provided a zone of uniform temperature, 40 mm long, the sample temperature distribution being shown in Fig. 3.7. Any samples which failed outside this zone of uniform temperature was discarded. Tests were conducted in a flowing argon atmosphere, and samples were strained to failure using a Hounsfield Tensometer, with a constant crosshead speed of  $0.04 \text{ mm s}^{-1}$ . Assuming that the effective sample gauge length is 50 mm, this corresponds to an initial strain rate of  $10^{-3} \text{ s}^{-1}$ . Repetition of 5 tests gave a standard deviation of 5% about the mean reduction in area values of 45%.

### 3.2.4 Measurement and Comparisons of Reduction in Area

To obtain reduction in area values from fractured tensile samples,

the fractured ends were examined under a low power (X10) microscope, and 10 measurements of the diameter at fracture to the nearest 0.1 mm taken. Reduction in area values were then calculated, assuming that the cross section of the fractured samples remained circular.

Fig. 3.8 compares reduction in area values measured from samples fractured using Gleeble, Instron and induction testing apparatus. These results show a good correspondence between the tests, so that results from the various testing apparatus can be interchanged with confidence.

### 3.3 CARBON EXTRACTION REPLICA PREPARATION AND EXAMINATION

Samples for replication were first ground flat, and the area to be examined was defined by the application of a non-conducting lacquer. The sample was then electropolished for three minutes using an electropolishing solution consisting of 200 parts ethanol, 100 parts 2 - butoxyethanol and 52.5 parts perchloric acid. The electropolishing solution was cooled to 0°C, and electropolishing carried out at IIV, using a stainless steel cathode. After electropolishing, the sample was etched for approximately 30 s using a 2% nital solution, and then a carbon film was evaporated onto the prepared surface at a pressure of  $10^{-4}$  torr. The carbon film was then scribed into 3 mm squares, and the replicas removed by immersion in a 5% nital solution. The replicas were then washed in distilled water, and finally collected on 4 mm diameter copper grids. In the case of replicas taken directly from fracture surfaces, the carbon film was deposited directly on the fracture surface, and removed as described previously.

Replicas were examined using a JEOL 100B microscope operating at 60 KV. The microscope was equipped with an EDAX X-ray analysis system, capable of identifying elements with atomic number greater than 11. The system was therefore, not capable of distinguishing between carbide and nitride precipitates. The smallest spot size available was 50 nm in diameter, and this determined the minimum distance between precipitates which could be analysed separately. Precipitate sizes were measured directly from the negatives. To calculate a mean precipitate diameter, assuming spherical precipitates, at least 200 measurements were taken from 3 separate replicas taken from the same sample. The procedure adopted to calculate the mean precipitate diameter,  $D_m$ , for a precipitate

distribution was that used by Weiss and Jonas (1980). It is assumed that precipitates of diameter  $d_i$  are extracted from a layer of matrix  $d_i$  thick, as illustrated in Fig. 3.9.  $N_{si}$ , the number of precipitates per unit area of diameter  $d_i$ , is measured directly from the negative. However, it is  $N_{vi}$ , the number of precipitates per unit volume of diameter  $d_i$  which is required to calculate  $D_m$ . As shown in Fig. 3.9,  $N_{si}$  and  $N_{vi}$  are related by:-

$$N_{vi} = N_{si}/d_i \dots\dots\dots 3.2$$

$D_m$  is then calculated using the formula:-

$$D_m = \left[ \frac{\sum_i N_{vi} d_i^3}{\sum_i N_{vi}} \right]^{1/3} \dots\dots 3.3$$

To gain at least a semi-quantitative estimate of the particle distribution at the austenite grain boundaries, the number of particles in a measured length of grain boundary was counted, and hence the distance between particle centres, the interparticle spacing, was calculated. For any particular steel, these measurements were based on approximately 200 particle counts taken from different grain boundary regions, and from different replicas. Such measurements, although not providing absolute measurements of the grain boundary precipitate distributions, are adequate for making comparisons between different steels.

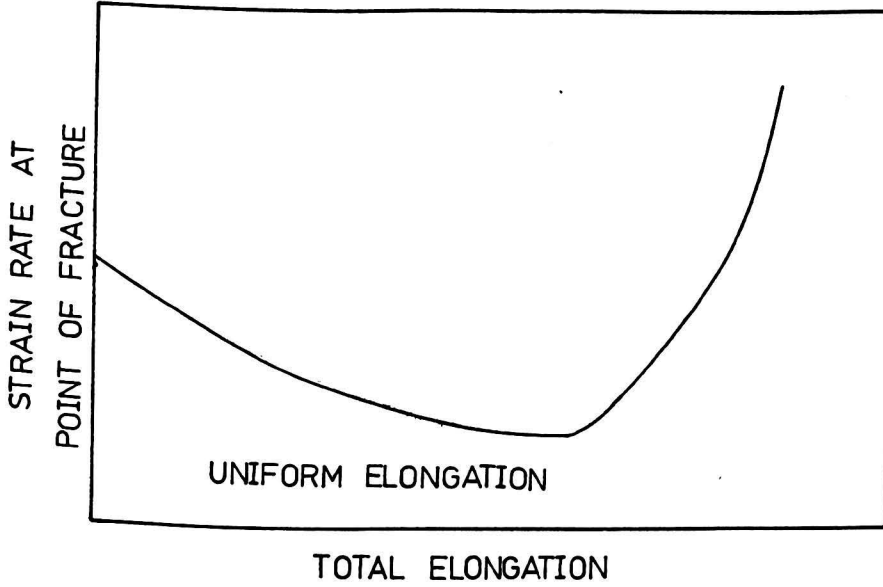
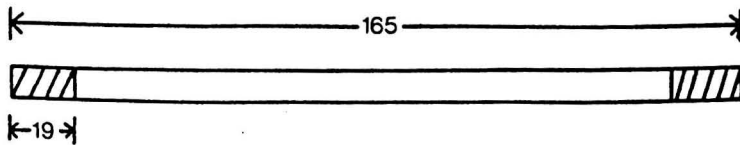
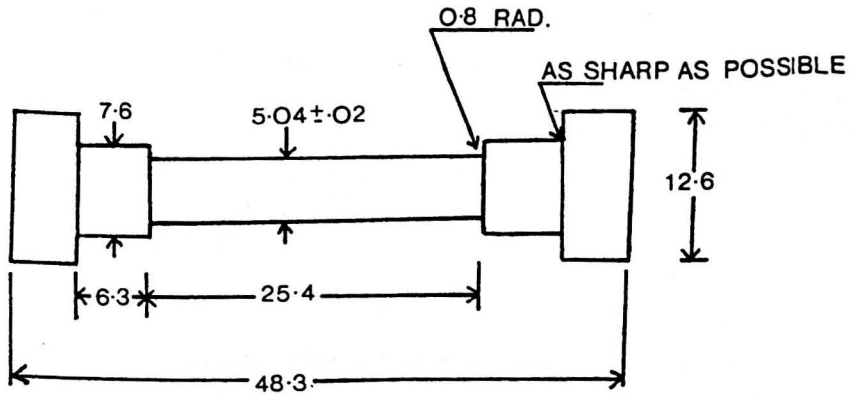


Fig. 3.1 Schematic illustration of variation of strain rate at point of fracture with total elongation of test piece.



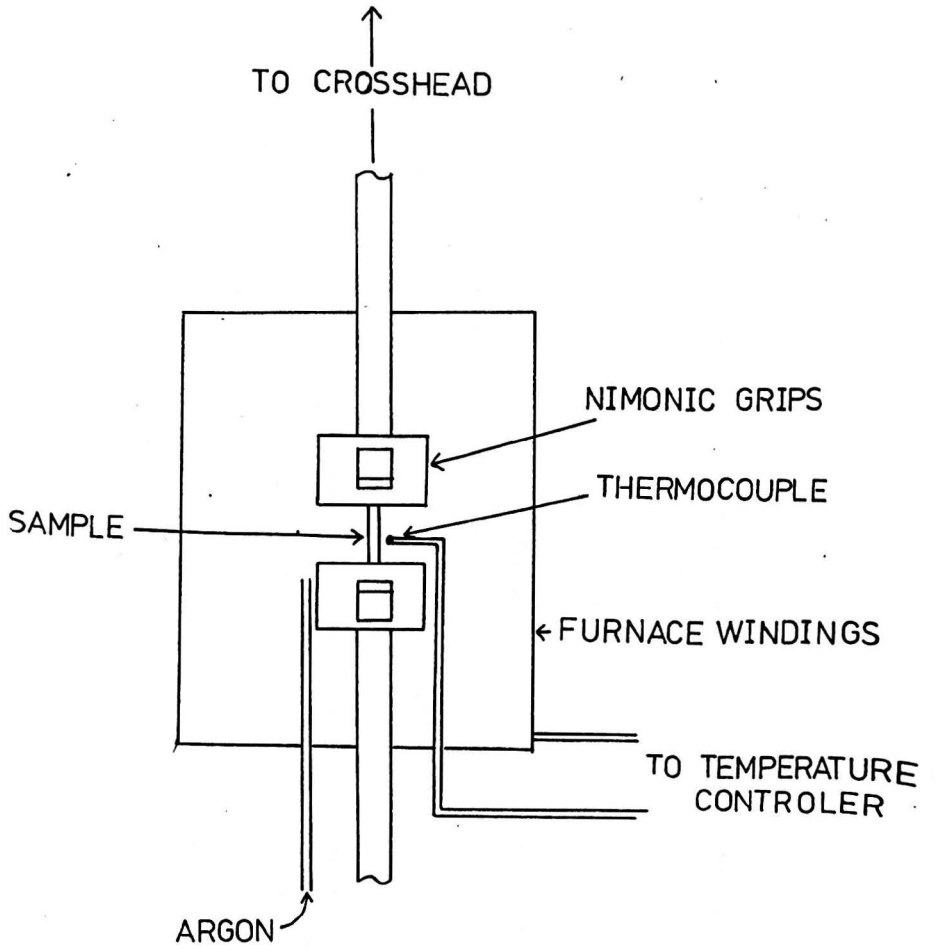
GROUND FINISH  
 DIAMETER  $6.35 \pm 0.025$   
 THREAD  $1/4"$  B.S.W.  
 ALL DIMENSIONS IN mm

Fig. 3.2 Gleeble Test piece



FINE MACHINE FINISH  
 ALL DIMENSIONS IN mm

Fig. 3.3 Instron test piece



**Fig.3.4** Schematic illustration of Instron high temperature testing equipment.

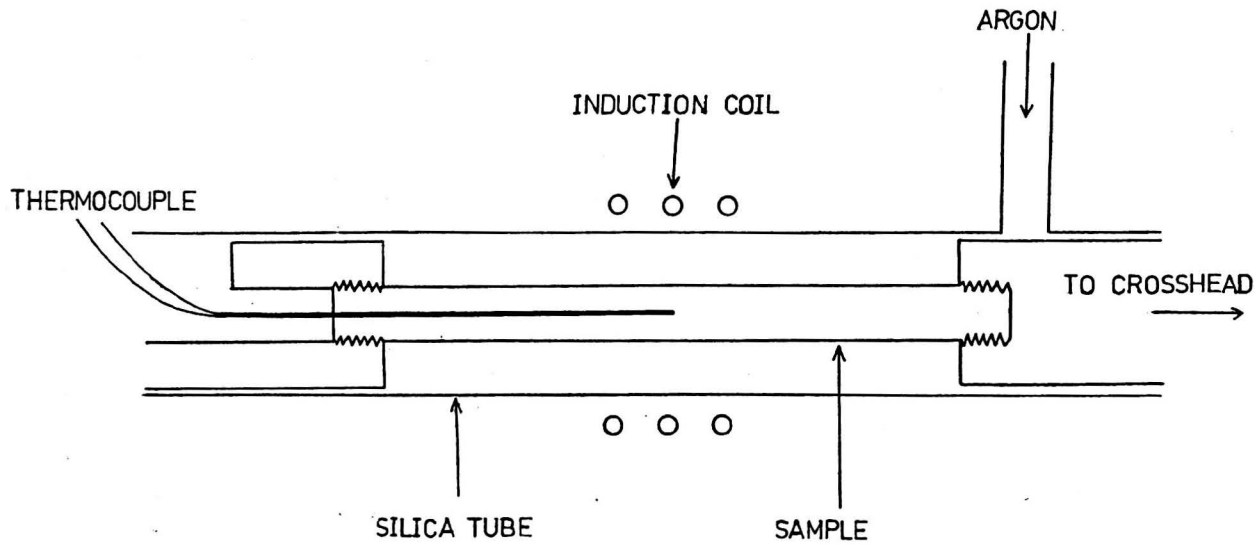
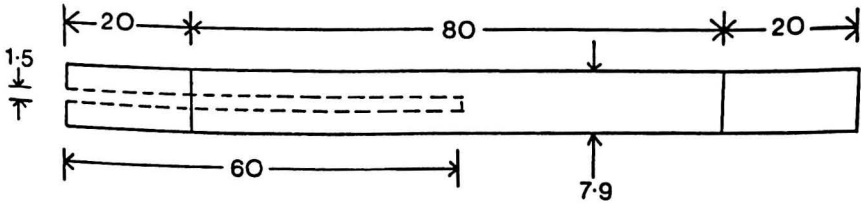


Fig. 3.5 Schematic illustration of induction heating equipment for high temperature tensile testing.



GROUND FINISH

THREAD 5/16 B.S.F.

ALL DIMENSIONS IN mm

Fig. 3.6 Induction test piece

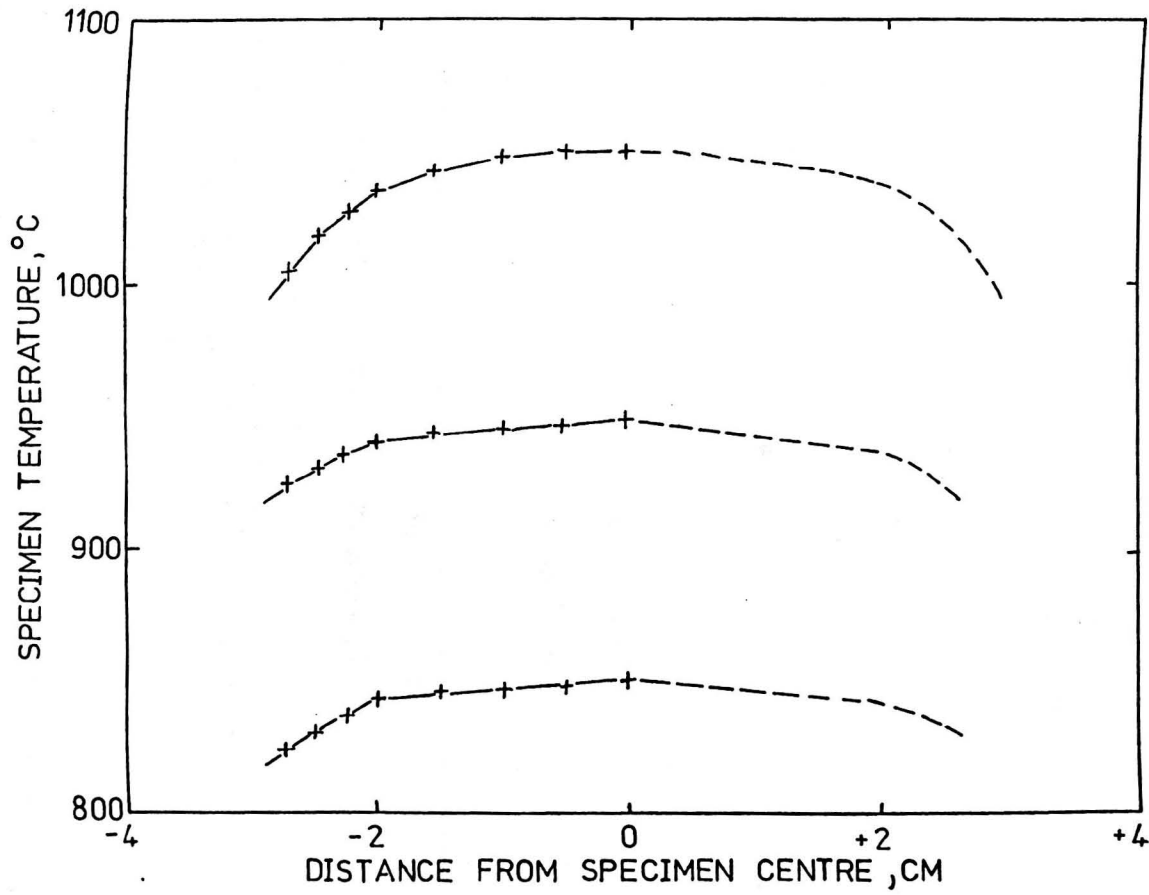


Fig. 3.7 Temperature distribution in Induction test piece at three different temperatures

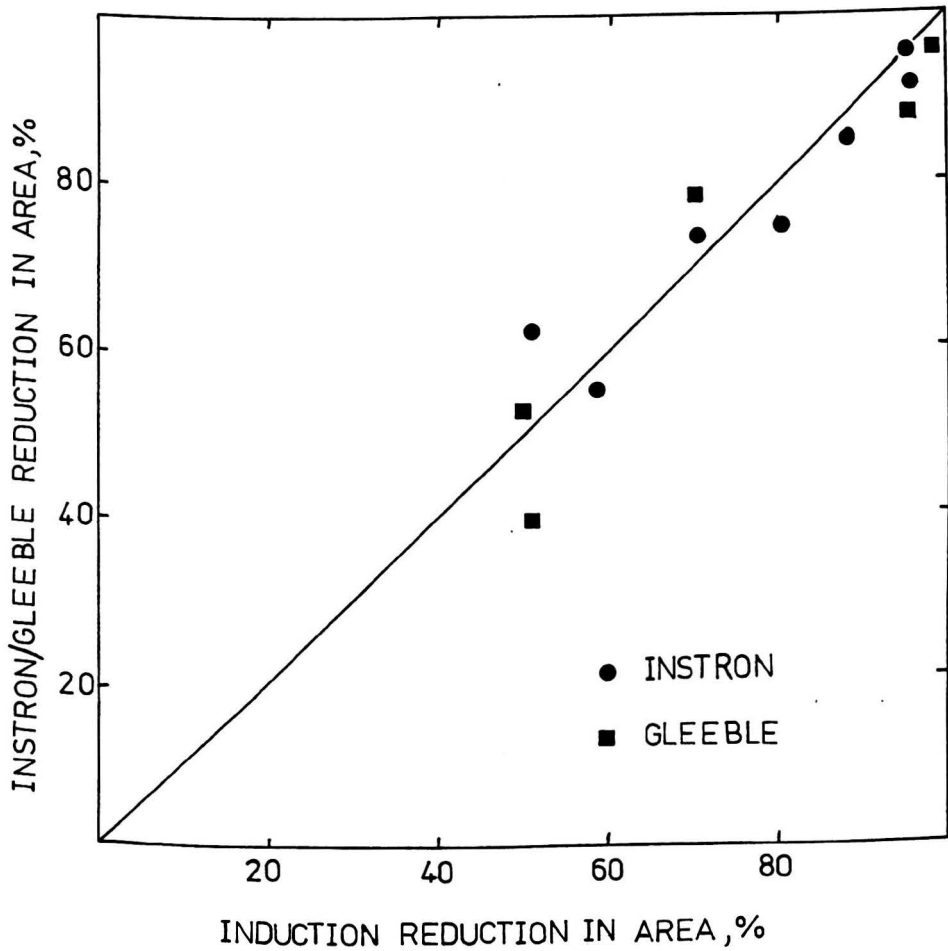


Fig. 3.8 Comparison of reduction in area values from different testing equipment, tests performed under identical conditions

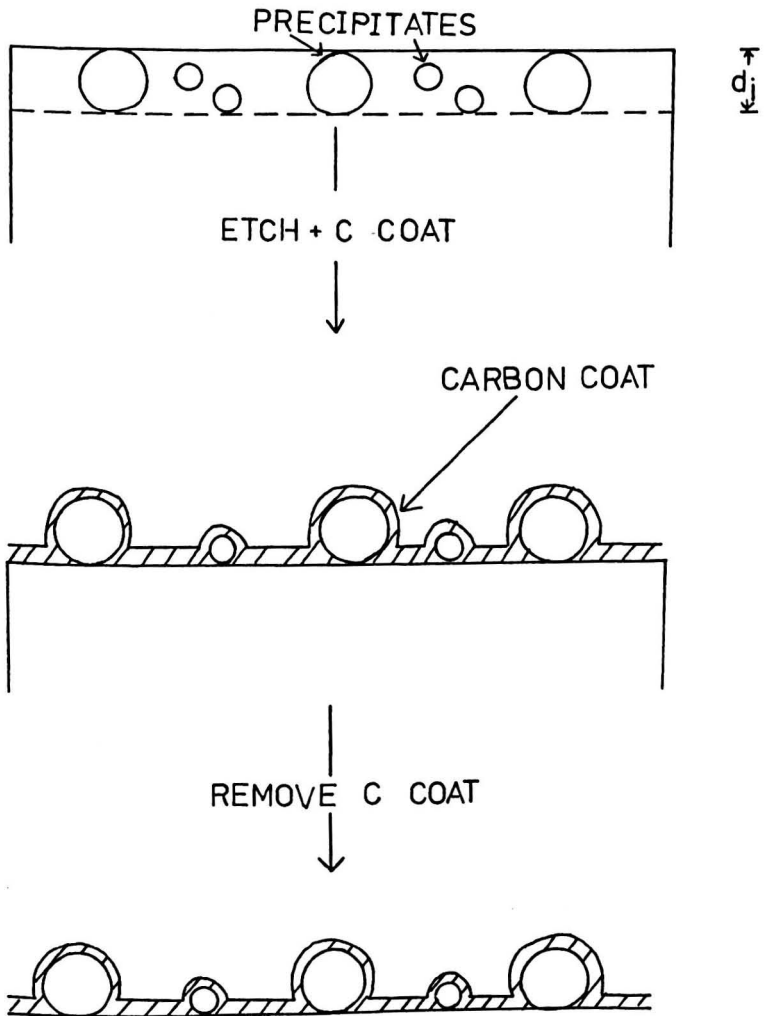


Fig.3.9 Extraction of precipitates using single stage carbon replicas.

## CHAPTER 4

### The Influence of C Content on the Hot Ductility of Plain C-Mn Steels

#### 4.1 INTRODUCTION

It is now well known that micro-alloyed steels, and particularly C-Mn-Nb-Al grades, can show a ductility trough in the temperature range 700 - 1000°C, when tested using intermediate strain rates, as described in section 2.9. This loss of ductility can lead to transverse cracking in continuously cast slabs. The precipitation of NbCN and AlN during cooling have been shown to be important factors in reducing the hot ductility of micro-alloyed steels. A smaller but nevertheless marked ductility trough is known to occur even in the absence of micro-alloying additions. (Mintz and Arrowsmith, 1979; Yamanaka et al, 1980; Wray, 1981). In this case the fall in reduction in area is believed to be due to the onset of the transformation from austenite to ferrite, causing strain concentration to take place in the softer ferrite phase, which forms as thin films around the austenite grains. Because of the generally higher minimum ductility values given by plain C-Mn steels compared to micro-alloyed steels these do not give problems on continuous casting and have therefore received less attention. Nevertheless for a complete understanding of these ductility troughs a detailed knowledge of the ductility trough in the absence of micro-alloying additions is required, and obtaining this information has formed the basis of this chapter. If transformation is the only controlling factor in dictating the position of the hot ductility trough in a plain C-Mn steel, then raising the C content would be expected to lower the transformation temperature and move the hot ductility trough to lower temperatures. Examining the influence of carbon content on the position of the ductility trough should therefore give useful information as to the origins of the hot ductility troughs in plain C-Mn steels.

## 4.2 EXPERIMENTAL

Plain C-Mn steels with the same base composition (1.4% Mn, 0.2% Si) but with C contents in the range 0.04 to 0.65% were cast as 50 kg laboratory vacuum melts and rolled to 37 mm plates, finish rolling at 1050°C. The chemical compositions are given in Table 4.1. Longitudinal tensile samples having the dimensions shown in Fig. 3.2 were machined from all the steels and hot ductility tests carried out using the Gleeble equipment at BSC Swinden Laboratories, as described in section 3.2.1. The test pieces were given a homogenizing treatment of 5 min. at 1330°C prior to cooling at 60°C/min. (similar to the cooling rate at the surface of the continuously cast slab) to a test temperature in the range 600 - 950°C and strained to failure at a rate of  $3 \times 10^{-3} \text{ S}^{-1}$ . One steel, the 0.65% steel, was tested under the same conditions, but using the induction heating equipment described in section 3.2.3. The results obtained from both sets of equipment can be compared directly quite confidently. (section 3.2.4)

The austenite grain size prior to testing was established by heating samples to 1330°C for 5 minutes using a muffle furnace, temperature being established by a thermocouple embedded in the sample. The samples were then cooled at a rate to give outline-ment by ferrite. Austenite grain sizes were then determined using the linear intercept method. Carbon extraction replicas were also taken close to the point of fracture on selected steels in the temperature range 700 to 850°C, and the inclusions present analysed. Longitudinal sections, including the place of fracture, were taken from the broken samples and also prepared for metallographic examination. Although cooling rates after fracture were fast, they were not always fast enough to prevent further transformation occurring during cooling to room temperature. However, ferrite

formed after fracture could readily be distinguished from that present before, as the former showed side plate formation. The thickness of the austenite grain boundary ferrite present before cooling was measured using an oil immersion lens. Measurements were taken within 5 mm of the fracture surface, and the apparent grain boundary ferrite thickness was taken as the mean of approximately 70 measurements. This apparent ferrite thickness is an over estimate of the true ferrite thickness, due to the sectioning effect.

Examination of fracture surfaces was carried out using a JEOL T100 scanning electron microscope operating at 25 KV.

The  $A_{r3}$  and  $A_{r1}$  temperatures after heating to 1330°C, holding for 5 minutes, and cooling at 60°C/min. were obtained for all the steels using a Theta dilatometer. Equilibrium transformation temperatures were calculated using the method of Andrews (1965). The transformation temperatures for the fractured tensile samples were estimated metallographically, the  $A_3$  temperature being taken as the temperature at which ferrite was first observed in the metallographic specimens. of fractured tensiles.

## 4.3 RESULTS

### 4.3.1 Hot Tensile Tests

The curves of reduction in area against test temperature are given in Fig. 4.1. All the steels show a marked ductility trough, reduction in area falling from 90% to about 30%. The depth of the trough is similar for all the steels, but the position and width vary with C content. The ductility of the 0.04%C steel starts to fall at about 900°C, and reached a minimum in the temperature range 750 to 820°C. Ductility is fully recovered when the temperature is further lowered to 700°C. As the C content is raised from 0.04 to 0.28%C, there is a gradual movement of the ductility trough to lower temperatures. At the 0.28%C level, the ductility trough has been shifted to lower temperatures by approximately 90°C. The 0.35 and 0.65%C steels show different trends and both of these steels have similar hot ductility curves with ductility troughs extending over a very wide temperature range of 250°C. The results of Fig. 4.1 have been re-plotted in Fig. 4.2 to show the variation in ductility with C content at 600 and at 900°C. At 900°C, reduction in area values are independent of C content up to 0.35%C, when there is a large drop in hot ductility resulting from the extended ductility troughs of the 0.35 and 0.65%C steels. At 600°C, reduction in area values are again independent of C content. Fig. 4.3 shows the variation in peak stress,  $\sigma_p$ , with test temperature for all six steels.  $\sigma_p$  decreases as temperature increases for all six steels. Fig. 4.4 shows the influence of C content on peak stress at 900°C and at 600°C. At 600°C, there is a clear increase in hot strength with increasing C content, peak stress increasing from 170 to 215 MPa as the C content increases from 0.04 to 0.35%C. At 900°C, hot strength decreases slightly

from 50 to 42 MPa as the C content increases from 0.04 to 0.65%C.

#### 4.3.2 Metallography

Austenite grain size measurements as a function of C content are shown in Fig. 4.5. This shows that grain size is independent of C content, and is approximately 300  $\mu\text{m}$  for all six steels.

The form of the grain boundary ferrite is shown in Fig. 4.6. In addition to grain boundary ferrite, this micrograph shows ferrite sideplates, formed during cooling after fracture, and a bainitic matrix. Measurement of apparent grain boundary ferrite thickness for steels 2 to 5, along with the appropriate hot ductility curve, are shown in Figs. 4.7 - 4.10. Figs. 4.7 - 4.9 indicate that the minimum of the ductility trough is associated with very thin films ( - 4  $\mu\text{m}$ ) of grain boundary ferrite, and ductility only begins to recover as the ferrite thickness increases rapidly as the temperature is lowered. Fig. 4.10 illustrates that for the 0.35%C steel, the ductility minimum is reached at temperatures well above that at which grain boundary ferrite is observed. The 0.65%C steel is of near eutectoid composition, and only very small amounts of grain boundary ferrite were observed, and only at temperatures below 700°C.

Figs. 4.11 - 4.13 show micrographs taken just behind the fracture surfaces of samples of the .19% steel, fractured at temperatures above, below and within the ductility trough. Fig. 4.12, which shows failure at the ductility minimum, displays the features common to all observed failures at the ductility minimum; coarse, un-recrystallized austenite grains, showing outlining by thin films of ferrite; and cracks forming within this ferrite, due to the nucleation and growth of voids at inclusions within the ferrite. Fig. 4.14 shows such a crack in greater detail. The 0.35 and 0.65%C steels again showed intergranular failure at the ductility

minimum, but for these steels, intergranular failure occurred in the single phase austenite. Fig. 4.15 shows intergranular cracking in the .35%C steel, tested at 850°C. These cracks generally occur at 45° to the tensile axis, and appear to be 'W' type cracks.

SEM examination of fracture surfaces revealed four distinct modes of fracture; low temperature ductile rupture; intergranular microvoid coalescence; intergranular decohesion; and high temperature ductile rupture. An example of low temperature ductile rupture (LTDR) is shown in Fig. 4.16. This mode of fracture has been well documented, and is associated with the nucleation, growth and coalescence of voids at second phase particles. In the present study, void nucleation occurs mainly by decohesion of the matrix-inclusion interface at MnS inclusions, and for this mode of fracture, reductions of area of greater than 80% were produced. LTDR was observed for all six steels at test temperatures of 600°C and below, at 650°C for the 0.04 and 0.10%C steels, and at 700°C for the 0.04%C steel.

Fig. 4.17 illustrates the features of the intergranular microvoid coalescence (IMC) mode of fracture. Microvoids, often associated with second phase particles cover the facets of the austenite grains. Analysis of the second phase particles using energy dispersive analysis of X-rays (EDX) indentified these particles as MnS. Steels 1 to 5 exhibit this fracture mode, over temperature ranges corresponding to the existence of this ferrite films at the grain boundaries, and the reduction of area values associated with IMC are approximately 35%.

The third mode of fracture, intergranular decohesion (ID) is shown in Fig. 4.18. This mode of fracture is distinguished from IMC by the flat austenite grain facets, which, although showing MnS

inclusions, lack micro-voids. In some cases, wavy ridges are apparent on the grain facets, similar to those observed by Ouchi and Matsumoto (1982) in micro-alloyed steels, and to those observed by Ohmori and Maehara (1984) in an Nb containing austenitic stainless steel. It seems likely that these wavy ridges are due to the intersection of slip bands with the grain boundary during deformation, as suggested by Ohmori and Maehara. ID was the mode of fracture observed for the 0.65%C steel at temperatures below 900°C, and in the 0.35%C between 700°C and 900°C. ID was also occasionally observed in the lower carbon steels, at temperatures near the high temperature extent of the ductility trough.

Fig. 4.19 illustrates the fourth mode of fracture, high temperature ductile rupture (HTDR). Large voids are apparent on the fracture surface, greater in size than those associated with LTDR, and apparently not associated with second phase particles. All six steels show this failure mode. For steels 1-4, HTDR occurs at test temperatures greater than 850°C, whilst for steels 5 and 6, HTDR occurs at temperatures greater than 900°C. Reduction in area values for HTDR are greater than 80% for all six steels.

Wray (1975) has observed this mode of failure in austenitic iron. It is believed that the large voids apparent on SEM fractographs were originally intergranular cracks, formed at an early stage of deformation. As deformation proceeds, the original grain boundary crack is distorted into an elongated void, until final failure occurs by necking between these voids.

It should be noted that in most fractured tensile samples, more than one of the fracture modes described previously has contributed to final failure, although usually, one mode is dominant.

Figs. 4.7 - 4.10 and Fig. 4.20 - 4.21 show the temperature range

over which each failure mode occurs for each steel, together with ductility and transformation data.

### 4.3.3 Dilatometry

Table 4.2 shows the  $Ar_3$  and  $Ar_1$  temperatures determined by dilatometry. A change in C content from 0.04 to 0.65% has led to a fall of 174°C for the  $Ar_3$  and 119 for the  $Ar_1$  temperatures. Also shown are the metallographically determined  $Ar_3$  temperatures, which are typically 100°C greater than the dilatometric  $Ar_3$  temperatures. Unfortunately, the 0.04%C was cooled too slowly after fracture to allow  $Ar_3$  temperatures to be reliably determined metallography. The  $Ae_3$  and  $Ae_1$  temperatures determined using the formula of Andrews (1965) are also shown. The  $Ae_3$  temperatures fell from 865° to 720°C as the content increased from 0.04 to 0.65%. The  $A_1$  temperature remained constant at 713°C. The dilatometric  $Ar_3$  and  $Ar_1$  temperatures, and the calculated  $Ae_3$  and  $Ae_1$  temperatures and their relationship to the hot ductility curves are shown in Figs. 4.7 - 4.10, and Figs. 4.20 - 4.21.

#### 4.4 DISCUSSION

The foregoing results clearly show the existence of a ductility trough in the high temperature tensile behaviour of C-Mn steels with a wide range of C contents. These results compare well with those obtained by previous workers, using steels of similar compositions, and tested using similar strain rates. (Fig. 4.22) The influence of C content on peak stress is in agreement with that reported by other workers. (Wray, 1984 ). The present results have also shown that when the failure mode is HTDR, reduction of area values are independent of C content. This is in conflict with the results reported by Robbins et al (1967) using hot torsion tests. They observed an increase in hot ductility with increasing C content, and further work by Gittins (1971) showed that this increase was due to the decrease in O content, and hence oxide inclusions, associated with higher C contents. In the present study, O analysis was unfortunately, not available, but it is likely that all six steels had similar, low O contents, since all were vacuum melts. This would account for the lack of sensitivity of hot ductility to C content in the austenitic state.

The hot ductility and metallographic observations also show the importance of the austenite to ferrite transformation in controlling hot ductility in the lower carbon steels (1-4 inclusive). Raising the C content in these steels lowers the transformation temperatures, and as a consequence, moves the ductility trough to lower temperatures. Fracture occurs by intergranular microvoid coalescence. Strain is concentrated in the softer ferrite phase, allowing ductile voiding to occur around the MnS inclusions, these cavities eventually linking. The difference in dilatometric and metallographic  $A_{r3}$  temperature imply that the ferrite surrounding the

austenite grains is deformation induced. Previous work by Bernard et al (1978) also showed that transformation temperatures determined metallographically from fractured tensile samples were higher than those determined by dilatometry, using the same cooling rates. Work by Kozasu et al (1976) and by Roberts et al (1980) has also shown that deformation raised the temperature at which the austenite to ferrite transformation commences. For large deformations their work has shown that the transformation temperature may be increased by over 100°C. This effect is due to an increase in the effective ferrite nucleation area per unit volume accompanying deformation. These additional ferrite nucleation sites are believed to be at deformation bands and bulges at austenite grain boundaries caused by deformation. Recovery of ductility on lowering the test temperature seems to be related to the thickening of the ferrite films, in agreement with the results of Ouchi and Matsumoto (1982). It should be noted that even at temperatures which give reduction in area values of 50% at the low temperature end of the ductility trough, the actual amount of ferrite is very small. Hence only a very thin film is required to give intergranular failure in the coarse grained steels, and these films, although thin when deformation induced, thicken rapidly once the  $A_{r3}$  temperature is reached. Indeed the temperature at which ductility first starts to recover does correspond approximately to the dilatometric  $A_{r3}$ , and this indicates that the width of the trough may be controlled by the difference in temperature between the deformation induced transformation temperature and the dilatometric  $A_{r3}$ . Under more equilibrium conditions, the width would be expected to become narrower, and results confirming this are discussed in subsequent chapters. In the present instance where cooling rates are high, it seems likely that deformation can

raise the transformation temperature ( $A_{r3}$ ) close to equilibrium values.

An additional factor which may lead to the recovery of ductility at low test temperatures is the fact that the strength differences between austenite and ferrite decreases slightly as the temperature is reduced. (Wray, 1981). This would be expected to reduce strain concentration in the ferrite, and hence improve ductility. Support for this idea is shown by the fact the the .10%C steel requires a much thicker ferrite film to restore ductility than either the .19%C or the .28% steel, the ductility of which recovers at lower temperatures.

For the higher C steels hot ductility behaviour is clearly very different. Raising the C level from 0.28 to 0.35%C causes the temperature at which ductility starts to fall to increase by over 100°C. Intergranular fracture now takes place in the austenite at as high a temperature as 850°C. The extended nature of the ductility trough in the higher C steels arises not only because C appears to promote intergranular failure in the austenite, but also because increasing C content lowers the transformation temperature. Furthermore, in the case of the .35%C steel, it is likely that when transformation does finally occur, strain concentration in the softer deformation induced ferrite will then take place, as for the .28%C steel.

The influence of C in encouraging failure to occur in the austenite is apparent even at C contents of less than 0.35%. Examination of Figs. 4.7 - 4.9 clearly shows that the difference between the  $A_{e3}$  temperature and the temperature at which ductility first starts to fall increases with C content. This difference increases from zero for an 0.1%C steel to 50°C for an 0.28%C steel. Loss of ductility in this range must be controlled by processes occurring

in the austenite, and this is confirmed by the absence of ferrite films and the first appearance of some flat faced fracture surfaces characteristic of intergranular failure in the austenite. However, it is not until the C content reaches 0.35% that full intergranular failure in the austenite occurs.

To try to establish possible reasons to account for the difference in fracture behaviour between high and low carbon steels, careful examination was made both optically and using carbon extraction replicas of the sulphide distribution. No significant differences were found between the sulphide distribution in low and high C steels. In order to obtain more information on the hot ductility behaviour of low and high C steels, it was decided to perform hot tensile tests at a variety of strain rates to determine the activation energy for deformation,  $Q$ . The steels chosen were the .19%C steel, and the .65%C steel. Hot tensile tests were performed as before, but using the Instron equipment described in section 3.2.2. Strain rates in the range  $3 \times 10^{-2}$  -  $3 \times 10^{-4} \text{ s}^{-1}$  were used, and tests performed in the temperature range 850 to 1050°C.

Stress strain rate and temperature can be correlated using equation 2.3 for low stresses, equation 2.3 reduces to:

$$\dot{\epsilon} = A \sigma^n \exp - Q/RT \dots\dots\dots 4.1$$

where  $\dot{\epsilon}$  is the strain rate, A and n constant,  $\sigma$  stress, R the universal gas constant, and T the test temperature.

The validity of equation 4.1 under the present conditions is shown by Figs. 4.23 and 4.24 which shows a linear relationship between  $\ln \sigma_p$  and  $1/T$  for the .19 and .65%C steel at a constant strain rate.

The activation energy for deformation,  $Q$ , is obtained from the gradient of the plot of  $\ln \dot{\epsilon}$  against  $1/T$  at constant stress, Figs. 4.25 and 4.26. The stress exponent, n, is determined from the gradient of the plot of  $\ln \dot{\epsilon}$  against  $\ln \sigma_p$  at constant temperature, Figs. 4.27

and 4.28. The values of  $Q$  and  $n$  are shown in Table 4.3, together with other values of  $Q$  and  $n$  from previous work. It can be seen that the present results are in good agreement with the results of previous workers. In Fig. 4.29, values of the activation energy for deformation are plotted against C content, and it can be seen that there is a systematic increase in  $Q$  with C content. It is suggested that this increase in activation energy is sufficient to retard the onset of dynamic recrystallization or to decrease the rate of dynamic recrystallization if it occurs. This would be expected to decrease hot ductility by reducing the rate of grain boundary migration, and hence allowing intergranular failure to occur in the austenite.

Fig. 4.30 shows the sample elongation to peak stress for the .19%C and .65%C steels at various strain rates and test temperatures. This sample elongation to peak stress is simply related to  $\epsilon_c$ , the critical strain for the nucleation of dynamic recrystallization, as discussed in section 2.3.3., and Fig. 4.30 shows the expected trends with strain rate and temperature, i.e.  $\epsilon_c$  decreases with decreasing strain rate and increasing temperature. Unfortunately, the results were not accurate enough to confirm whether increasing C content did in fact retard the onset of dynamic recrystallization behaviour of the .19 and the .65%C steels. Hopefully, further tests will be able to clarify more precisely any differences in recrystallization behaviour between low and high C steels.

#### 4.5 CONCLUSIONS

1. The existence of ductility troughs in the high temperature tensile behaviour of C-Mn steels tested using intermediate strain rates has been confirmed.
2. For steels with C content less than .35% low ductility failures are intergranular in nature, and are due to strain concentration in the soft, ferrite films at the austenite grain boundaries.
3. For steels with C content less than .35%, decreasing the C content raised the ductility trough to higher temperatures, due to the increase in transformation temperature.
4. For steels with C contents  $> 0.35\%C$ , low ductility intergranular failures occur in the austenite, fundamentally different behaviour to that observed in lower C steels.
5. The activation energy for deformation has been shown to increase the increasing C content and it is proposed that this increase is responsible for the low ductility failures observed above the  $A_3$  temperature in higher C steels.

Code No.	C	Si	S	P	Mn	N	Ni	Cr	Mo
1	.04	.20	.013	.002	1.50	.004	.04	.03	.01
2	.10	.20	.013	.002	1.50	.004	.04	.03	.02
3	.19	.20	.013	.002	1.40	.004	.04	.03	.02
4	.28	.20	.013	.002	1.50	.004	.04	.03	.02
5	.35	.17	.009	.002	1.31	.004	.04	.06	.02
6	.648	.275	.003	.002	1.39	.005	NV	NV	NV

Table 4.1 Compositions of the steels examined (wt.%)

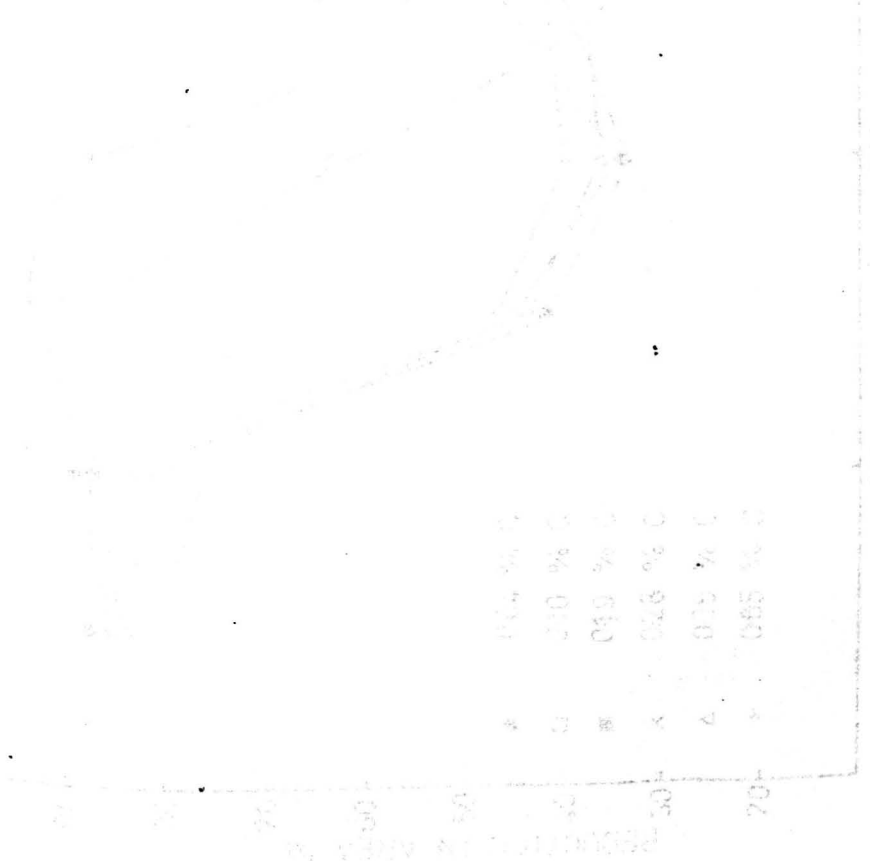
NV = no value

Code No.	C content (wt.%)	Transformation temperatures (°C)				
		Dilatometric		Metallographic	Calculated	
		Ar <sub>3</sub>	Ar <sub>1</sub>	Ar <sub>3</sub>	Ae <sub>3</sub>	Ae <sub>1</sub>
1	0.04	772	644	-	865	713
2	0.10	744	584	790	840	713
3	0.19	697	560	775	813	713
4	0.28	650	550	750	782	713
5	0.35	600	480	710	770	713
6	0.65	598	525	-	720	713

Table 4.2 Transformation temperatures determined by dilatometer, metallographically, and by the method of Andrews (1965)

Reference	C Content (wt.%)	Q (KJ mol <sup>-1</sup> )	n
Sellars and Tegart (1966)	-	280	4.7
Sankar et al, (1979)	0.14	308	5.1
Present work	0.19	290	5.2
Sellars and Tegart (1966)	0.25	300	4.6
Present work	0.65	330	5.5
Sellars and Tegart (1966)	0.85	339	4.55
Sellars and Tegart (1966)	1.2	390	4.55

Table 4.3 Influence of C content in C-Mn steels on the activation energy for deformation, Q, and stress exponent, n.



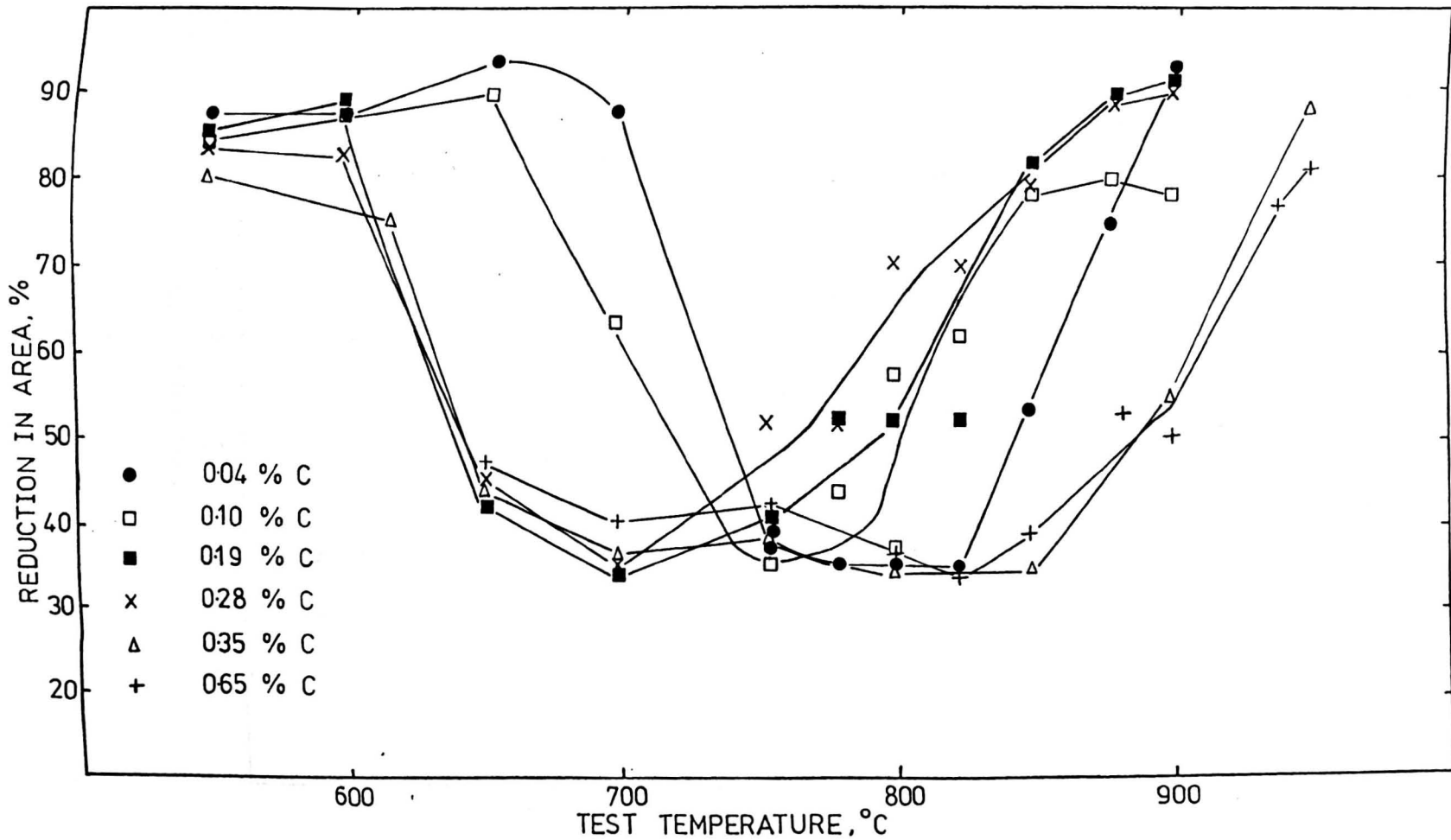


Fig. 4.1 Variation of reduction in area with test temperature for steels 1 - 6

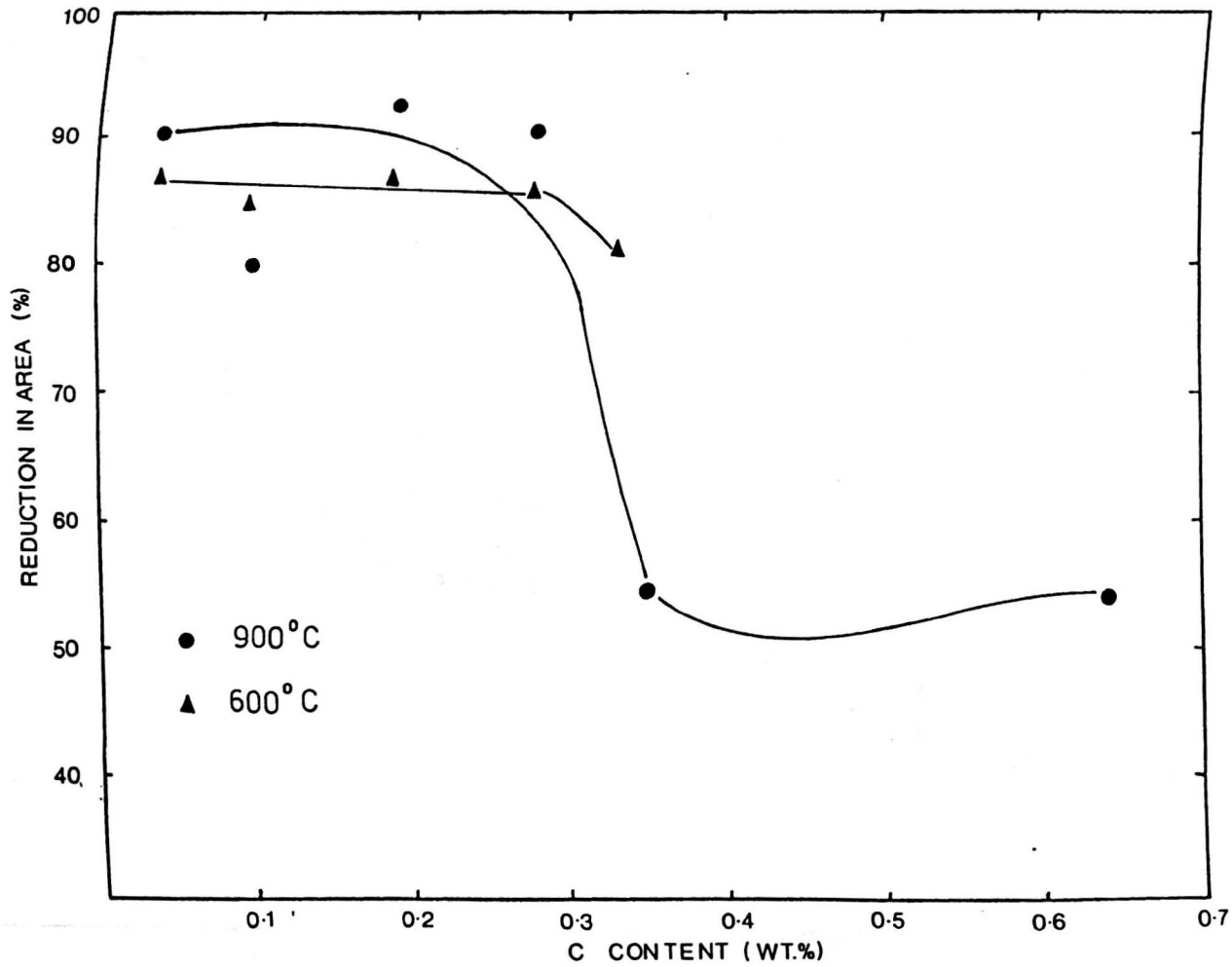


Fig. 4.2 Variation of reduction in area with C content at 900 and 600°C

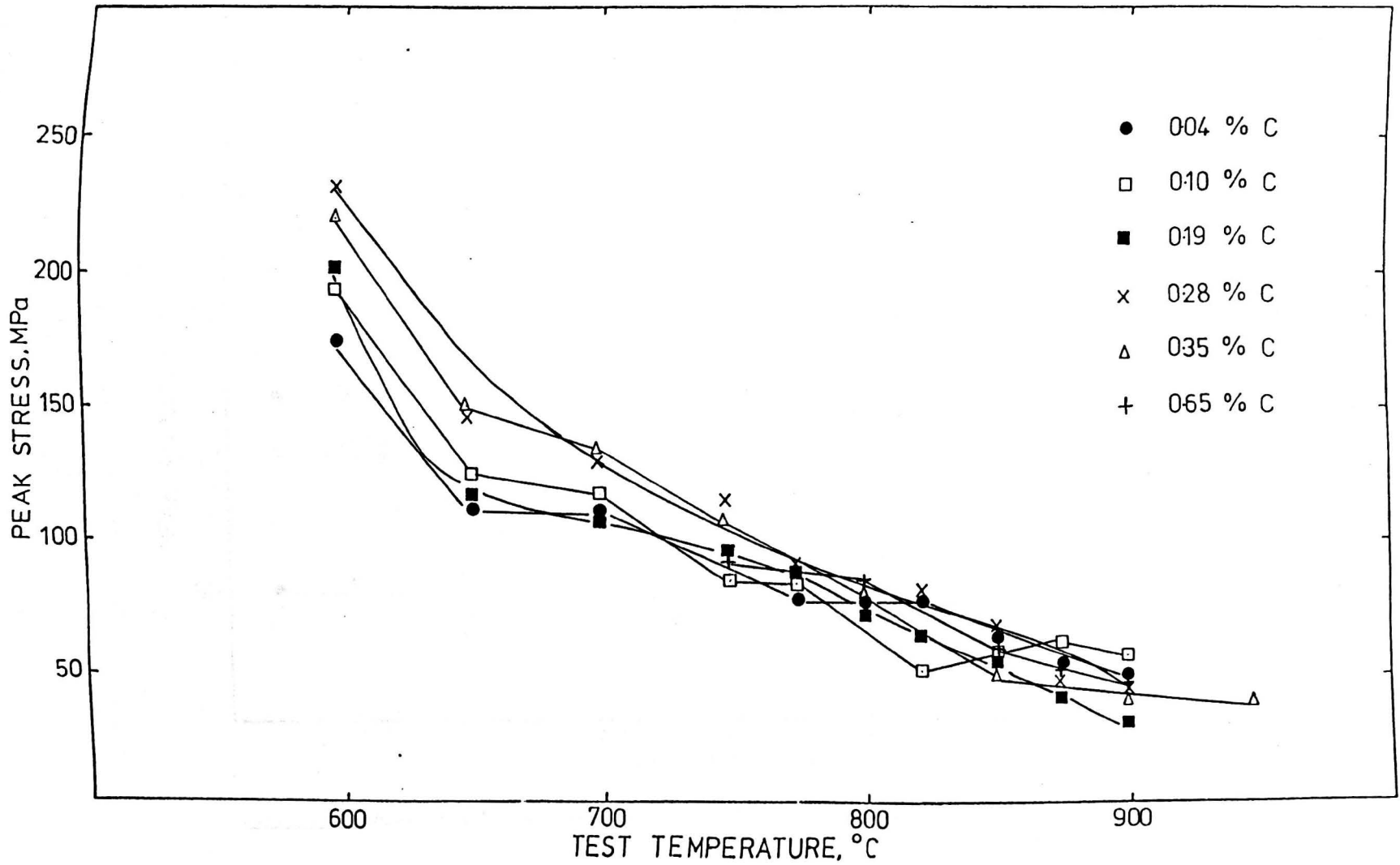


Fig. 4.3 Variation of peak stress with test temperatures for steels 1 - 6.

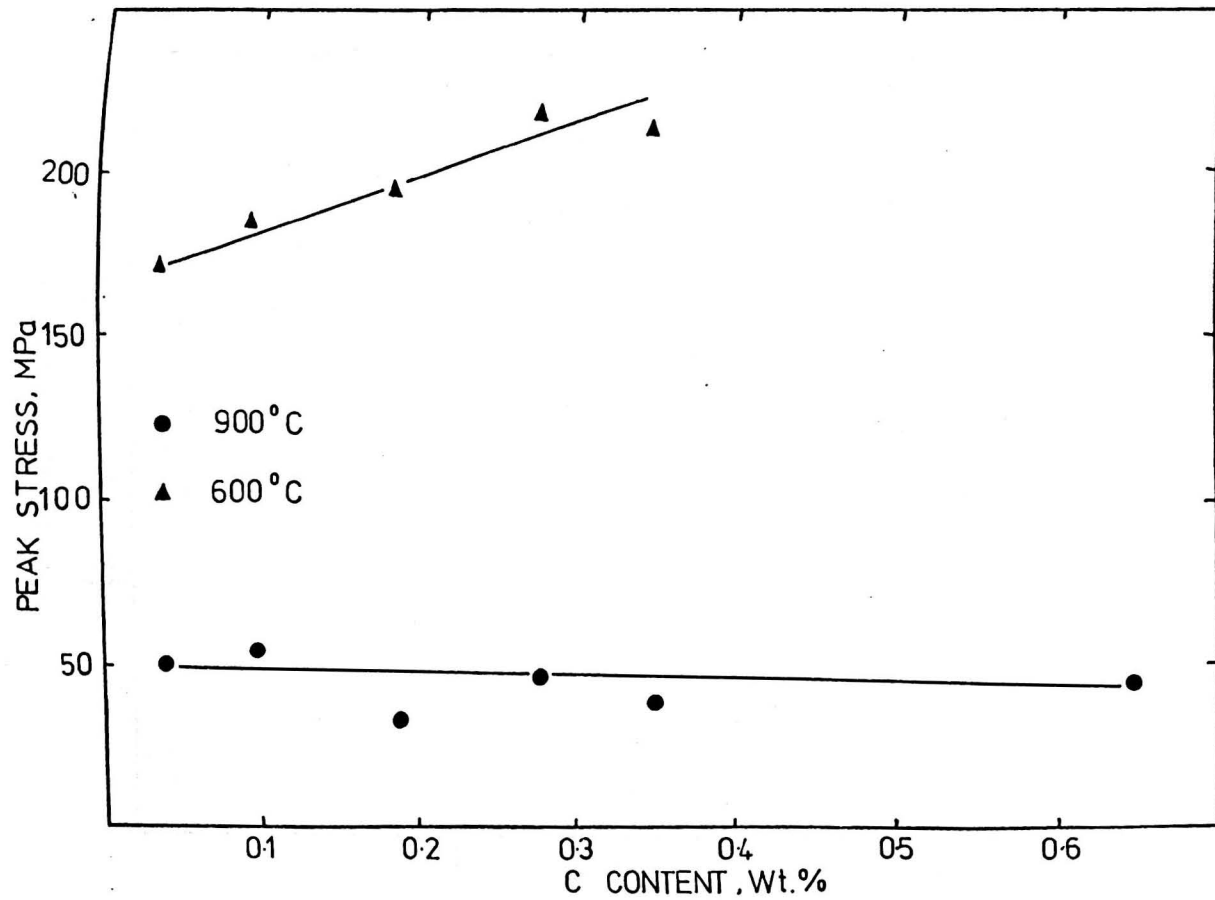


Fig. 4.4 Variation in peak stress with C content at 900 and 600°C

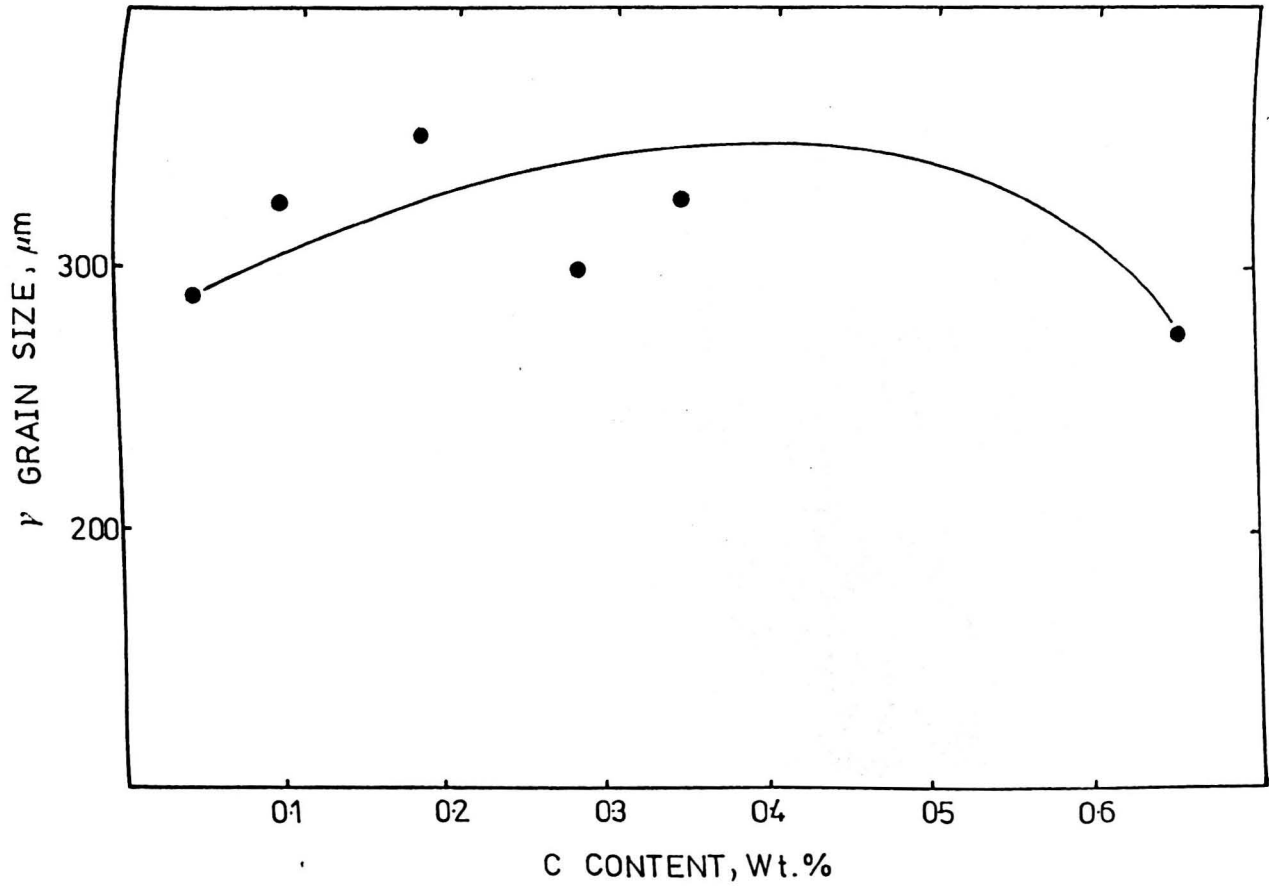


Fig. 4.5 Influence of C content on austenite grain size at 1330°C

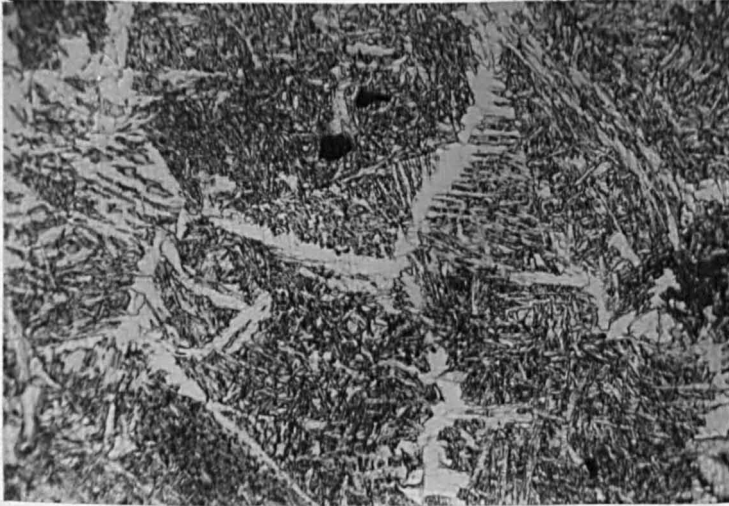


Fig. 4.6 Grain boundary ferrite and side plate formation in .10% C steel, tested at 600°C.

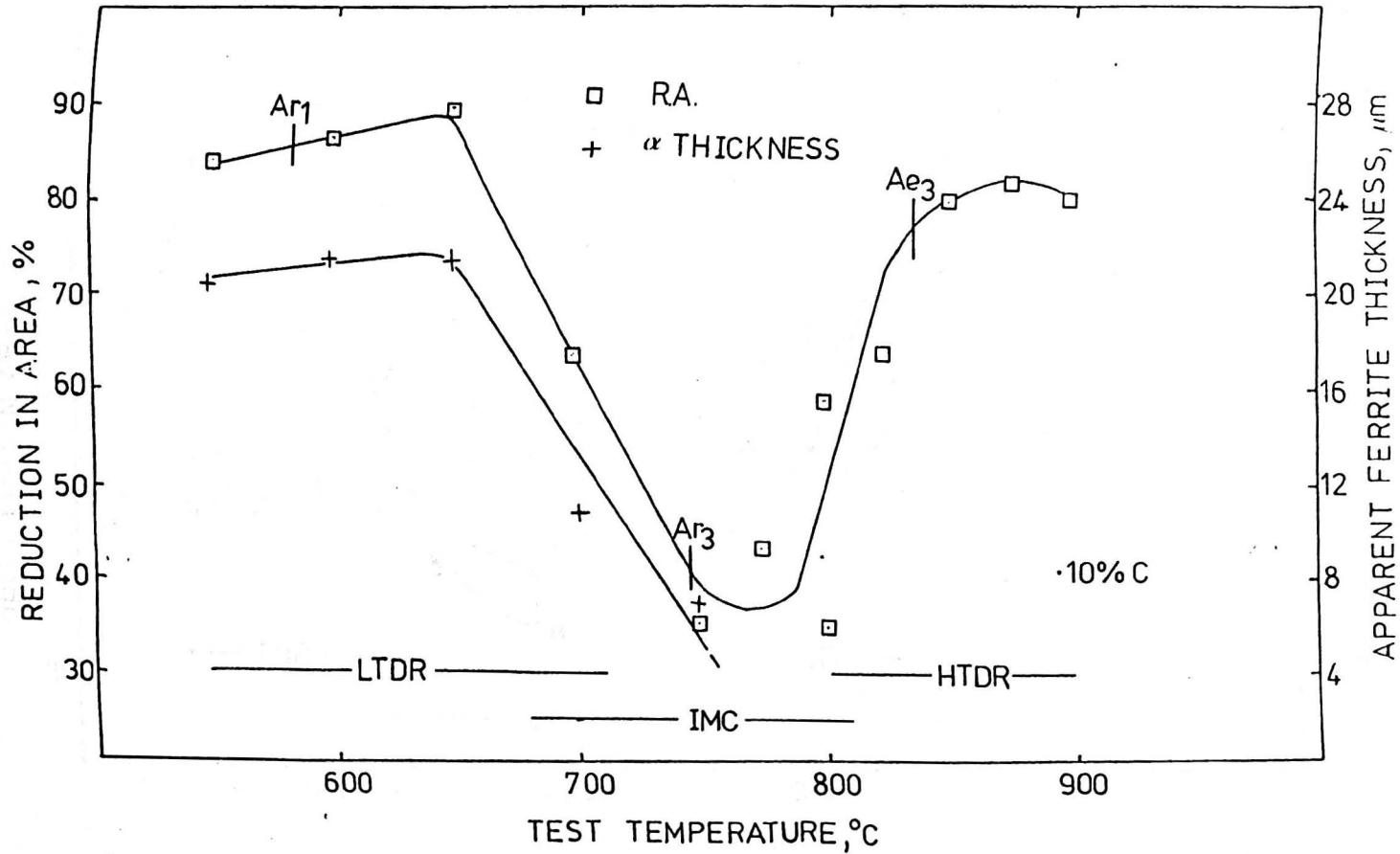
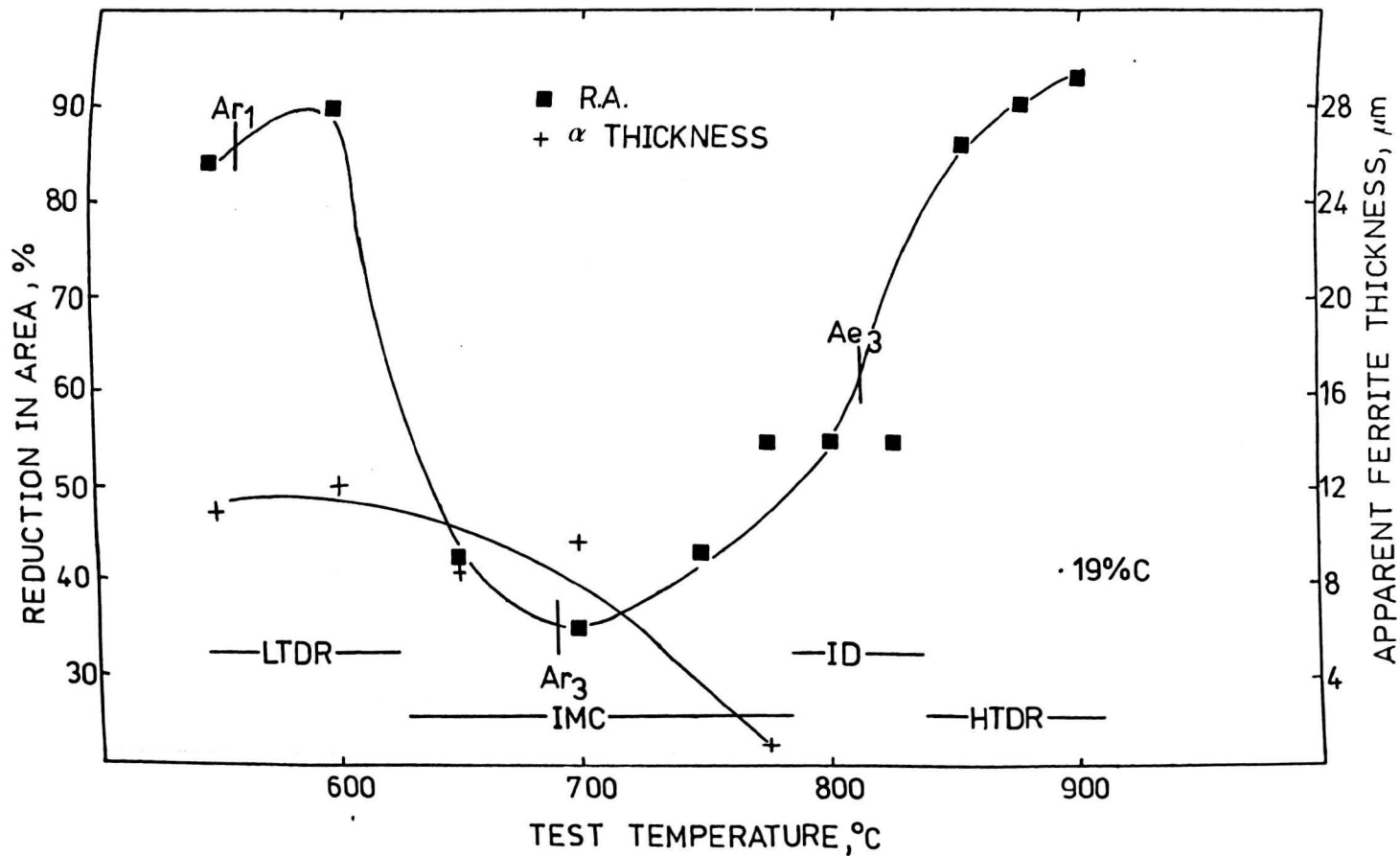


Fig. 4.7 Hot ductility, transformation and fracture data for the 0.10% C steel



**Fig. 4.8** Hot ductility, transformation and fracture data for the 0.19% C steel

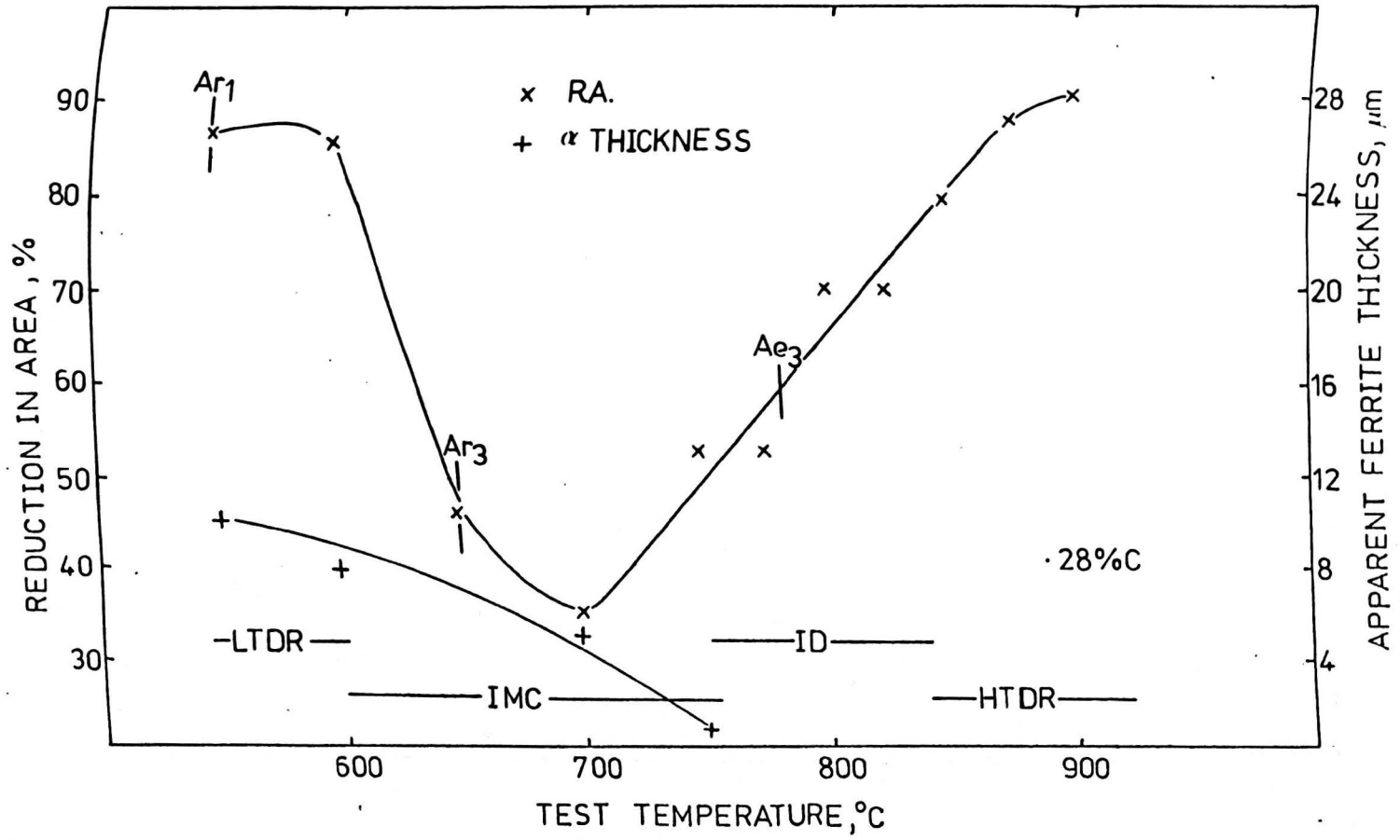


Fig. 4.9 Hot ductility, transformation and fracture data for the 0.28 C steel

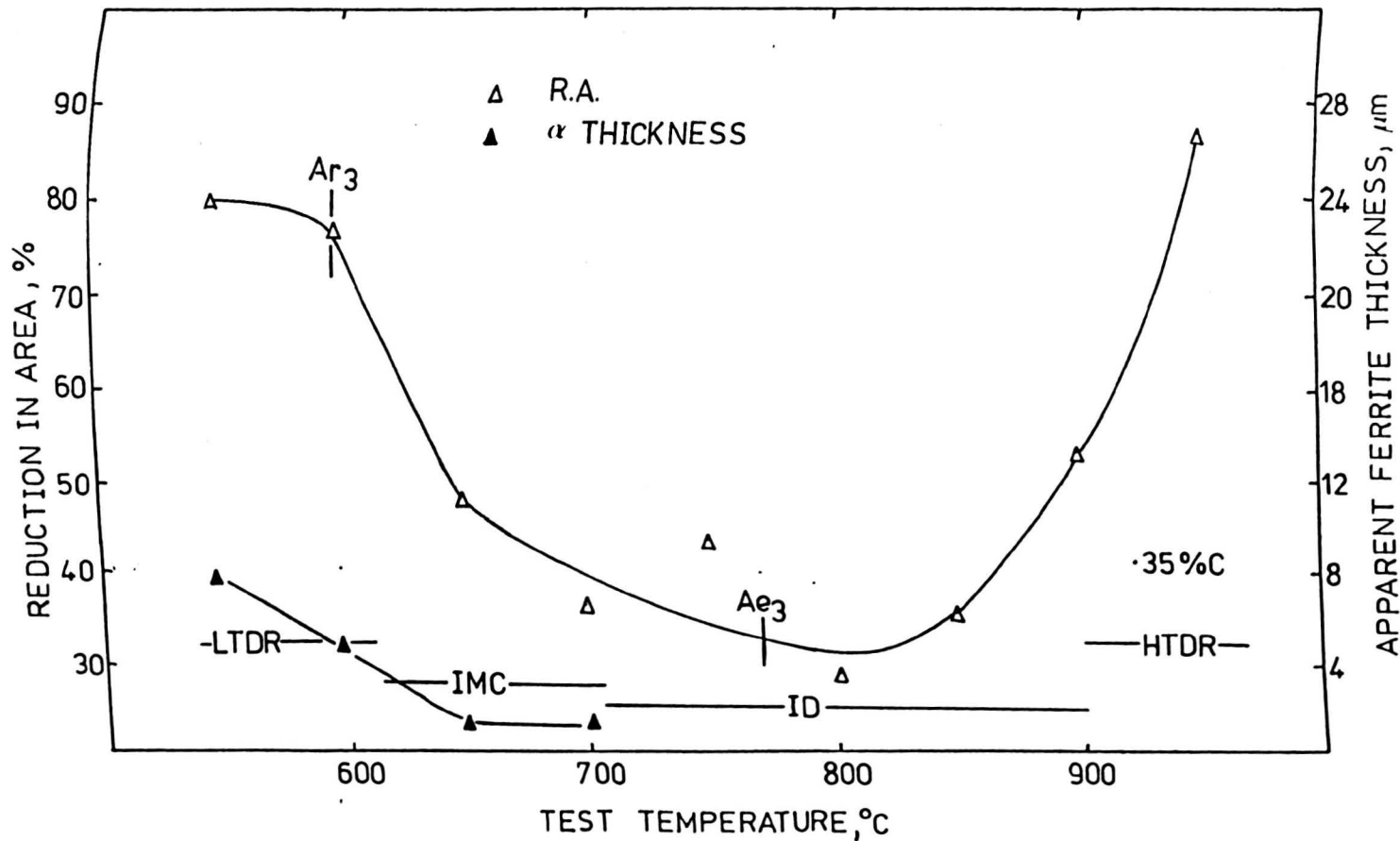


Fig. 4.10 Hot ductility, transformation and fracture data for the 0.35% C steel

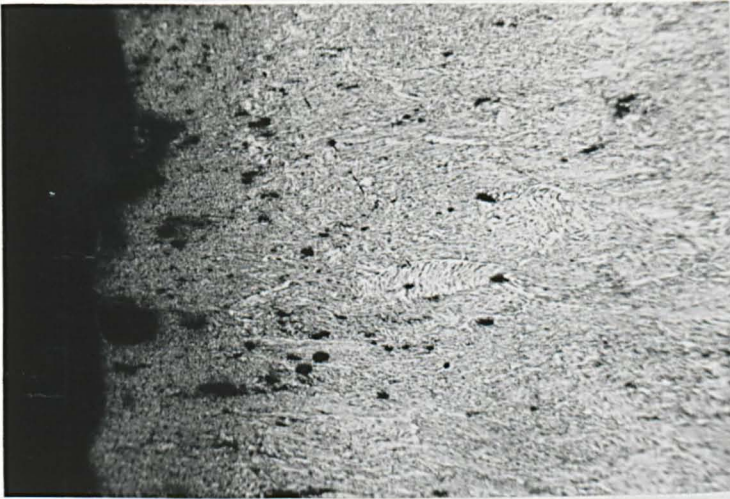


Fig.4.11 Optical micrograph showing point of fracture of the 0.19%C steel tested at 600°C. (R of A 90%)

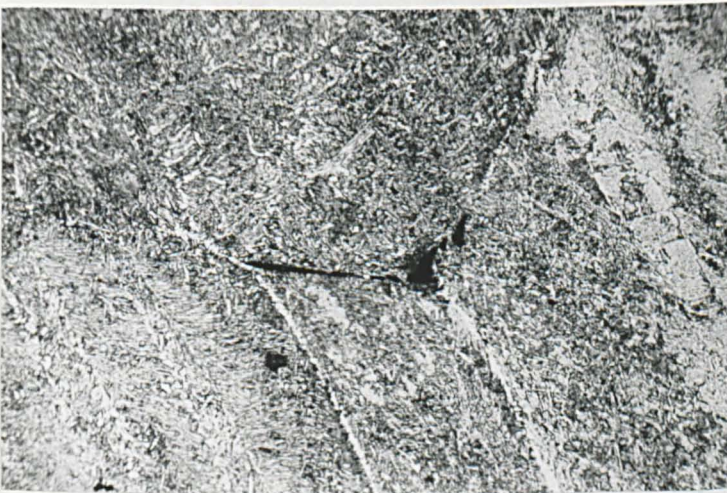


Fig.4.12 Micrographs illustrating grain boundary crack formation in the 0.19%C steel tested at 650°C (R of A 43%)

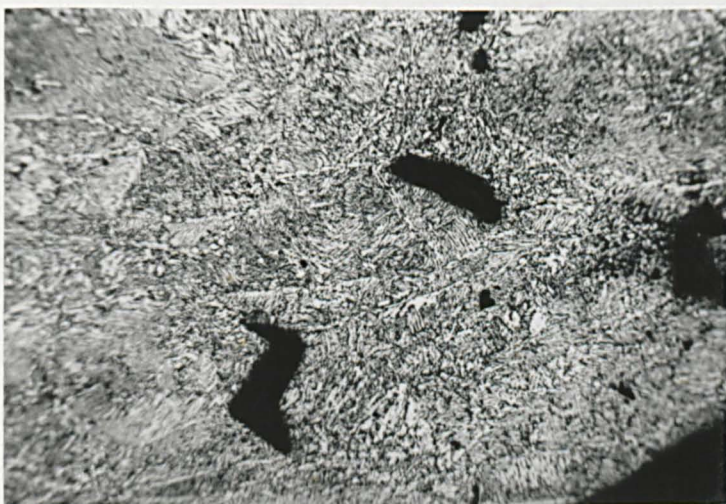


Fig. 4.13 Micrograph showing point of fracture of the 0,19%C steel tested at 650°C.

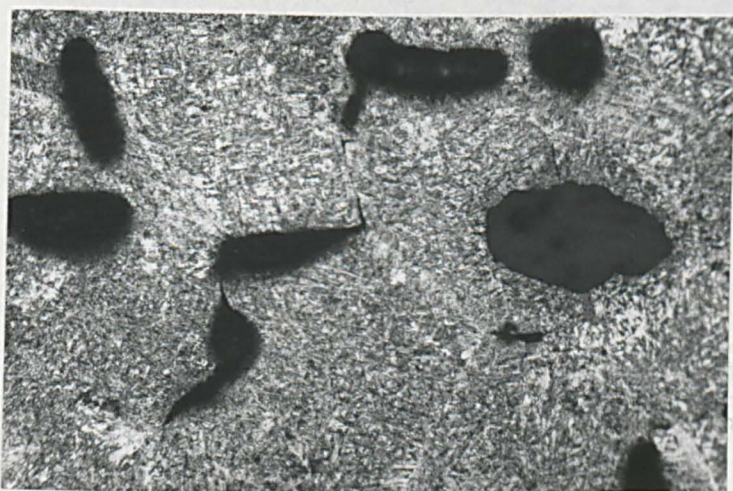


Fig. 4.15 Crack formation in the 0.35%C steel tested at 850°C.

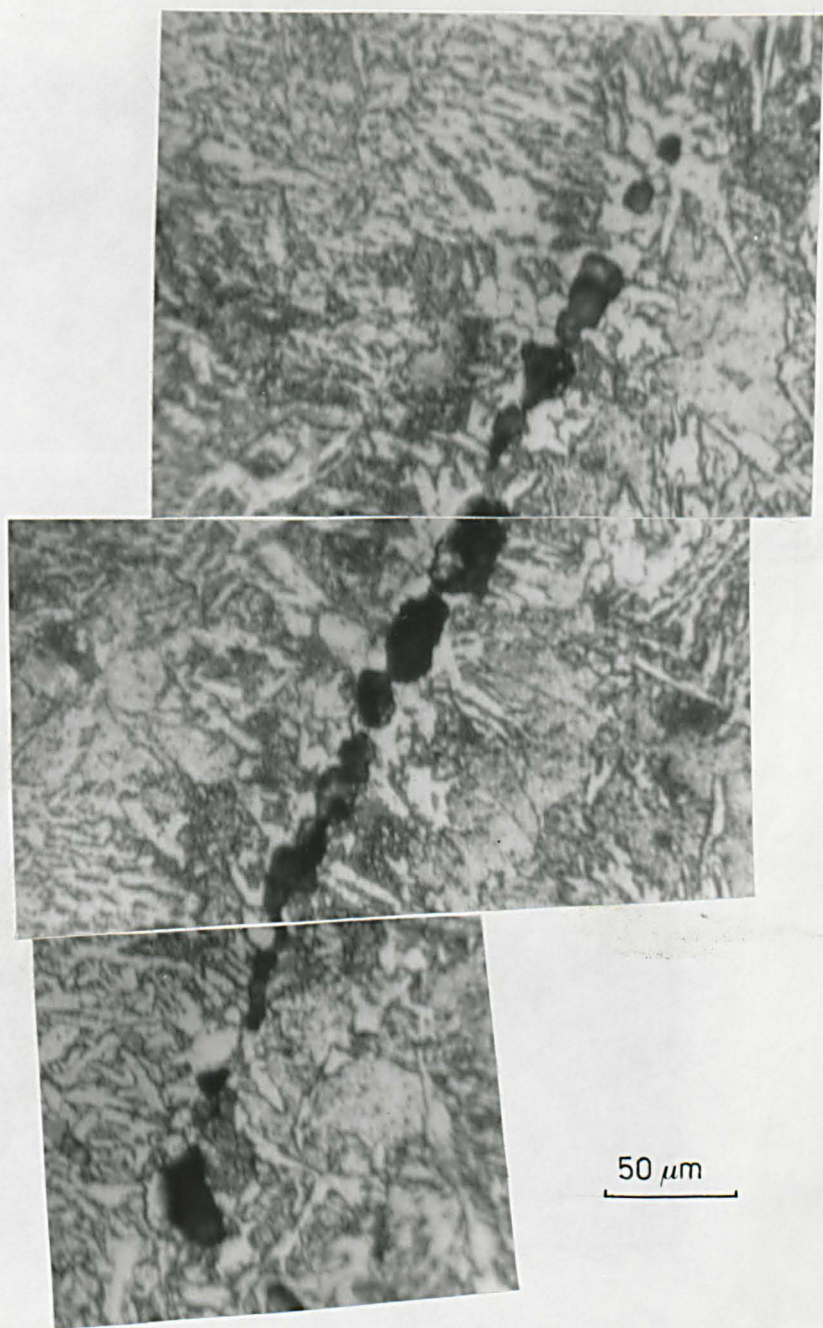
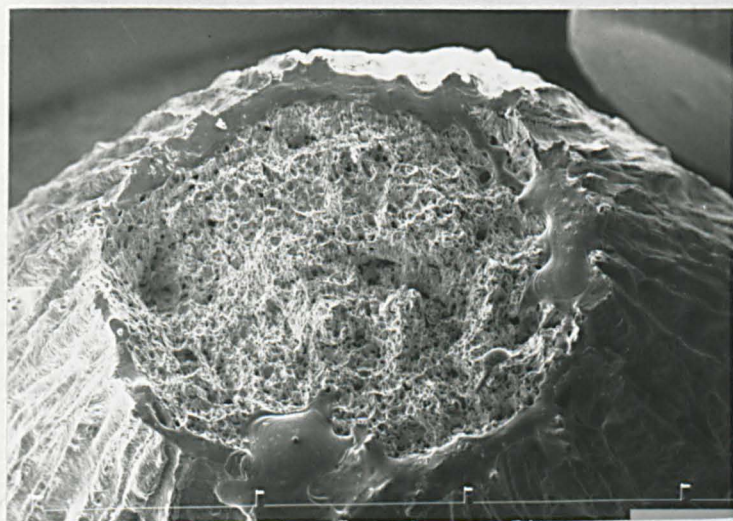
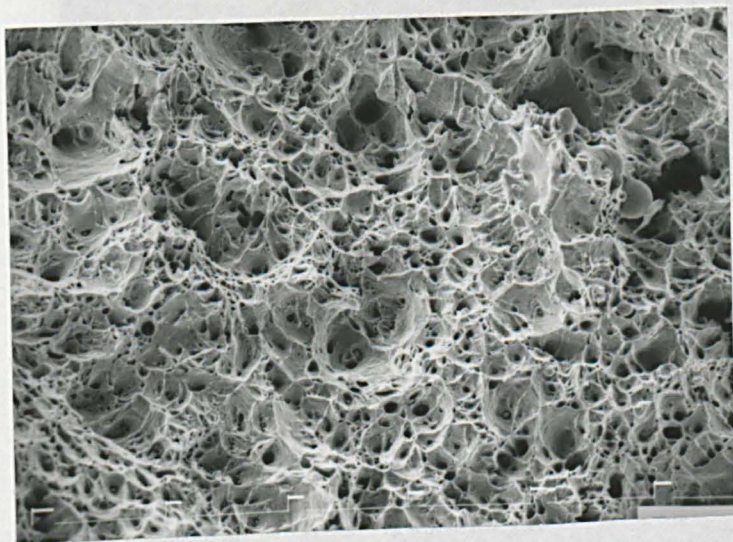


Fig. 4.14 Detail of crack formation in .19%C steel tested at 650°C

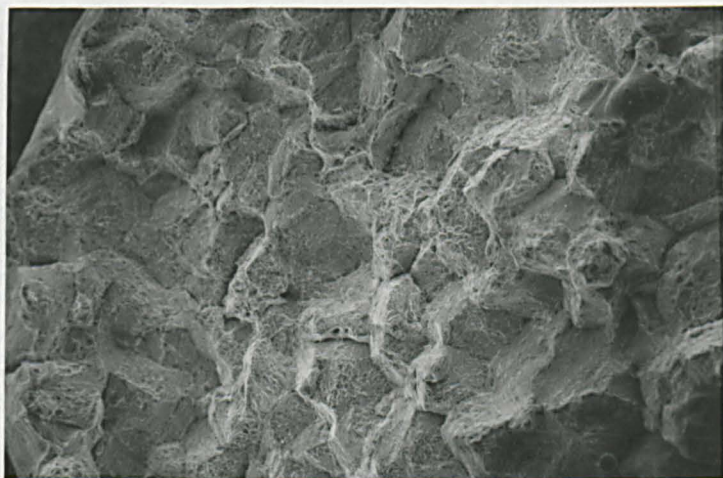


500  $\mu\text{m}$

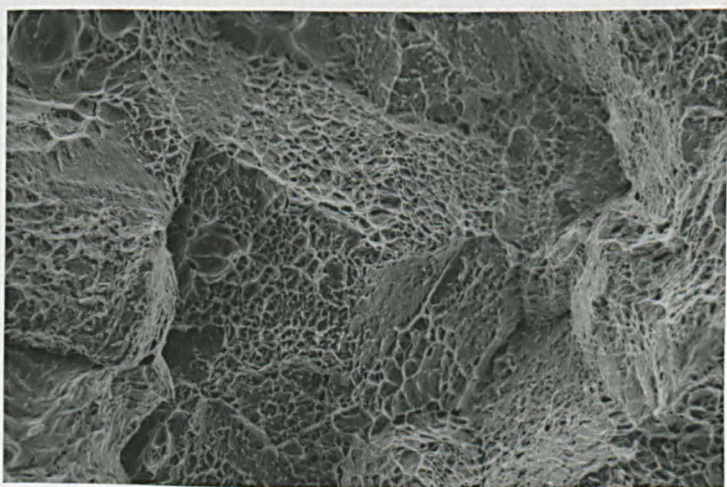


100  $\mu\text{m}$

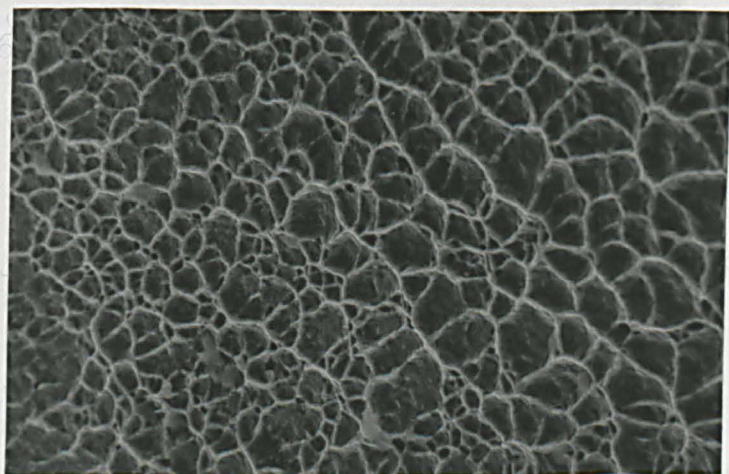
Fig. 4.16 Low temperature ductile rupture (LTDR) fracture mode, showing void formation at second phase particles. 0.04% C steel, tested at 550°C.



400 μm

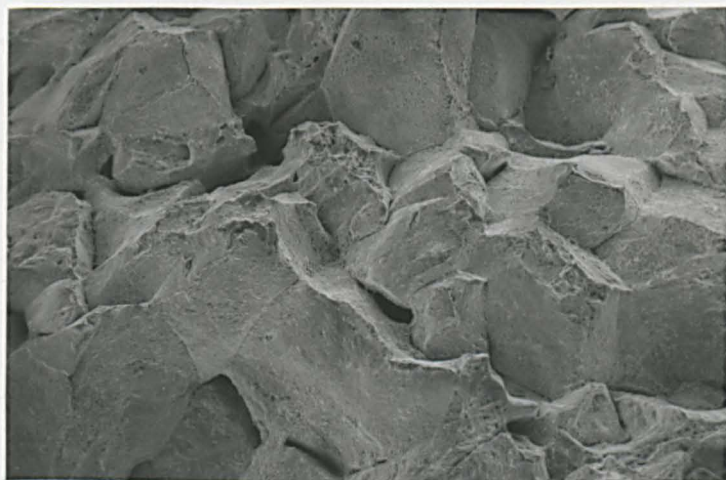


100 μm

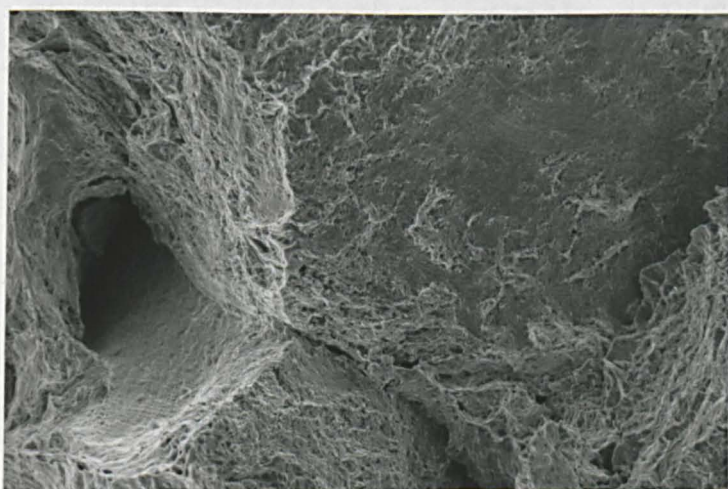


20 μm

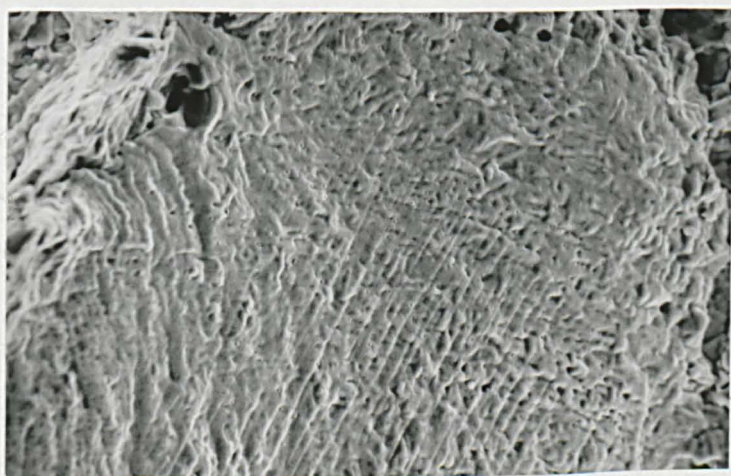
Fig.4.17 Intergranular micro void coalescence (IMC) fracture mode, showing void formation on grain facets. 0.10%C steel tested at 775°C.



200  $\mu\text{m}$

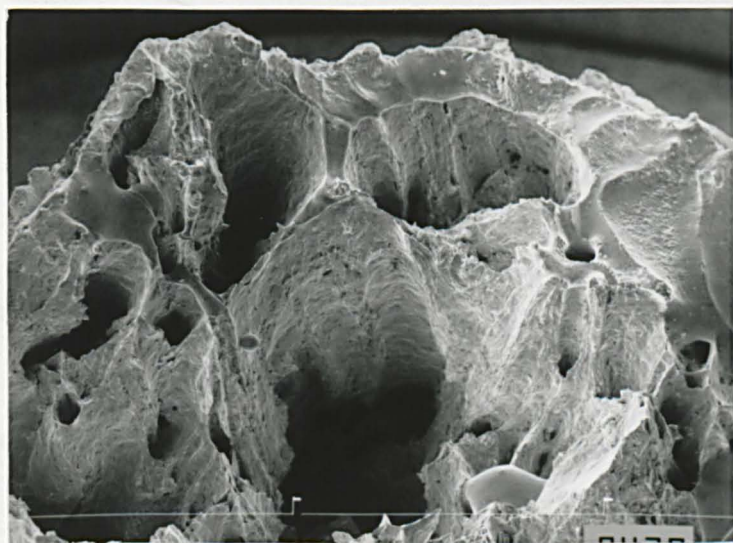


50  $\mu\text{m}$



20  $\mu\text{m}$

Fig. 4.18 Intergranular decohesion (ID) fracture mode, showing relatively smooth grain facets, some with wavy ridges. 0.35% C steel tested at 750°C.



400 $\mu$ m

Fig. 4.19 High temperature ductile rupture (HTDR) fracture mode, showing large voids on fracture surface. 0.04%C steel tested at 900°C.

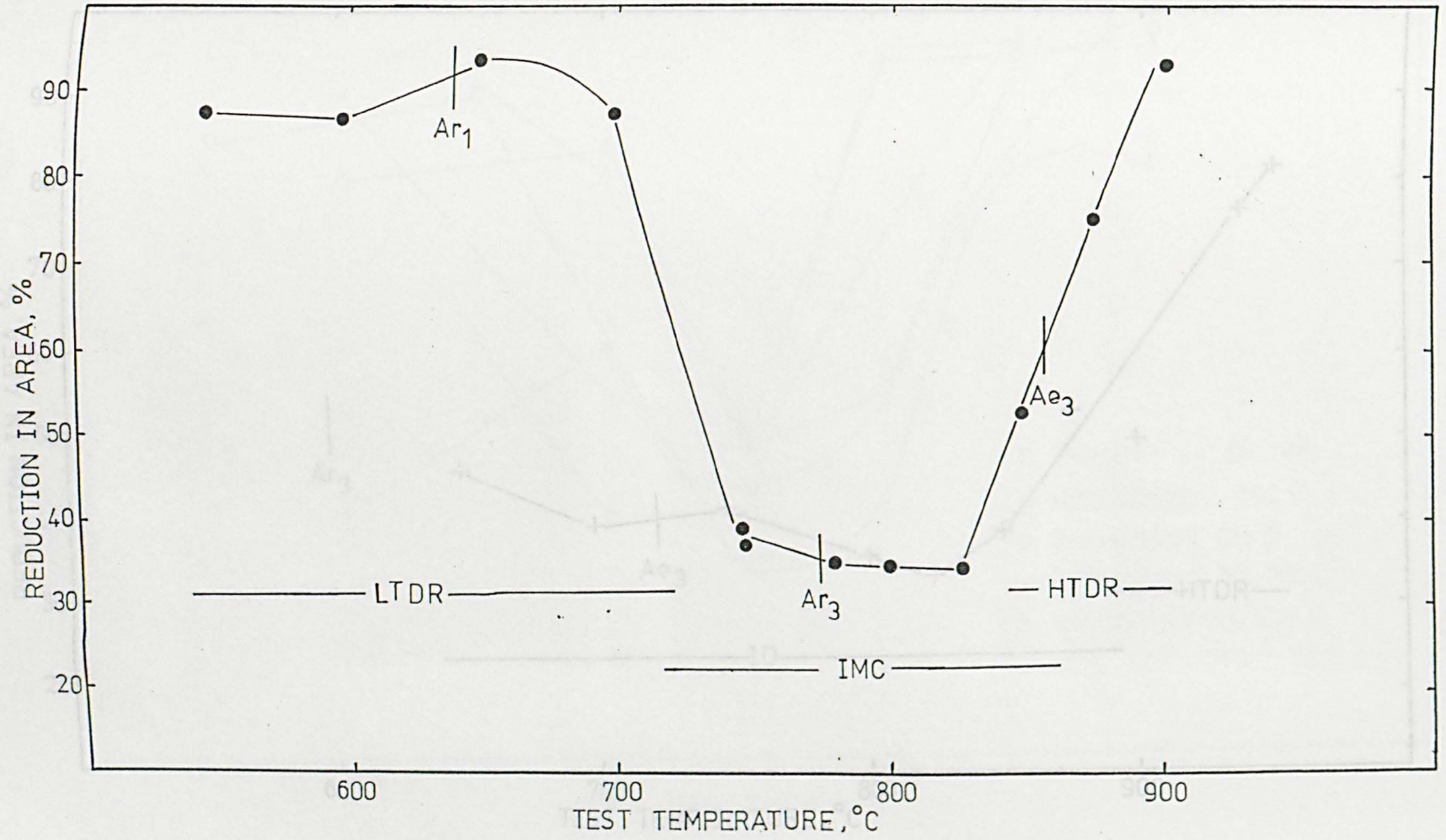


Fig. 4.21 Hot ductility, fracture and transformation data for the .65% C steel

Fig. 4.20 Hot ductility, fracture and transformation data for the .05% C steel.

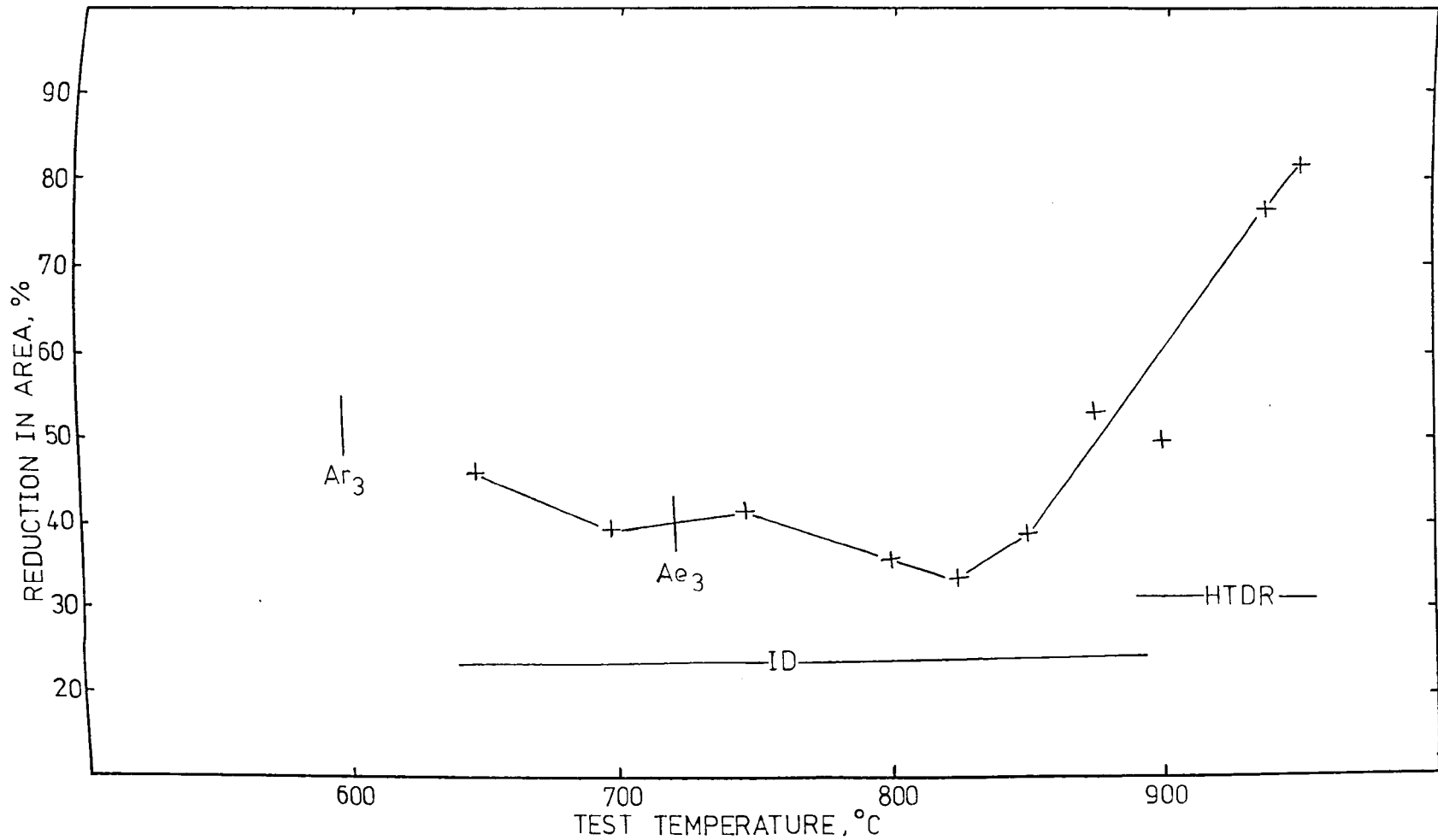


Fig. 4.21 Hot ductility, fracture and transformation data for the .65% C steel

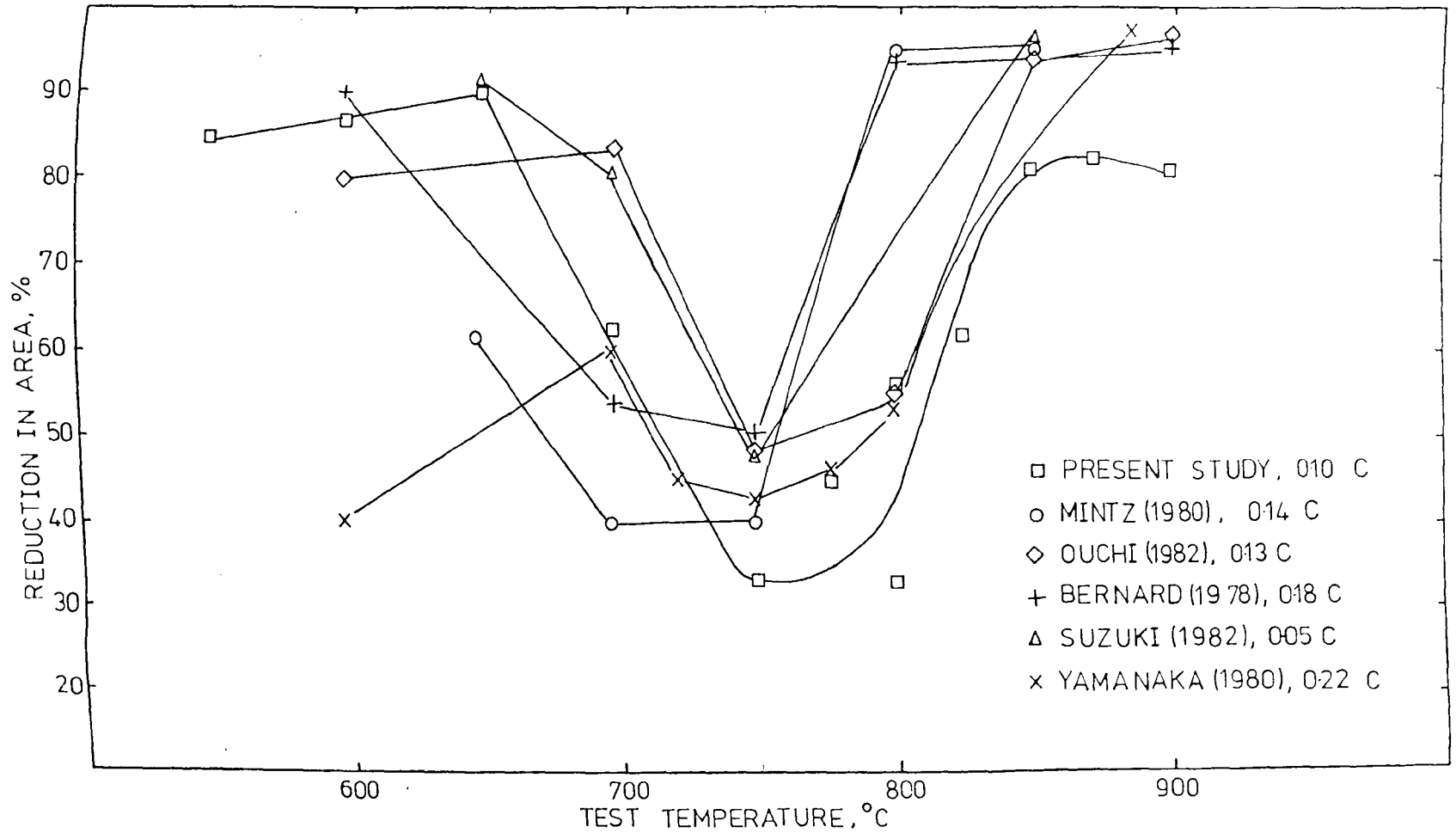


Fig. 4.22 Comparison of present hot ductility results with previous work

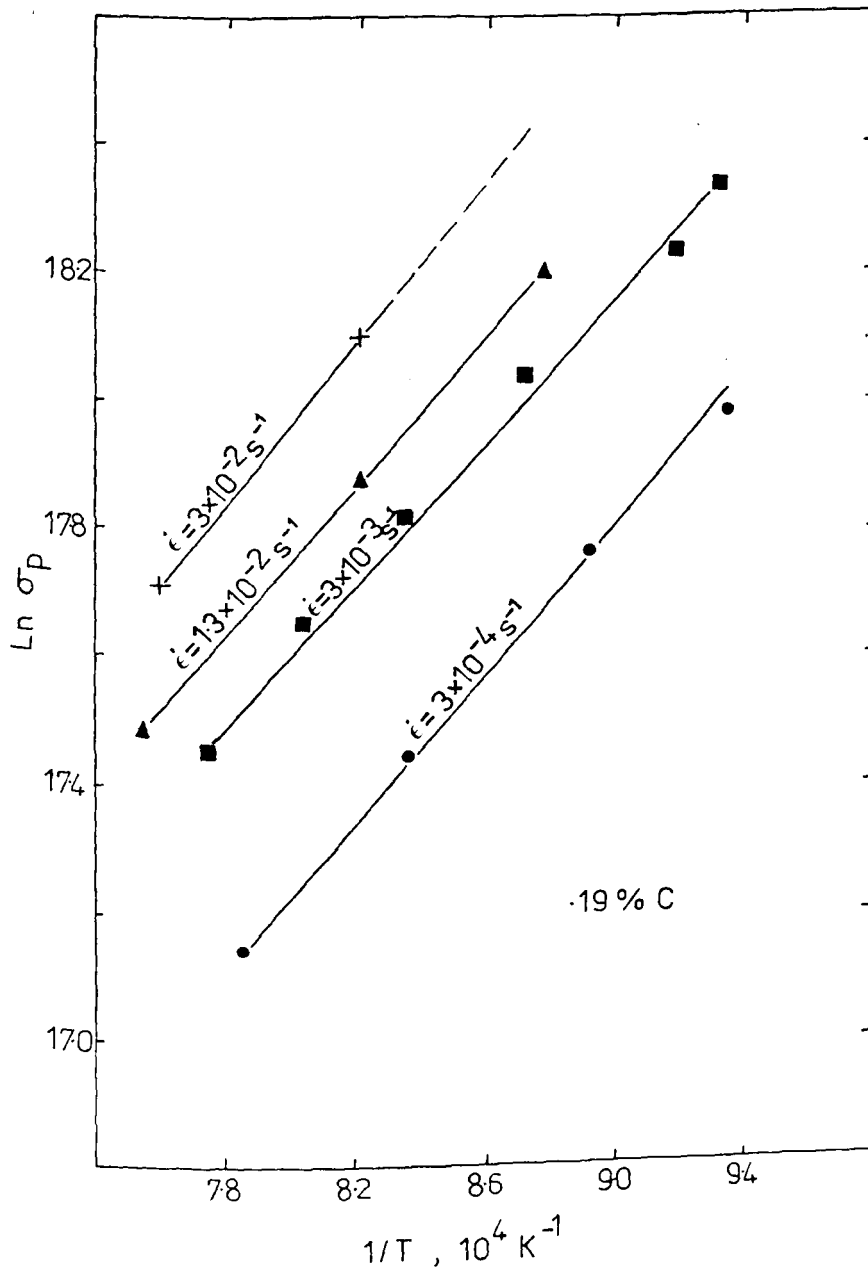


Fig. 4.23 Variation of peak stress,  $\sigma_p$ , with absolute temperature,  $T$ , at different strain rates for the 0.19% C steel

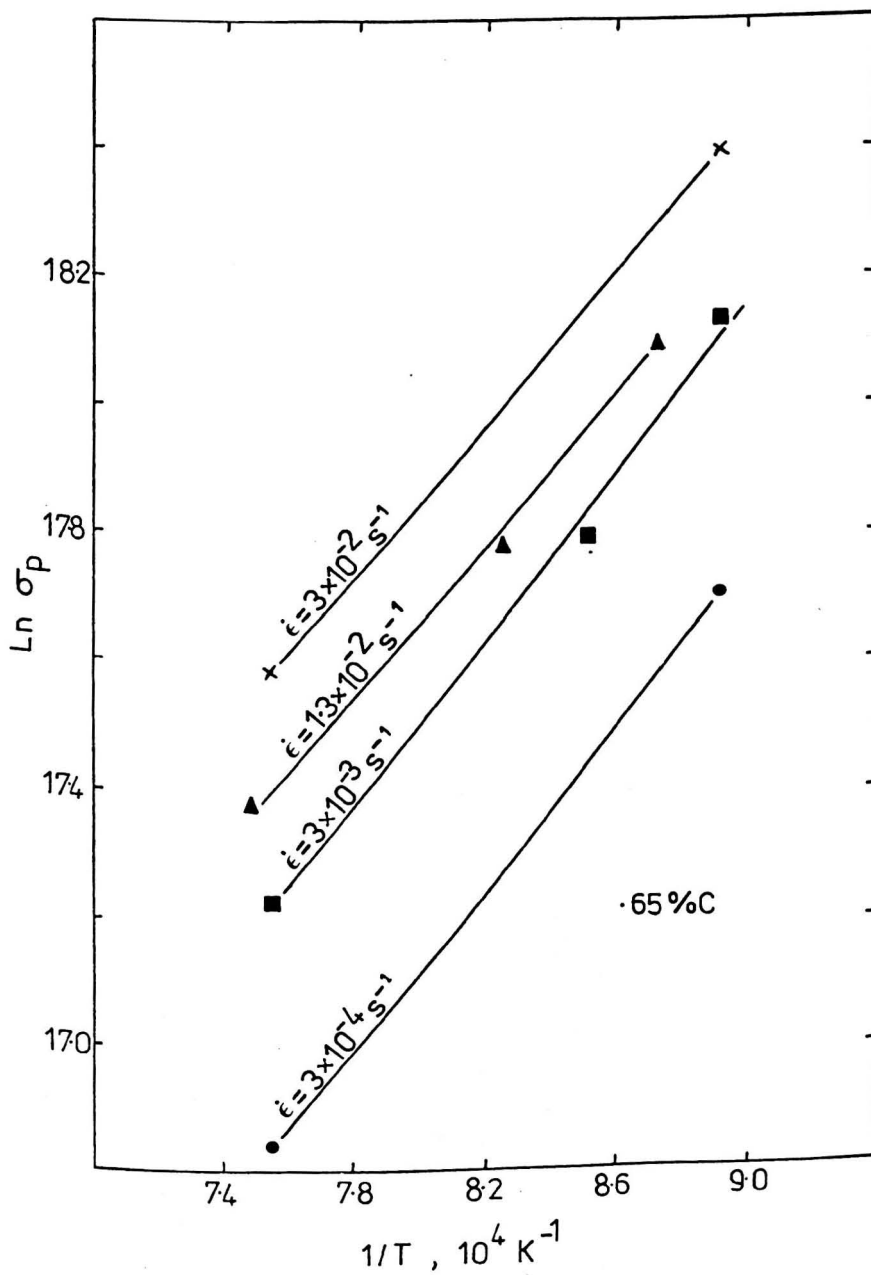


Fig. 4.24 Variation of peak stress,  $\sigma_p$ , with absolute temperature,  $T$ , at different strain rates for the 0.65% C steel

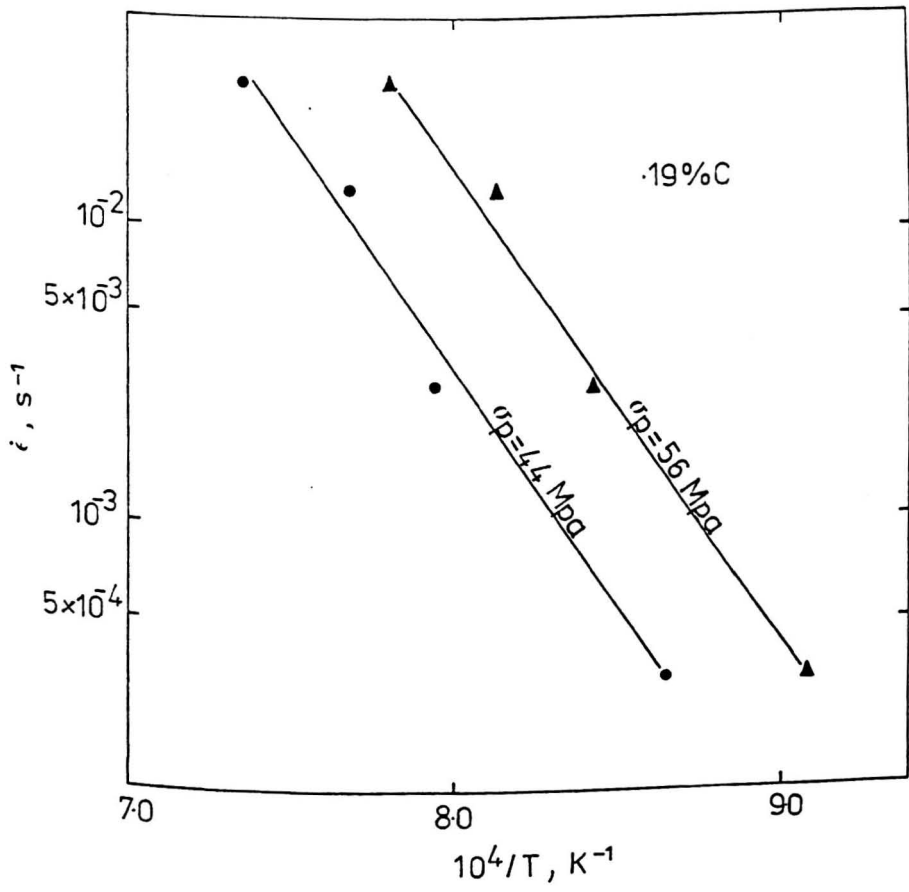


Fig. 4.25 Plot of strain rate,  $\dot{\epsilon}$ , against  $1/T$ , where  $T$  is the absolute temperature for the 0.19%C steel

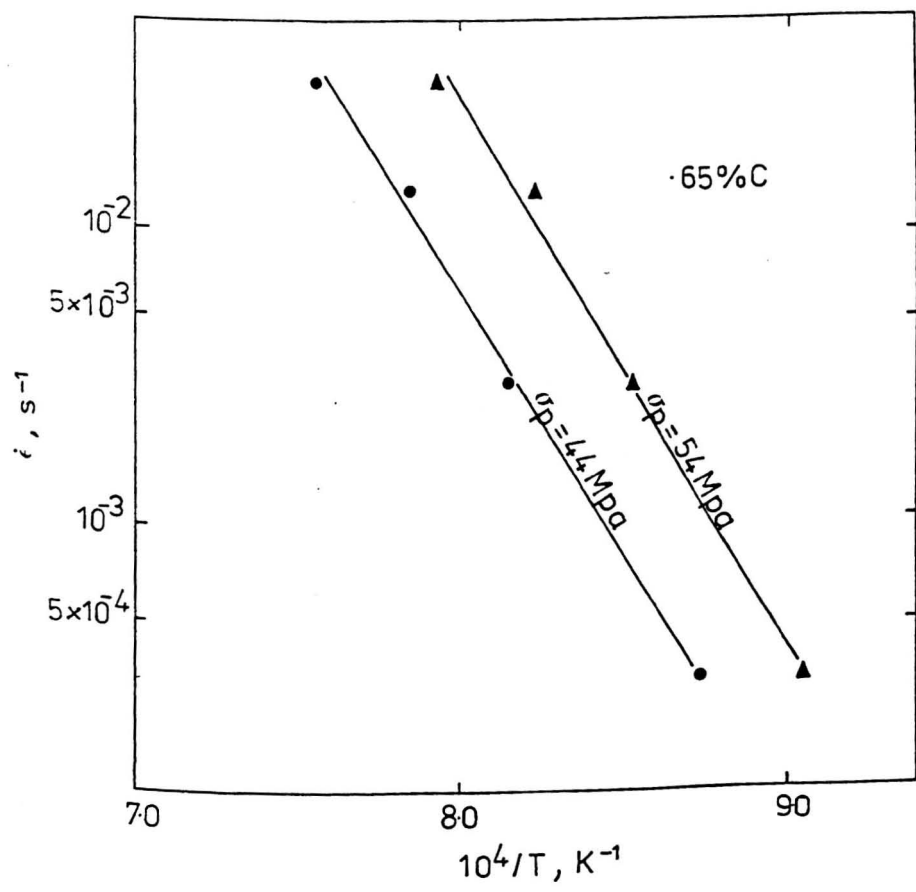


Fig. 4.26 Plot of strain rate,  $\dot{\epsilon}$ , against  $1/T$ , where  $T$  is the absolute temperature for the 0.65% steel

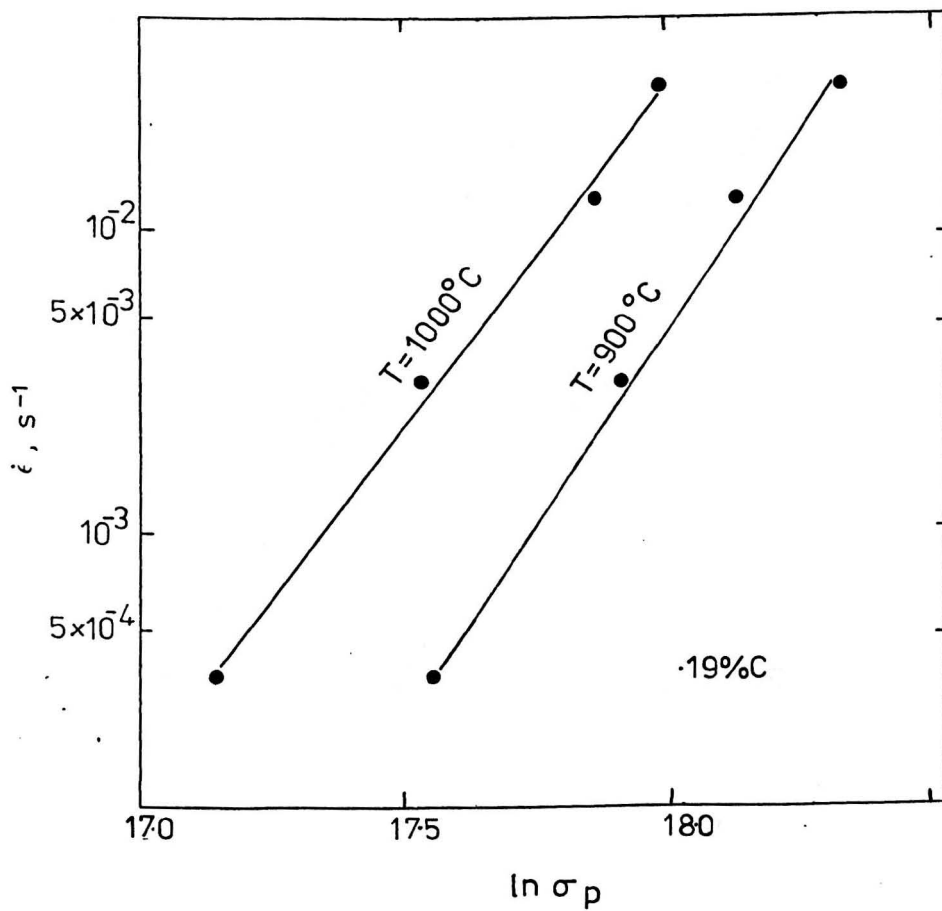


Fig. 4.27 Plot of  $\ln \dot{\epsilon}$  against  $\ln \sigma_p$  for the 0.19% C steel.

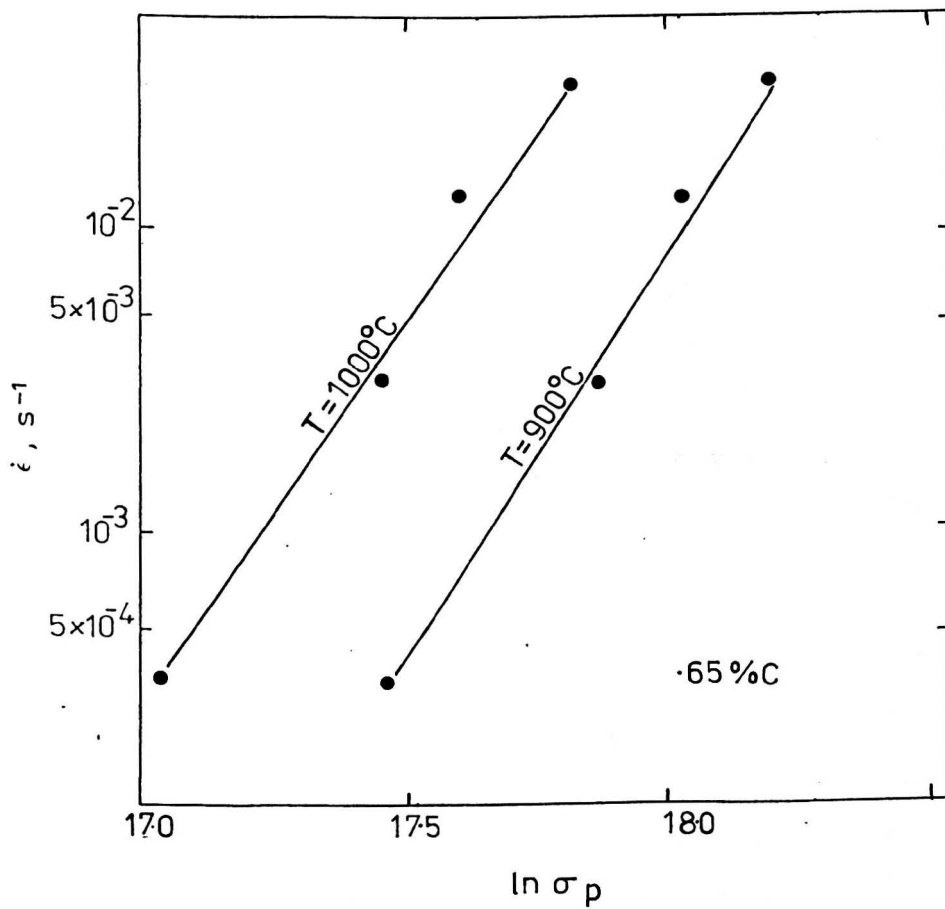


Fig. 4.28 Plot of  $\ln \dot{\epsilon}$  against  $\ln \sigma_p$  for the 0.65% C steel.

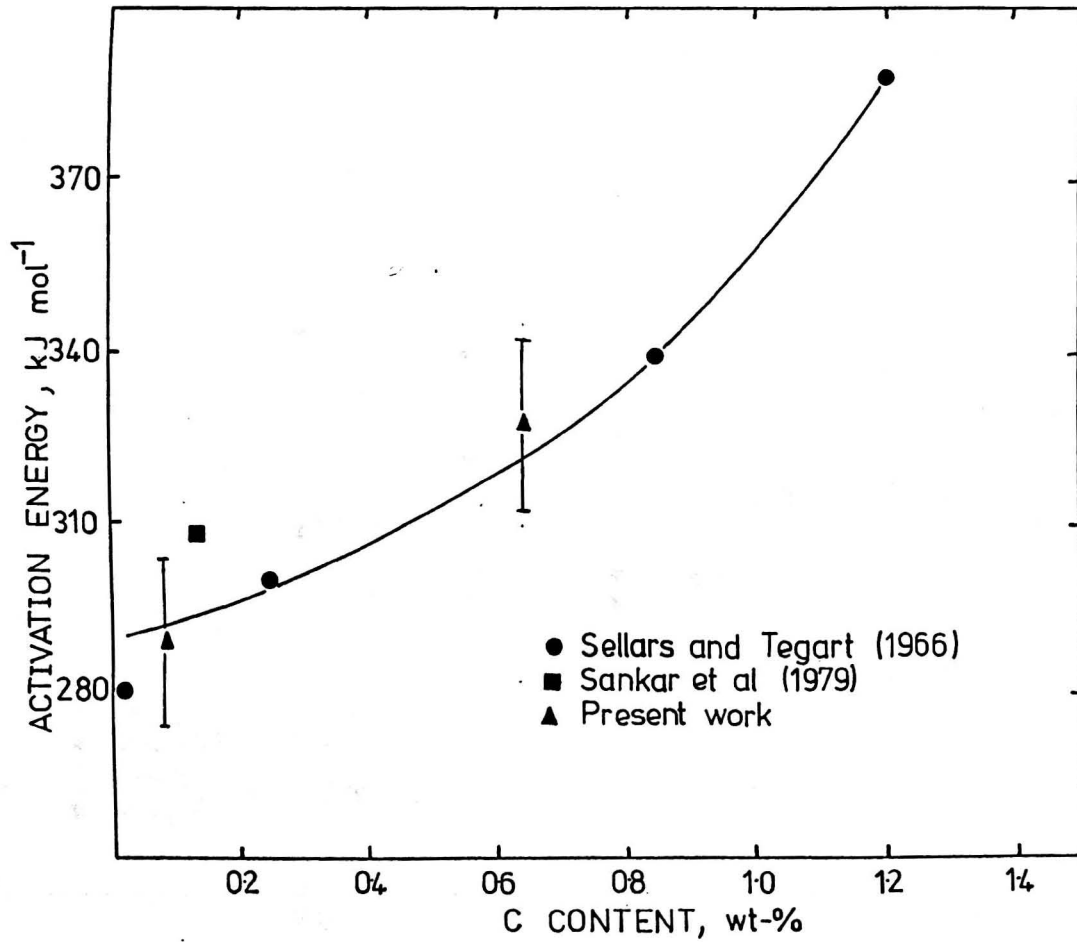
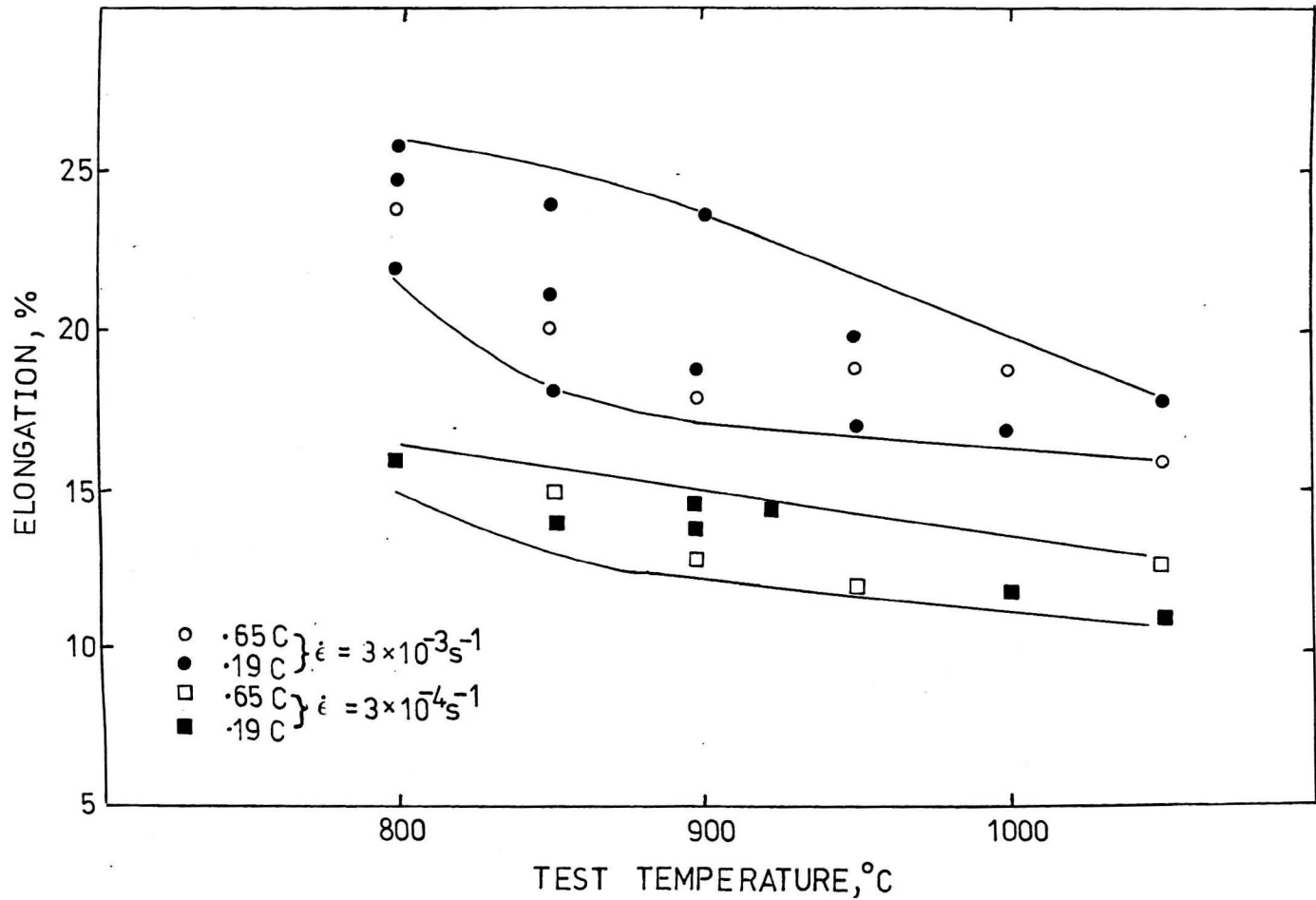


Fig. 4.29 Variation of activation energy for deformation with C content



**Fig. 4.30** Sample elongation at peak stress for the 0.19% C steel, and for the 0.65% C steel, at different temperature and strain rates.

## CHAPTER 5

### The Influence of Grain Size on the Hot Ductility of C-Mn steels

## 5.1 INTRODUCTION

Extensive studies in the field of creep have generally shown that high temperature ductility increases with decreasing grain size. (Bywater and Gladman, 1976; H.E. Evans, 1969; Katumba Rao et al 1975; Reynolds and Gladman, 1980) Similarly hot ductility in tensile testing is improved with refinement in grain size, the ultimate situation being reached in those alloys which give super plastic behaviour at ultra-fine grain sizes. In the case where failure is intergranular, the beneficial effect on ductility of refining grain size in creep tests is believed to be due to either a decrease in the grain boundary sliding rate or more likely the difficulty in propagating grain boundary cracks formed on sliding through triple points. (Bywater and Gladman, 1976; Kutumba Rao et al, 1975). It has also been suggested that the crack aspect ratio which controls the stress concentration at the crack tip will be higher in coarse-grained materials, and encourage crack propagation (Kutumba Rao et al, 1975).

In the case of micro-alloyed steels, there has been little indication from hot tensile tests that grain size has any significant influence on hot ductility. Work by Carlsson (1964) and Ouchi and Matsumoto (1982) on C-Mn-Al and C-Mn-Nb-Al steels showed no influence of austenite grain size on hot ductility after brittle intergranular failures. However, Schmidt and Josefsoon (1974) have observed that in the straightening of hot, continuously cast strands, cracks are associated with coarse austenite grains and that such cracking is reduced when the formation of coarse austenite grains is prevented by the use of suitable secondary cooling patterns. Since many micro-alloyed steels are susceptible to transverse cracking during continuous

casting, it is important to define the role of grain size in controlling hot ductility. In order to do this, it is necessary to separate the effect on hot ductility of micro-alloying precipitates from that of grain size. Therefore, the influence of grain size on hot ductility in plain C-Mn steels needs to be established before progress can be made in establishing its influence on micro-alloyed steels, and this has formed the basis of this chapter, whilst micro-alloyed steels are investigated in the subsequent chapter.

The results of chapter 4 established that raising the carbon content changes the mode of intergranular fracture from failure along thin films of ferrite surrounding the harder austenite grains, to intergranular fracture caused by grain boundary sliding in the austenite. Because these two modes of fracture may be influenced differently by grain size, a low carbon and a high carbon steel investigated in the previous chapter were chosen for the present study.

## 5.2 EXPERIMENTAL

The compositions of the low, 0.19%C, and high 0.65%C steels are given in Table 5.2, being the same as those investigated in the previous chapter. Processing details are given in section 4.2. Tensile samples were machined from the plates with their axes parallel to the rolling direction. For the 0.19%C steel, hot ductility tests were carried out using the Instron equipment described in section 3.2.2, the dimensions of the samples used being shown in Fig. 3.4. The initial grain sizes prior to testing were varied by heating to temperatures of 925°C, 1070°C and 1220°C. After 15 minutes at one of these temperatures, the samples were cooled at  $10^{\circ}\text{C min}^{-1}$  to test temperatures in the range 650 to 925°C, and after holding for 15 minutes, strained to failure at a rate of  $3 \times 10^{-3} \text{ s}^{-1}$ . For the 0.65%C steel, tests were performed using the induction heating equipment described in section 3.2.3, with tensile sample dimensions given in Fig. 3.6. The temperatures used to produce a similar variation in initial grain size were 950, 1250 and 1330°C, and after holding for 5 minutes, the samples were cooled at  $60^{\circ}\text{C min}^{-1}$  to test temperature.

The results shown in Fig. 3.8 show that for similar strain rates, comparable results are obtained from both Instron and induction equipment, and so results from the 0.19%C steel and 0.65%C can be compared directly.

The austenite grain size prior to testing was established by simulating the heat treatments given to the tensile samples to achieve the various grain sizes and then cooling at a rate to give outlining by ferrite. In the case of the 0.19%C steel, the heat treatment given to samples prior to testing using the Instron were simulated on small samples which were then quenched.

In this way the presence and amount of ferrite prior to tensile testing could be determined. Rapid cooling could not be carried out on tensiles immediately after fracture using the Instron, so that the amount of ferrite present after deformation could not be deduced. However, some indication of the influence of deformation on transformation could be obtained from samples which had been cooled rapidly after the Gleeble testing performed in the previous chapter. The higher C steel was close to eutectoid composition, so that at the test temperatures used, intergranular fracture would always occur in the austenite. Fracture examinations were carried out using a JEOL T100 SEM. Some limited dilatometry work using a Theta dilatometer was also carried out on these steels to try and establish the  $A_{r3}$  temperature under the conditions used.

### 5.3 RESULTS

#### 5.3.1 Metallography

The austenite grain sizes corresponding to each reheating temperature for the .19%C steel and the .65%C are shown in Table 5.2. Grain sizes for the steels after reheating to 1330°C were taken from the results shown in Fig.4.5. For the .19% steel, grain size increased from 70 to 290  $\mu\text{m}$  as the reheating temperature increased from 925 to 1220°C. For the .65%C steel, grain size increased from 50 to 300  $\mu\text{m}$  as the reheating temperature increased from 950 to 1330°C.

Fig. 5.1 shows the variation of ferrite volume fraction with test temperature for grain sizes in the range 70 to 290  $\mu\text{m}$  for the .19%C. The rate of the  $\gamma \rightarrow \alpha$  transformation is progressively decreased as grain size increased. Fig. 5.1 also shows the precise determination of the  $A_{r3}$  temperature by metallographic techniques is difficult, due to the asymptotic nature of the curve, but the temperature for 1% transformation for all three grain sizes appear to be in the range 750 - 770°C. Calculated equilibrium temperatures for the .19%C steel using Andrews' formula (1965) gave values of 813 and 712°C for the  $A_{e3}$  and  $A_{e1}$  temperatures respectively. Examination of C extraction replicas taken from samples of the .19%C steel reheated to 925°C and a Gleeble sample reheated to 1330°C during the tests described in chapter 4, showed similar sulphide distributions, consisting of randomly distributed sulphides.

#### 5.3.2 Hot Ductility

The curves of percentage reduction in area against test temperature in the range 600 - 900°C for the 0.19%C steel for the three grain sizes are shown in Fig. 5.2. Also included in this figure is

the curve obtained in chapter 4 for the 0.19%C steel under Gleeble test conditions, i.e. reheated to 1330°C, and cooled to test temperature at 60°C min.<sup>-1</sup>.

In the case of the finer grained steels (70 and 180  $\mu\text{m}$ ), ductility started to fall markedly at temperatures below 775°C, and reached a minimum at 750°C. Ductility recovered rapidly as the test temperature is lowered further. In the case of the coarse grained material (290  $\mu\text{m}$ ), the ductility started to drop at 810°C, and minimum ductility occurred close to 800°C. For the Gleeble tested samples, ductility began to fall at a temperature of 800°C, reaching a minimum at 700°C. The minimum ductility value for the Gleeble tested samples was 35%, compared with about 55% for the finer grained, Instron tested material.

Fig. 5.3 shows the curve of reduction in area against test temperature for the 0.65%C steel at the three grain sizes (50, 180 and 300  $\mu\text{m}$ ). For the two finer grained materials, ductility remained good over the entire range of test temperature, whilst for the coarse grained material, low ductility failures occurred below test temperatures of 950°C.

### 5.3.3. Fractography

SEM fracture examinations have shown that the failure mode in the low ductility temperature range was always intergranular, and typical examples are shown in Fig. 5.4. The majority of intergranular fracture surfaces in the 0.19%C steel were of the intergranular microvoid coalescence type described in chapter 4, consisting of ductile dimples associated with MnS inclusions on the grain facets. The results of chapter 4 indicate that this fracture mode is usually associated with failure occurring in the thin ferrite film formed around austenite grains on trans-

formation. At test temperatures near the  $A_{e_3}$  temperature, occasional flat grain facets were observed, which are thought to be indicative of failure occurring in the austenite due to grain boundary sliding, as described in chapter 4.

The low ductility failure which occurred in the coarse grained 0.65% C steel were again intergranular, but of the intergranular decohesion type described in chapter 4 (see Fig. 4.18)

#### 5.4 DISCUSSION

The results of chapter 4 have confirmed the existence of a ductility trough associated with the  $\gamma$  to  $\alpha$  transformation in C-Mn steels and shown that altering the transformation temperature by varying the C content produces a corresponding shift in the position of the ductility trough. Coarsening the grain size would be expected to lower the transformation temperature, but there is little indication that changes in grain size have a corresponding effect on the position of the ductility trough. Indeed coarsening the grain size from 180 to 290  $\mu\text{m}$  raises the temperature at which ductility first starts to fall by 50°C, Fig. 5.2.

In the case of the two finer grained steels (70 and 180  $\mu\text{m}$ ), the temperature at which hot ductility began to fall corresponded fairly well to the  $A_r3$  temperature determined from Fig. 5.1.

Reference to Figs. 5.1 and 5.2 shows that at the minimum ductility temperature of 750°C, the finer grained material (70  $\mu\text{m}$ ) has 5% ferrite present prior to deformation, whilst the coarser grained material (180  $\mu\text{m}$ ) has 1% present. Full recovery of ductility below 750°C occurs when approximately 30% ferrite is present prior to deformation, and this increased volume fraction of ferrite, together with the decrease in strength difference between austenite and ferrite which occurs on lowering the temperature, (Wray, 1981) would be expected to reduce strain concentration at austenite grain boundaries as discussed in chapter 4.

In the case of the coarsest grained material examined, (290  $\mu\text{m}$ ), the ductility started to drop close to the calculated equilibrium temperature of 813°C, and minimum ductility occurred close to 800°C, Fig. 5.2. From an examination of Fig. 5.1, it is reasonable to suggest that the  $A_r3$  temperature for this steel was about 720°C.

It therefore seems likely that for this grain size, deformation can raise the transformation temperature at the boundaries so that it is possible for ferrite to be formed at high temperatures, giving rise to a much extended ductility trough.

Unfortunately, the Instron testing arrangements did not allow rapid quenching of samples after failure so the presence of ferrite after deformation could not be determined. However, the Gleeble tests of chapter 4 involved rapid cooling after testing which enabled ferrite formed during deformation to be detected. The same steel, when cooled rapidly to the test temperature from 1330°C so that the  $A_{r3}$  temperature was lowered to 697°C (using a Theta dilatometer) gave an extended ductility trough, Fig. 5.2. The austenite grain size prior to deformation in this case was coarse (350  $\mu\text{m}$ ) and examination of samples fast cooled after fracture showed the presence of thin films of the softer ferrite phase surrounding the austenite grains at temperatures well in excess of the  $A_{r3}$ . Evidence for deformation induced ferrite was found for temperatures up to 800°C. It therefore appears that in coarse grained material, deformation induced ferrite can have a considerable influence widening the hot ductility trough. At the coarser grain sizes it seems that deformation can raise the  $A_{r3}$  temperature to almost the  $A_{e3}$ . Because of this, the portion of the hot ductility curve between A and B in Fig. 5.2 is not significantly influenced by the large change in  $A_{r3}$  which takes place on altering the cooling conditions.

These results would seem to indicate that in the finer grained steels, (70 and 180  $\mu\text{m}$ ) deformation between the  $A_{e3}$  and  $A_{r3}$  temperatures has little influence on the position of the ductility

trough.

Possible reasons for this are (a) the high surface area/volume ratio of the grains reduced the local deformation at the boundaries so that it is insufficient to produce ferrite, (b) the ferrite films produced are discontinuous thus not allowing easy crack linkage, or (c) nucleation sites are so numerous in the fine grained steel that deformation has little influence in providing extra sites. Certainly the ferrite formed in coarse grained material tends to grow along the  $\gamma$  boundaries and as a consequence only a very small amount is required to produce a continuous network and this can be compared to finer grained materials where growth is more equiaxed, Figs. 5.5 and 5.6 respectively.

In order to substantiate that hot ductility was not being influenced by deformation at finer grain sizes, the finest grained (70  $\mu\text{m}$ ) steel was given slightly faster cooling to test temperature (15°C/min.) and tested immediately to failure on the Instron, Fig. 5.7.

The ductility trough moved to lower temperatures by 30° to 40°C in accord with the change in the  $A_{r3}$  temperature as measured by the Theta dilatometer (Fig. 5.7). This contrasts with the behaviour of the coarse grained material where ductility at the high temperature end of the trough did not alter even though marked changes in the  $A_{r3}$  were noted, Fig. 5.2.

The high carbon steel behaves in a fundamentally different manner to the low carbon steel as described in chapter 4. In this chapter, it was shown that raising the C content in a coarse grained steel causes intergranular failure to occur by grain boundary sliding in the austenite, and not, as with low C steels, on phase transformation. Raising the C level was found to increase

the activation energy for dynamic recrystallization and hence encourage more grain boundary sliding and crack linkage. However, the results of Fig. 5.3 show that low ductility, intergranular failures only occur in the coarsest grained material, and the finer grained materials fail with high ductilities. As already mentioned refining the grain size would be expected to make it more difficult for cracks to move through the triple points as well as reducing the crack aspect ratio giving rise to a lower stress concentration. Whether failure occurs at high temperatures in the austenite or at lower temperatures on transformation is very finely balanced and just as changes in C content can have an influence on the fracture mode, so grain size can have a similar powerful effect.

In addition to extending the width of the ductility trough, there is also evidence to suggest that increasing the grain size increases the depth of the trough. For the low C steel increasing grain size from 350  $\mu\text{m}$  reduced the minimum ductility value from 57 to 35% reduction of area whilst for the higher C steel a similar change in grain size produced a change in the reduction of area from 95 to 37%. Similar behaviour has been noted by Carlsson et al (1980) for intergranular failure in the austenite of 17Cr-17Ni-4.5Mo stainless steel tested in the temperature range 950° to 1050°C.

The reduction of area values obtained at a particular temperature are dependent on strain rate, carbon content and grain size and all of these variables alter the position and extent of the hot ductility trough.

It should be noted however, that whereas C content influences the extent and position of the ductility trough, but not minimum reduction of area values, (see Fig. 4.2 from chapter 4), grain

size also influences the minimum value of reduction of area associated with intergranular failures. The minimum reduction of area values for the temperature range 700° to 1000°C are plotted against grain size in Fig. 5.8. Included in this curve are results from previous examinations on plain C-Mn and C-Mn-Ti steels. (Mintz et al, 1980) The latter steels have been included because although precipitates are present in these steels, they have been shown to be randomly distributed and are not situated at the austenite grain boundaries. In addition, the 0.19%C steel after normalising was heated directly to temperatures in the range 700° to 950°C, held for 15 minutes at temperature and then tested to failure at the same strain rate of  $3 \times 10^3 \text{ s}^{-1}$  using the Inston equipment. It can be seen from Fig. 5.9 that there is little evidence of a ductility trough and although grain size increased with temperature in the range normally associated with low ductility (700 to 900°C), the austenite grain size was fine, being approximately 30  $\mu\text{m}$ . These results suggest that ductility for the strain rate examined will always be very high for plain C-Mn steels in the temperature range 700° to 1000°C if grain size can be kept below 50  $\mu\text{m}$ . Steels with grain sizes which are typical of continuously cast steel ( - 700  $\mu\text{m}$ ) would, when tensile tested in this temperature range, always have low minimum ductility values (<30% reduction of area) with associated intergranular failures.

## 5.5 CONCLUSIONS

1. Refining the grain size is beneficial to hot ductility as it reduces the width of the ductility trough and increases the minimum reduction of area values.
2. The temperature for the start of the ductility trough in a fine grained 0.19%C plain C-Mn steel corresponds approximately to the  $Ar_3$  temperature. Recovery in ductility quickly occurs on lowering the test temperature due to the introduction of a greater volume fraction of ferrite at the  $\gamma$  grain boundaries and by reducing the relative strength difference between the  $\gamma$  and  $\alpha$ . Coarsening the grain size causes the temperature for the start of the ductility trough to increase up to the  $Ae_1$  temperature due to the production of long thin films of deformation induced ferrite round the  $\gamma$  grain boundaries. Because of this a much extended trough is produced.
3. Refining the grain size in the higher C-Mn steels (0.65%) has even more marked effect in improving hot ductility. Low ductility intergranular failure occurs in coarse grained high C-Mn steels by grain boundary sliding in the  $\gamma$ . Refining the grain size prevents this taking place and ductility can be kept high to temperatures as low as 700°C, the lowest testing temperature examined.

C	Si	Mn	P	S	N	Ni	Cr	Mo
.19	0.20	1.50	.002	.013	.004	.04	.03	.02
.65	0.28	1.40	.002	.003	.005	NV	NV	NV

Table 5.1 Compositions of the steels examined, (wt.%)

NV = no value

Reheating Temperature °C	925	950	1070	1220	1250	1330
Grain size, $\mu\text{m}$ , 0.19%C	70	-	180	290	-	350
Grain size, $\mu\text{m}$ , 0.65%C	-	50	-	-	180	300

Table 5.2 Variation of austenite grain size with reheating temperature for both steels.

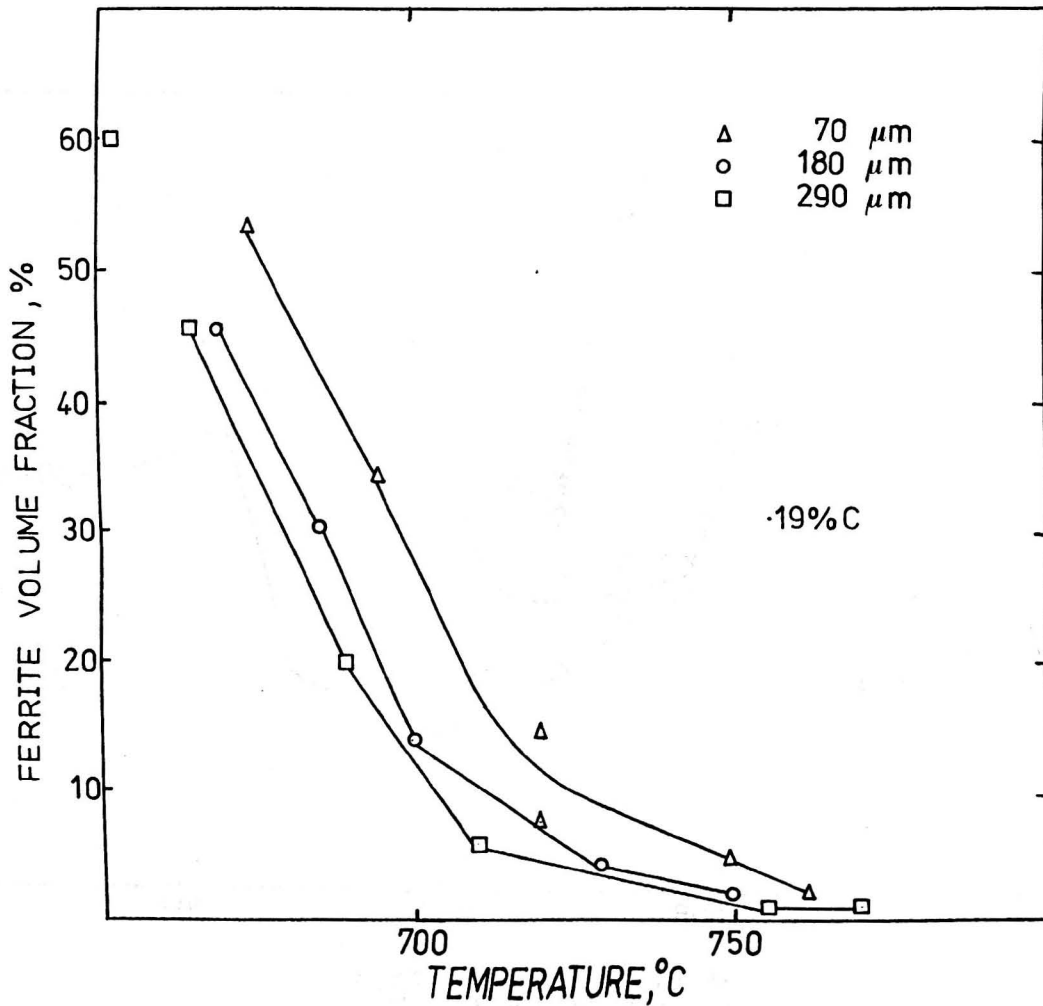


Fig. 5.1 Ferrite volume fraction after quenching small samples of varying initial grain size from various temperatures, .19%C steel.

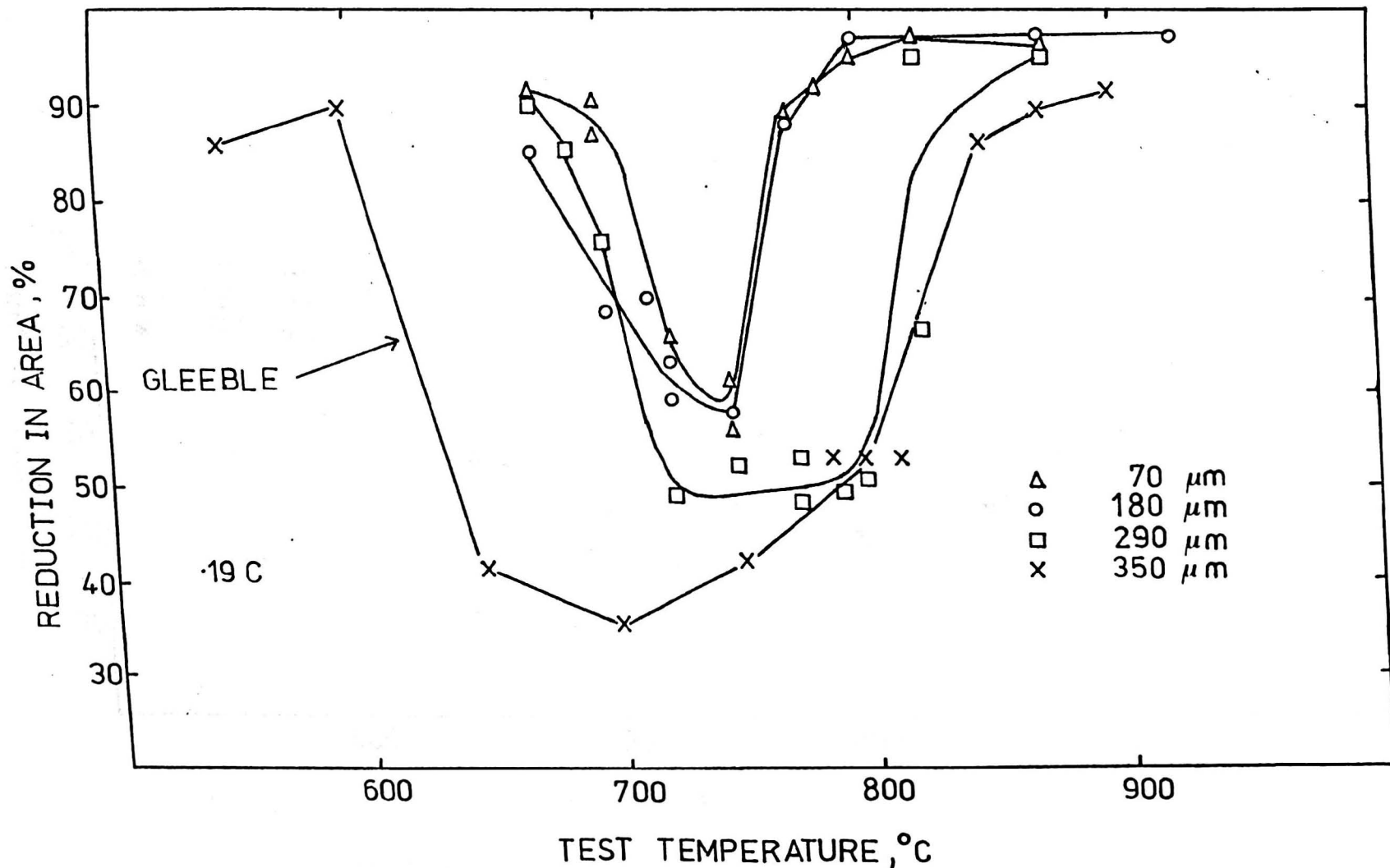


Fig. 5.2 Hot ductility curves for the .19% steel after reheating to various temperatures to produce grain sizes in the range 70 - 210  $\mu\text{m}$  prior to testing. Also included are the Gleeble test results of chapter 4.

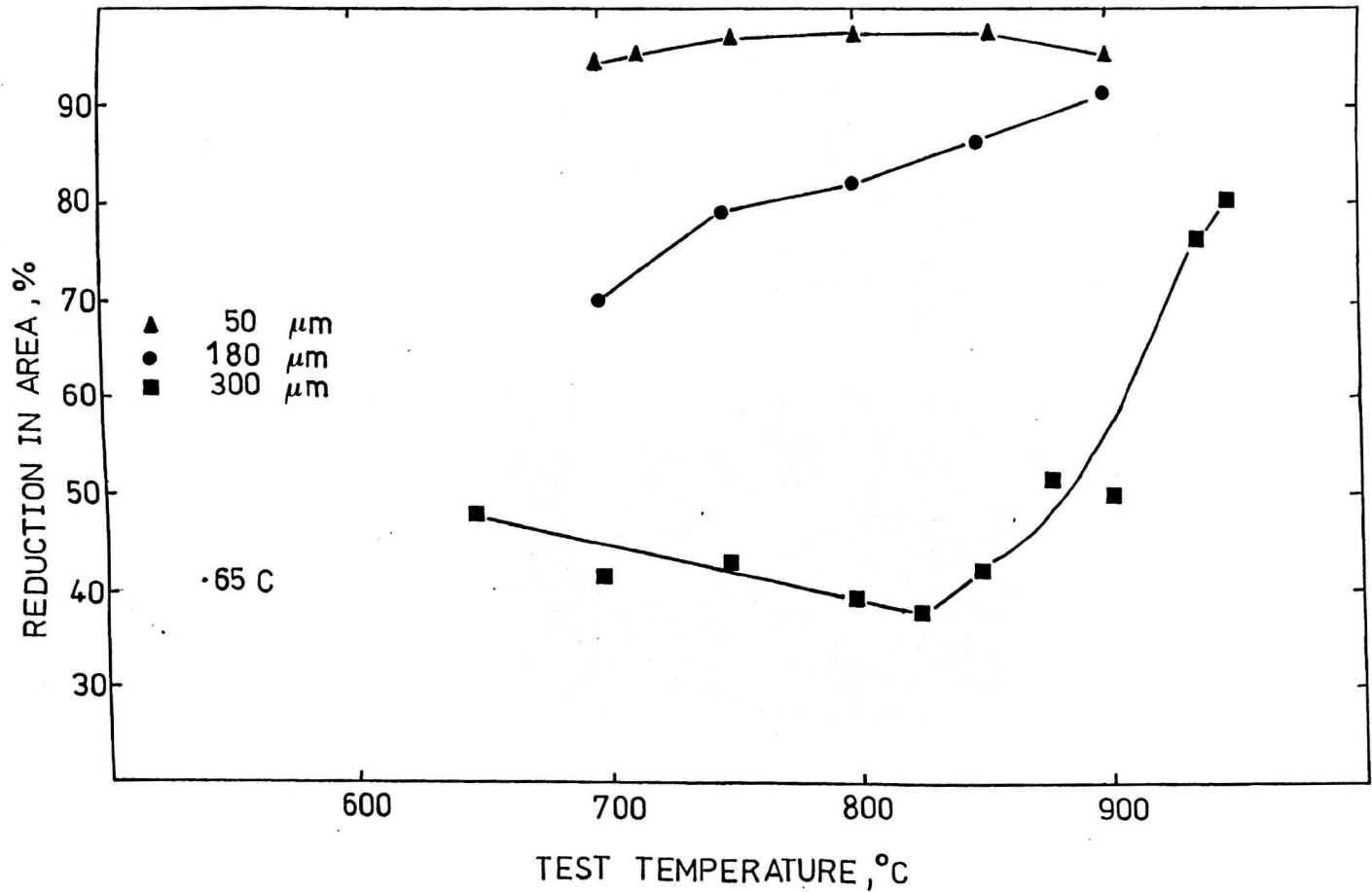
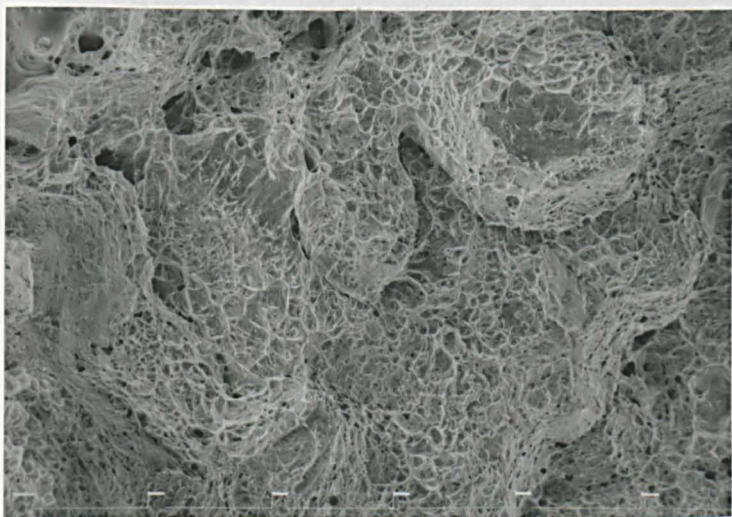


Fig. 5.3 Hot ductility curves for the .65% C steel after reheating to various temperatures to produce grain sizes in the range 50-30 μm prior to testing.



100  $\mu\text{m}$

Fig. 5.4

Intergranular fracture showing microvoids on grain facets, grain size  $290 \mu\text{m}$ , test temperature  $750^\circ\text{C}$ .

200  $\mu\text{m}$

Fig. 5.5

Form of grain boundary ferrite in  $70 \mu\text{m}$  grain size steel, prior to testing at  $750^\circ\text{C}$ .

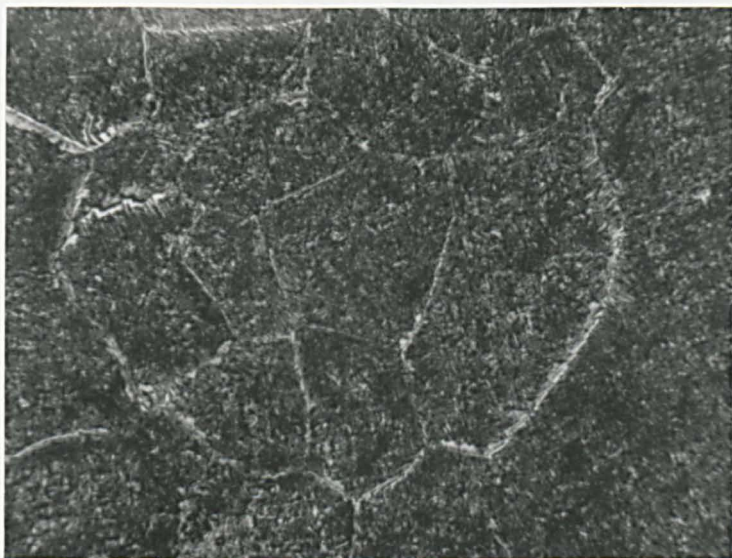


Fig. 5.5

Form of grain boundary ferrite in 290  $\mu\text{m}$  grain size steel, prior to testing at 750°C.



Fig. 5.6

Form of grain boundary ferrite in 70  $\mu\text{m}$  grain size steel, prior to testing at 750°C.

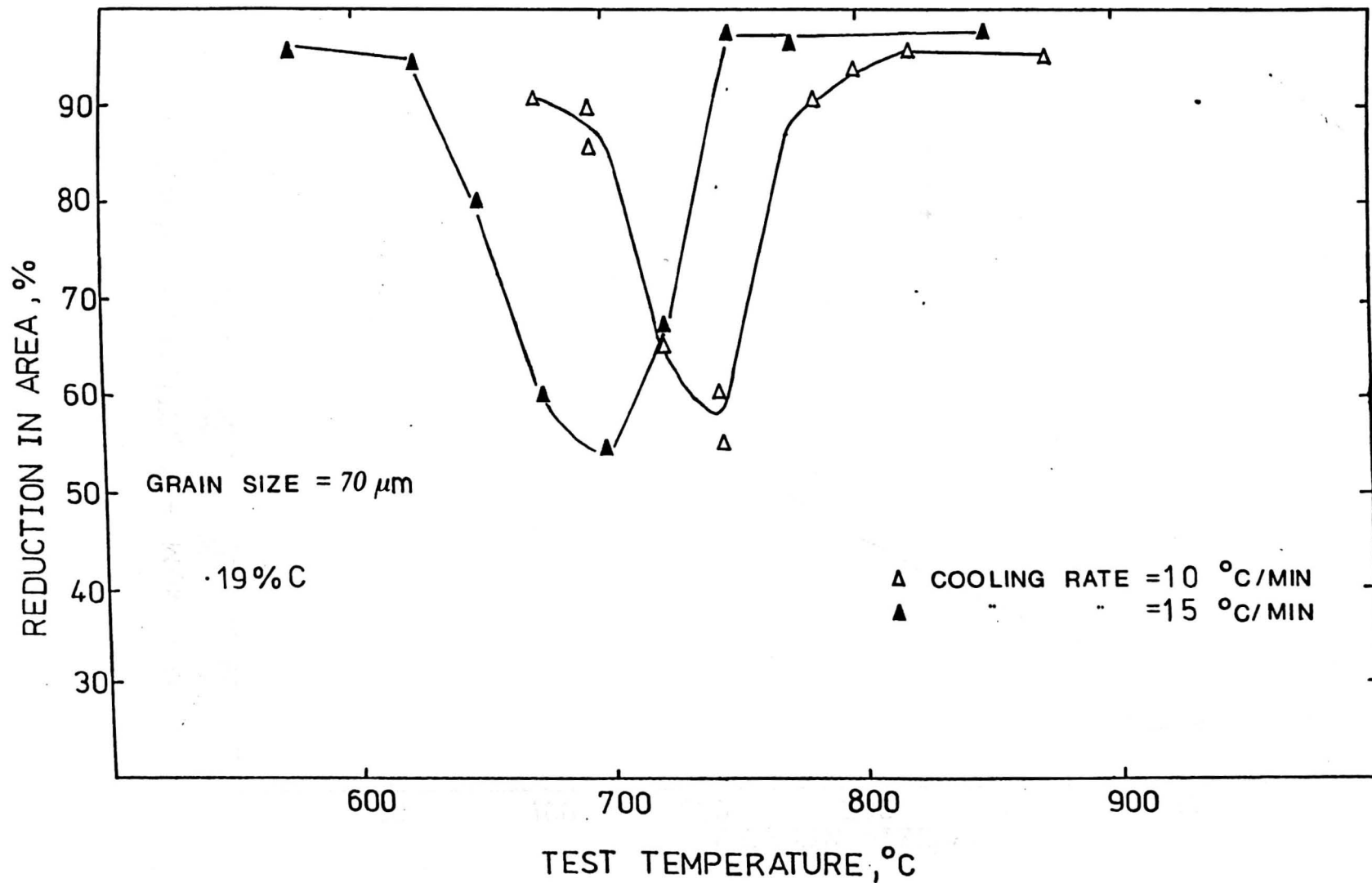


Fig. 5.7 Hot ductility curves for the .19% C steel following heating to 925 $^{\circ}\text{C}$  and cooling at either 10 $^{\circ}\text{C}/\text{min}$  or 15 $^{\circ}\text{C}/\text{min}$ . to test temperature.

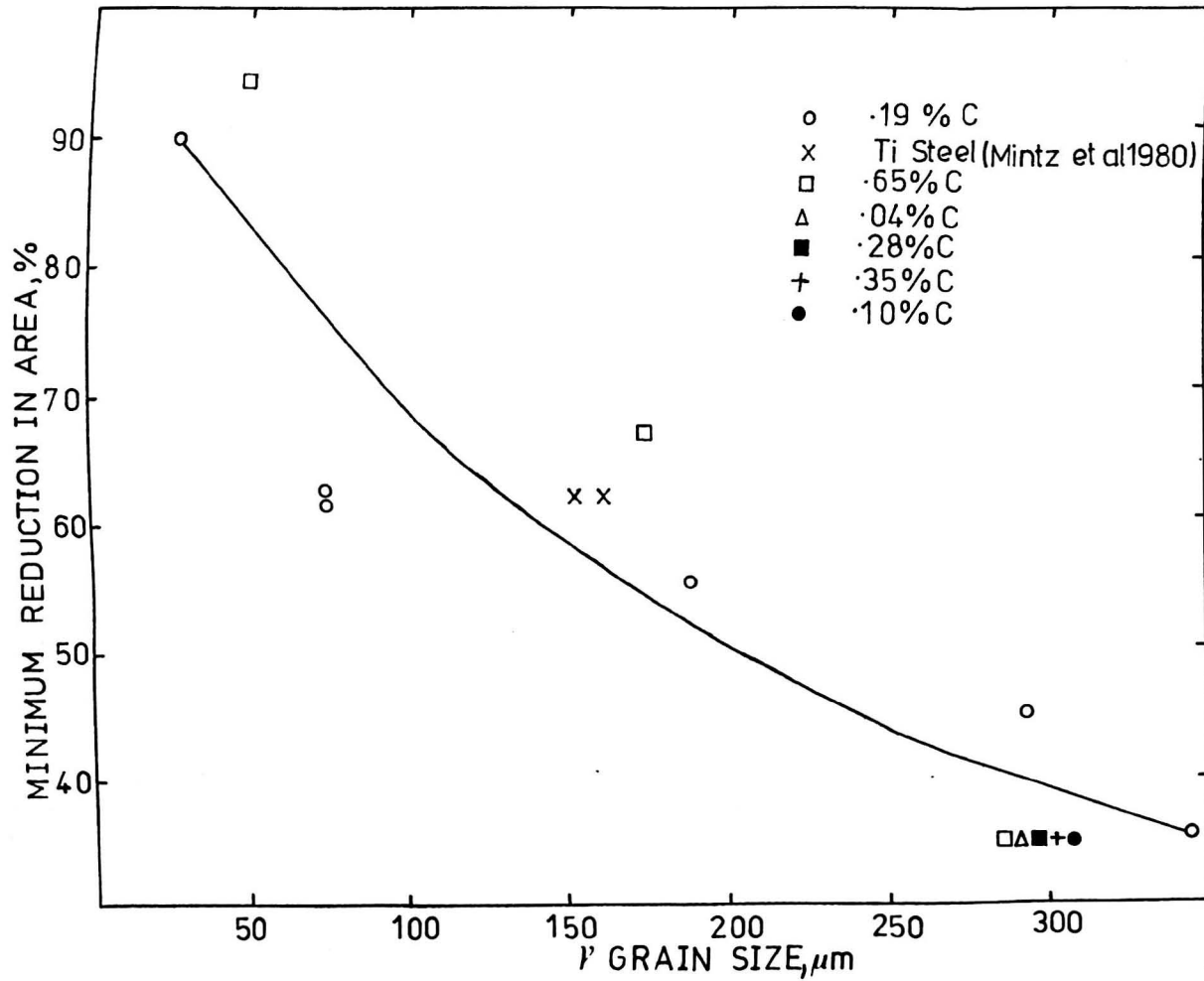


Fig. 5.8 Variation of minimum reduction in area values with austenite grain size following testing in the range 700 - 1000°C.

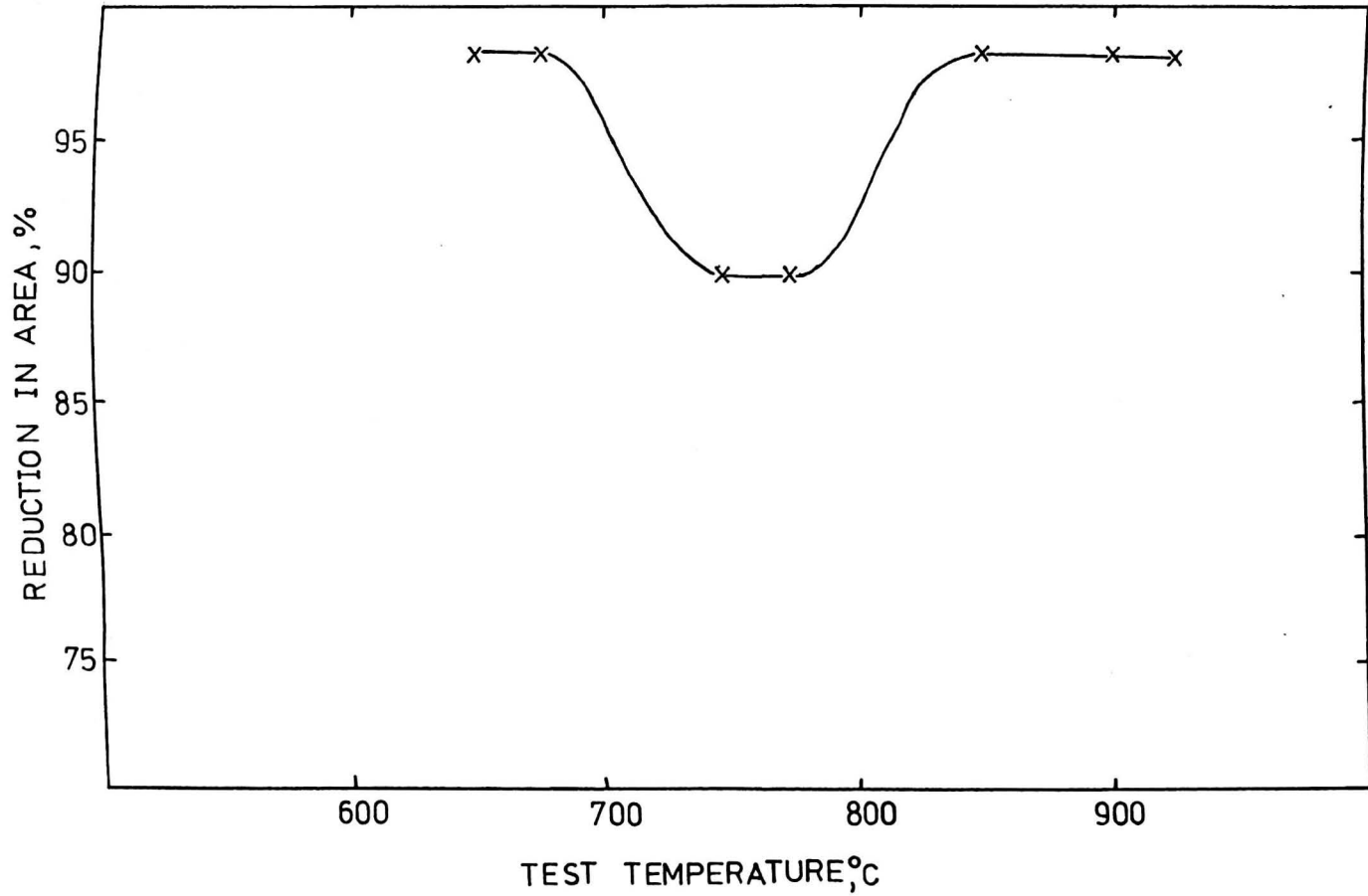


Fig. 5.9 Hot ductility curve for the .19%C steel after normalising and heating directly to test temperature.

## CHAPTER 6

### The Influence of Grain Size on the Hot Ductility of the Micro-Alloyed steels

## 6.1 INTRODUCTION

In section 2.6, the influence of grain size on creep ductility, and on hot tensile test ductility, was described, and it was also noted that grain size could influence the transverse cracking of continuously cast slab, coarse austenite grains promoting cracking. (Schmidt and Josefsson, 1974). In chapter 5, the influence of austenite grain size on the hot ductility behaviour of two C-Mn steels of differing C contents was investigated, and it was shown that increasing grain size generally has a detrimental effect on hot tensile ductility, and can produce increases in both the width and the depth of the ductility trough. However, such plain carbon steels are not usually susceptible to transverse cracking, and it is micro-alloyed steels which are most prone to this type of defect. Few reports have been made of the influence of grain size on the hot ductility of micro-alloyed steels, (Carlsson, 1964; Ouchi and Matsumoto, 1982), and these have concluded that grain size has little influence on hot ductility. The major problem in such studies has been in distinguishing between the effects of grain size and precipitation on hot ductility, as precipitation and grain size are often closely related. In this chapter the influence of grain size on the hot ductility of C-Mn-Al, C-Mn-V-Al and C-Mn-Nb-Al will be investigated, and compared with the behaviour of one of the C-Mn steels investigated in chapter 5. Hot tensile tests will be performed only in the single phase austenitic state.

## 6.2 EXPERIMENTAL

The compositions of the steels examined are given in Table 6.1. The steels were cast as 50 kg vacuum melts, and hot rolled to 37 mm plate, finish rolling 1050°C. Tensile samples, shown in Fig. 3.6 were machined from the plate with their tensile axes parallel to the plate rolling direction, having gauge length 80 mm and diameter 7.9 mm. These samples were then tested using the induction heating equipment described in section 3.2.3 To produce a wide range of austenite grain sizes prior to testing, each sample was reheated to temperatures in the range 850 - 1360°C, and held for 5 minutes. The samples were then cooled to a test temperature of 850°C at a rate of 60°C/min., and held for 5 minutes prior to straining to failure at a rate of  $3 \times 10^{-3} \text{ s}^{-1}$ . Fractured samples were then prepared for metallographic and SEM examination. Carbon extraction replicas were taken from -1 mm behind the fracture surface, and in some cases, carbon extraction replicas were taken directly from the fracture surfaces. To determine austenite grain sizes prior to deformation, small samples were heat treated in a muffle furnace to simulate the thermal cycle of the tensile samples. After solution treatment, these samples were cooled at a rate sufficient to produce ferrite outlinement of austenite grain boundaries. Grain sizes were measured from these samples using the linear intercept method, counting approximately 100 grains.

In the present study, it was very important to distinguish between the effects on hot ductility of grain size, and of precipitation, and therefore, it was important to determine the solution temperature for the appropriate precipitate in each steel. Equilibrium solubility calculations are not entirely reliable for the present study, due to the short reheating times used. Solubility

temperatures were therefore determined using the method of loss of secondary hardening potential. Small samples were heated using a muffle furnace to reheating temperatures in the range 850 - 1360°C, quenched in iced brine, and then tempered for one hour at 600°C. The hardness of the samples was taken as the mean of 10 readings from a Vickers Dp machine using a 20 kg load. This method proved successful in determining the solution temperature of the C-Mn-Nb-Al and C-Mn-V-Al steels, and the results are described in the subsequent section. However, for the C-Mn-Al steel, no changes in hardness were observed on tempering, and so an alternative method was used to determine the solubility of AlN. Small samples of the C-Mn-Al steel were heated in a muffle furnace to various reheating temperatures, and then quenched into iced brine. Carbon extraction replicas were then taken from the small samples, and then solubility temperatures determined from the presence or absence of AlN.

## 6.3 RESULTS

### 6.3.1 Hot Tensile Tests and Metallography

Fig. 6.1 shows the influence of reheating temperature on the austenite grain size for all 4 steels. The C-Mn steel shows a continual increase in austenite grain size with temperature, from a grain size of 70  $\mu\text{m}$  at 925°C to 300  $\mu\text{m}$  at 1330°C. The C-Mn-Al, C-Mn-V-Al and C-Mn-Nb-Al steels all show a temperature range over which grain size is approximately constant at 30  $\mu\text{m}$  for each steel. Above a temperature of 1050°C, grain coarsening commences for these three steels, until at a reheating temperature of 1360°C, grain sizes were in the range 250 - 350  $\mu\text{m}$ .

Fig. 6.2 shows the influence of reheating temperature on the hot ductility of all 4 steels at a test temperature of 850°C. The C-Mn steel shows excellent hot ductility for all the reheating temperatures investigated. For the C-Mn-Al steels, reduction in area values rose from 65% at 850°C to 96% at 1100°C, and remained at - 96% for reheating temperatures up to 1360°C. The reduction in area values for the C-Mn-V-Al steel increased from 66% for the sample heated to 850°C, to 75% for the sample reheated to 950°C. As the reheating temperature was raised above 950°C, reduction in area values fell continuously, reaching 50% at a reheating temperature of 1360°C. For the C-Mn-Nb-Al steel, reduction in area values increased from 52% at 850°C to 80% at 1100°C. As the reheating temperature was increased further, reduction in area values fell continuously reaching 26% at 1360°C.

The hot ductility results of Fig. 6.2 are replotted in Fig. 6.3 to show the variation of reduction in area with austenite grain size, the grain size for a particular reheating temperature being obtained from Fig. 6.1.

Load elongation curves for the C-Mn-Al, C-Mn-V-Al and C-Mn-Nb-Al

steels are shown in Figs. 6.4 - 6.6. Some of these curves show an abrupt drop in load as deformation proceeds, distinct from that normally associated with the onset of sample necking. Similar load-elongation curves have been observed during hot tensile tests by Wray and Holmes (1975) and by Wilcox (1982), and are attributed to the onset of dynamic recrystallization. Thus it is sometimes possible by examination of the load elongation curves, to determine whether dynamic recrystallization has occurred before fracture. In some cases, however, the form of the load-elongation curve makes it difficult to state unambiguously whether recrystallization has occurred or not. The temperature range over which dynamic recrystallization occurs before fracture for each steel is shown in Fig. 6.3. For the C-Mn steel, dynamic recrystallization occurred prior to fracture in all tests. Similarly for the C-Mn-Al steel, dynamic recrystallization occurred prior to fracture in all tests, with the exception of the sample heated directly to 850°C. For the C-Mn-V-Al steel, recrystallization did not occur in samples reheated to 1300°C or above prior to testing at 850°C. At reheating temperatures below 1300°C, it was not possible to determine unambiguously whether dynamic recrystallization had occurred for this steel. For the C-Mn-Nb-Al steel, only the sample reheated to 1100°C prior to testing showed evidence of recrystallization (Fig. 6.6).

SEM fractography revealed three distinct fracture modes, high temperature ductile rupture (HTDR), intergranular decohesion (ID), and intergranular microvoid coalescence (IMC). These three fracture modes were also observed in the plain carbon steels examined in chapter 4. However, it should be noted that whilst in C-Mn steels, the IMC fracture mode seems to be associated with pro-eutectoid ferrite films at austenite grain boundaries, in micro-alloyed steels,

this fracture mode can occur in single phase austenitic structures. Fig. 6.7 shows the temperature range over which each fracture mode occurs for all four steels. The C-Mn steel shows HTDR for all reheating temperatures. The C-Mn-Al steel shows HTDR for all tests, except the sample heated directly to 850°C and tested. This fracture has also been classed as ID, but appears radically different to other ID failures, because of the very fine grain size of this steel. The C-Mn-V-Al shows predominantly ID for reheating temperatures greater than 1250°C. For reheating temperatures below 1250°C, the fracture mode is mixed HTDR and ID. The C-Mn-Nb-Al steel shows the ID failure mode for all the samples tested, except that reheated to 1100°C prior to fracture, which showed HTDR. For reheating temperatures greater than 1250°C, regions of the IMC fracture mode were present, but ID was the predominant fracture mode. Figs. 6.8 - 6.9 shows examples of each fracture mode. For the C-Mn-Nb-Al steel, carbon extraction replicas were taken directly from the fracture surfaces of samples which had failed in an intergranular manner after reheating to 1330 and 1360°C. Those replicas showed a random precipitation of NbCN on the grain facets, Fig. 6.10.

Examination of carbon extraction replicas taken from transverse sections of the fractured samples revealed no precipitation in any of the fractured C-Mn samples, or in samples of the C-Mn-Al steel reheated above 1000°C. However, the C-Mn-Al samples reheated to 850 and to 1000°C showed extensive AlN precipitation at the austenite grain boundaries, and also some intragranular precipitation. (Figs. 6.11 - 6.12).

For the C-Mn-V-Al steel heated directly to 850°C, grain boundary and matrix precipitation of V(CN) was observed, and also present were large angular platelets of AlN, which were randomly distributed.

(Fig. 6.13). Samples of this steel heated to 1050°C and above prior to testing at 850°C showed only V(CN) precipitates, and no AlN. (Fig. 6.14) These VCN precipitates were generally randomly distributed, although occasionally these precipitates outlined grain boundaries.

In the C-Mn-Nb-Al steel heated directly to 850°C and tested, replica examination revealed extensive precipitation of NbCN and AlN at austenite grain boundaries, and within the grains (Fig. 6.15). The sample reheated to 1100°C prior to testing at 850°C showed no grain boundary precipitation, but a coarse random distribution of NbCN (Fig. 6.16), and no AlN precipitation. The samples reheated to temperatures in the range 1200 to 1360°C all displayed similar precipitation patterns after fracture at 850°C. Extensive fine precipitation of NbCN was observed at austenite grain boundaries and within the grains themselves. (Fig. 6.17)

### 6.3.2. Determination of Solution Temperatures

Fig. 6.18 shows the influence of reheating temperature on the hardness of the C-Mn-Nb-Al steels after quenching from the reheating temperature and tempering at 600°C for one hour. Hardness remains constant at VH.230 for reheating temperatures of 1050°C and less, and gradually increases to VH.295 as the reheating temperature is increased to 1150°C. Hardness remains constant at VH.295 as the reheating temperature increases from 1150 to 1360°C. The interpretation of these results relies on the assumption that only Nb(CN) formed during tempering at 600°C makes a significant contribution to the secondary hardening of the steel, and thus the greatest secondary hardening occurs when all the Nb is in solution at the reheating temperature. Using this assumption, the hardness values in Fig. 6.18 can be

interpreted as follows: up to reheating temperatures of 1050°C, little Nb is in solution, and hence not available to cause secondary hardening during tempering; between reheating temperatures of 1050 and 1150°C, the amount of Nb in solution rises rapidly and leads to an increase in hardness on tempering; at reheating temperatures of 1150°C and above, all the available Nb is in solution, and produces the maximum secondary hardening. Therefore, the results of Fig. 6.18 indicate that 5 minutes at reheating temperatures greater than 1150°C is sufficient to dissolve all the Nb in the C-Mn-Nb-Al steel.

To confirm this result, carbon extraction replicas were taken from a sample of the steel which had been reheated to 1150°C and quenched, and examination of the replicas revealed no precipitation of either NbCN or AlN.

In a similar fashion, the solution temperature of V(CN) in the C-Mn-V-Al steel was determined by examination of Fig. 6.18 which shows the hardness of samples quenched from various reheating temperatures, and then tempered for 1 hour at 600°C. These results indicated a solution temperature of 1110°C, and this was again confirmed by the examination of extraction replicas.

For the C-Mn-Al steel, examination of extraction replicas taken from samples quenched from various reheating temperatures indicated a solution temperature of approximately 1100°C.

#### 6.4 DISCUSSION

The C-Mn steel shows excellent hot ductility over a wide range of austenite grain sizes when tested at 850°C, and it is only in the two phase region that this steel shows a ductility trough, as detailed in chapters 4 and 5. When tested at 850°C, dynamic re-crystallization occurs before failure, leading to the isolation of developing grain boundary cracks, and hence producing high ductility failures. As described in chapter 4, the large voids apparent on the HTDR type fracture surfaces are grain boundary cracks, which developed prior to dynamic recrystallization, and were subsequently isolated from the grain boundaries, and distorted as deformation proceeded. The high ductility values obtained for the C-Mn steel irrespective of prior austenite grain size indicate that when the fracture mode is HTDR, grain size has no effect on ductility, as opposed to the quite marked effects on ductility which grain size has when the fracture mode is intergranular, as described in chapter 5. For reheating temperatures of 1100°C and above, the C-Mn and C-Mn-Al steels have similar hot ductility, and this is due to the complete dissolution of AlN at 1100°C, and the suppression of AlN precipitation on cooling to 850°C, owing to the fairly rapid cooling rate of 60°C/min. As mentioned in section 2.9.2 it is thought that for the precipitation of AlN to occur after solution treatment, cooling rates of less than 1°C/min. are required. Reheating temperatures of 1000 and 850°C are insufficient to dissolve all the AlN present, and so on cooling to 850°C, AlN is present prior to deformation in these samples. For the sample reheated to 1000°C, the relatively coarse distribution of AlN is not effective in retarding the onset of dynamic recrystallization, and high ductility failure results. For the sample heated directly to 850°C, the AlN

distribution produced is much finer, and delays the onset of dynamic recrystallization, allowing low ductility, intergranular failure to occur.

The C-Mn-V-Al steel heated to 850°C and tested directly has similar hot ductility to the C-Mn-Al steel tested after the same treatment, and again this is due to the delay of the onset of dynamic recrystallization due to the precipitation of V(CN) and AlN. The results of section 6.3 indicate that reheating at 1100°C for 5 minutes is sufficient to dissolve all the AlN and VCN. Replica examination also reveals that reheating above 1100°C produces a precipitate distribution which is independent on reheating temperature, consisting of a random distribution of V(CN), with occasional grain boundary precipitation AlN is not present due to the relatively fast cooling rates used after reheating. Therefore, for the C-Mn-V-Al steel, the gradual decrease in hot ductility with increasing reheating temperature is not due to a change in precipitate distribution, but is more likely to be caused by the increase in grain size.

For the C-Mn-Nb-Al steel, reheating to 1000°C prior to testing at 850°C, and testing directly on heating to 850, a precipitate distribution of NbCN and AlN is produced, which is sufficient to delay the onset of dynamic recrystallization until fracture has occurred. Reheating to 1100°C produces a coarse random distribution of NbCN, which is ineffective in retarding dynamic recrystallization, and hence high ductility failure occurs. Reheating to temperatures of 1200°C and above leads to complete dissolution of all the NbCN, and subsequent precipitation occurs prior to testing during cooling from the reheating temperature, or during the test. The fine distribution of NbCN formed at grain boundaries and within the grains themselves after reheating to

1200°C and above, retards dynamic recrystallization and allows low ductility, intergranular failures to occur. Precipitate distributions formed by reheating above 1200°C are independent of the reheating temperature, samples reheating to 1200 and to 1360°C both having similar precipitate distributions after testing at 850°C, (Fig. 6.17). Therefore, it appears likely that the small decrease in reduction of area values from 36% to 28% as the reheating temperature increases from 1200 to 1360°C is due to the change in austenite grain sizes as was the case for the C-Mn-V-Al steel. The foregoing results indicate that the hot ductility behaviour of this C-Mn-Nb-Al steel is dominated by the precipitation of NbCN and AlN, and that austenite grain size has a secondary influence on hot ductility, if intergranular failure occurs. Both the C-Mn-V-Al and the C-Mn-Nb-Al shows similar trends of decreasing hot ductility with increasing grain size, when the precipitate distribution remains constant. However, the reduction in area values of the C-Mn-Nb-Al are considerably lower than those of the C-Mn-V-Al steel, at any given reheating temperature. This is probably due to the grain boundary precipitation of NbCN, which restricts grain boundary migration, and hence allows grain boundary cracks to develop and grow; also the fine matrix precipitation of NbCN will concentrate strain at the grain boundaries more effectively than the coarser distribution of V(CN).

The foregoing results indicate that at least in C-Mn-V-Al and C-Mn-Nb-Al steels, increasing grain size has a slight, detrimental effect on hot ductility, although precipitation is the major factor. Creep studies have produced a number of suggestions as to the mechanism by which grain size influences ductility, as described in section 2. These include the retardation of grain

boundary crack propagation by triple points, possible increases in grain boundary sliding rates with increasing grain size, and the increase in stress concentration at the grain boundary crack tip with increasing grain size. However, the present study does not indicate which, if any, of the above mechanisms are responsible for the effect of grain size on hot ductility.

## 6.5 CONCLUSIONS

1. For a test temperature of 850°C and strain rate of  $3 \times 10^{-3} \text{ s}^{-1}$ , grain size has no influence on the hot ductility of an 0.19%C plain C-Mn steel. This is because dynamic recrystallization easily occurs at this temperature giving high reduction of areas and ductile fractures.
2. In the case of C-Mn-Al steel grain boundary precipitation of AlN is effective in reducing hot ductility provided it is in a fine form. Reheating temperatures of 1000°C coarsened the precipitates sufficiently to allow dynamic recrystallization to occur when tested at 850°C. Higher reheating temperatures cause dissolution of the AlN and because of its sluggishness in reprecipitating at the boundaries did not influence hot ductility, giving rise to high reduction in area values.
3. Hot ductility in micro-alloyed Nb and V steels is dominated mainly by the precipitation processes. Ductility is worse when precipitation takes place both at the  $\gamma$  grain boundaries and in fine form in the matrix as with Nb containing steels in which the NbCN is first taken into solution and then precipitates out dynamically during test. Ductility is best in those steels when the precipitates are presented in a coarse form randomly precipitated in the structure. This occurred in the Nb containing steel when reheated to 1100°C which coarsened the precipitates without taking much back into solution and more generally in the V containing steel throughout the whole temperature range, precipitation being in general coarse and randomly distributed.
4. When low ductility intergranular failures occur in micro-alloyed steels grain refinement is likely to give some benefit. Refining the grain size from 300 to 150  $\mu\text{m}$  might be expected to

raise the R of A values at 850°C by 15 to 20%. Such an improvement may be useful in reducing transverse cracking in Nb grades of steel.

Steel	C	Si	Mn	P	S	Al	Nb	V	N
1. C-Mn	.19	.20	1.40	.002	.013	-	-	-	.004
2. C-Mn-Al	.15	.29	1.45	.003	.008	.017	-	-	.006
3. C-Mn-V-Al	.13	.30	1.44	.003	.003	.017	-	.066	.009
4. C-Mn-Nb-Al	.12	.29	1.44	.003	.009	.015	.034	-	.010

Table 6.1 Compositions of the steels examined (wt.%)

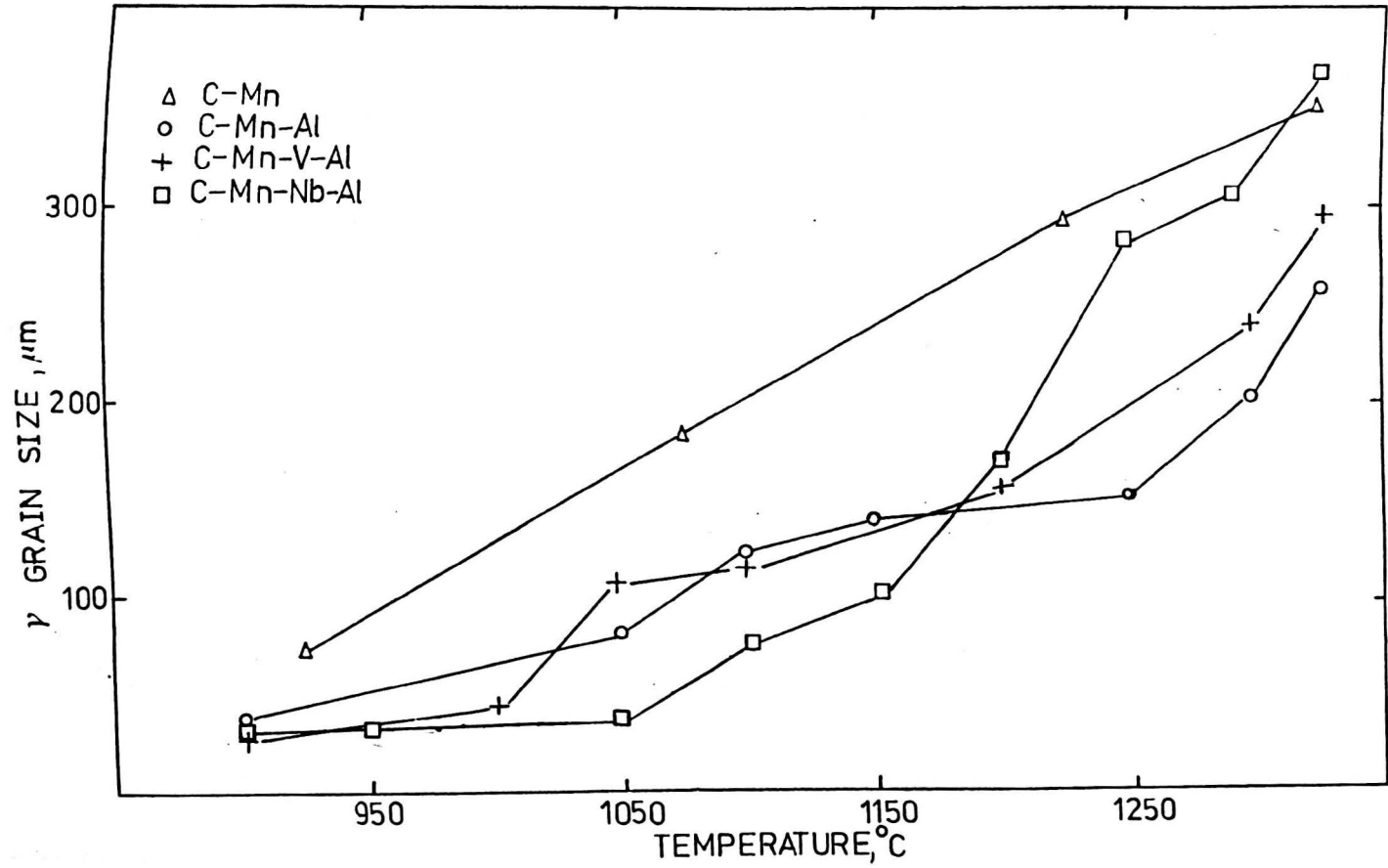


Fig. 6.1

Influence of reheating temperature on the austenite grain size of the C-Mn, C-Mn-Al, C-Mn-V-Al, and C-Mn-Nb-Al steels.

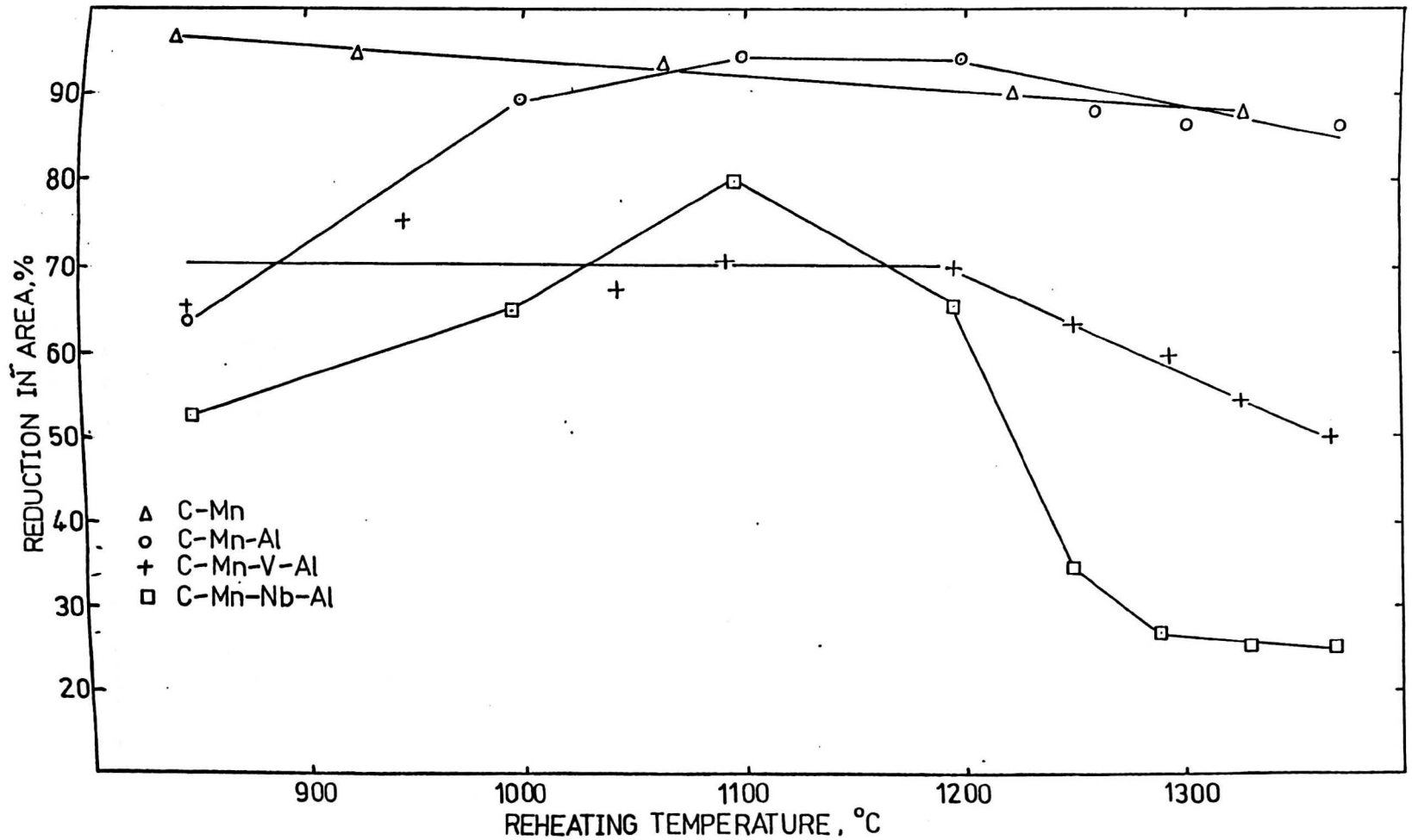


Fig. 6.2 Reduction of area values following tensile testing at 850°C after reheating to various temperatures, for C-Mn, C-Mn-Al, C-Mn-V-Al and C-Mn-Nb-Al steels.

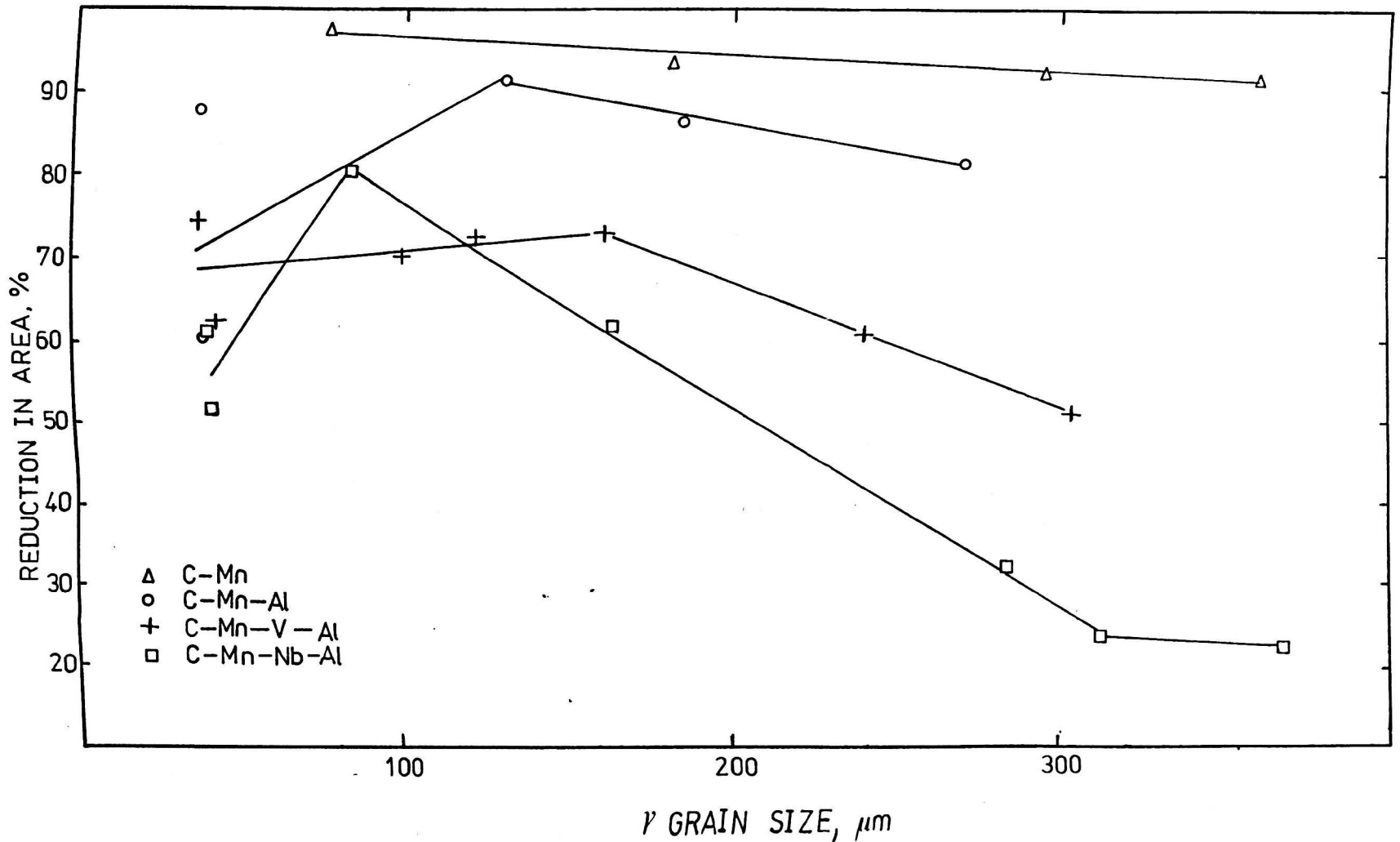


Fig. 6.3 Variation of reduction in area values with austenite grain size.

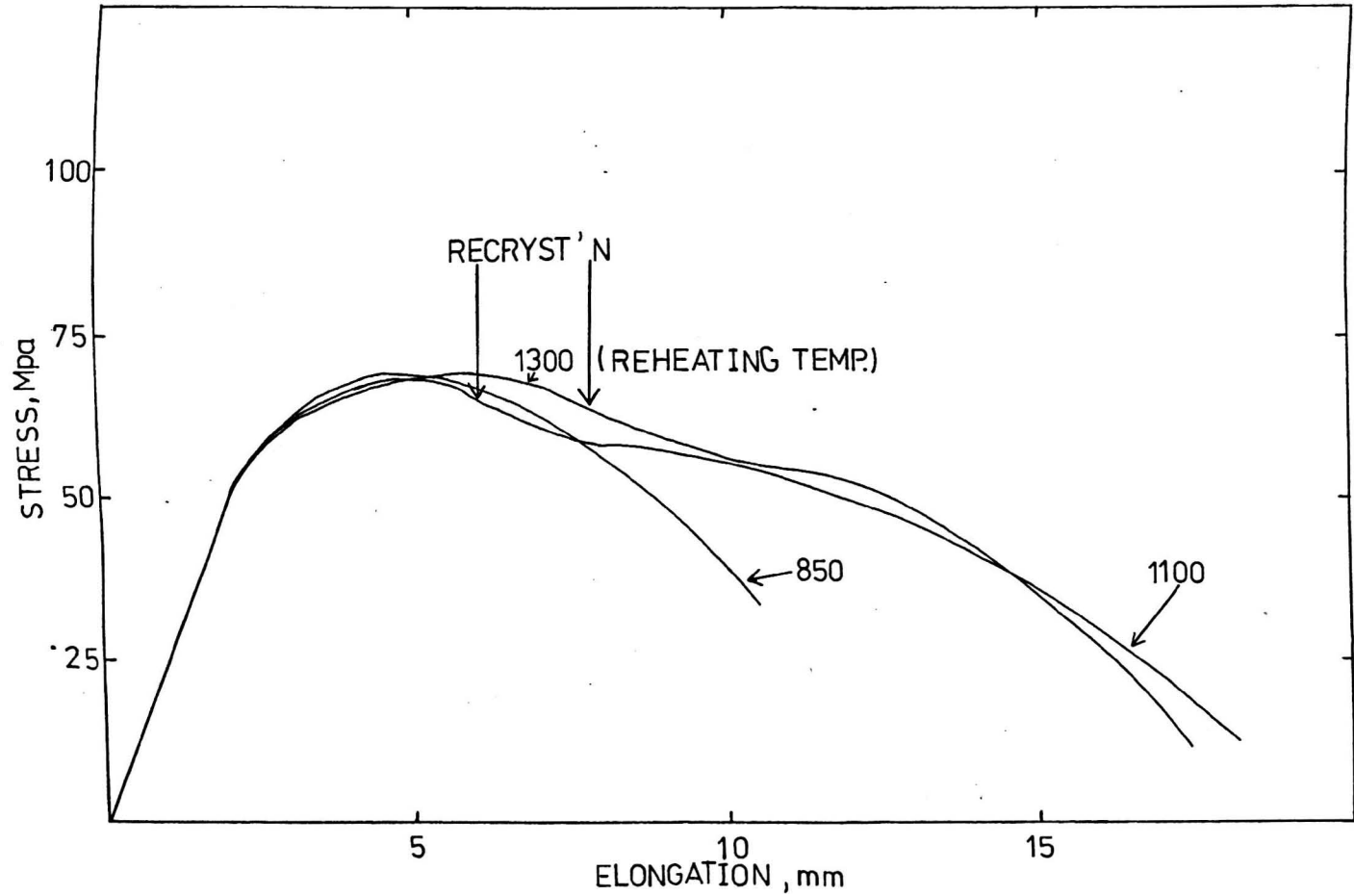


Fig. 6.4 Load-elongation curves for the C-Mn-Al steel

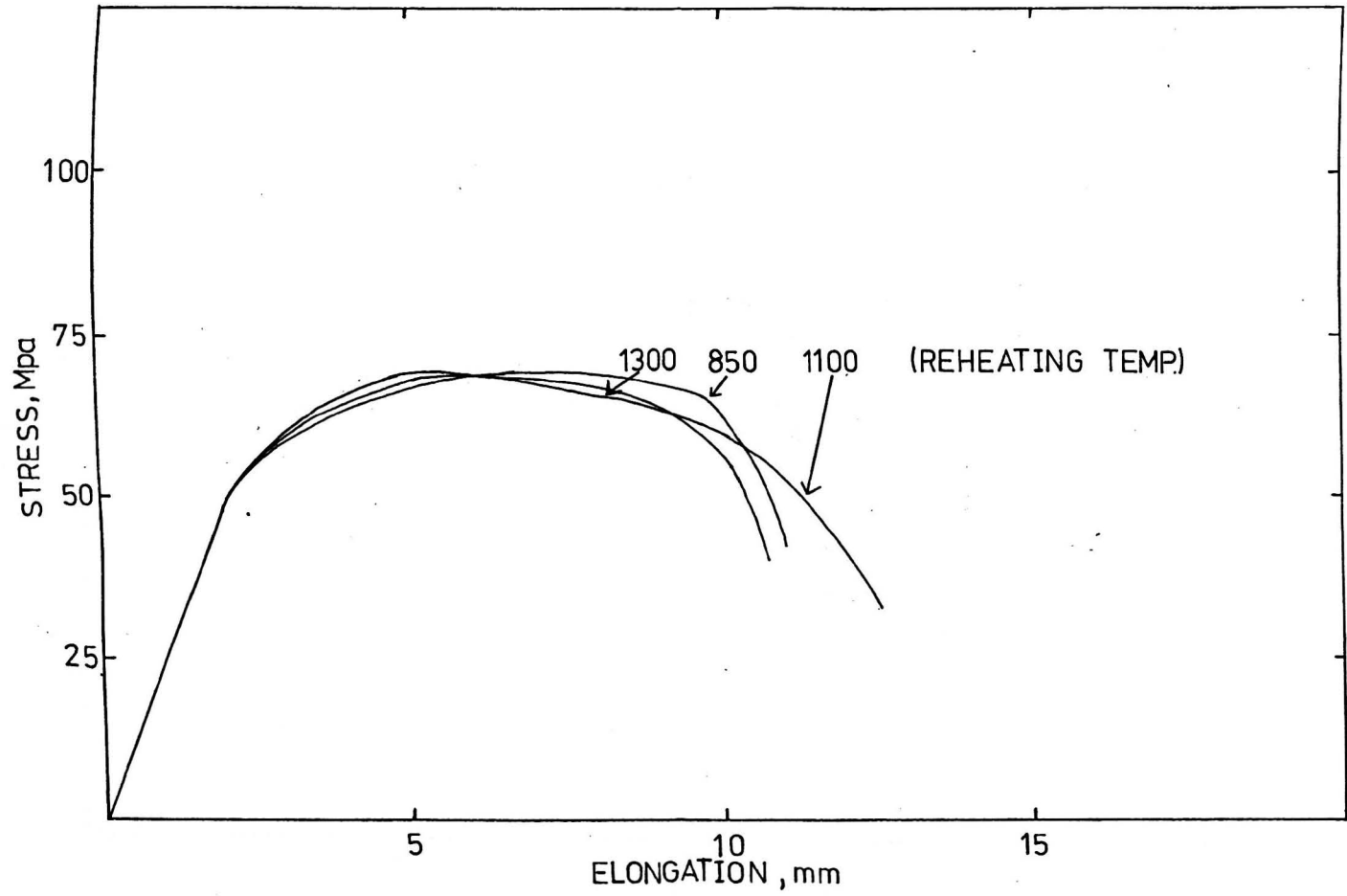


Fig. 6.5 Load-elongation curves for the C-Mn-V-Al steel

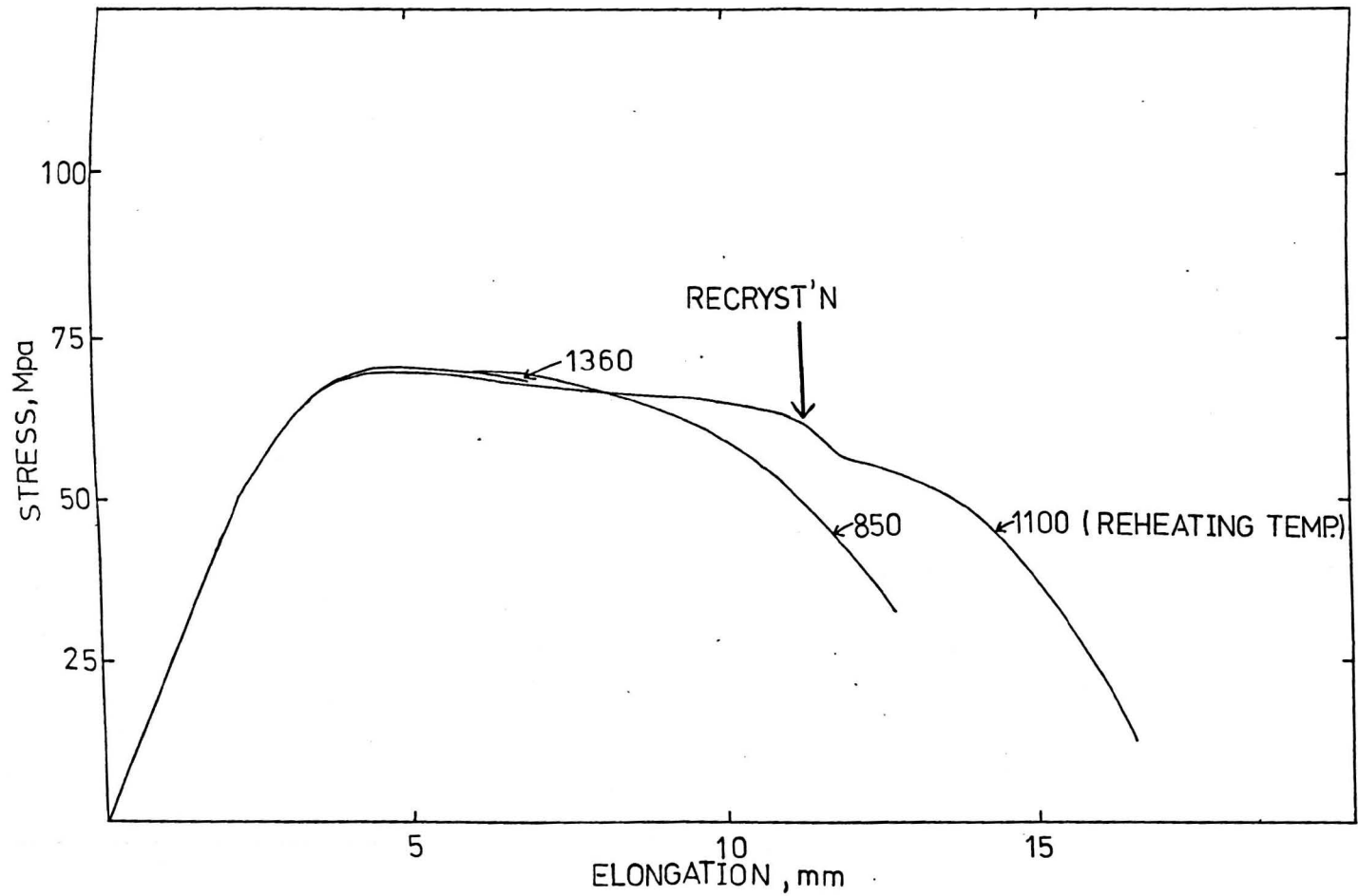


Fig. 6.6 Load elongation curves for the C-Mn-Nb-Al steel

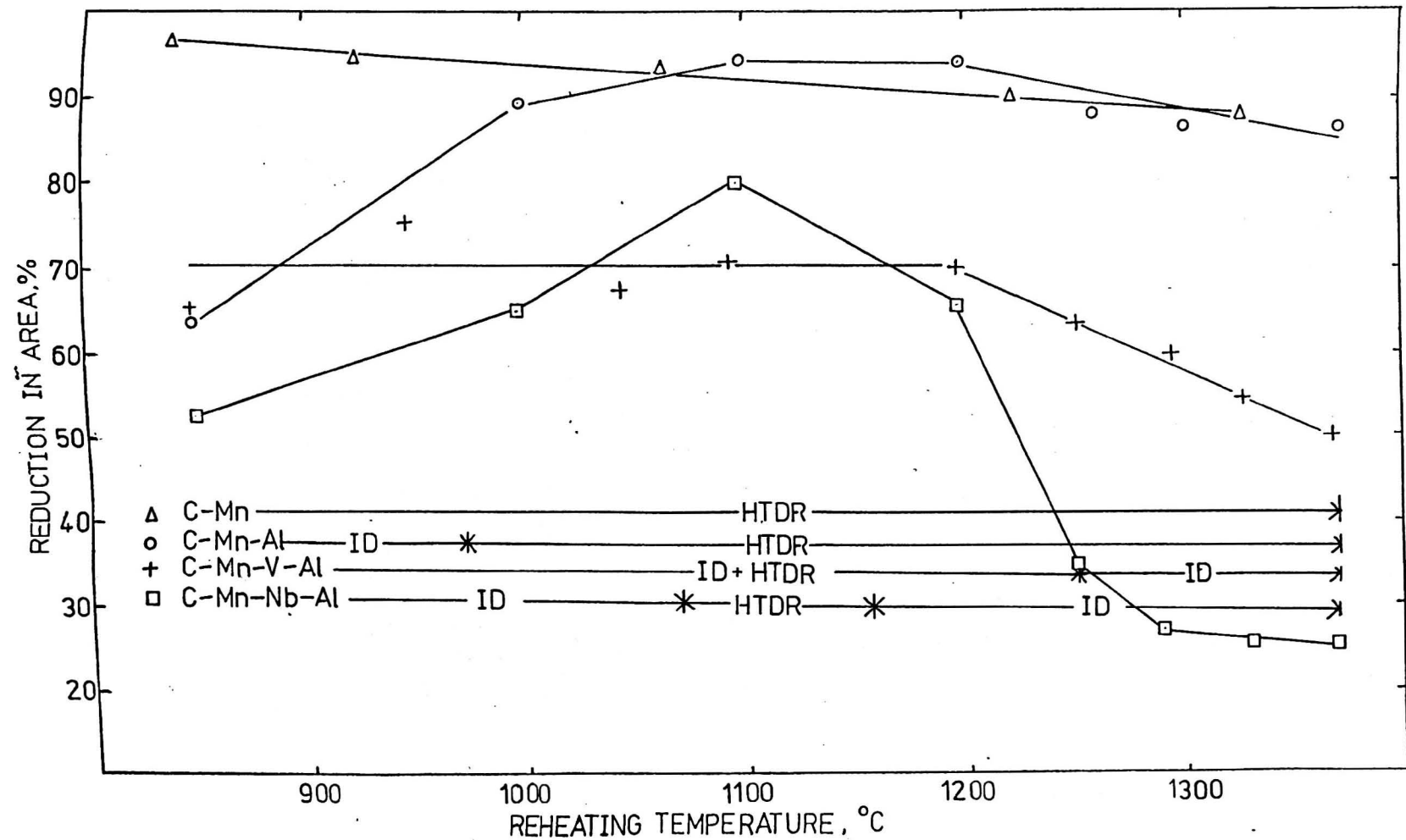
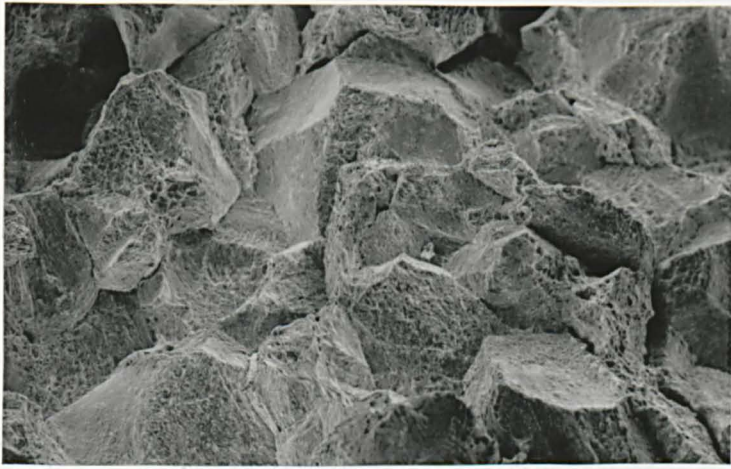
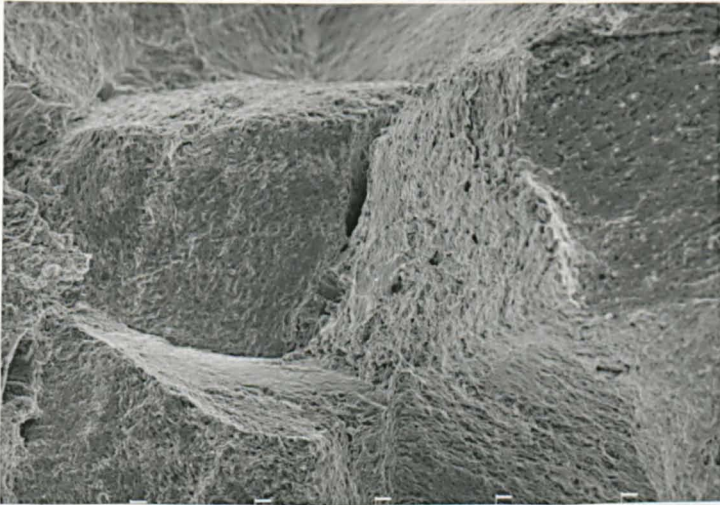


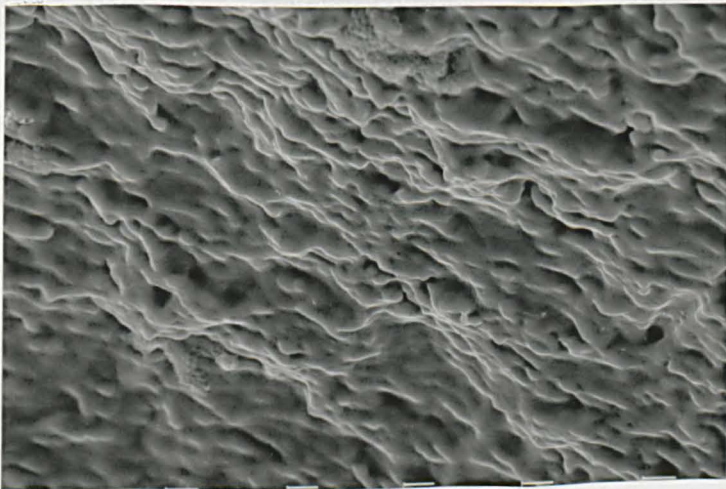
Fig. 6.7 Extent of fracture mode for each steel.



200  $\mu\text{m}$



50  $\mu\text{m}$



20  $\mu\text{m}$

Fig. 6.8

Example of ID fracture mode in C-Mn-Nb-Al steel after reheating to 1330°C and testing at 850°C.

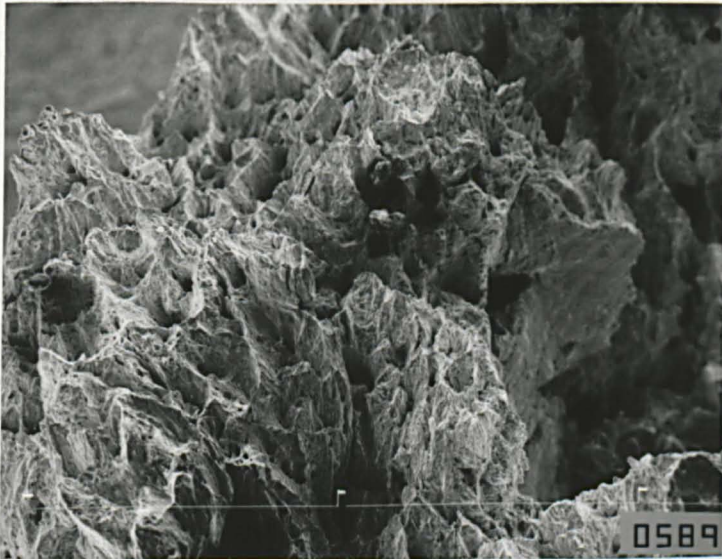


Fig.6.9

Example of HTDR fracture mode in C-Mn-Nb-Al steel after reheating to 1100°C and testing at 850°C.

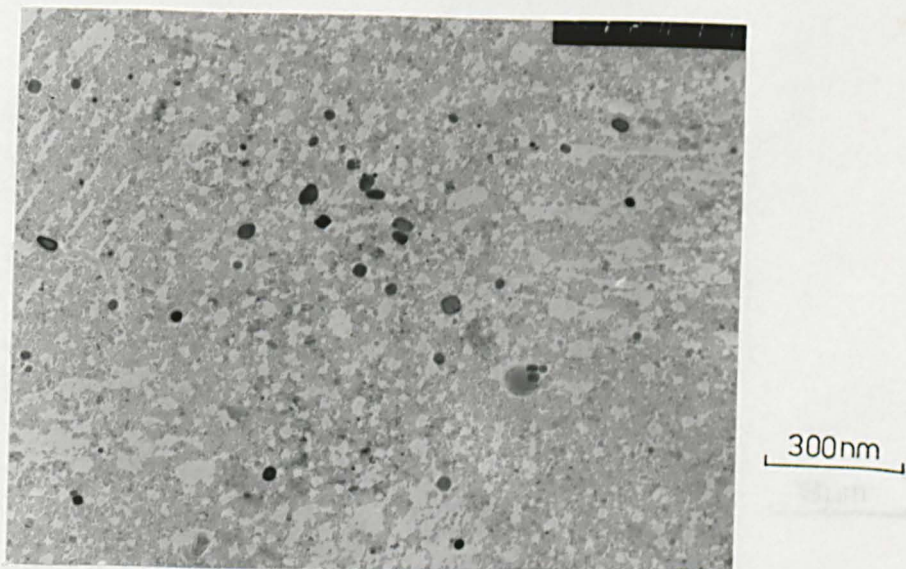


Fig. 6.10 NbCN precipitates extracted from fracture surface of C-Mn-Nb-Al steel after reheating to 1330°C



Fig. 6.11 C-Mn-Al steel heated directly to 850°C, showing grain boundary precipitation of AlN.



05-AUG-84 11:38:29 EDAX READY  
 RATE: 324886CPS TIME: 33LSEC  
 00-20KEY:10EV/CH PRST: 200LSEC  
 A: B:  
 FS= 1233 MEM: A FS= 200  
 |00 |02 |04 |06 |08 |10 |12 |14 |16 |18

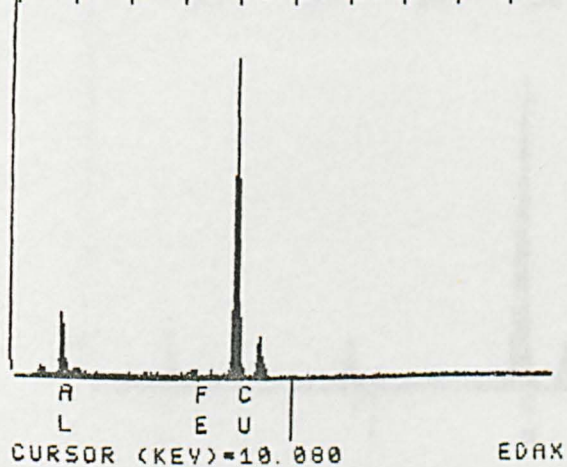


Fig. 6.12

C-Mn-Al steel reheated to 1000°C, tested at 850°C with associated X-ray spectrum.



18-SEP-84 10:16:32 PEAK IDENT  
 RATE: 1820CPS TIME: 85LSEC  
 00-20KEV:10EV/CH PRST: 200LSEC  
 A: B:  
 FS= 2531 MEM: A FS= 200  
 |02 |04 |06 |08 |10

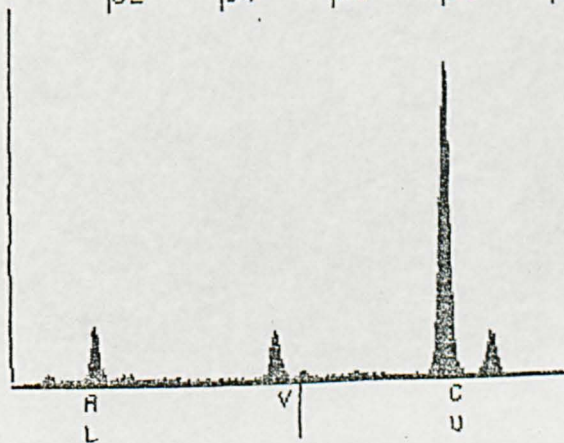


Fig.6.13 Precipitation in C-Mn-V-Al steel heated to 850°C and tested, showing VCN and AlN precipitation and associated X-ray spectra.

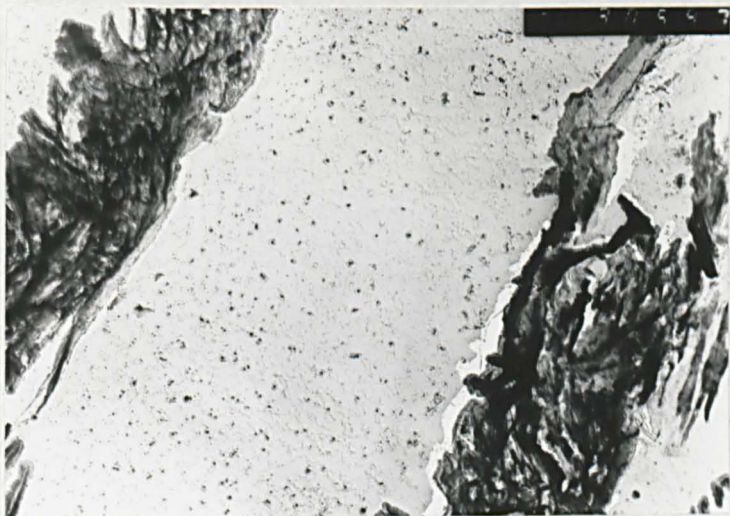


Fig. 6.14 Precipitation in C-Mn-V-Al steel after reheating to 1050°C and testing at 850°C.

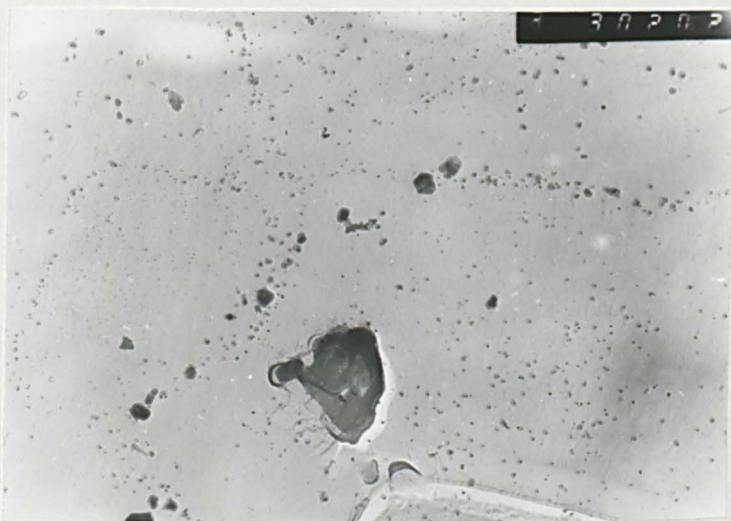


Fig. 6.15 Precipitation in C-Mn-Nb-Al steel heated to 850°C and tested, showing AlN and NbCN precipitation.

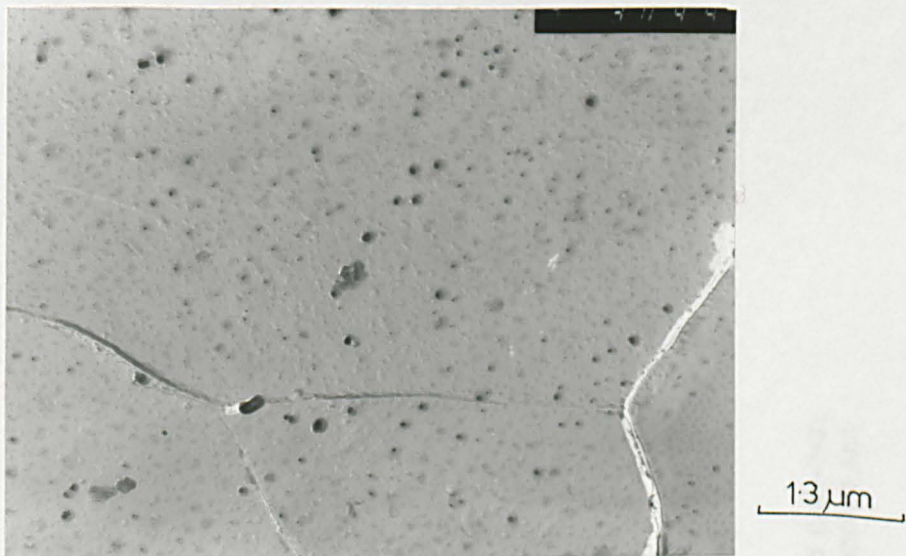


Fig. 6.16 Precipitation in C-Mn-Nb-Al steel heated to 1100°C prior to testing at 850°C

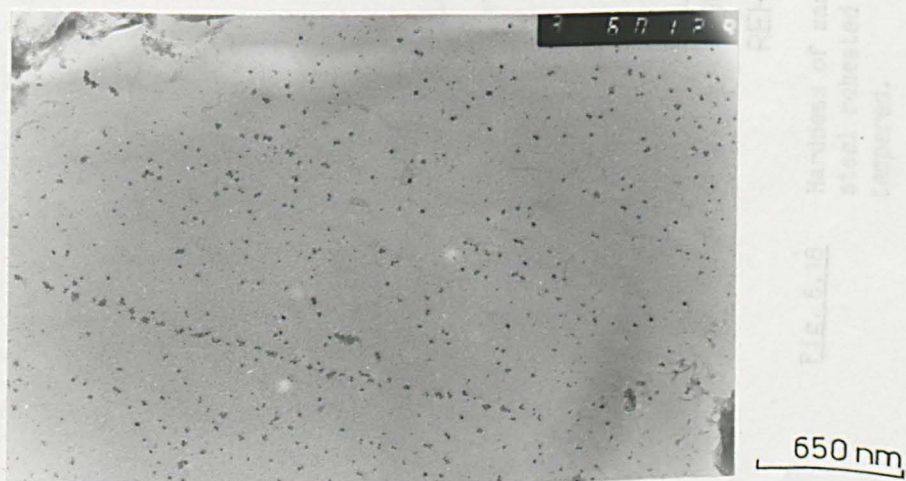


Fig.6.17 Precipitation in C-Mn-Nb-Al steel heated to 1330°C prior to testing at 850°C.

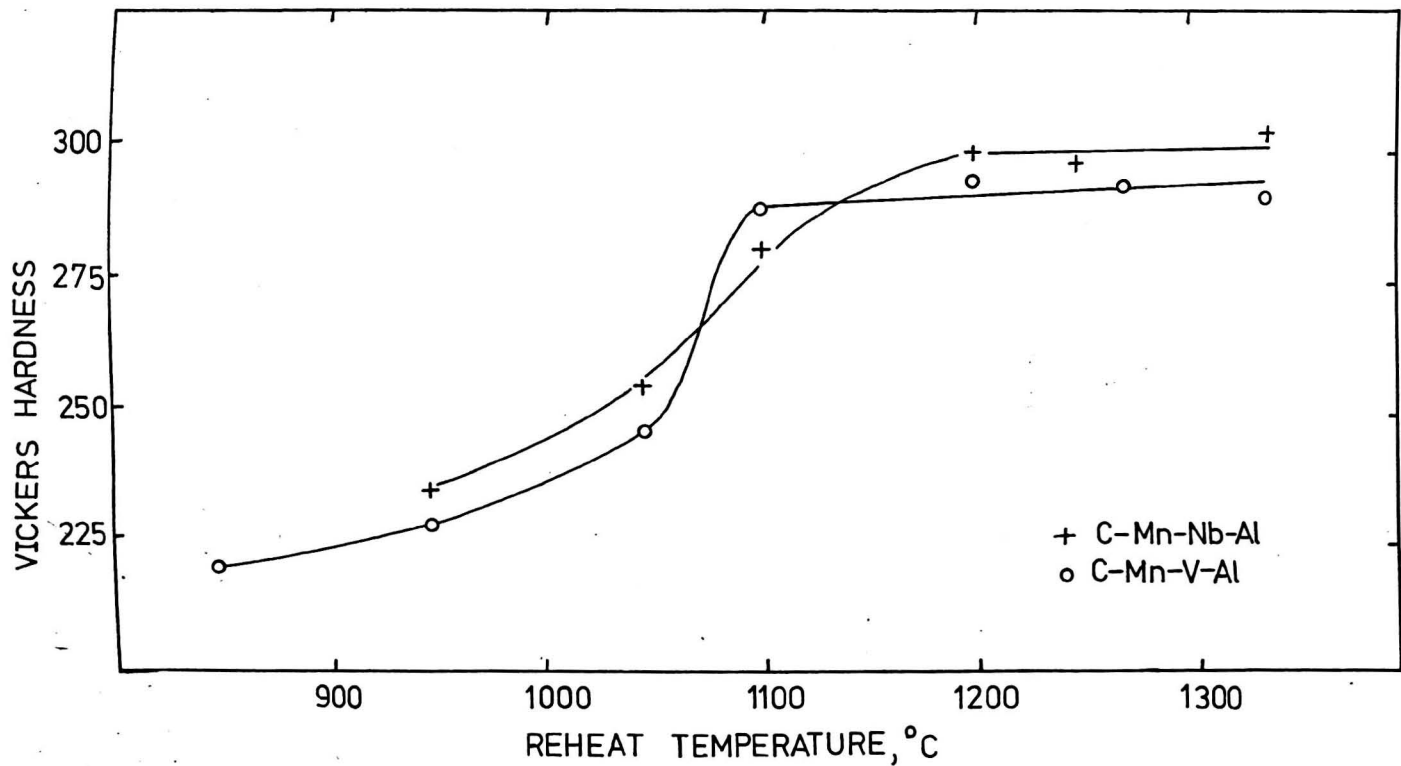


Fig. 6.18 Hardness of samples of the C-Mn-Nb-Al steel and C-Mn-V-Al steel reheated to various temperatures, and quenched and tempered.

## CHAPTER 7

### The Influence of static and Dynamic Precipitates on Hot Ductility

## 7.1 INTRODUCTION

Numerous investigations into the hot ductility of micro-alloyed steels have confirmed that the precipitation of carbides and/or nitrides play an important role in the fracture behaviour of such steels after certain thermal cycles, and at intermediate strain rates. The precipitate size and volume fraction are recognised as being particularly important parameters. (Bernard et al, 1978; Mintz and Arrowsmith, 1979; Ouchi and Matsumoto, 1982) During hot working, these precipitates may be present prior to deformation, or alternatively, they may be formed during deformation. It is well known that the precipitation of AlN, NbCN and VCN is accelerated by deformation, compared to precipitation rates measured during isothermal transformations in undeformed structures at the same temperature. (Vodopivec, 1973; Le Bon et al, 1975; Weiss and Jonas, 1979; Akben et al, 1981). It is believed that this acceleration of precipitation is due to the introduction of favourable nucleation sites by the deformation process. The exact nature of these nucleation sites cannot be determined directly for transformable steels, but it seems likely that these sites are dislocation networks and vacancy clusters. This is supported by the observation of NbC precipitated on dislocations in austenitic stainless steels following high temperature testing. (Ohmori and Maehara, 1984). The proportion of static and dynamic precipitates present at a particular temperature after deformation is dependent on the cooling rate from the solution temperature, and also on the deformation rate. Slow cooling rates are likely to favour static precipitation. For the particular case of AlN, cooling rates of approximately 1°C/min. are believed to be required for the precipitation of AlN during continuous cooling, a particularly sluggish reaction. (Gladman and Pickering,

1967) Dynamic precipitation may not occur at very high strain rates, since deformation usually ceases before the incubation time for dynamic precipitation has been reached. However, static precipitation may subsequently occur in the deformed structure. This static precipitation in a deformed structure occurs at rates intermediate between that of dynamic precipitation, and static precipitation in undeformed metal. (Weiss and Jonas, 1979) The investigation of Weiss and Jonas (1979) showed that for the dynamic precipitation of NbC, strain rates of less than  $10^{-1} \text{ s}^{-1}$  were required, the exact values being temperature dependent. A later study by Akben et al (1981) showed that a similar strain rate was required for the dynamic precipitation of VN. Another important result from a study by Weiss and Jonas (1980) was that dynamically precipitated NbCN was finer than the equivalent static precipitates formed at the same temperature.

It can be seen from the foregoing that precipitate volume fraction and size are dependent on whether the precipitate is formed in a dynamic or in a static situation. Therefore, since both precipitate volume fraction and size play an important role in determining the hot ductility of micro-alloyed steels, it would be expected that dynamic and static precipitates would each have a distinct influence on hot ductility.

Investigations into the influence of the static and dynamic precipitation of AlN have concluded that precipitates present before deformation are more detrimental to hot ductility than those formed during the test. (Vodopivec, 1978; Wilcox, 1982) Wilcox has also concluded that NbCN formed during deformation is more detrimental to hot ductility than that existing prior to deformation.

It was therefore, decided in this chapter to investigate the relative influences of the static and dynamic precipitation of

of AlN, NbCN and VCN on the hot ductility of three micro-alloyed steels.

## 7.2 EXPERIMENTAL

The C-Mn-Al, C-Mn-V-Al and C-Mn-Nb-Al steels examined in chapter 6 were chosen for the present investigation. The compositions of these steels are given in Table 6.1 (code numbers 2, 3 and 4), and processing details are given in section 6.2. Tensile samples having a gauge length of 80 m.m. and a diameter of 7.9 m.m. (Fig. 3.6) were machined from the plates with their axes parallel to the rolling direction, for testing using the induction heating apparatus described in section 3.2.3. All three steels were solution treated for 10 minutes at 1330°C, prior to cooling to test temperature at an average rate of 100°C/min. to suppress pre-test precipitation. For the C-Mn-Nb-Al steel, tests were performed at 950°C, since it is close to this temperature that NbCN precipitation is most rapid. (Weiss and Jonas, 1979)

Samples were either tested immediately on reaching this temperature, or held for up to 21,000 s before testing. This enabled the proportion of static precipitates to be varied from 0 for the samples tested immediately, to approximately 100% for the longest holding times prior to testing. For the C-Mn-Al and C-Mn-V-Al steels, the test temperature was reduced to 850°C since AlN and VCN precipitate most rapidly at lower temperatures than NbCN. (Leslie et al, 1954; Akben et al, 1981)

It should be noted that 850°C is above the  $A_e$ , temperature calculated using Andrews' formula (1965) for both the C-Mn-Al steel and the C-Mn-V-Al steel.

Longitudinal sections including the point of fracture were taken from broken tensiles and prepared for metallographic examination. Fracture surfaces were examined using a JEOL T100 SEM operating at 25 KV. Carbon extraction replicas were prepared from sections approximately 1m.m. behind the fracture surface, as described in section 3.3.

To investigate the static precipitation of NbCN at 950°C, the method of loss of secondary hardening potential was used, as described in chapter 6.

Small samples of the C-Mn-Nb-Al steel were solution treated at 1330°C for 10 minutes, rapidly cooled to 950°C, and maintained at this temperature in a muffle furnace for varying periods of time. After the appropriate length of time, the samples were quenched into iced brine, and then tempered at 600°C for 1 hour. Hardness measurements were then taken from sectioned and polished samples using a Vickers DP machine. An attempt was made to follow the static precipitation of VCN in the C-Mn-V-Al steel using this same method, but unfortunately, only very small hardness changes were obtained, which could not be confidently interpreted.

## 7.3 RESULTS

### 7.3.1 Hot Tensile Tests

Figs. 7.1 - 7.3 show the variation of reduction in area and peak stress,  $\sigma_p$ , with holding time prior to testing at 950°C for the C-Mn-Nb-Al steel, and at 850°C for the C-Mn-Al and C-Mn-V-Al steels. The hot ductility of the C-Mn-Nb-Al steel increases slightly as the holding time increases, rising from 30% reduction in area for 1 s holding time, to 45% for 21,000 s holding time. Peak stress falls from 57 MPa to 52 MPa as the holding time increases to 21,000 s. For the C-Mn-V-Al steel tested at 850°C, reduction in area values fall from 52% to 40%, as the holding time prior to testing increases to 21,000 s, whilst peak stress remains approximately constant at 69 MPa. The C-Mn-Al steel has reduction in area values of over 95% for all holding times, and a constant peak stress of 69 MPa. Figs. 7.4 - 7.6 illustrate the load-elongation curves for all three steels, for various holding times prior to testing. For all holding times, the load-elongation curves of the C-Mn-Al steel show a sudden fall, which is characteristic of the onset of dynamic recrystallisation, (Wray, 1975) illustrating that dynamic recrystallization occurred during all tests involving this steel. Conversely, the load elongation curves for the C-Mn-Nb-Al steel indicated that in all cases, fracture occurred before the onset of recrystallization. For the C-Mn-V-Al steel, the load elongation curves showed that the steel held for 1 s prior to testing had undergone recrystallization, whilst for holding time greater than 1 s, fracture had occurred before recrystallization.

### 7.3.2 Metallography

Optical and SEM fractography revealed that the C-Mn-V-Al and C-Mn-Nb-Al steel fractured at the austenite grain boundaries for all holding times. Two intergranular failure modes were observed

in these two steels, i.e. intergranular decohesion (ID) and intergranular microvoid coalescence (IMC), the former mode predominating. These fracture surfaces were essentially similar to the intergranular failures described in chapter 6. Examination of the austenite grain structure after fracture revealed a coarse, unrecrystallized structure for both the C-Mn-V-Al and C-Mn-Nb-Al steels, the former having a grain size of 300  $\mu\text{m}$ , the latter having a grain size of 360  $\mu\text{m}$ . Holding time prior to testing had no influence on grain size in either steel. The C-Mn-Al steel showed the high temperature ductile rupture mode of failure described in previous chapters for all holding times. Examination of carbon extraction replicas taken from the C-Mn-Al steel showed no precipitation in any of the fractured samples. The C-Mn-Nb-Al steel showed extensive precipitation of NbCN for all holding times prior to testing. No AlN precipitation was evident. For the sample tested after 1 s holding time, extensive matrix and grain boundary precipitation of NbCN was observed, (Fig. 7.7) and in some cases, precipitate free zones adjacent to the grain boundaries. After 7200 s holding time, in addition to the fine NbCN precipitates, a coarser form of NbCN precipitate was present, and after 21,000 s holding time, only the coarse NbCN precipitate was observed. (Fig. 7.7). Fig. 7.8 shows the evolution of precipitate size distribution with holding time prior to testing. For holding times of 1 s, the precipitate frequency distribution is uni-modal, with a mean diameter of 15 nm. After 7200 s holding time, the frequency distribution is bi-modal, and remains bi-modal after 21,000 s holding time, although the peak at the smaller precipitate size was much reduced. These results compare well with the NbCN size measurements of Weiss and Jonas (1980)

The C-Mn-V-Al steel showed precipitation of VCN in all the fractured

samples (Fig. 7.9). In the sample held for 1 s prior to fracture, VCN precipitates are randomly precipitated. However, for the samples held for 21,000 s prior to testing, precipitation occurs predominantly at the austenite grain boundaries (Fig. 7.9). No AlN precipitation was observed in the C-Mn-V-Al steel. Fig. 7.10 shows the evolution of precipitate size with holding time prior to testing. For all holding times, the size distribution is unimodal, and mean precipitate diameter increases from 12 nm for 1 s holding time to 50 nm for 21,000 s holding time.

### 7.3.3 Static Precipitation of NbCN

The hardness results used to follow the static precipitation kinetics of NbCN at 950°C in the C-Mn-Nb-Al steel are shown in Fig. 7.11. Quenching directly from 1330°C followed by tempering at 600°C for one hour resulted in a hardness value of 304 Vickers. This hardness value corresponds to zero NbCN precipitation at 950°C. When samples are held at 950°C for more than 300 s prior to quenching and tempering, hardness values begin to fall, and after holding for 21,000 s at 950°C the hardness values reach 255 Vickers. Assuming that NbCN precipitated at 950°C makes no contribution to hardness after quenching and tempering, these results can be interpreted as showing that NbCN precipitation at 950°C begins after approximately 300 s, which agrees approximately with the results of other workers. (Watanabe et al, 1977; Weiss and Jonas, 1979) The hardness values show no sign of attaining a constant value after 21,000 s, which indicates that NbCN precipitation at 950°C is still not complete after this time.

#### 7.4 DISCUSSION

The absence of precipitation in the C-Mn-Al steel tested after 1s holding time indicates that fracture occurs before the incubation period necessary for dynamic precipitation of AlN has been reached. The time to failure for this test was - 300s, and so the incubation time for the dynamic precipitation of AlN must exceed this period. No precipitation of AlN was observed in the sample held for 21,000 s prior to testing, and this indicates that the incubation time for the static precipitation of AlN is greater than 21,000 s. Unfortunately, the very slow precipitation rates of AlN (both dynamic and static) mean that no conclusions can be drawn on the relative influences of dynamically and statically precipitated AlN. The absence of grain boundary pinning precipitates in the C-Mn-Al steel means that dynamic recrystallization could occur rapidly, isolating grain boundaries from the developing cracks, and producing high ductility failures.

For the C-Mn-Nb-Al steel, the rapid static precipitation rate of NbCN, as indicated by the hardness results shown in Fig. 7.11 mean that only the sample tested with holding time of - 1s prior to deformation, will show a precipitation pattern formed solely during deformation. The remaining samples all contain a proportion of NbCN formed prior to testing. The particle size distributions shown in Fig. 7.8, which are similar to those determined by Weissand Jones (1980), indicate that the dynamic precipitates have a mean diameter of 15 n.m., whilst the static precipitates are larger, having a diameter of 60 nm. Examination of Fig. 7.7 shows that dynamic precipitates of NbCN form both at grain boundaries, and within the grains themselves. This matrix precipitation of NbCN is sufficient to produce a slight increase

in peak stress. In contrast, static NbCN precipitates appear to form mainly at austenite grain boundaries, with little matrix precipitation.

The observation of coarse, un-recrystallized grain structures in all the fractured samples indicates that both the dynamic and static distributions of NbCN are effective in retarding the onset of dynamic recrystallization. A possible explanation for the inferior hot ductility of the samples containing a large proportion of dynamic precipitates is the extensive matrix precipitation of NbCN, and the tendency to form precipitate free zones in these samples, which lead to strain concentration at the grain boundaries, and hence reduce hot ductility.

For the C-MN-V-Al steel tested after a holding time of 1s, the random distribution of dynamically precipitated VCN is only partially effective in preventing dynamic recrystallization.

Fig. 7.6 shows some evidence of dynamic recrystallization before fracture, the load elongation curve for the 1s holding time test showing the characteristic drop in load associated with the onset of dynamic re-crystallization. However, dynamic recrystallization has occurred at a far later stage of deformation than for the C-Mn-Al steel, and this has led to the relatively low reduction in area value of 52%. Thus it can be said that the randomly distributed dynamic VCN retards dynamic recrystallization to some extent, but recrystallization does occur before final fracture is complete. There seem to be few reports in the literature on VCN precipitation kinetics, but for dynamic precipitation kinetics the PTT curve for NbCN and VN are similar, with the nose of the latter curve occurring at lower temperatures than the NbCN curve. (Akben et al, 1981) Also, there seems to be distinct differences in precipitation.

patterns for the steel tested after 1s, and after 6 hours, the latter being larger and distributed at austenite grain boundaries, and this would seem to indicate that the static precipitation of VCN is well advanced after 6 hours. This array of static VCN precipitates at austenite grain boundaries is effective in preventing dynamic recrystallization before fracture, leading to low ductility intergranular failures. Thus it can be concluded that for the C-Mn-V-Al steel, dynamically precipitated VCN is less effective in retarding recrystallization than statically precipitated VCN, and this leads to static VCN having the greater detrimental effect on hot ductility.

## 7.5 CONCLUSIONS

1. In a C-Mn-Nb-Al steel tested at 950°C, both dynamic and static arrays of precipitates were effective in delaying the onset of dynamic re-crystallization long enough for brittle, intergranular failure to occur.
2. The dynamic precipitates of NbCN were formed at grain boundaries, and within the matrix, and were finer than the equivalent static precipitates, which formed predominantly at the grain boundaries.
3. Samples of the C-Mn-Nb-Al steel held for short times prior to testing, and hence having a greater proportion of dynamic precipitates, had inferior hot ductility to those samples held for longer times. It is believed that this is due to the extensive matrix precipitation, and the existence of precipitate free zones in the samples held for only short times prior to testing, leading to strain concentration at the grain boundaries.
4. In a C-Mn-V-Al steel tested at 850°C, the static precipitate distribution formed after long holding times prior to testing was more effective in retarding re-crystallization than the dynamic precipitate distribution, leading to inferior hot ductility in the samples held for longer times prior to testing.

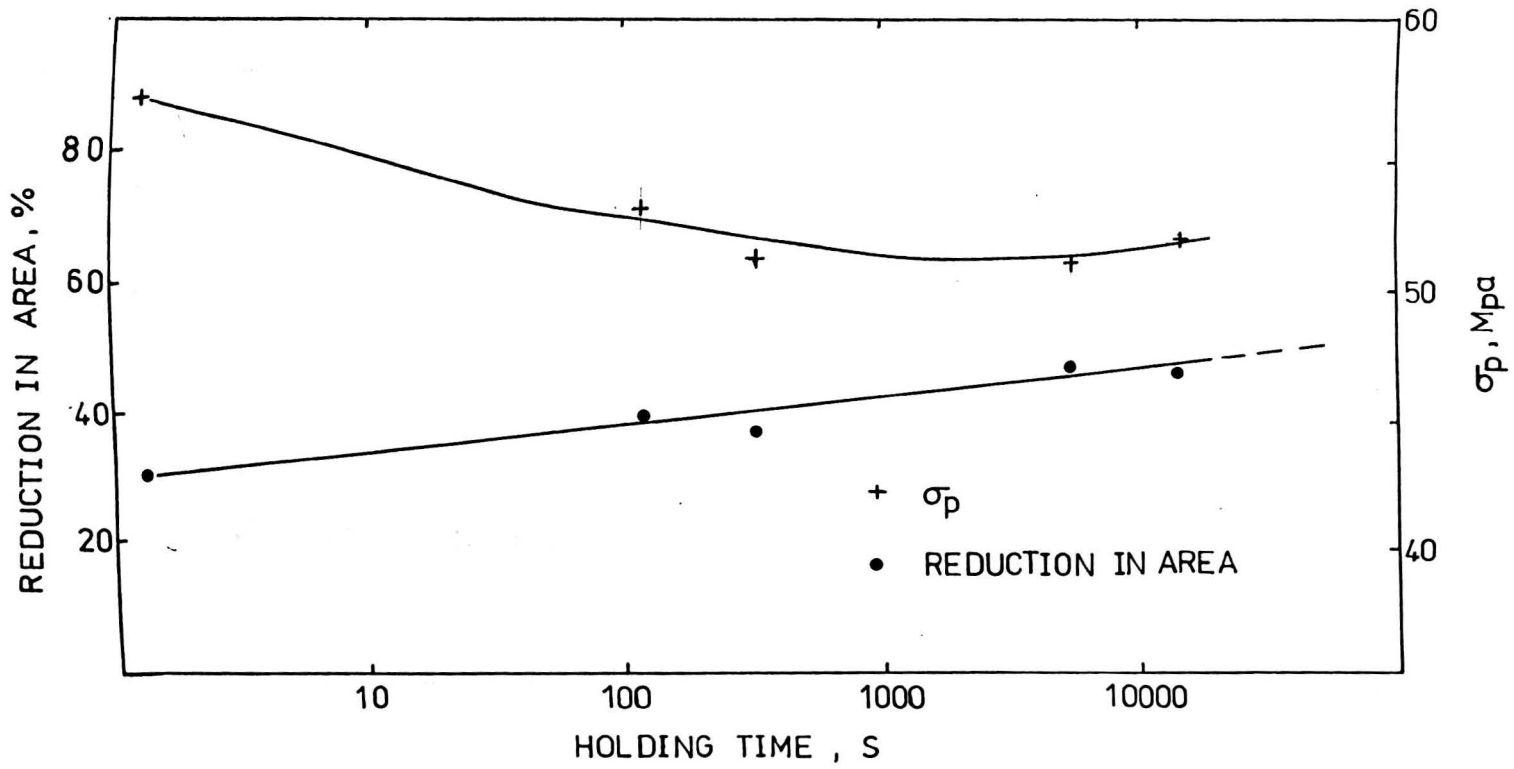


Fig. 7.1 Influence of holding time prior to testing on peak stress and hot ductility of the C-Mn-Nb-Al steel, tested at 50°C.

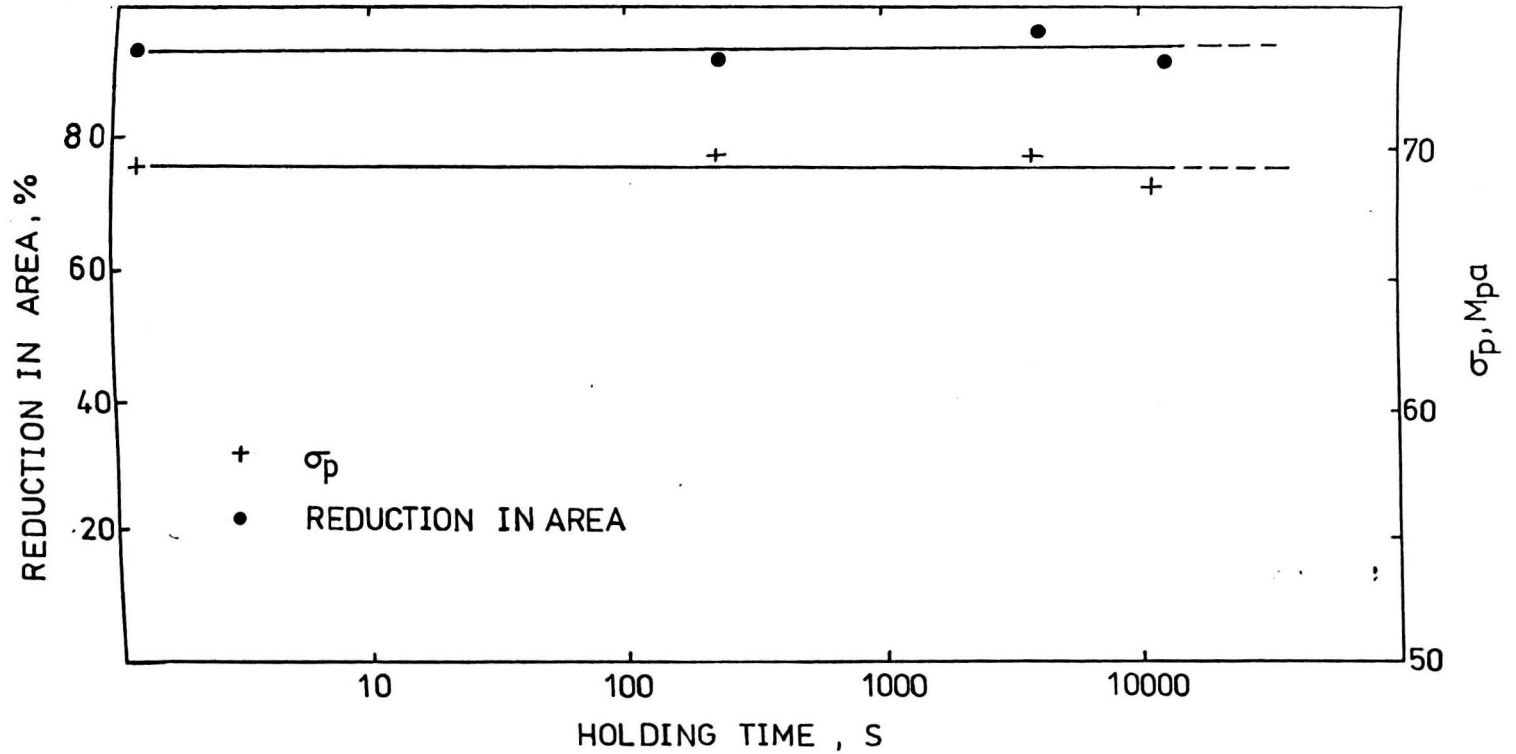
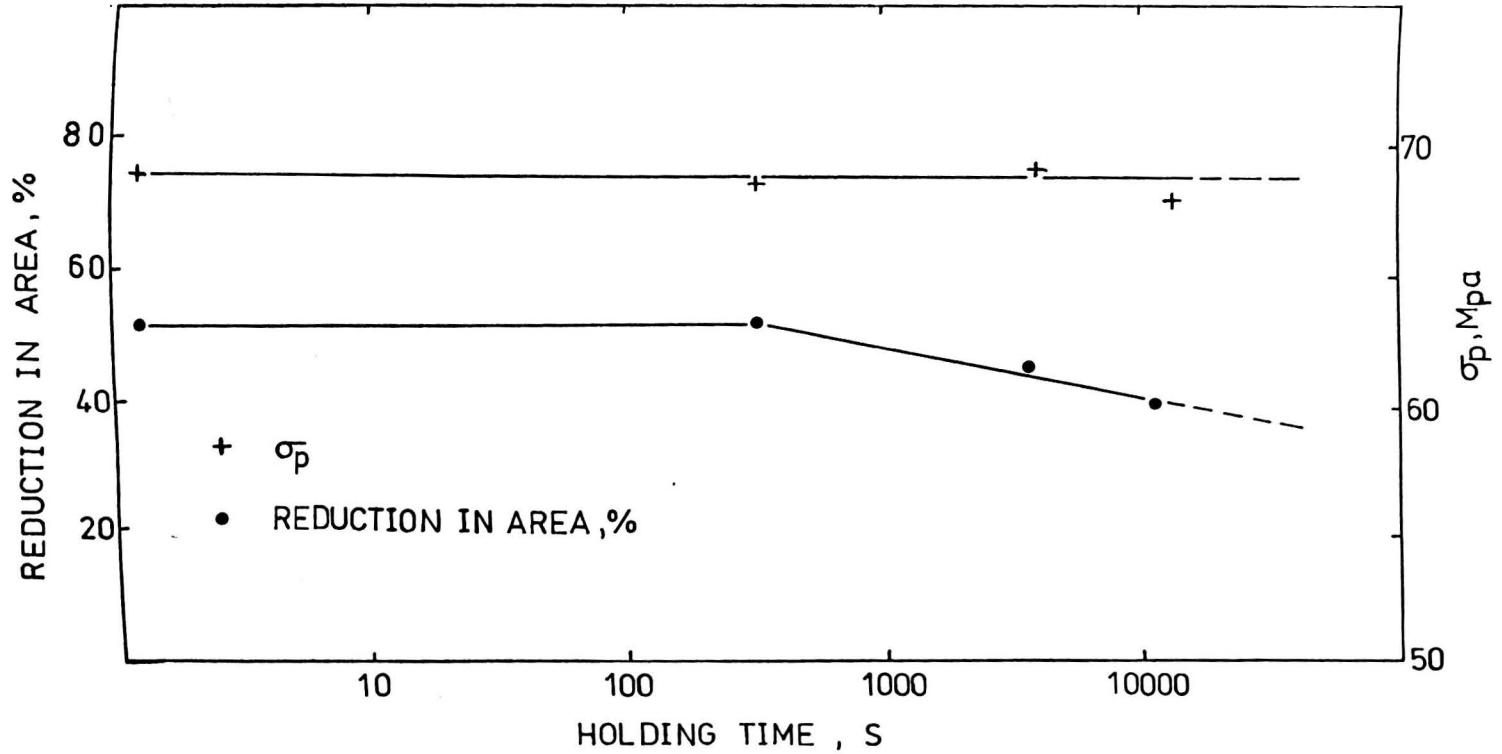


Fig. 7.2 Influence of holding time prior to testing on peak stress and hot ductility of the C-Mn-Al steel tested 850°C.



**Fig. 7.3** Influence of holding time prior to testing on peak stress and hot ductility of the C-Mn-V-Al steel, tested at 50°C.

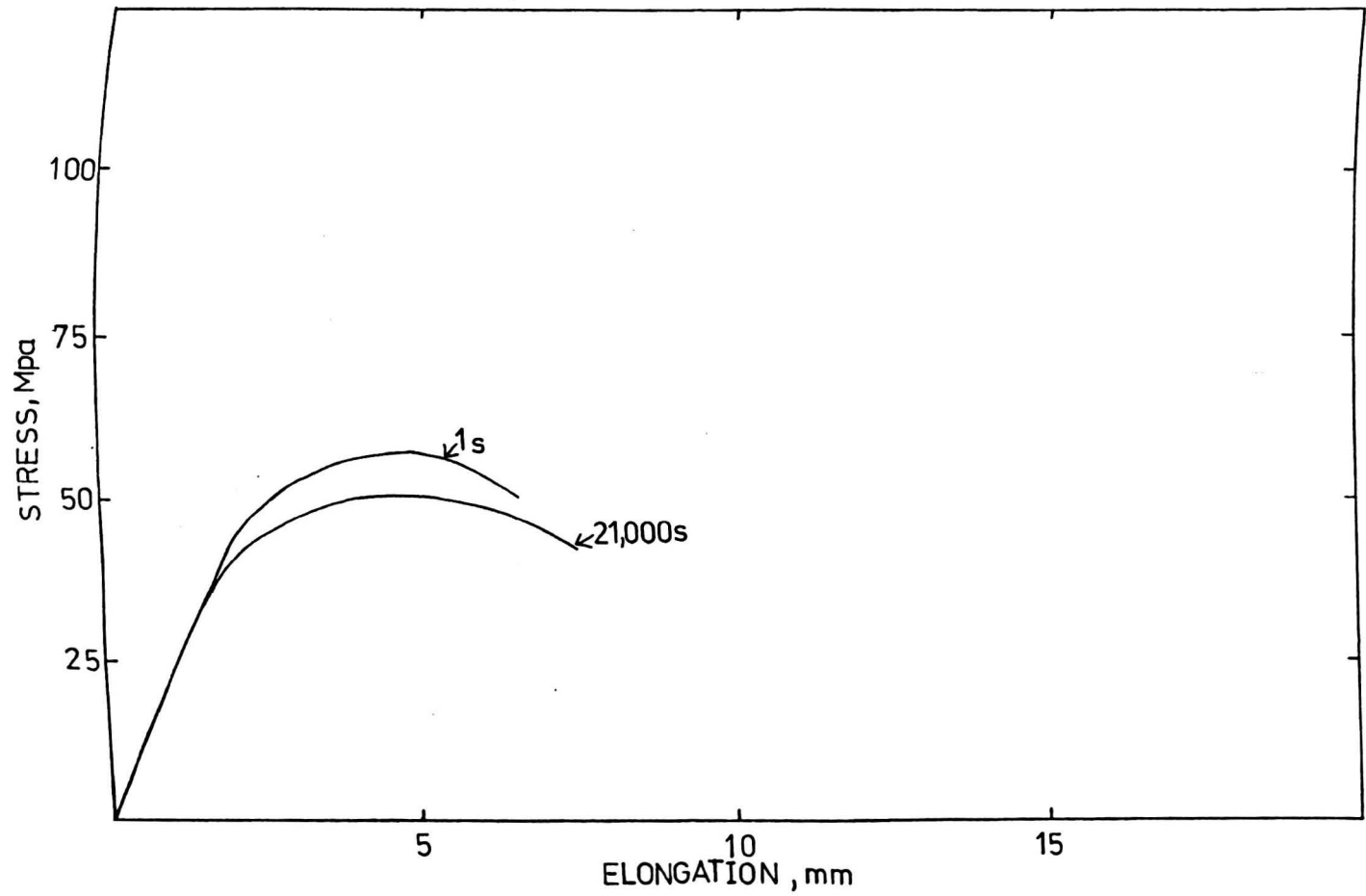


Fig.7.4

Stress-elongation curves for the C-Mn-Nb-Al steel held at 950°C for various times prior to testing.

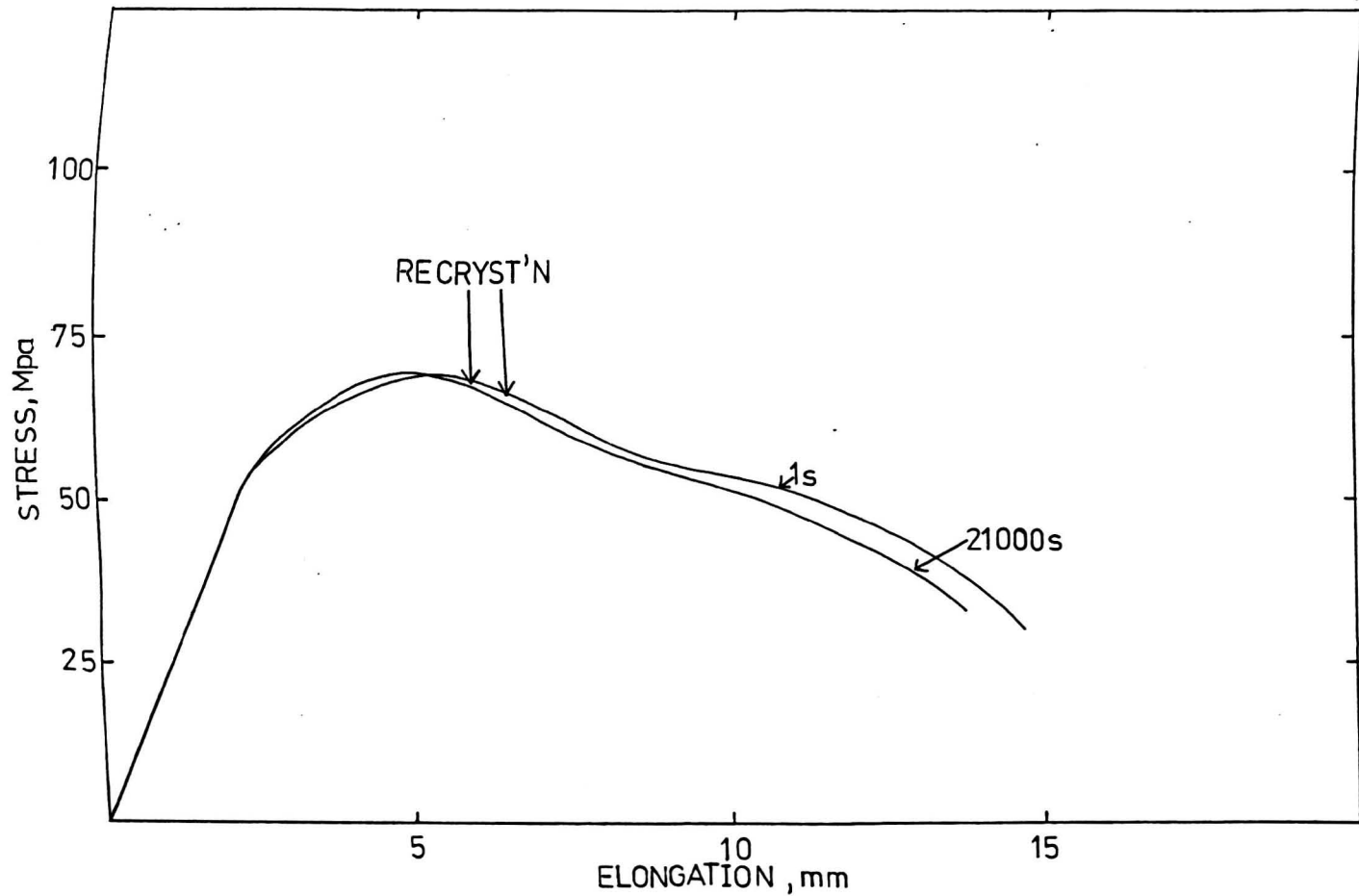


Fig. 7.5

Stress elongation curves for the C-Mn-Al steel held at 850°C for various times prior to testing.

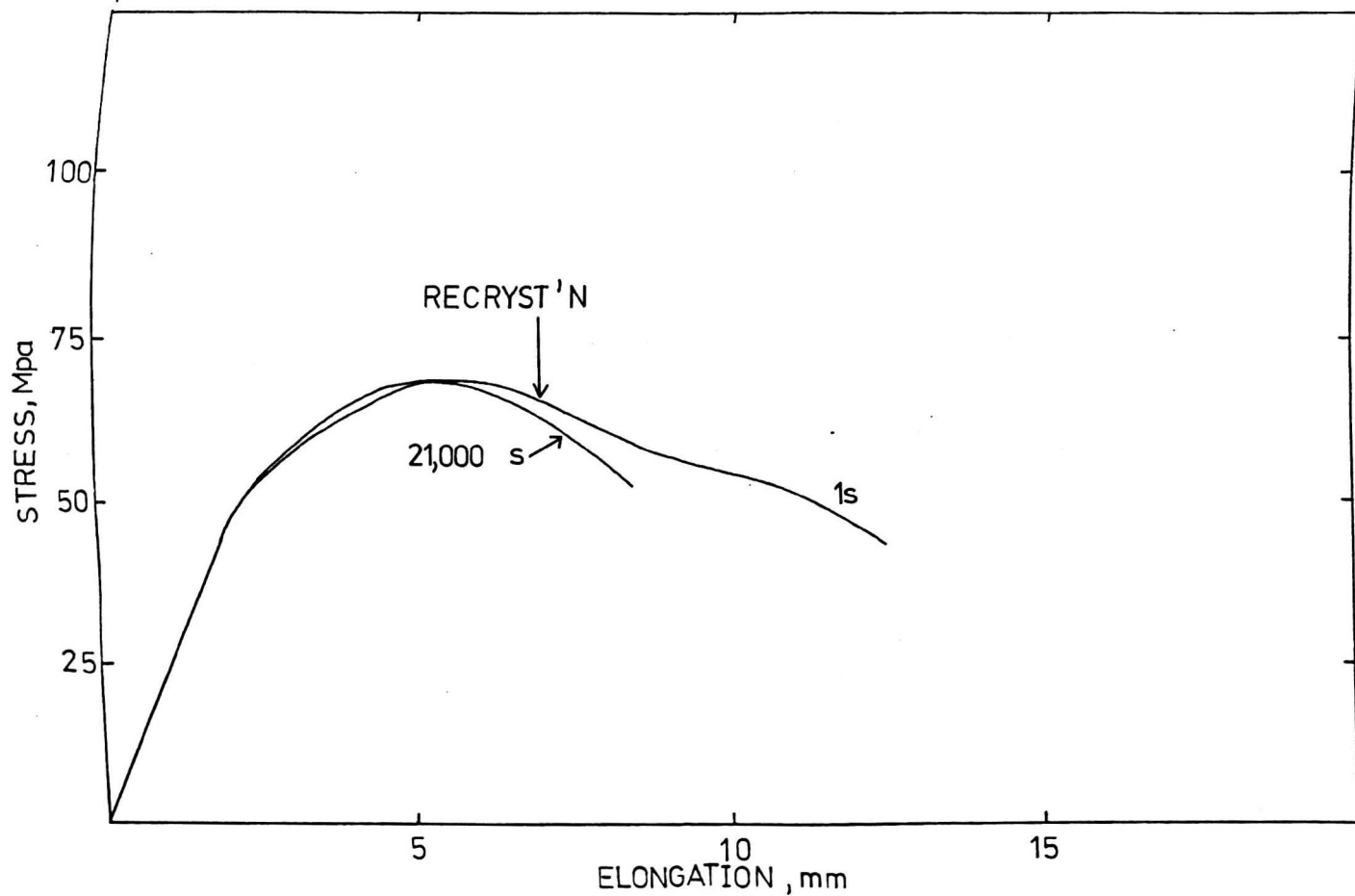
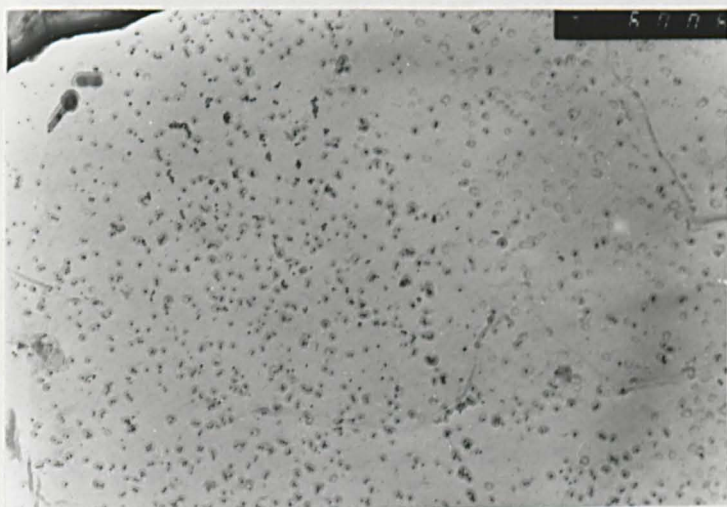


Fig. 7.6

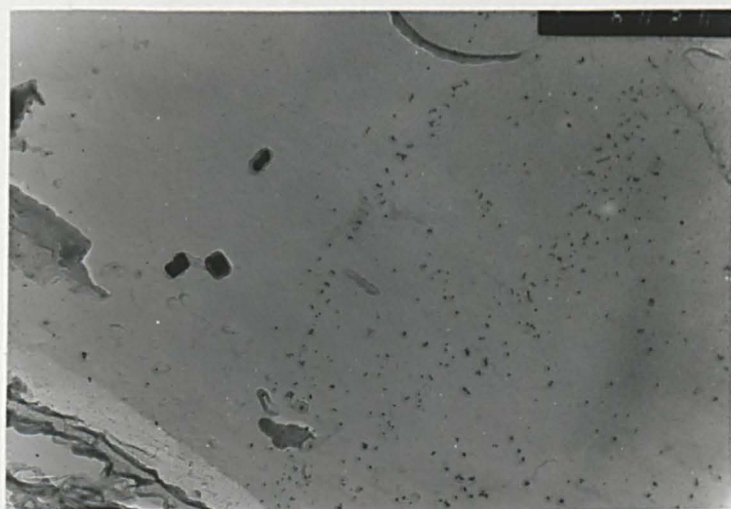
Stress elongation curves for the C-Mn-V-Al steel held at 850°C for various times prior to testing.

a



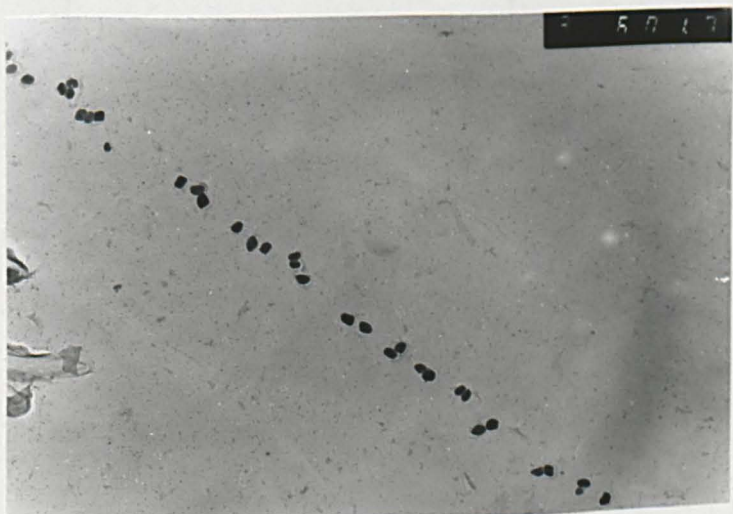
650nm

b



650nm

c



650nm

Fig. 7.7

NbCN precipitation in C-Mn-Nb-Al steel after holding for  
a) 1 s b) 7200 s and c) 21000 s prior to testing at 950°C

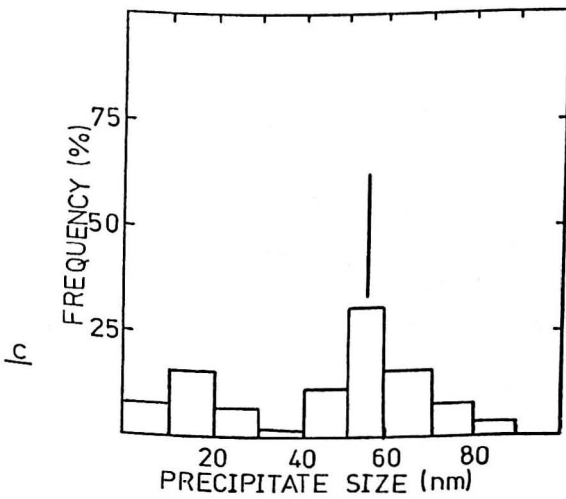
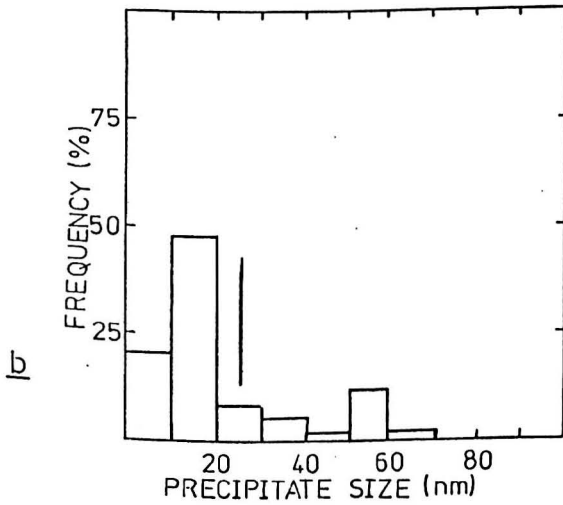
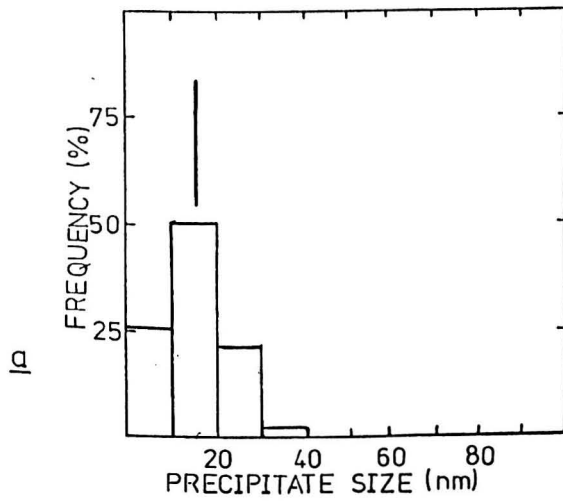
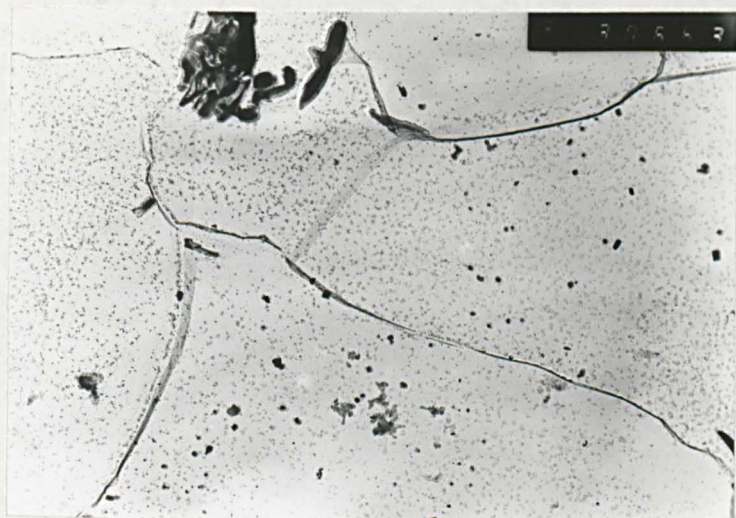


Fig. 7.8

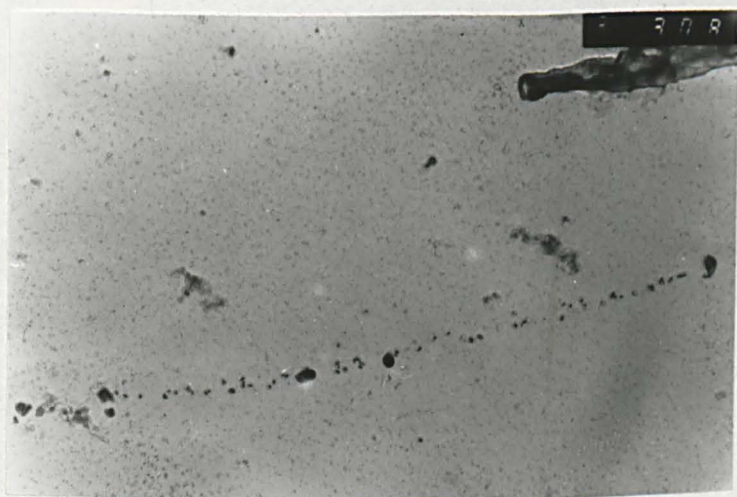
Precipitate size distributions in C-Mn-Nb-Al steel after holding for a) 1 s b) 7200 s and c) 21000 s prior to testing at 950°C.

a



13 μm

b



13 μm

Fig. 7.9

Precipitation in C-Mn-V-Al steel after holding for a) 1 s and b) 21000 s prior to testing at 850°C

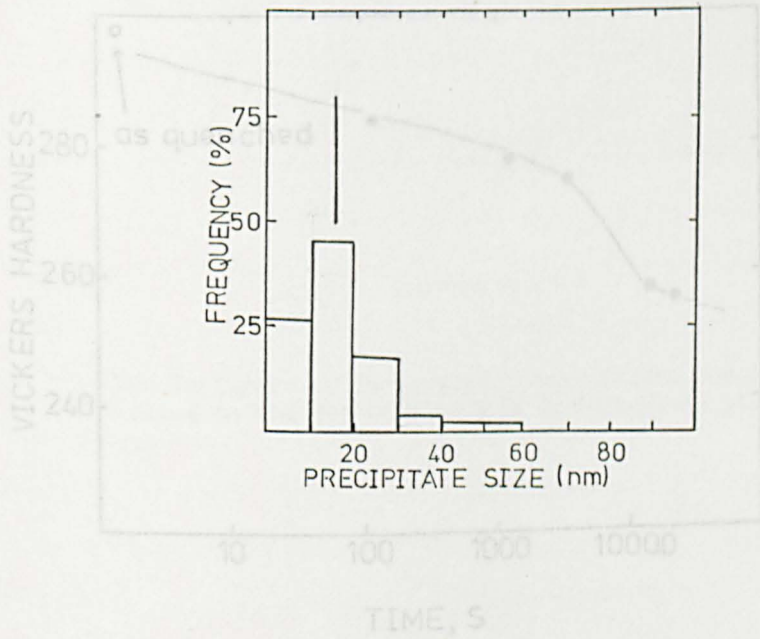


Fig. 7.11

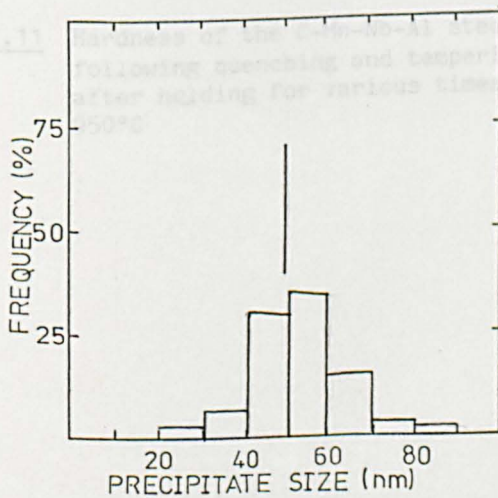


Fig. 7.10

Precipitate size distributions in C-Mn-V-Al steel after holding for a) 1s and b) 21000 s prior to testing at 850°C.

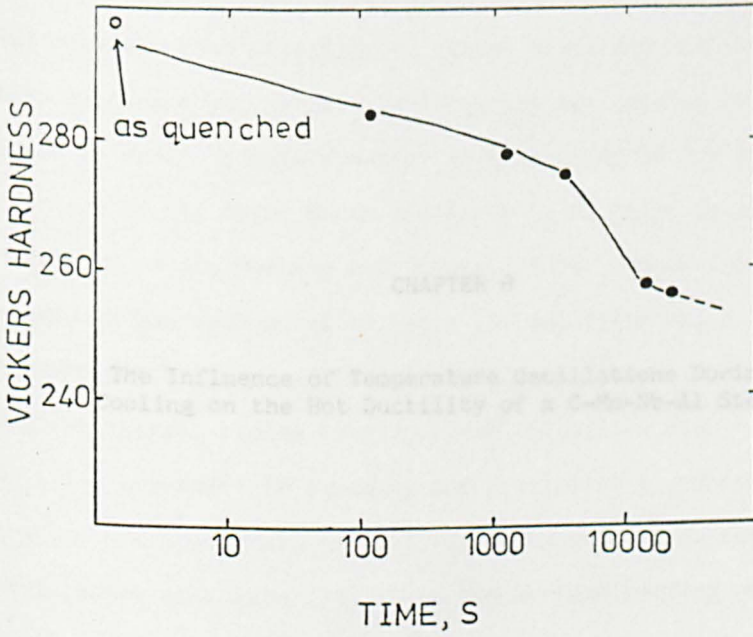


Fig. 7.11 Hardness of the C-Mn-Nb-Al steel following quenching and tempering, after holding for various times at 950°C

## CHAPTER 8

The Influence of Temperature Oscillations During  
Cooling on the Hot Ductility of a C-Mn-Nb-Al Steel

## 8.1 INTRODUCTION

The problem of transverse cracking in continuously cast slabs has received much attention in recent years and many workers have performed hot tensile tests on the susceptible grades of steel in order to gain a better understanding of the phenomenon. (Bernard et al, 1978; Mintz and Arrowsmith, 1979; Ouchi and Matsumoto, 1982; Maehara and Ohmori, 1984). In performing such tests, it has been usual to use a thermal cycle which simulates to some extent that experienced by the continuously cast slab. Typical thermal cycles have involved an initial high temperature solution treatment to dissolve any precipitates present and to produce a coarse grain size, followed by cooling to test temperature at a rate similar to the surface cooling rate of the continuously cast slab. However, the actual thermal cycle experienced at the continuously cast slab surface, where transverse cracks form, is highly complex, and usually a temperature oscillation is set up in the slab surface by the alternate impingement of water sprays and rolls on the slab. Such a temperature oscillation is shown in Fig. 2.5. This cooling pattern differs drastically from the constant cooling rate after solution treatment employed in the majority of previous hot ductility studies.

As discussed in section 2.9, the precipitation of NbCN and AlN is an important factor in determining the hot ductility of microalloyed steels, and the rate of cooling after solution treatment would be expected to have an important effect on precipitation, and hence hot ductility. Indeed, Nozaki et al (1978) showed that this precipitation of AlN after solution treatments was accelerated when a temperature oscillation was introduced into the cooling pattern. As well as influencing precipitation, cooling patterns effect the

thermal stresses set up, and Tomono (1977) has shown that these stresses alone are sufficient to cause cracking in steel slabs, when the slab temperature is oscillated rapidly by the impingement of water sprays.

To date, it appears that only Offerman et al (1981) have investigated the hot ductility of micro-alloyed steels using a cooling pattern which incorporated cyclic temperature oscillation, following solution treatment. They found that the ductility trough observed in micro-alloyed steels following continuous cooling was broadened by the introduction of temperature oscillations. The work of Wilcox (1982) is also of some relevance, as he investigated the hot ductility of micro-alloyed steels following solution treatment, continuous cooling to an intermediate temperature, followed by testing at a higher temperature. For such a thermal cycle, the temperature range of the ductility trough was extended, as compared with direct cooling to test temperature, due to the increased precipitation occurring at the intermediate temperature.

The foregoing results would indicate that the majority of previous hot ductility studies relating to the continuous casting process would tend to over estimate hot ductility, and therefore the aim of this chapter is to investigate the influence of cooling patterns involving temperature oscillations on the hot ductility of an Nb micro-alloyed steel.

## 8.2 EXPERIMENTAL

The steel chosen for this examination was the C-Mn-Nb-Al steel used in the previous two chapters. Composition is given in Table 8.1 and processing details are given in section 6.2. Tensile samples of gauge length 80 mm and diameter 7.9 mm (Fig. 3.6) were machined from the plate with their axes parallel to the rolling direction, for testing using the induction heating equipment described in section 3.2.3. This equipment is capable of producing very rapid cooling rates, suitable for the simulation of rapid temperature oscillations in the tensile samples.

Ideally, cooling patterns which simulate exactly that of the continuous casting process would have been used, but, as the computer simulations of Nozaki et al (1978) shows, such a cooling pattern is complex, involving variable cooling rates and temperature oscillations of varying amplitude, which would be difficult to reproduce consistently in a hot tensile test. For this investigation, it was decided to choose three relatively simple cooling patterns, involving constant cooling rates, and temperature oscillations of constant amplitude.

The three cooling patterns investigated are shown schematically in Fig. 8.1. In each case, the tensile sample was heated to a solution temperature of 1330°C in approximately 10 minutes, and held at this temperature for 5 minutes prior to cooling to test temperatures in the range 850 - 1100°C. Cooling pattern 1 (CP1) involved cooling at a constant rate of 60°C/min. (approximately that of the continuously cast slab surface) to test temperatures. Cooling pattern 2 (CP2) used an overall cooling rate of 60°C/min., but at temperatures below 1100°C, a temperature oscillation was introduced, having a minimum to maximum amplitude of 50°C, and period of 45s. Cooling pattern 3 (CP3) was similar to CP2, but the amplitude of

the temperature oscillation was 100°C, and the period 90s. All three cooling patterns were produced by manual adjustment of the induction heating unit. For all three cooling patterns, the sample temperature was stabilised at the test temperature for 5 minutes, and then the samples strained to failure using a strain rate of  $3 \times 10^{-3} \text{ s}^{-1}$ . After fracture, the samples were cooled rapidly to room temperature in approximately 2 minutes. Examples of the actual cooling patterns for samples tested at 870°C and 1050°C are shown in Fig. 8.2.

Fractured surfaces were examined using a JEOL.T.100 SEM, and carbon extraction replicas prepared and examined, as described in section 3.3. In order to see how closely the precipitation pattern in fractured hot tensile samples resemble that formed in continuously cast slab, carbon extraction replicas were also prepared from a continuously cast slab of thickness 229 mm. The composition of the slab is similar to that of the steel used in the hot ductility tests, and is given in Table 8.1. Carbon extraction replicas were taken from 2 mm below the slab surface, and from the slab centre.

## 8.3 RESULTS

### 8.3.1 Hot Ductility Tests

The variation of reduction in area with test temperature for all three cooling patterns is shown in Fig. 8.3, and in each case, a severe ductility trough is apparent, the depth and width of which varies for each cooling pattern. For CP1, reduction in area falls from 90% to 24% as the test temperature is reduced from 1,000 to 850°C. For CP2 the ductility trough is deeper and broader than that of cooling pattern 1, reduction in area falling from 87% to 19% as the test temperature is reduced from 1050 to 850°C. For CP3 the depth of the ductility trough is similar to that of CP2, but the ductility trough extends to a temperature of 1075°C.

The load-elongation curves for each cooling pattern are shown in Figs. 8.4 - 8.6. Peak load values at a given temperature are similar for each cooling pattern. The onset of dynamic recrystallization as determined by the abrupt drop in load during deformation, varies for each cooling pattern. The temperature range over which dynamic recrystallization occurs for each cooling pattern is indicated on Fig. 8.3. For CP1 dynamic recrystallization occurs in samples tested at 1,000°C or above, whilst for CP3, this temperature is raised to 1100°C.

### 8.3.2 Metallography

SEM fractography revealed that low ductility failures were intergranular in nature, and similar to the intergranular decohesion (ID) and intergranular microvoid coalescence (IMC) fracture modes described in previous chapters, the former fracture mode predominating. High ductility failures were of the ductile rupture type described previously.

Examination of carbon extraction replicas taken from samples fractured using cooling patterns 1 and 3 in the temperature range 870 - 1050°C revealed extensive precipitation of NbCN in all cases. AlN precipitation was not observed. At 870°C, for both cooling patterns, similar precipitation patterns were observed (Fig. 8.7), consisting of extensive grain boundary precipitation of NbCN, and also a fine, matrix precipitation of NbCN. Grain boundary particle size and spacing were 15 nm and 60 nm respectively, and matrix particle size was 7 nm. At a test temperature of 970°C, precipitation was again similar for each cooling pattern, but grain boundary precipitate size and spacing are greater than at 870°C (Fig. 8.8) being 30 nm and 75 nm respectively. At test temperature of 1050°C, grain boundary precipitation of NbCN is still apparent, but little matrix precipitation was observed. However, grain boundary precipitate size and spacing differ for each cooling pattern: for CP1 precipitate size and spacing are 45 nm and 150 nm respectively, whilst for CP3, the values are 35 nm and 70 nm (Fig. 8.9)

Typical precipitation in the continuously cast slab at the surface, and at the centre, is shown in Fig. 8.10. At the slab surface, much grain boundary and matrix precipitation of NbCN was observed. At the slab centre, precipitation was more

random in nature, and only occasionally were grain boundaries decorated by precipitates. At the slab centre, in addition to NbCN, a larger, angular particle was present (Fig. 8.10) analysis of these particles indicated (Mn, Fe)s, typically containing approximately 7 wt.% Fe. The precipitation observed at the slab surface is similar in size and nature to that observed in tensile samples tested in the temperature range 1,000 - 1050°C. Therefore, it would seem reasonable to assume that the majority of the precipitates observed at the slab surface were formed in the temperature range 1,000 - 1,050°C, and that precipitation patterns observed in hot tensile tests are similar to those found in the actual continually cast slab.

#### 8.4 DISCUSSION

The ductility trough observed in the temperature range 850 - 1000°C is typical for C-Mn-Nb-Al steels tested using low strain rates after high temperature solution treatment (see section 2.9). The unusual feature of the hot ductility curves shown in Fig. 8.3 is the dependence of the width of the ductility trough on the cooling pattern used. This behaviour is similar to that observed by Offerman et al (1981). Tomono (1973) showed that when steel slabs are subject to rapid temperature fluctuations due to the impingement of water sprays, the thermal stresses generated were sufficient to cause cracking. This seems an unlikely explanation for the present situation, as cooling rates are far less severe in the hot tensile test, compared with cooling by water sprays. However, to ensure that tensile samples were not cracked by thermal stresses prior to testing, a sample was cooled using cooling pattern 3, but not tested. Inspection using low power microscopy and dye penetrant techniques failed to indicate any cracks.

The observation of enhanced NbCN precipitation at 1050°C using cooling pattern 3 provides an explanation for the increased width of the ductility trough. As indicated in Fig. 8.3, this increased precipitation has led to the onset of dynamic recrystallization being delayed to test temperatures of 1100°C for cooling pattern 3, presumably due to increased grain boundary pinning by the NbCN precipitated. It is this delay in recrystallization which produced the extended ductility trough when cooling pattern 3 was used, by allowing time for the nucleation and growth of intergranular cracks. It should be noted that even when dynamic recrystallization is not occurring, hot ductility tends to increase with test temperature, in a similar fashion to

that observed by Wilcox and Honeycombe (1984) in C-Mn-Nb and C-Mn-Nb-Al steels. This increase may be due to the increase in the rate of dynamic recovery as the temperature is raised, leading to a decrease in the stress levels at grain boundary triple points and other crack nucleation sites. In addition, matrix hardening by NbCN precipitates decreases as the temperature increases, due to the decreased volume fraction of NbCN precipitates.

Cooling pattern 2 shows ductility intermediate between that of patterns 1 and 3, but any changes in precipitation were not large enough to be detected by carbon extraction replicas, as precipitate distributions after using cooling patterns 1 and 2 were similar.

Thus the hot ductility behaviour of a C-Mn-Nb-Al steel after using different cooling patterns can be explained in terms of the differences in the precipitation of NbCN which these cooling patterns produce. Nozaki et al (1978) observed that temperature oscillations above and below the transformation temperature led to enhanced precipitation of AlN, but such an explanation cannot be used to account for the enhanced NbCN precipitation observed in the present study, as the lowest temperature reached during the oscillations was approximately 800°C. The  $A_{e3}$  temperature calculated for this steel using Andrews's equation (1965) is 840°C, but the  $A_{r3}$  temperature is still likely to be well below 800°C, due to the very rapid cooling rate during the temperature oscillations. Therefore, at no time is the steel cooled below the  $A_{r3}$  temperature.

A possible explanation for the enhanced precipitation of NbCN during temperature oscillations becomes apparent when it is noted that using CP3 and a test temperature of 1050°C, the lowest

temperature reached is approximately 950°C, and that the time spent at temperatures near 950°C is approximately 2 minutes. The studies on the precipitation kinetics of NbCN by Le Bon et al (1975), Watanabe et al (1977) and Weiss and Jonas (1979) have all shown that NbCN precipitation is most rapid around 950°C. The incubation time for precipitation appears to vary with the method used for the precipitation study, but at 950°C, incubation times are usually in the range 1 - 5 minutes. Thus by cooling to 950°C prior to testing at 1050°C, an opportunity is given for the rapid precipitation of NbCN to occur at 950°C, leading to higher volume fractions of NbCN at 1050°C than would be expected simply by direct cooling to 1050°C. The study of the static precipitation kinetic of NbCN at 950°C using hardness measurements performed in Chapter 7 support this argument, as they demonstrate that for this particular C-Mn-Nb-Al steel, precipitation of NbCN commences after approximately 5 minutes (Fig. 7.11).

With regards to continuous casting, it is apparent from Fig. 8.3 that the cooling pattern used is only likely to influence transverse cracking if the slab straightening temperature is above 970°C. For straightening temperatures above 970°C, when hot ductility is strongly influenced by cooling pattern, it is obviously important to maintain uniform cooling of the slab surface.

In the present study, temperature oscillations have occurred entirely in the austenite. During the actual continuous casting process, temperature oscillations are likely to occur which lead to cycling through the  $\gamma$  -  $\alpha$  transformation. Under such conditions, hot ductility would be expected to be reduced still further, due to such effects as the enhanced precipitation of AlN (Nozaki et al, 1978) and the introduction of transformation stresses. (Coleman and Wilcox, 1985). Therefore, under actual continuous casting

conditions, transverse cracking is likely to be reduced by the use of a uniform cooling pattern even if the slab straightening temperature is less than 970°C.

## 8.5 CONCLUSIONS

1. Introducing temperature oscillations into the cooling pattern of a C-Mn-Nb-Al steel after solution treatment leads to an extension in the temperature range of the ductility trough normally associated with such steels after uniform cooling from solution temperature.
2. This extension of the ductility trough is due to the retardation of dynamic recrystallization introduced by the temperature oscillations during cooling. This is caused by enhanced NbCN grain boundary precipitation during the temperature oscillations.
3. If the straightening of continuously cast slab is performed at temperatures above 970°C, it is important to keep the slab surface cooling as uniform as possible.

Steel	C	Si	Mn	P	S	Al	N	Nb
1	.12	.29	1.44	.003	.009	.015	.010	.034
2	.14	.22	1.36	.005	.011	.030	.009	.030

Table 8.1 Compositions of the steels examined (wt. %)

- 1 - C-Mn-Nb-Al steel for hot tensile testing
- 2 - continuously cast slab

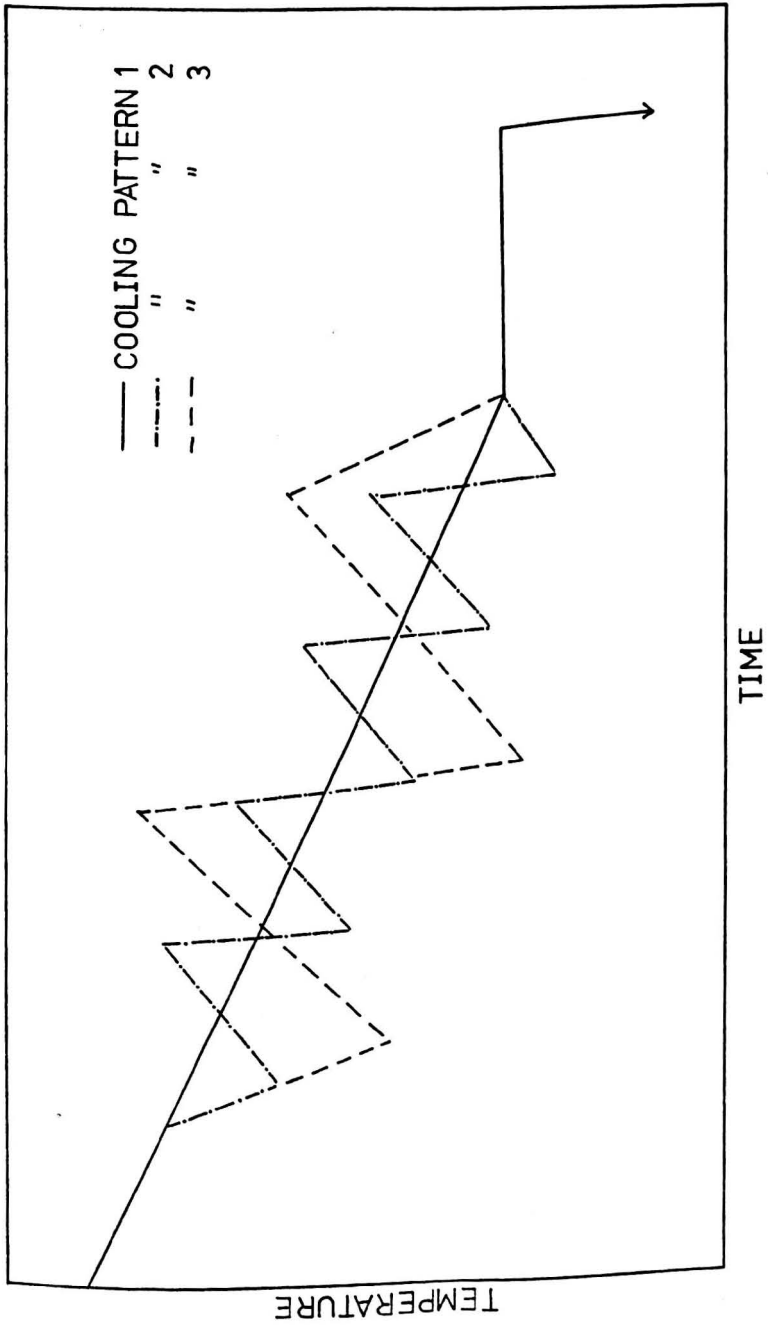


Fig. 8.1 Schematic illustration of cooling patterns from solution temperature.

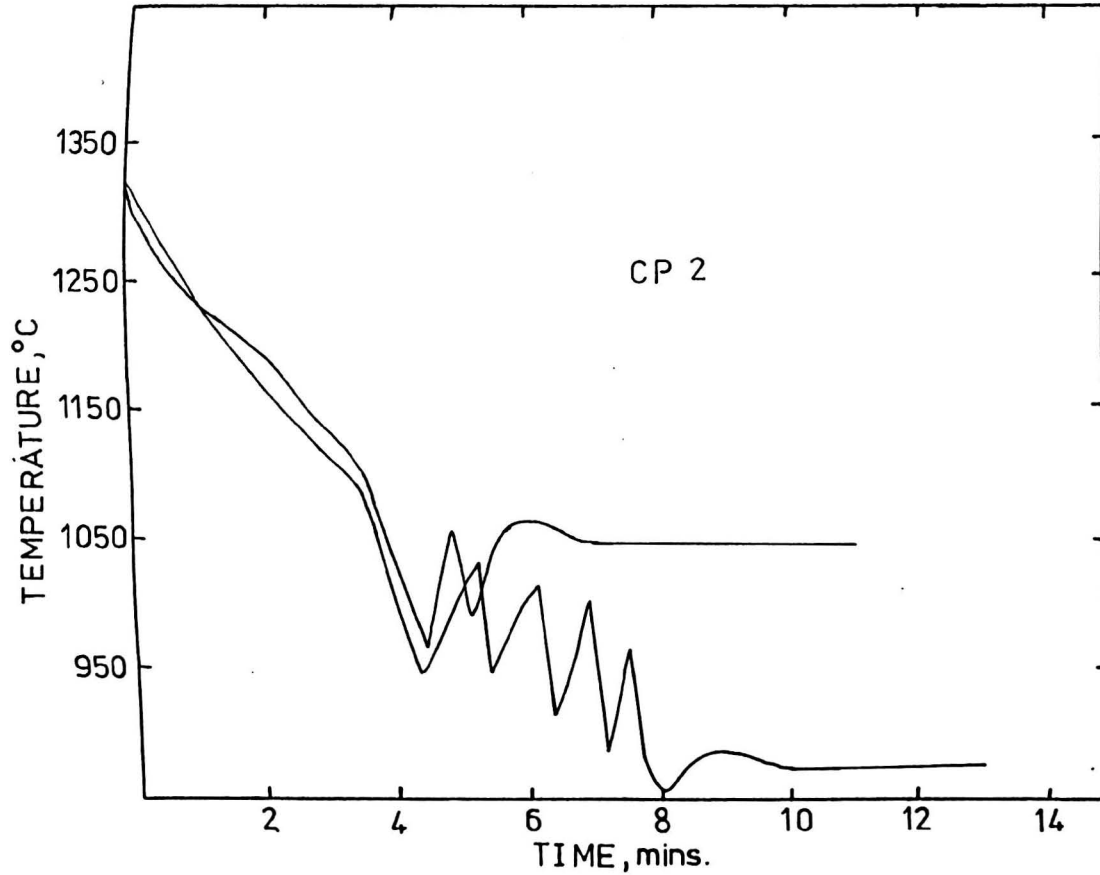


Fig. 8.2a Actual cooling curves for cooling pattern 2, test temperatures 870 and 1050°C

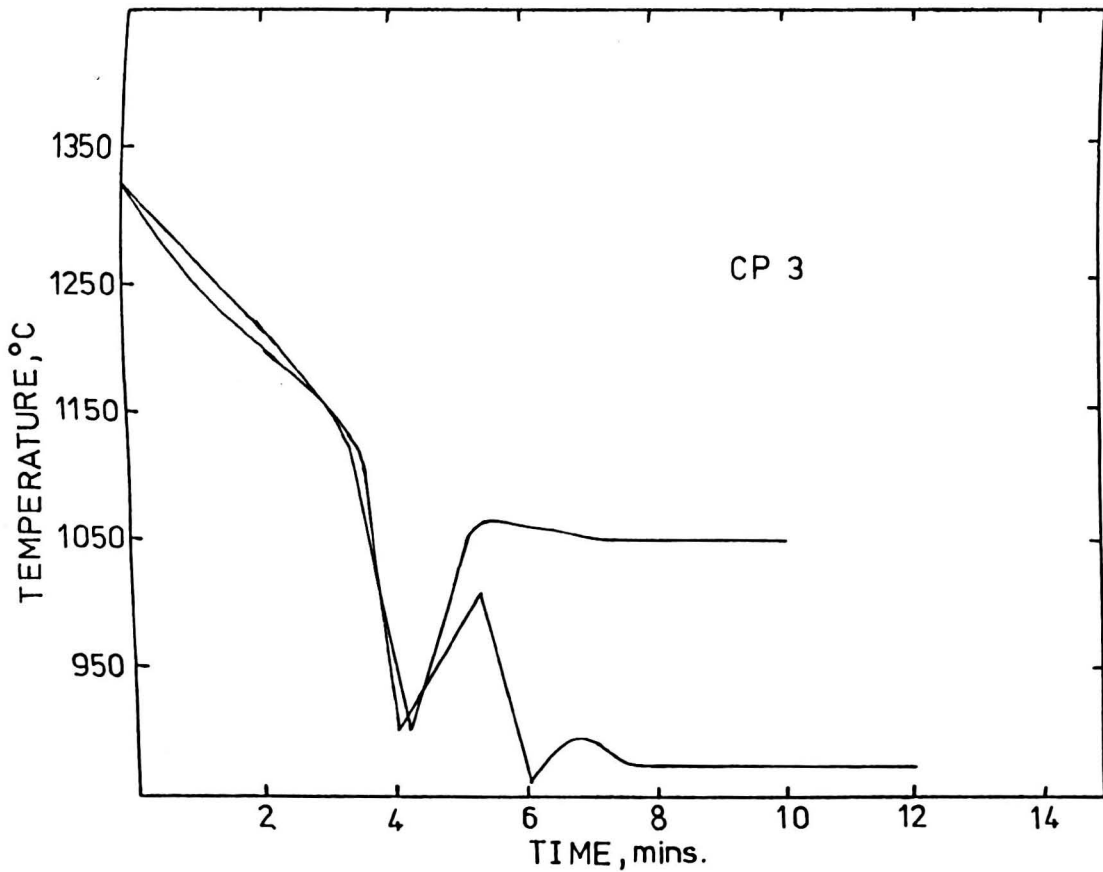


Fig. 8.2b Actual cooling curves for cooling pattern 3, test temperatures 870 and 1050°C.

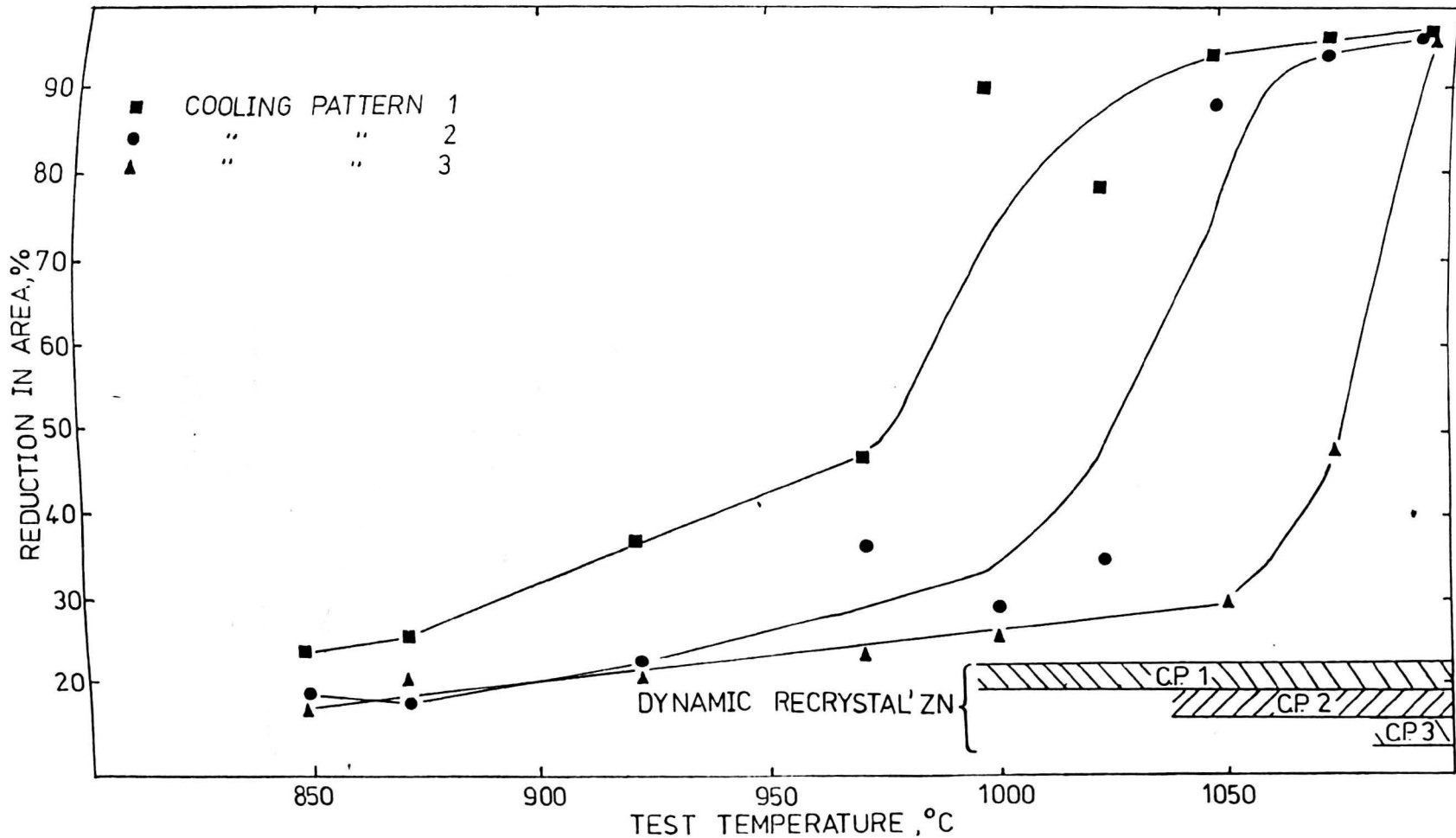


Fig. 8.3 Hot ductility curves for each cooling pattern, occurrence of dynamic recrystallization indicated by shaded regions.

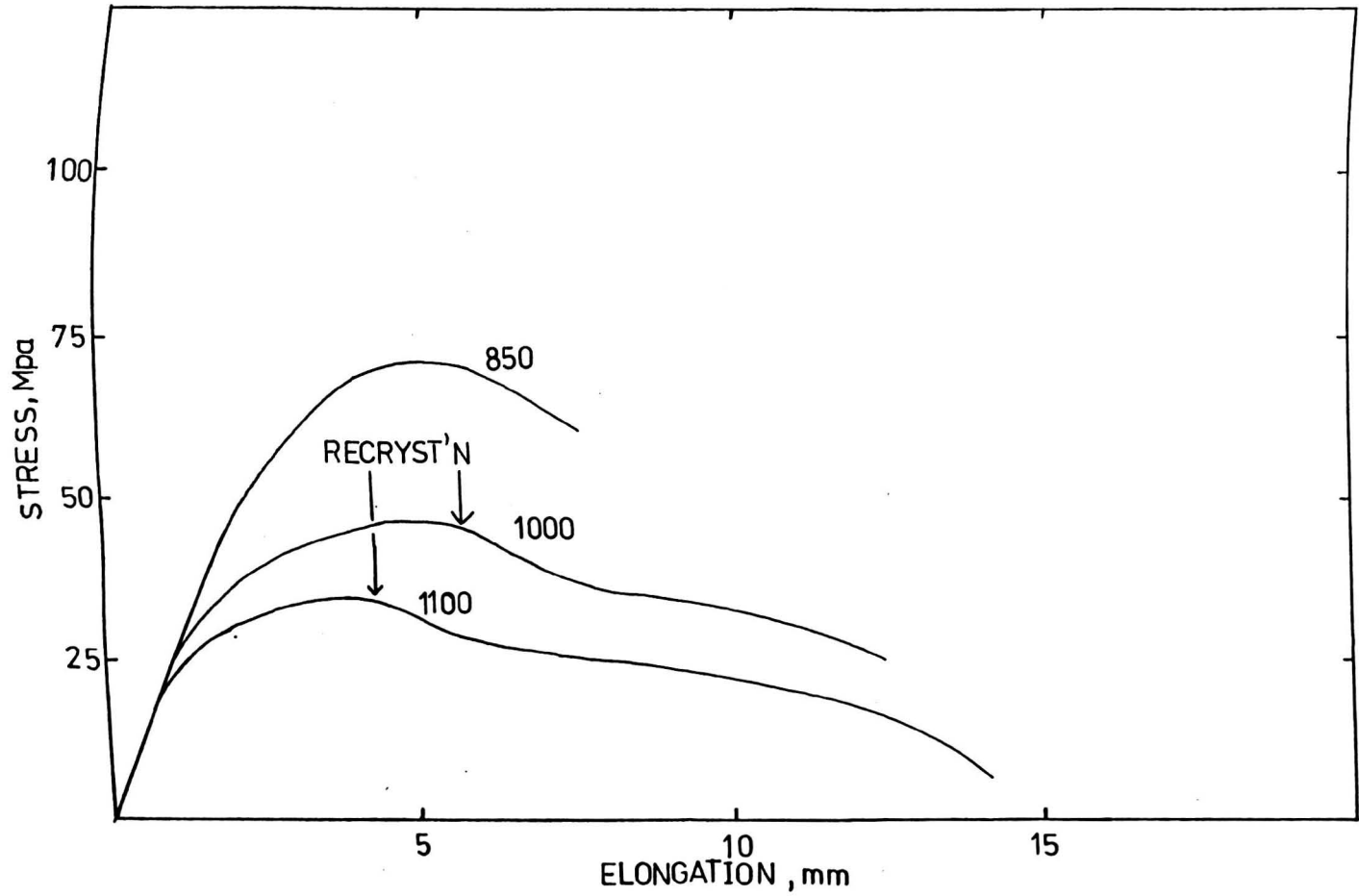


Fig. 8.4 Representative load-elongation curves for cooling pattern 1.

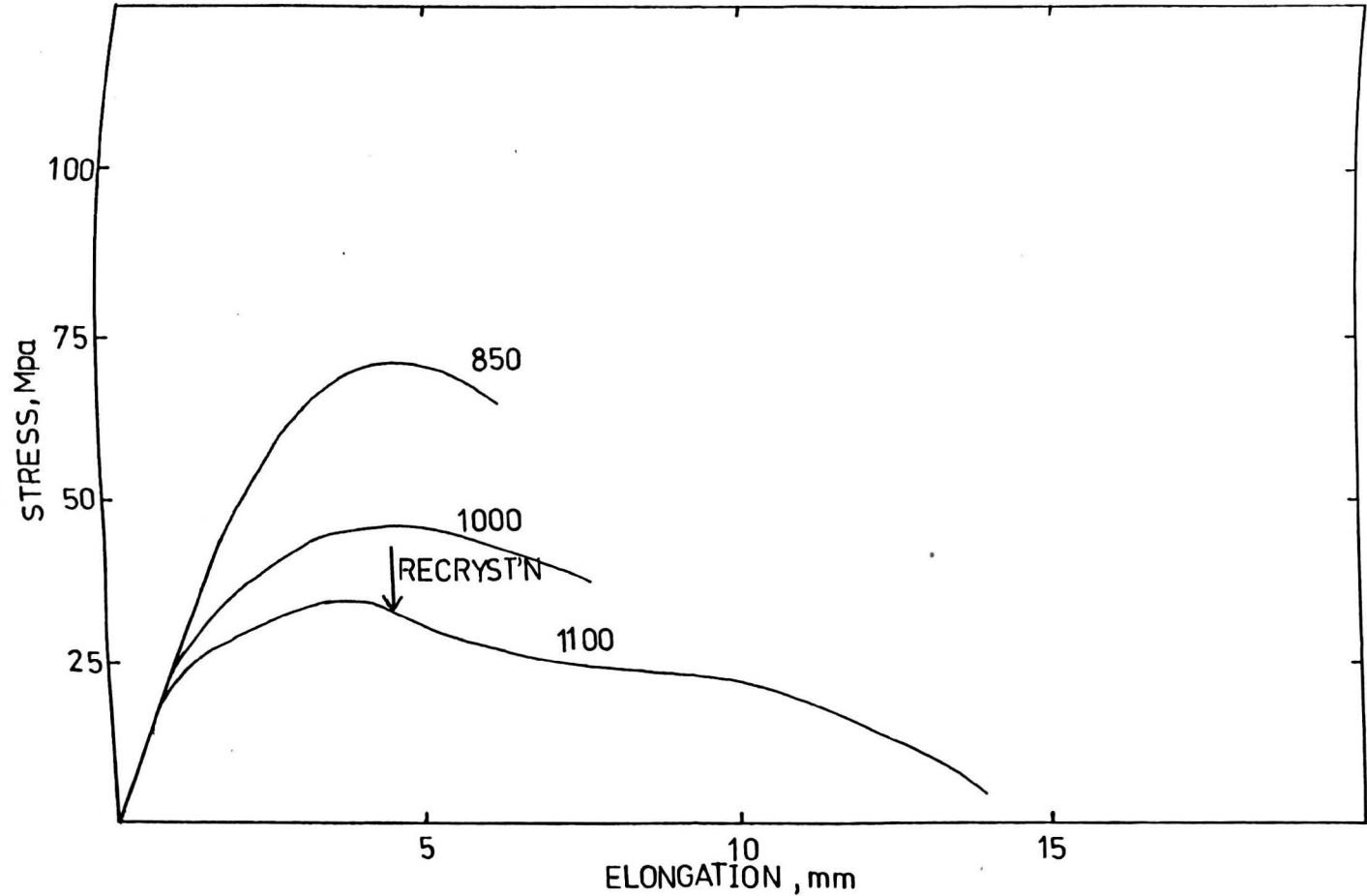


Fig.8.5 Representative load-elongation curves for cooling pattern 2.

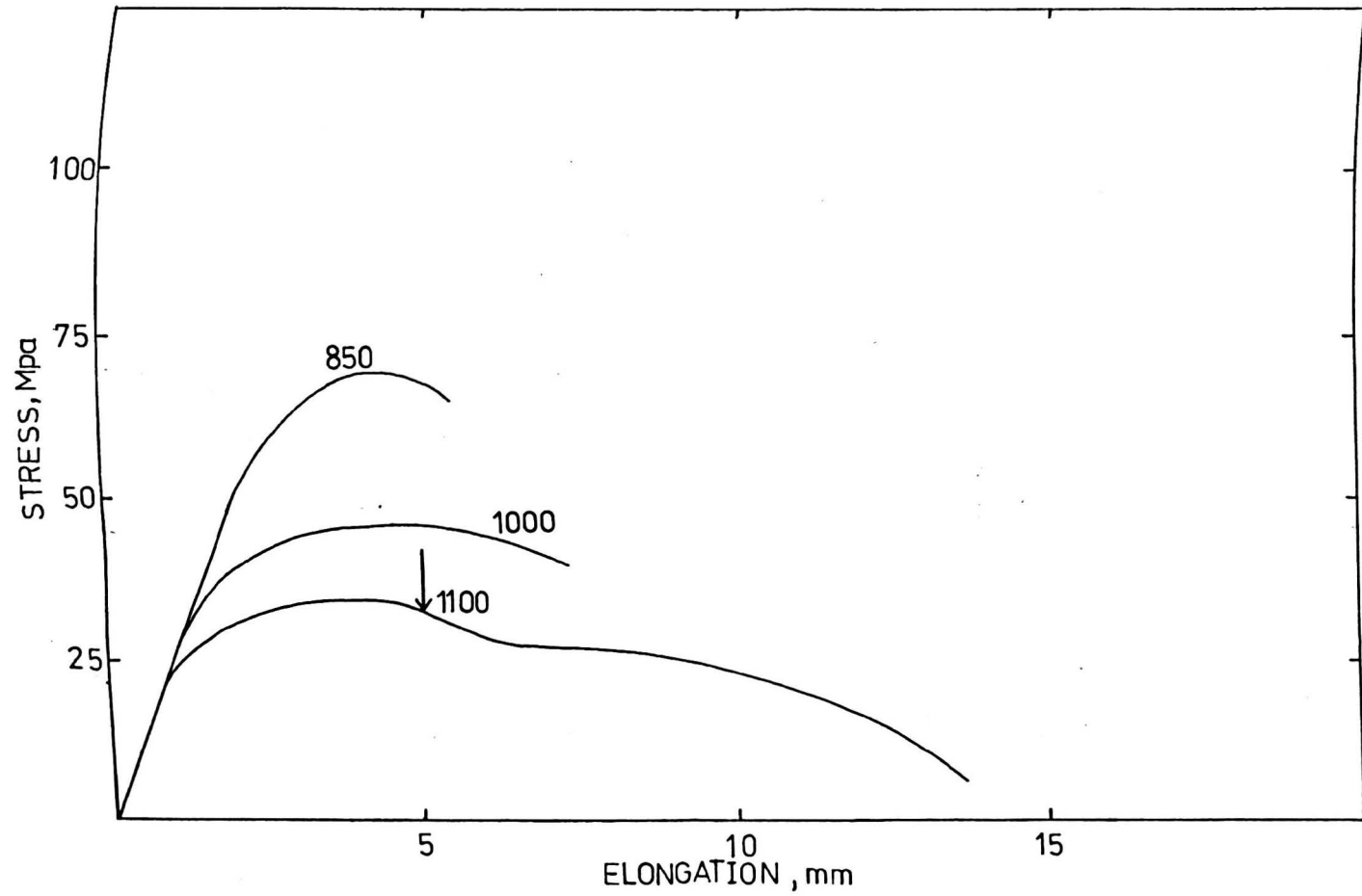


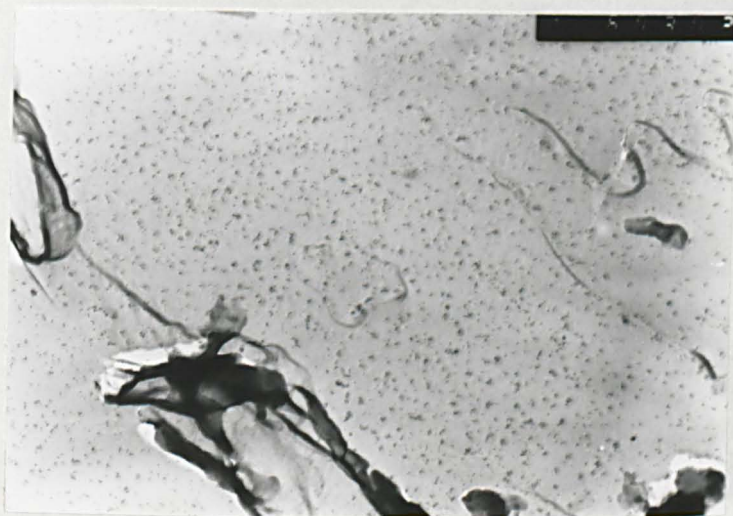
Fig. 8.6 Representative load-elongation curves for cooling pattern 3.

a



13 μm

b



650 nm

Fig. 8.7 Precipitation in steels tested at 870°C after a) cooling pattern 1 and b) cooling pattern 3.

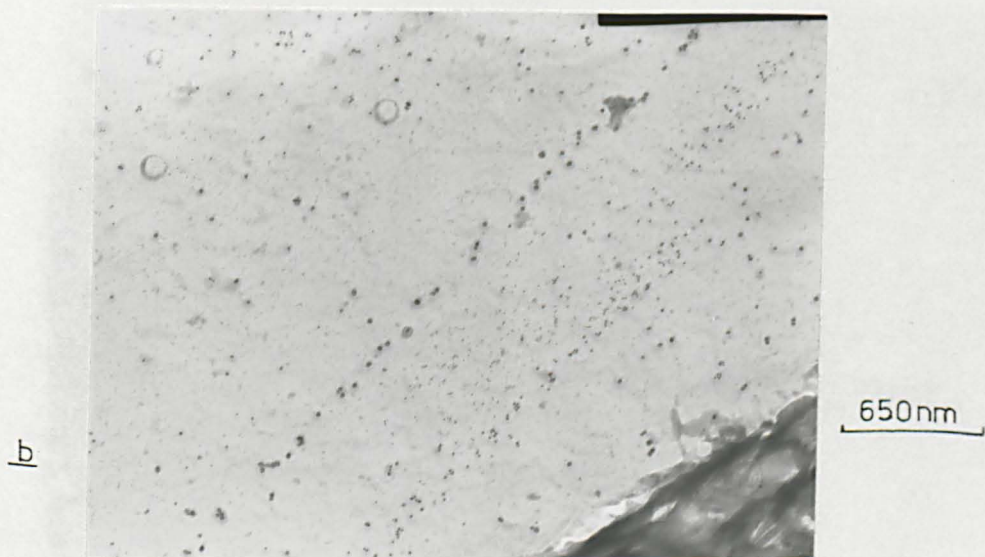
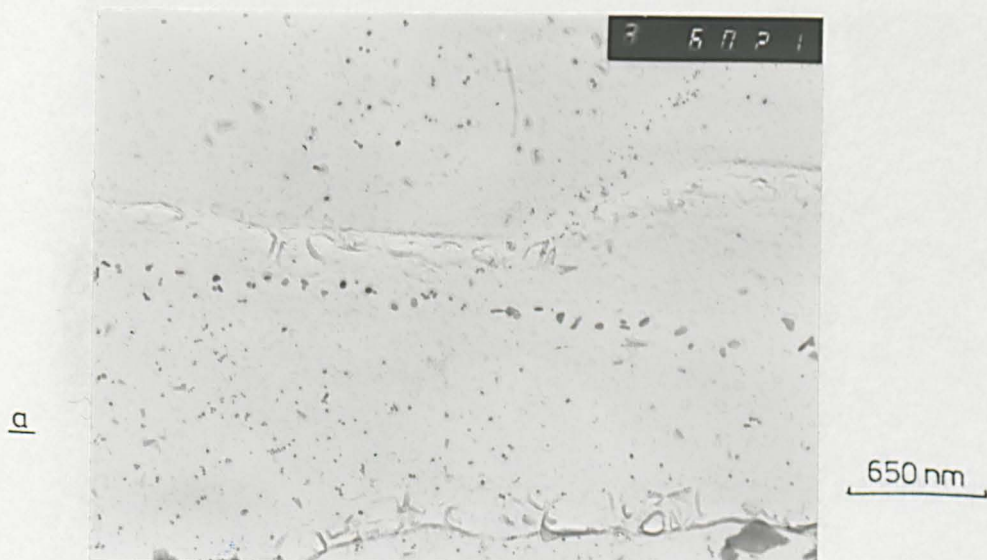


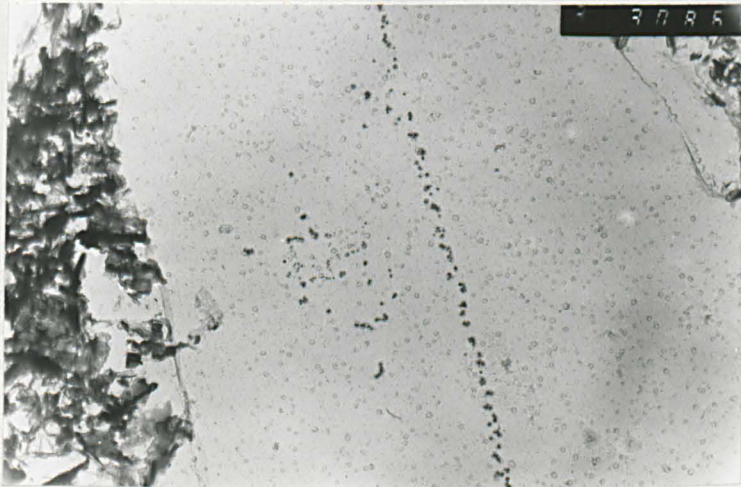
Fig.8.8 Precipitation in steels tested at 970°C after a) cooling pattern 1 and b) cooling pattern 3.

a



13 μm

b



13 μm

Fig.8.9 Precipitation in steels tested at 1050°C after a) cooling pattern 1 and b) cooling pattern 2.

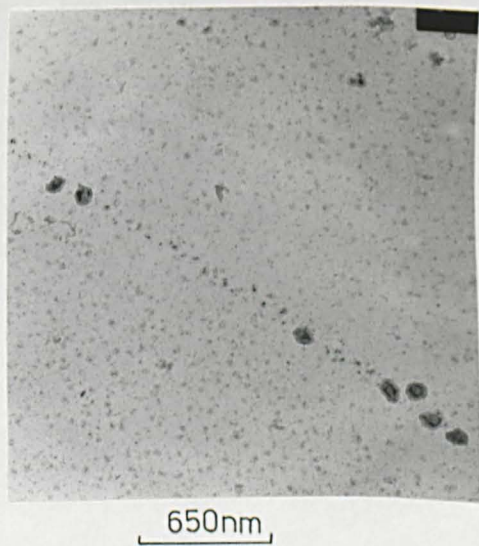
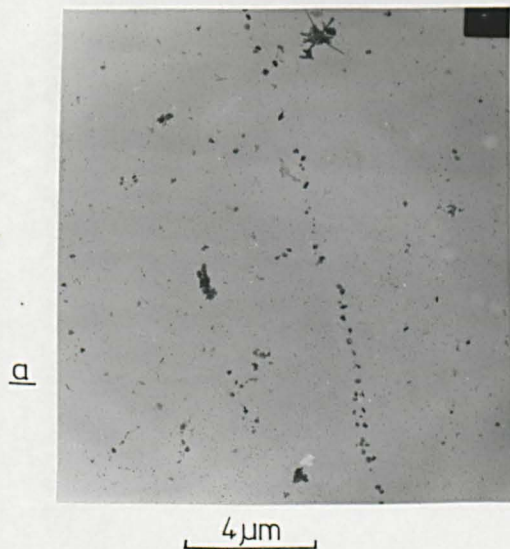


**Fig. 8.10** Precipitation in continuously cast C-Mn-Nb-Al slab a) surface  
b) centre.

CHAPTER 9

THE HOT DUCTILITY OF A DIRECTLY CAST

C-Mn-Nb-Al STEEL

## 9.1 INTRODUCTION

In chapter 8, it was noted that the majority of previous hot ductility studies simulate only approximately the thermal cycle experienced by the continuously cast slab, and an attempt was made to produce a cooling pattern similar to that experienced during continuous casting. However, as in the majority of previous studies, these tests were performed on wrought, as opposed to cast, materials. The wrought material might be expected to have improved hot ductility when compared to the as cast material, owing to such factors as the refinement of the as cast grain size, and also due to the formation of new grain boundaries, which are away from the original highly segregated, as cast, austenite grain boundaries.

Of the few studies conducted on the hot ductility of as cast material, (Lankford, 1972; Harding et al, 1977; Suzuki et al 1982; Rogberg, 1983) none have used C-Mn-Nb-Al steels, and only the studies of Lankford and Suzuki were aimed at simulating the continuous casting process. Therefore, it was decided to investigate the hot ductility of a C-Mn-Nb-Al steel conforming to BS 4360 grade 50D composition limits, (a grade particularly prone to transverse cracking) directly after casting. It was hoped to simulate more closely the continuously cast structure. In addition, it was decided to compare the hot ductility of these cast samples with samples which had been cooled to room temperature after casting, and then solution treated prior to hot tensile testing.

## 9.2 EXPERIMENTAL

The composition of the steel examined is given in Table 9.1. The steel was supplied as a slice off a corner of an as-cast ingot. Tensile samples 100 mm in length and having an approximate gauge length of 50 mm were individually machined so as to fit inside silica tubes with a 0.2 mm diametrical clearance. A 1.2 mm diameter hole was drilled from one end of each sample so that a thermocouple could be inserted (Fig. 9.1). The samples were heated using the induction heating unit described in section 3.23 so that approximately 20 mm of the gauge length at the mid length position could be melted. The molten region was contained in the tolerance fitted silica sheath.

Samples were melted at 1560°C, re-solidified and cooled at 60°C min<sup>-1</sup> to test temperatures in the range 850-1200°C and then strained to failure at a rate of  $1.3 \times 10^{-2} \text{ S}^{-1}$ . This strain rate is slightly faster than the rate used in previous tests.

In addition to obtaining the hot ductility directly after casting, (samples referred to in text as 'as cast') samples were allowed to cool to 60°C, reheated to 1330°C, held for 5 minutes, cooled at 60°C min<sup>-1</sup> to the test temperature and either held for 5 minutes or strained immediately to failure (samples referred to in text as 'reheated').

Comparison with previous work (Mintz and Arrowsmith, 1979; Ouchi and Matsumoto, 1982) was made by obtaining the Gleeble hot ductility data over the same temperature range using the as supplied ingot steel which had been reheated to 1330°C and cooled at 60°C min<sup>-1</sup>. (Samples referred to in text as 'reheated Gleeble'.) The strain rate in these Gleeble tests was  $3 \times 10^{-3} \text{ S}^{-1}$ .

Austenite grain sizes were obtained using the linear intercept measurement on transverse sections prior to straining from both 'as cast' and 're-heated' samples.

Carbon extraction replicas were taken close to fracture surfaces for samples of both 'reheated' and 'as cast' conditions. In addition, the progress of sulphide precipitation during reheating was followed by heating samples to temperatures in the range 1200 - 1300°C and quenching into iced brine. Precipitates extracted using carbon replicas were analysed using an EDAX attachment, and semi-quantitative analysis obtained using the EDAX programme SW.9100 version 2.3.

To examine sulphide composition and the composition of the steel surrounding the sulphides, polished sections were examined using an SEM with EDAX attachment.

### 9.3 RESULTS

#### 9.3.1 Hot Ductility Tests

The hot ductility curves of reduction in area against test temperature for 'reheated' 'reheated Gleeble' and 'as cast' conditions are given in Fig. 9.2. For the reheated and as cast conditions, reduction in area values fell from 90% to 25% over the temperature range 1050 - 850°C. Of the two conditions, the 'as cast' material gave the better hot ductility, its hot ductility trough being approximately 80°C lower in temperature. Samples given long hold times (approximately 1 hour) at the solution treatment temperature did not give significantly different reduction in area values to those samples given standard holding times. The curve for the 'reheated Gleeble' falls in between the 'as cast' and 'reheated'. However, the slower strain rate used in the Gleeble test would be expected to reduce hot ductility (see section 2.5) so that although an exact comparison cannot be made, there is no doubt that the 'reheated Gleeble' samples have better hot ductility than samples reheated after induction melting.

#### 9.3.2 Metallography

The austenite grain sizes prior to straining for the 'as cast' and 'reheated' samples were 700 and 260  $\mu\text{m}$  respectively. The 'as cast' grain size compares favourably with grain size measurements taken at the surface of continuously cast slabs.

SEM examinations of fracture surfaces of samples broken at temperatures giving low ductilities showed three distinct fracture modes; high temperature ductile rupture (HTDR), intergranular microvoid coalescence (IMC), and interdendritic failure (IDF), Figs. 9.3 - 9.5. The first two fracture modes were essentially similar to those described in chapter 6, and formed the majority

of the fracture surface. It is believed that the IDF fracture mode occurs during solidification, and is due to a shortage of feed metal to the interdendritic regions, resulting in shrinkage cavities. In the 'as cast' condition, lines of angular, type III MnS inclusions could be seen on the IDF regions of the fracture surface, (Fig. 9.5) which probably mark the regions where a number of dendrites meet. Smaller MnS inclusions were also observed on the nodule surfaces. In contrast, reheated samples showed few of these MnS inclusions.

These coarse angular precipitates were not observed on carbon extraction replicas suggesting that they were either of a very localised nature, or were not extracted. However, replicas did reveal an hexagonal sulphide ( - 100 nm in diameter) at the prior austenite grain boundaries (Fig. 9.6). This precipitate tended to be sparse in the 'as cast' condition, but very marked in the 'reheated' condition. The amount present in the 'reheated' condition could be reduced by lowering the soaking temperature in the reheating part of the thermal cycle from 1330°C to 1200°C (Figs. 9.6 and 9.7) These facts suggest that the austenite grain boundary sulphides originated through partial solution and re-precipitation of the coarser interdendritic sulphides.

Carbon extraction replicas also revealed precipitation of NbCN in a fine form at austenite grain boundaries, sub-boundaries and within the matrix in all the strained samples examined (Figs. 9.8 - 9.9) However, there was significantly more of this grain boundary precipitation in the 'reheated' condition compared to the 'as cast' (compare Figs. 9.8 and 9.9) In addition to the fine NbCN, a coarse NbCN eutectic was also present in the 'as cast' condition (Fig. 9.10), but a large proportion of this was observed to redissolve on reheating to 1330°C.

Sulphide particles extracted by replicas from both 'as cast' and 'reheated' samples were analysed, and the majority of the smaller sulphides (100 - 200 nm diameter) extracted from the boundaries were shown to contain iron, generally between 5 - 10%, although isolated inclusions gave much higher values of 20%. Typical X-ray spectra for those sulphides are shown in Fig. 9.5. Within the accuracy of the measurement, there was no significant difference in iron content between inclusions found in 'as cast' and 'reheated' samples.

Micro-analysis of polished samples of 'as cast' material indicated that the Mn content of the matrix surrounding a (Mn, Fe)S inclusion was 20 - 25% that of the Mn content of the bulk of the material (see Table 9.2). Analyses of a continuously cast slab are also shown.

Replicas taken from the 'reheated Gleeble' samples close to the fracture indicated that the degree of precipitation both of MnS and NbCN at grain boundaries was somewhere in between that shown by the 'as cast' and 'reheated' conditions, in accord with hot ductility behaviour (Fig. 9.11).

#### 9.4 DISCUSSION

Mintz and Arrowsmith (1979) and Funnell and Davies (1978), and also the results of chapter 8, have all shown that the hot ductility of micro-alloyed steels is very much influenced by the degree of precipitation at the grain boundaries, the more finely spaced being this precipitation, the worse the hot ductility. Of the previous studies carried out to evaluate the hot ductility of directly cast steel (Lankford, 1972; Harding et al, 1977; Suzuki et al, 1982; Rogberg, 1983), the work of Harding again shows it is the degree of grain boundary precipitation which controls hot ductility. In this work, better hot ductility was obtained in an Al containing steel in the reheated, as opposed to the as cast condition. It was suggested that in the reheated condition, the AlN was taken back into solution, and because of slow rate of AlN precipitation during cooling, remained in solution on cooling to the test temperature. In the present investigation, the hot ductility of the 'as cast' material was superior to the 'reheated'. Such behaviour is unusual in that the hot ductility of wrought material is generally superior to 'as cast' since hot working refines and homogenises the micro structure. (Sellars and Tegart, 1972) It may be explained by the presence of only isolated particles at the grain boundaries in the 'as cast' state, but continuous fine networks of both MnS and NbCN in the 'reheated' condition. Although fracture examinations (Figs. 9.3 - 9.5) did show extensive coverage of the dendrite nodules by MnS inclusions, most of these do not lie along the austenite grain boundaries. NbCN eutectics were observed in the 'as cast' state, but these eutectics were not continuous and were in coarse form. The re-distribution of MnS and NbCN on reheating to give fine net-

works would be likely to reduce hot ductility and give rise to the observed interangular failures for a number of reasons. Grain boundaries would be more effectively pinned by the finer distribution of particles and cavitation processes would therefore be able to take place more readily. A fine continuous network would provide easy linkage for crack propagation. Finally, the grain boundary network of precipitates were often associated with precipitate free zones (Fig. 9.8) and this would tend to concentrate the strain into the boundary region. The major problem in the above interpretation is accounting for the extensive networks of sulphide precipitates which have not been observed in previous work.

The observation of coarse NbCN eutectics and coarse MnS inclusions in the 'as cast' tensile samples indicates that there has been intense segregation to the interdendritic boundaries during solidification. This form of precipitation can be found at the centre-line of a continuously cast slab, where segregation is most marked. Because of the intense segregation of S during solidification, the finer sulphides were formed as (Mn, Fe) S inclusions. These would be gradually converted to a pure MnS given time if the temperature was sufficiently high, and in the process these inclusions absorb Mn from the surrounding matrix. This has been shown by the Mn content of the matrix in the vicinity of the inclusions being reduced to about a quarter to approximately 0.3%. This reduced level of Mn would, according to Turkdogan et al (1955) increase the solubility of S in austenite at 1330°C, so that approximately 0.005% S would be available for precipitation on cooling after reheating. Salmon Cox and Charles (1965) have also noted that (Mn, Fe)S can form in ingot steels of relatively high Mn/S ratio when segregation has been intense, and in reverting to a purer

MnS level in the neighbourhood of the inclusion is considerably reduced. They also point out that the manganese to sulphur ratios obtained by bulk analysis may be misleading as it is the ratio in the actual liquid from which the sulphide is formed which is important. To summarise, it is believed that the poorer hot ductility of the 'reheated' condition compared to the 'as cast' is due to the dissolution of 'as cast' sulphides at the reheating temperature and their subsequent reprecipitation in a fine form at the austenite grain boundaries at the test temperature. The high solubility of the 'as cast' sulphides is explained by a high level of segregation during solidification after re-melting which resulted in Fe-rich sulphides surrounded by Mn-depleted matrix. It is clear from the foregoing that the casting condition used after melting a small section of a tensile specimen are very different to those encountered during commercial continuous casting close to the slab surface, where transverse cracking occurs. This is evident by comparing the precipitate distribution in material taken from the surface of continuously cast slab, (Fig. 8.10) and the precipitate distribution in the present 'as cast' samples. Segregation in the laboratory sample has been found to be more intense, and this suggests that the cooling rate is too slow, allowing concentration of elements into the last liquid to solidify around the interdendritic boundaries. This leads to the production of (Mn, Fe) S which can subsequently redissolve more readily on reheating giving poor hot ductility. By encouraging the formation of pure MnS by faster cooling as found in commercially continuously cast slab the tendency to re-dissolve will be reduced and the hot ductility of the 'as cast' and 'reheated' states would then be expected to be similar.

Thus the laboratory hot ductility test in its current form, although

giving much useful information on the importance of the precipitate distribution at the austenite grain boundaries in controlling hot ductility, cannot at present, satisfactorily simulate the commercial casting condition encountered during continuous casting. It is intended to develop the test further by increasing the cooling rate, introducing a cyclic rise and fall in temperature to simulate the undergone by the commercial strand.

## 9.5 CONCLUSIONS

The hot ductility of C-Mn-Nb-Al steel cast in situ and subsequently tested in the temperature range 850-1300°C has been shown to be superior to that of the steel after cooling below the transformation, resolution treated and tested in the same temperature range.

This difference in hot ductility can be related to the presence of a dense, finely divided precipitation of sulphide and NbCN precipitates along the grain boundaries in 'reheated' samples but not in 'as cast' samples. In contrast, in the 'as cast' sample, because of the slow cooling rate during solidification, marked segregation occurred resulting in coarse NbCN eutectics and manganese sulphide containing small amounts of Fe, being produced close to the interdendritic boundaries. These were able to subsequently largely re-dissolve on reheating to 1330°C and precipitate out in a fine form at the new grain boundaries formed on reheating.

C	Si	S	P	Sol Al	N	Nb	Mn
.14	.35	.013	.009	.038	.006	.040	1.40

Table 9.1 Analysis of steel examined (Wt.%)

Sample	Mn/S ratio of sulphide	Mn content of steel surrounding sulphide relative to bulk Mn
As cast tensile	1.11	0.24
Concast slab surface	1.28	1.08
Concast slab centre-line	1.58	1.02

Table 9.2 Results of EDAX micro-analysis of sulphides and surrounding matrix.

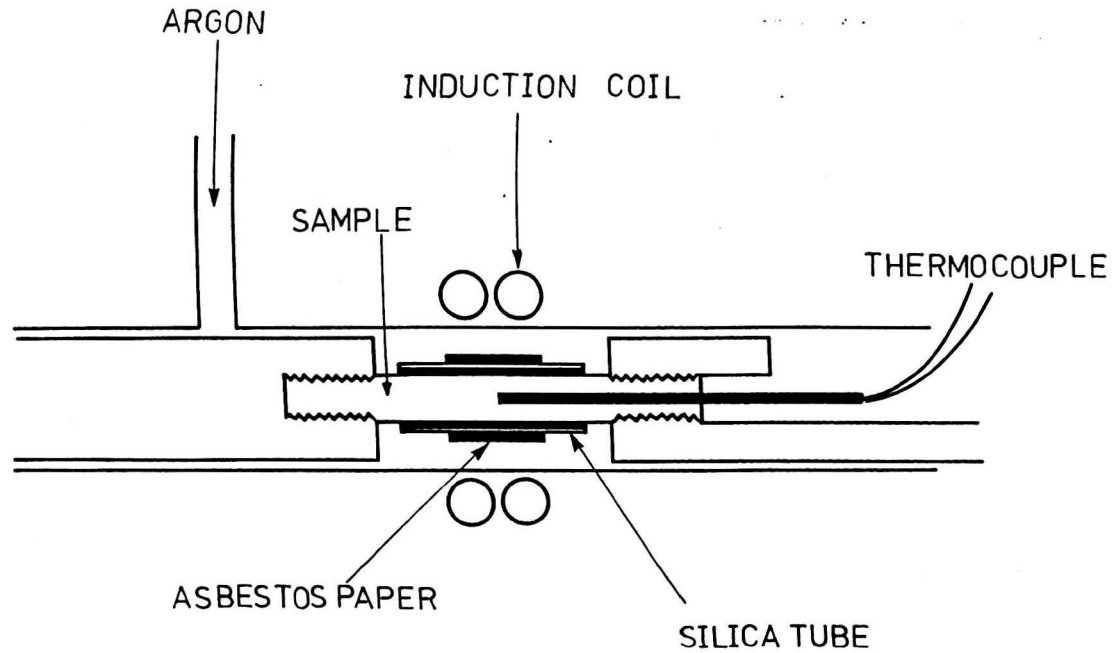


Fig. 9.1 Induction heating equipment for the high temperature tensile testing of 'directly cast' samples.

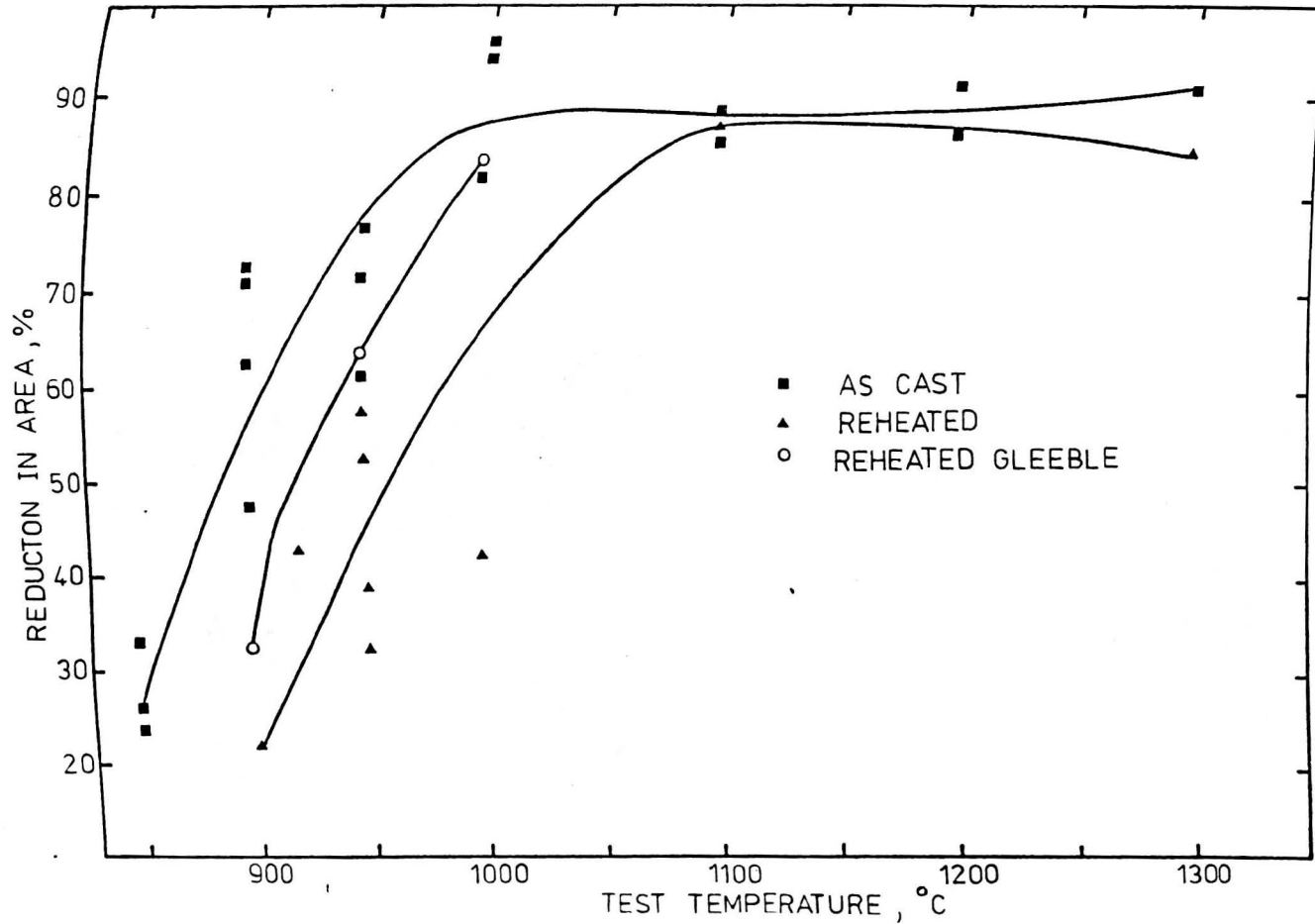
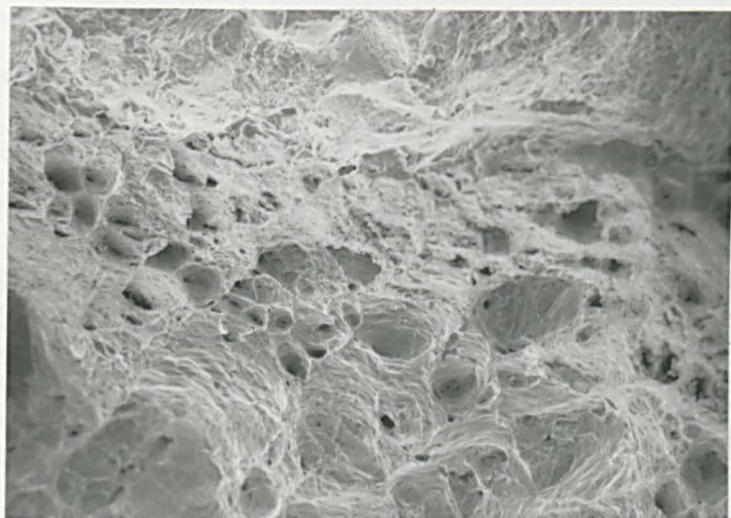
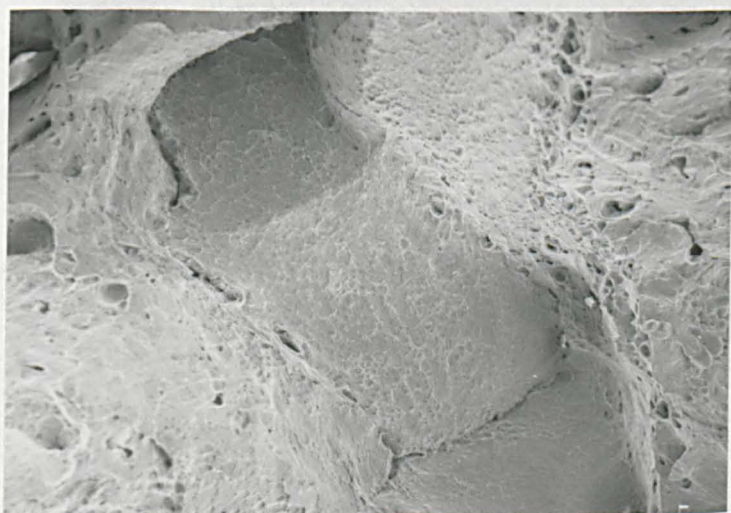


Fig. 9.2 Variation of Reduction in area with test temperature for samples in 'as cast', 'reheated' and 'reheated Gleeble' samples.



60 $\mu$ m

Fig.9.3 High temperature ductile rupture fracture mode, from 'as cast' samples fractured at 950°C.



60 $\mu$ m

Fig.9.4 Intergranular microvoid coalescence fracture mode, from 'as cast' sample fractured at 950°C.

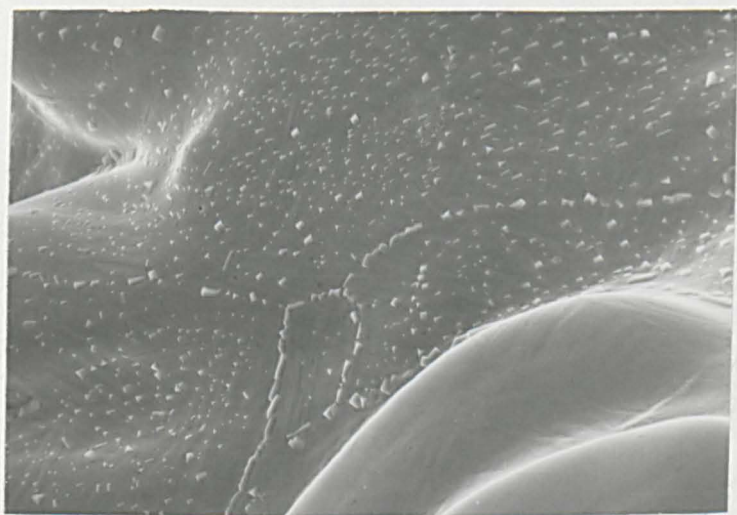
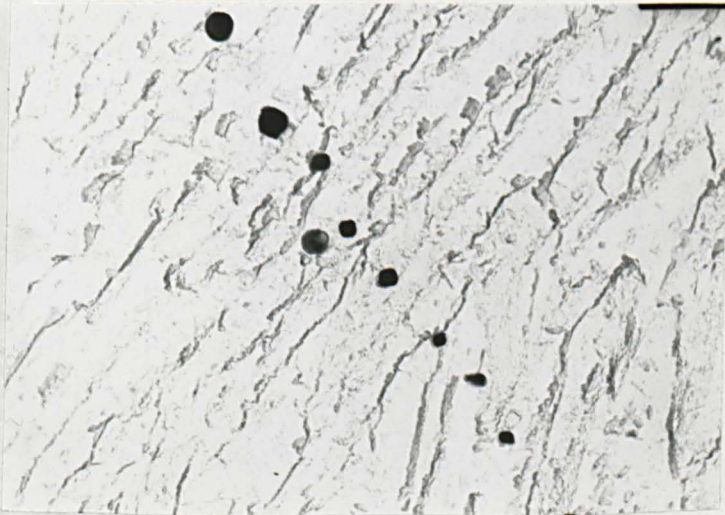


Fig.9.5 Interdendritic failure in 'as cast' sample fractured at 950°C, showing rows of sulphide inclusions



1  $\mu\text{m}$

Fig.9.6 Sulphide and NbCN precipitation at grain boundaries in 'reheated' sample tested at 950°C.



1  $\mu\text{m}$

Fig.9.7 Sulphide precipitation after reheating to 1200°C prior to cooling to 950°C.

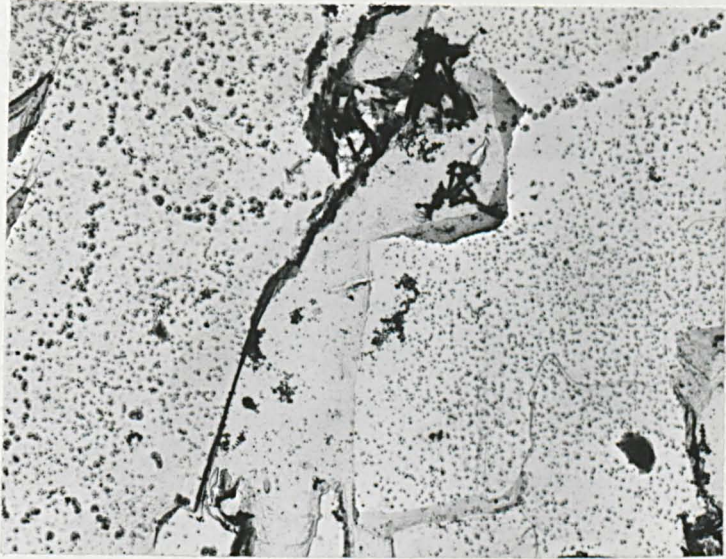
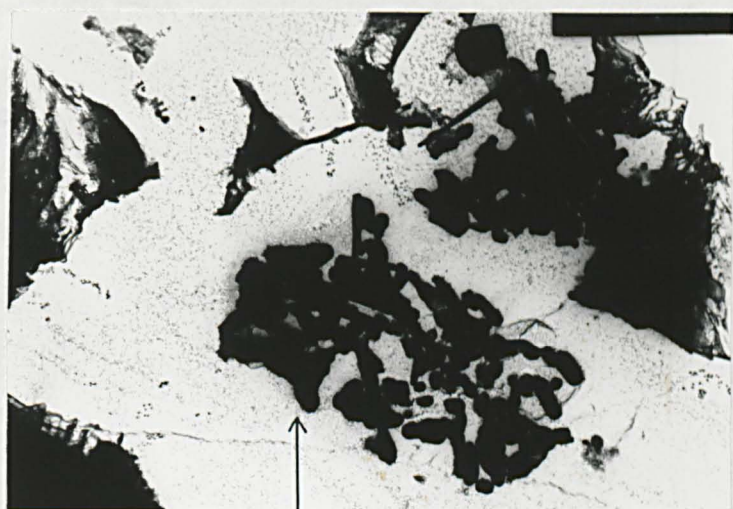


Fig.9.8 Precipitation in 'reheated' sample tested at 950°C. N.B. precipitate free zones.

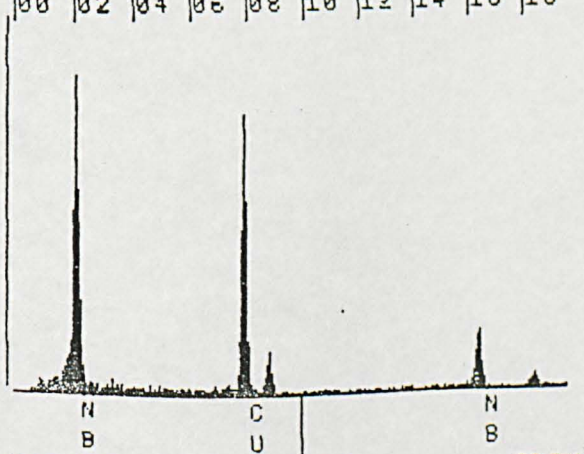


Fig.9.9 Precipitation in 'as cast' sample tested at 950°C.



13 μm

31-AUG-84 10:18:48 PEAK IDENT  
 RATE: 6CPS TIME: 38LSEC  
 00-20KEV:10EV/CH PRST: 200LSEC  
 A: B:  
 FS= 700 MEM: A FS= 700  
 |00 |02 |04 |06 |08 |10 |12 |14 |16 |18



CURSOR (KEV)=10.000 EDAX

Fig.9.10 Coarse NbCN extracted from 'as cast' sample tested at 950°C, with associated X-ray spectrum.

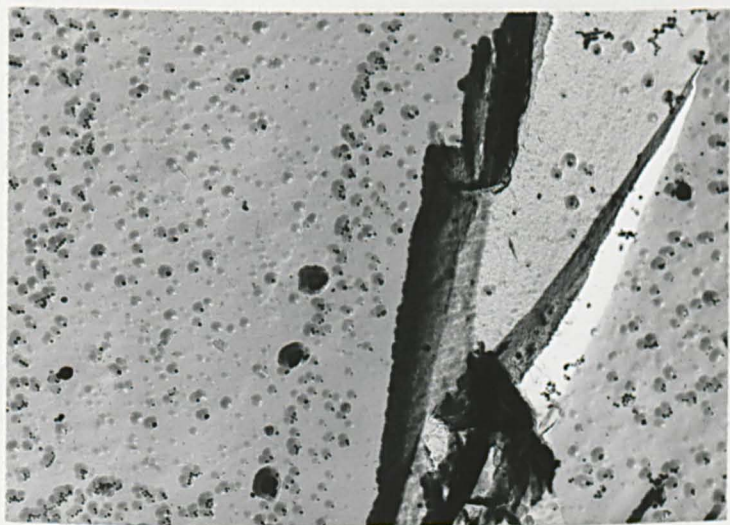


Fig.9.11 Precipitation in 'reheated Gleeble' sample tested at 950°C.

CHAPTER 10

The Hot Ductility of Micro-Alloyed Steels  
Heated Directly to Test Temperature

## 10.1 INTRODUCTION

The hot ductility results presented in the previous chapters have all used thermal cycles involving a high temperature solution treatment prior to testing. This has been a common procedure for the majority of hot ductility studies carried out on micro-alloyed steels in the past, and is designed to simulate to some extent the 'as cast' microstructure found in the continuously cast slab. Other investigations (Wilcox, 1982; Ouchi and Matsumoto, 1982) have involved intermediate heat treatments at temperatures below the final test temperatures in order to deduce the influence of a variety of precipitate distributions on hot ductility. Other investigations, whilst examining the hot ductility of micro-alloyed steels when heated directly to test temperature, have used high strain rates to simulate hot rolling processes. (Sankar et al, 1979) To date it appears that only Wray (1981) and Ouchi and Matsumoto (1982) have examined the hot ductility of micro-alloyed steels when heated directly to test temperature, using intermediate strain rates. It is intended in this chapter to examine the influence of temperature and strain rate on the hot ductility and hot strength of a variety of micro-alloyed steels heated directly to test temperature. Although not directly relevant to the continuous casting process, it was hoped that such results would provide further information to aid in understanding the hot ductility of these steels by producing precipitate distributions and grain sizes very different to those produced after high temperature solution treatments. Also, many hot forming processes do involve direct heating followed by deformation, e.g. the production of pipeline fittings, which commonly use micro-alloyed steels, and thus it was hoped that the hot ductility and strength data obtained

by carrying out directly heated hot tensile tests would be of some relevance to such processes.

## 10.2 EXPERIMENTAL

Six steels were examined having similar base compositions of 0.15%C, 1.4% Mn and 0.3% Si and varying additions of such elements as Nb, V, Al, Ti and Ca. The compositions are shown in Table

10.1. The steels were cast as 50 kg laboratory melts, and rolled to 37 mm plates, finishing rolling 1050°C. Tensile samples with diameter 5.04 mm and gauge length 25.4 mm (Fig. 3.3) were machined longitudinally from each plate.

Hot tensile tests were performed using the Instron equipment described in section 3.2.2. The samples were heated to test temperatures in the range 600 - 1100°C at a constant rate of 15°C/min., and held for 15 minutes prior to testing at initial strain rates in the range  $10^{-2}$  -  $10^{-4}$   $S^{-1}$ . After fracture, the samples were cooled to room temperature at a rate of approximately 25°C/min.

Metallographic sections were prepared from selected samples, and carbon extraction replicas prepared and examined as described in section 3.3. To ensure that the precipitates examined were not formed during the relatively slow cooling rate after testing, heat treatments were carried out on small samples of the C-Mn-Nb-Al steel in a muffle furnace. Two samples of this steel were heated to 1050°C for 15 minutes, and one cooled at 25°C/min. to room temperature, and the other quenched into iced brine. Replicas were prepared from each, and examination proved that the precipitation patterns were similar in each. This verifies that no significant precipitation occurs in this steel during cooling at 25°C/min. from temperatures up to 1050°C.

Fractographic examination was carried out using a JEOL T100 SEM. To establish austenite grain sizes prior to fracture, small samples were heated in a muffle furnace to simulate the thermal

cycle of the hot tensile test, and then cooled at a rate to produce ferrite outlining of the austenite grains. Austenite grain size was measured using the linear intercept method. For the C-Mn and C-Mn-V-Al steels, a Theta dilatometer was used to determine  $A_c$  transformation temperatures for heating rates of  $15^\circ\text{C}/\text{min}$ .

## 10.3 RESULTS

### 10.3.1. Hot Strength

Fig. 10.1 shows the influence of test temperature on peak stress,  $\sigma_p$ , for all six steels, when heated directly to test temperature and fractured using a strain rate of  $3 \times 10^{-3} \text{ s}^{-1}$ . There is a continuous decrease in  $\sigma_p$  as the test temperature is increased. Composition has little influence on  $\sigma_p$  above  $850^\circ\text{C}$ , when all the steels are expected to be austenitic. However, the C-Mn steel does appear to have slightly lower values of  $\sigma_p$  between  $850$  and  $950^\circ\text{C}$ , possibly due to slight precipitation hardening effects in the other steels. At test temperatures below  $700^\circ\text{C}$ , in the ferrite plus pearlite region, the steels with higher carbon contents, and hence higher pearlite volume fractions, have the higher strengths. The influence of strain rate on the hot strengths of the C-Mn, C-Mn-Al and C-Mn-Nb-Al steels is shown in Fig. 10.2 - 10.4. In these figures,  $\ln \sigma_p$  is plotted against  $1/T$ , where  $T$  is the absolute temperature, for strain rates in the range  $3 \times 10^{-2} - 3 \times 10^{-4} \text{ s}^{-1}$ . These plots show a linear relationship between  $\ln \sigma_p$  and  $1/T$  or at constant strain rate for all three steels in the austenite phase region, in agreement with equation 2.3. The activation energy for deformation,  $Q$ , is obtained by plotting  $\ln \dot{\epsilon}$  against  $1/T$  at constant  $\sigma_p$ .  $Q$  is determined from the gradient of the resulting straight lines, and these curves are shown in Figs. 10.5 - 10.7. For the C-Mn steel, the activation energy is  $290 \text{ KJ mol}^{-1}$ , which is the same as the result obtained for this steel in chapter 4, although in the previous case, a different thermal cycle was investigated. For the C-Mn-Al and C-Mn-Nb-Al steels, the activation energies were  $316 \text{ KJ mol}^{-1}$  and  $435 \text{ KJ mol}^{-1}$  respectively.

The stress exponents,  $n$ , for each steel are determined from the

gradients of the plots of  $\ln \dot{\epsilon}$  versus  $\ln \sigma_p$  at constant temperature, and are shown for the C-Mn, C-Mn-Al, and C-Mn-Nb-Al in Figs. 10.8 - 10.10. The values of  $n$  for the C-Mn, C-Mn-Al, and C-Mn-Nb-Al were 4.9, 5.7 and 7.7, respectively. These values of  $n$  and  $q$  are compared with the results of other workers in Table 10.2, and are shown to be in reasonable agreement with these previous values. For some tests performed at strain rates of  $3 \times 10^{-3}$  and  $3 \times 10^{-4} \text{ s}^{-1}$ , it was sometimes possible to detect the occurrence of dynamic recrystallization from the form of the load-elongation curves. Such curves were characterized by either an abrupt drop in flow stress, or by oscillations in the flow stress. Similar load elongation curves have been observed by other workers during the low strain rate tensile testing of steels. (Wray and Holmes, 1975; Wilcox, 1982). Unfortunately, in some cases it was not possible to determine unambiguously whether dynamic recrystallization was occurring from the load-elongation curves. Some representative examples of load-elongation curves are shown in Fig. 10.11. The onset of dynamic recrystallization as a function of temperature, composition and strain rate will be detailed in the following section, along with hot ductility results.

### 10.3.2. Hot Ductility

Reduction in area values as a function of test temperature for all six steels are shown in Fig. 10.12, the strain rate used being  $3 \times 10^{-3} \text{ s}^{-1}$ . The C-Mn and C-Mn-Ti-Al steels show reduction in area values greater than 90% over the entire temperature range examined, i.e. 650 - 1050°C. The C-Mn-Al, C-Mn-V-Al and C-Mn-Al-Ca steels show some loss of ductility in the temperature range 750 - 950°C, reduction in area values falling from 90% to approximately 65% for the C-Mn-Al and C-Mn-V-Al steels, and from 97% to 85% for the C-Mn-Al-Ca steel. The C-Mn-Nb-Al steel shows more severe

embrittlement in the temperature range 750 - 1000°C, with reduction in area values of 50%.

Fig. 10.12 also shows the temperature range over which dynamic recrystallization occurs for each steel, as determined from the load elongation curves. For the C-Mn-Nb-Al steel, dynamic recrystallization occurs only at temperatures above 950°C, whilst for the C-Mn-Al, C-Mn-V-Al, and C-Mn-Al-Ca steels the corresponding temperature is 850°C, and for the C-Mn and C-Mn-Ti-Al steels, 800°C. For the C-Mn-Al, C-Mn-V-Al and C-Mn-Nb-Al steels, the onset of dynamic recrystallization is associated with an increase in hot ductility.

The C-Mn, C-Mn-Al and C-Mn-Nb-Al steels were also tested using a variety of strain rates in the range  $3 \times 10^{-2}$  -  $3 \times 10^{-4}$  s<sup>-1</sup>.

Figs. 10.13 - 10.15 show the influence of strain rate on the hot ductility of these three steels, and also dynamic recrystallization and transformation data. The C-Mn steel showed excellent hot ductility when tested using the two highest strain rates, but a severe ductility trough was apparent for this steel when tested at a strain rate of  $3 \times 10^{-4}$  s<sup>-1</sup>, ductility dropping to 55% reduction in area at 900°C. Dynamic recrystallization occurred at all strain rates for test temperatures greater than 820°C.

Fig. 10.14 shows the influence of strain rate on the hot ductility of the C-Mn-Al steel, and shows the development of a ductility trough as strain rate is reduced. At a strain rate of  $3 \times 10^{-2}$  s<sup>-1</sup>, no loss of ductility is apparent, but as the strain rate is decreased, an increasingly deep and wide ductility trough is formed, and at the slowest strain rate, this trough extends from 800 - 1000°C, with minimum reduction in area values of 35%. Dynamic recrystallization occurs at temperatures greater than 820°C for the two higher strain rates, and at temperatures

greater than 970°C for the lowest strain rate. The hot ductility of the C-Mn-Nb-Al steel shows a similar decrease in hot ductility with decreasing strain rate (Fig. 10.15), the slowest strain rate producing a ductility trough in the temperature range 800 - 1050°C, with a minimum reduction in area value of 42%. Dynamic recrystallization commences at a test temperature of 1000°C for the C-Mn-Nb-Al steel.

### 10.3.3. Metallography

The variation in austenite grain size with temperature for all the steels examined is shown in Fig. 10.16. The C-Mn steel showed a continual increase in austenite grain size with temperature from 70  $\mu\text{m}$  at 875°C to 200  $\mu\text{m}$  at 1100°C. The other steels showed an approximately constant grain size of 30  $\mu\text{m}$  in the temperature range 900 - 1050°C. Above this temperature, grain growth occurred rapidly for each steel, and at 1100°C, grain sizes vary from 60  $\mu\text{m}$  for the C-Mn-Ti-Al steel to 140  $\mu\text{m}$  for the C-Mn-Al and C-Mn-V-Al steels.

SEM examination revealed three distinct fracture modes:- low temperature ductile rupture (LTDR), high temperature ductile rupture (HTDR) and intergranular failure (IG). These first two fracture modes were identical to those observed in the C-Mn steels studied in chapter 4. LTDR was observed in all steels and at all strain rates below a temperature of 800°C. HTDR was observed in the C-Mn and C-Mn-Ti-Al steels when tested above 900°C, and in the remaining steels at temperatures above 1000°C. The IG failure mode was observed in steels which failed with reduction in area values of less than 70%, and is illustrated in Fig. 10.17. This mode of intergranular failure appeared different to that observed in previous chapters, due to the fine austenite grain size ( - 30  $\mu\text{m}$ ). Micro voids were not present on the grain facets.

examination of carbon extraction replicas revealed fine precipitates in all steels except the C-Mn steel. The sizes, spacing and nature of the precipitates present in each steel are given in Table 10.3 at test temperatures of 950°C and 1050°C. The C-Mn-Al steel showed continuous networks of AlN precipitates at austenite grain boundaries at temperatures of 950°C and 1050°C, (Figs. 10.18 - 10.19) precipitation being coarser and more widely spaced at the higher test temperature. Little inter-granular precipitation was observed in this steel. Precipitation in the C-Mn-Al-Ca steel was essentially similar to that observed in the C-Mn-Al steel. (Figs. 10.20 - 10.21). The C-Mn-Ti-Al steel showed much randomly distributed precipitation of Ti (C, N), the precipitates varying greatly in size in any given replica (Figs. 10.22 - 10.23). No AlN precipitation was observed in this steel. The C-Mn-V-Al steel contained precipitates of both AlN and V(CN), the AlN being present in the form of large angular plates, whilst the V(CN) was present as smaller, round precipitates. (Figs. 10.24 - 10.25). The V(CN) was sometimes present at grain boundaries, but usually within the grains, the grain boundary precipitates being slightly coarser than those within the matrix.

Extensive precipitation of both Nb (C,N) and AlN was observed in the C-Mn-Nb-Al steel, both at austenite grain boundaries and within the grains (Fig. 10.26 - 10.27). In some cases precipitate free zones adjacent to the austenite grain boundaries were also observed (Fig. 10.26). Again, the AlN was present in the form of angular platelets, often closely associated with Nb(CN) precipitates (Fig. 10.27)

#### 10.3.4 Dilatometry and Transformation Data

The  $Ac_3$  and  $Ac_1$  temperatures for the C-Mn and C-Mn-V-Al steels heated at  $15^\circ\text{C min}^{-1}$  obtained by dilatometry are shown in Table

10.4, along with calculated  $Ae_1$  and  $Ae_3$  temperatures using the equation of Andrews (1965).

## 10.4 DISCUSSION

### 10.4.1. Hot Strength

Peak stress values appear to be little influenced by composition in the austenitic state, although the C-Mn steel shows slightly lower  $\sigma_p$  values, possibly due to a slight precipitation hardening effect in the other steels, or the generally coarser grain sizes in the C-Mn steel. When tested in temperature ranges producing a ferrite/pearlite structure, peak stress is influenced by the variations in C content between the different steels, since increases in C content, and hence pearlite volume fraction, lead to rapid increases in work hardening rates, producing high peak stresses.

The linear plots obtained in Figs. 10.2 - 10.10 again demonstrate the general applicability of equation 2.3. The values of Q and n obtained for the C-Mn, C-Mn-Al and C-Mn-Nb-Al steels are in general agreement with previous results (Table 10.3), which consistently show high Q and n values for Nb containing steels. It should be noted that these Q values are higher than the activation energy for the self diffusion of iron in austenite, which is  $285 \text{ KJ mol}^{-1}$  (Badia and Vignes, 1969). The high values of Q and n associated with Nb containing steels are due to the retardation of dynamic recrystallization in such steels (Sankar et al, 1979).

Previous studies (Maehara and Ohmori, 1984; Yasumoto et al, 1985) and the results of Chapter 7 have shown that increases in hot strength, due to extensive intragranular precipitation of carbides, nitrides and sulphides have a detrimental effect on hot ductility. The results in this chapter show a small precipitation hardening component in the hot strength results, but it is important to note that this precipitation hardening component is similar for

all the compositions examined. Thus, differences in hot ductility between these steels cannot be due only to hot strength differences between the steels.

#### 10.4.2 Hot Ductility

At a strain rate of  $3 \times 10^{-3} \text{ s}^{-1}$ , the C-Mn steel shows excellent hot ductility over a wide temperature range, in contrast to the hot ductility behaviour of this same steel when tested after solution treatment. Figs. 4.1 and 5.2 show that after solution treatment this steel can suffer severe embrittlement associated with the austenite to ferrite phase transformation. However, as shown in Fig. 10.12, heating directly to test temperature produces no ductility trough at strain rates greater than  $3 \times 10^{-4} \text{ s}^{-1}$ . This is likely to be due to differences in phase distribution and grain size produced by the differing thermal cycles. When the steel is cooled into the two phase region, the softer ferrite phase forms continuous networks at the austenite grain boundaries, and these continuous networks act as paths for crack propagation as described in chapter 4. However, in the case of heating directly into the two phase region, the austenite forms the continuous network, having nucleated at pearlite colonies and ferrite grain boundaries. Cracking in this case occurs predominantly in the ferrite, and at austenite/ferrite interfaces, and it appears that cracks rarely propagate across interphase boundaries. (Figs. 10.28 N.B. to obtain a coarse microstructure for examination, a heat treatment was used to produce a coarse ferrite grain structure prior to testing, and hence a coarse two phase mixture). Thus the phase distribution and fine grain size produced by direct heating shows good hot ductility in the two phase region due to the lack of continuous paths for crack propagation. Therefore, the hot ductility results

shown in Fig. 10.12 for all the steels examined are not influenced by phase transformation, and ductility will be influenced directly by composition and precipitation only. The C-Mn steel shows a continual increase in austenite grain size prior to deformation over the entire range of test temperatures as opposed to the micro-alloyed steels, which all show an approximately constant grain size below test temperature of 1050°C, due to pinning of grain boundaries by precipitates. Above 1050°C, grain growth occurs rapidly as these precipitates increase in size. Comparison of hot ductility and grain size results indicate that grain size can only be a secondary influence on hot ductility, since wide variations in hot ductility are observed, whilst the grain size remains constant, or alternatively hot ductility remains constant, whilst grain size varies.

The foregoing results indicate that hot strength, phase transformation and grain size have little significance in explaining the hot ductility results shown in Fig. 10.12, and to explain these results, it is necessary to examine both grain boundary and intra granular precipitation in more detail. Examination of Table 10.3 shows that all the steels having a ductility trough when tested using a strain rate of  $3 \times 10^{-3} \text{ s}^{-1}$  show grain boundary precipitation to some extent. The steels with good hot ductility, the C-Mn and C-Mn-Ti-Al steels, show no grain boundary precipitation, although the C-Mn-Ti-Al steel shows extensive random precipitation of Ti(C,N). Thus it appears that at this strain rate, ductility troughs are associated with grain boundary precipitation. It appears likely that these grain boundary precipitates influence hot ductility by retarding the onset of dynamic recrystallization, as Fig.

10.12 shows that lack of ductility failures are associated with a lack of dynamic recrystallization, so that brittle, intergranular failures can occur before the critical strain for the nucleation of dynamic recrystallization,  $\epsilon_c$ , is reached, as described by Wilcox and Honeycombe (1984). When dynamic recrystallization commences before failure, high ductility fractures occur, as migrating grain boundaries isolate the developing cracks. This retardation of dynamic recrystallization is due to the array of static precipitates at austenite grain boundaries present before deformation, as opposed to the dynamic precipitates formed continually during deformation, which retard dynamic recrystallization after solution treatment. These results indicate that the high temperature extent of the ductility trough is dependant on the temperature,  $T_c$ , at which the fracture strain equals the critical strain for the onset of dynamic recrystallization,  $\epsilon_c$ . As the test temperature is increased above  $T_c$ , recrystallization can occur before fracture, and ductility increases rapidly.  $T_c$  for the Nb containing steels is particularly high, due to the effect of grain boundary precipitates, and also due to the small amount of Nb in solution at the deformation temperature (equilibrium calculations using the formula of Irvine et al (1967) indicate 0.008wt.% for the C-Mn-Nb-Al steel).

The actual minimum value for hot ductility is expected to be controlled by such factors as grain size, strain rate, precipitation and composition. The results shown in Fig. 10.12 are at a constant strain rate of  $3 \times 10^{-3} \text{ s}^{-1}$ , and as discussed previously grain size is approximately constant for all but the C-Mn steel in the temperature range 850 - 1050°C, and therefore differences in the minimum ductility values between the steels are probably due to the differences in precipitation. The C-Mn-Nb-Al steel

has the lowest value of reduction in area, and one possible cause for this is the extensive grain boundary precipitation, providing an easy path for crack propagation, combined with the extensive intragranular precipitation. This intragranular precipitation leads to matrix hardening, and to the development of PFZ's, which tend to concentrate strain at the grain boundaries. The C-Mn-Al steel, although having similar grain boundary precipitation to the C-Mn-Nb-Al steel in terms of size and spacing, lacks the extensive intragranular precipitation of the C-Mn-Nb-Al steel, and hence the C-Mn-Al steel has the higher ductility values. The C-Mn-V-Al steel has similar hot ductility values to the C-Mn-Al steel, although extensive grain boundary precipitation is not often observed in this steel. However, the extensive intragranular precipitation in the C-Mn-V-Al steel leads to this steel having similar hot ductility values to the C-Mn-Al steel. The C-Mn-Al-Ca steel shows surprisingly high hot ductility considering that its precipitate distribution and grain size are very similar to that of the C-Mn-Al steel. The C-Mn-Al and C-Mn-Al-Ca steels have similar compositions, but the C-Mn-Al steel does contain 0.017 wt.% Al, compared to 0.037 wt.% Al for the C-Mn-Al-Ca steel. (see Table 10.1). This difference in Al content might be expected to give the C-Mn-Al-Ca worse hot ductility, whereas the reverse is actually observed. One possible explanation for the surprisingly high hot ductility of the C-Mn-Al-Ca steel is its very low S level of 0.001 wt.%, compared with .008 wt.% for the C-Mn-Al steel. Recent work by Heritier et al (1981) and by Osinkolv et al (1985) has shown that in experimental Fe-C alloys containing AlN and S, increasing S levels have a severe detrimental effect on hot ductility for a given AlN content. Thus the very low S level of the C-Mn-Al-Ca steel may be responsible for its relatively good hot

ductility. The low temperature extent of the ductility trough is not strongly dependent on composition, and for all steels showing a ductility trough, hot ductility starts to fall at approximately 800°C, which is close to the  $A_{e_3}$  temperature range (810 - 858°C, Table 10.4) for these steels, calculated using the equation of Andrews (1965). It appears likely that hot ductility first begins to fall when austenite formation is almost complete, and when considerable grain boundary sliding can occur between the austenite grains.

#### 10.4.3. The Influence of Strain Rate on Hot Ductility

Fig. 10.13 shows that when a sufficiently slow strain rate is used, a C-Mn steel containing no precipitates can fail in a brittle manner. Brittle intergranular failures in austenites containing no precipitates have been reported previously (Wray, 1984) if sufficiently slow strain rates are employed. The results of Figs. 10.14 - 10.15 shows that decreasing strain rates lead to broadening and deepening of the ductility troughs existing in the C-Mn-Al and C-Mn-Nb-Al steels. It should be noted that in these steels, the precipitate distributions are very stable with respect to time, and precipitate distributions present after fracture are identical for samples tested at the same temperature, but with different strain rates. Austenite grain size is also stable with respect to time. Thus the decrease in hot ductility with decreasing strain rate is not due to variations in microstructure due to long test times. This decrease in hot ductility is more probably due to the increase in the ratio  $\epsilon_{g.b.}/\epsilon_t$ , where  $\epsilon_{g.b.}$  is the strain due to grain boundary sliding and  $\epsilon_t$  the total strain, as discussed in section 2.5, which will favour intergranular failure. Also, if dynamic recrystallization occurs, grain boundary migration rates will be reduced as the strain rate is reduced, making the isolation of grain boundary cracks less

effective. Figs. 10.13 - 10.15 indicate that low ductility failures can occur even though dynamic recrystallization is proceeding at the lowest strain rate examined. Unlike the ductility results using a strain rate of  $3 \times 10^{-3} \text{ s}^{-1}$ , the high temperature extent of the ductility trough does not necessarily coincide with the onset of dynamic recrystallization. It seems likely that at the lowest strain rate examined, the slow rate of grain boundary migration associated with dynamic recrystallization is ineffective in preventing crack growth. In addition, at a strain rate of  $3 \times 10^{-4} \text{ s}^{-1}$ , recrystallization is periodic in nature, and it is possible that intergranular cracks may develop between each recrystallization cycle, further reducing ductility. Thus it appears that at strain rates of  $3 \times 10^{-4} \text{ s}^{-1}$ , dynamic recrystallization arguments alone cannot explain hot ductility behaviour, as it appears that at these slow strain rates, dynamic recrystallization becomes less effective in preventing low ductility failure.

## 10.5 CONCLUSIONS

1. Six micro-alloyed steels have been tested at temperatures in the range 1100°C using strain rates between  $3 \times 10^{-2}$  -  $3 \times 10^{-4} \text{ s}^{-1}$  after heating directly to test temperature, and their strengths have been shown to be described by the equation:-

$$\dot{\epsilon} = A \sigma^n \exp (-Q/RT)$$

2. At a strain rate of  $3 \times 10^{-3} \text{ s}^{-1}$ , the C-Mn-Al, C-Mn-Al-Ca, C-Mn-V-Al and C-Mn-Nb-Al steels show a loss of ductility in the temperature range 750 - 1000°C, due to the extensive grain boundary precipitation in these steels, which retards the onset of dynamic recrystallization.
3. Decreasing the strain rate from  $3 \times 10^{-3} \text{ s}^{-1}$  to  $3 \times 10^{-4} \text{ s}^{-1}$  deepens and broadens the ductility troughs in the C-Mn-Al and C-Mn-Nb-Al steels, and introduces a ductility trough in the behaviour of the C-Mn steel in the temperature range 800 - 900°C. It is believed that the adverse effect of decreasing strain rate on hot ductility is due to strain concentration at the grain boundaries, and to reduced grain boundary migration rates, which favour intergranular failure.

Steel	C	Si	Mn	P	S	Al	N	Nb	Ti	V	Ca
C-Mn	.19	.20	1.40	.002	.013	—	.004	—	—	—	—
C-Mn-Al	.15	.29	1.45	.003	.008	.017	.006	—	—	—	—
C-Mn-V-Al	.11	.32	1.34	.005	.006	.024	.004	—	—	.057	—
C-Mn-Nb-Al	.12	.29	1.44	.002	.009	.015	.010	.034	—	—	—
C-Mn-Ti-Al	.16	.23	1.50	.002	.013	.030	.004	—	.030	—	—
C-Mn-Al-Ca	.10	.41	1.30	.014	.001	.037	.008	—	—	—	.005

Table 10.1      Compositions of the steels examined (wt.%)

Steel	Reference	Q (KJmol <sup>-1</sup> )	n
C-Mn	Present work	290	4.9
C-Mn	Sellars and Tegart (1966)	300	4.6
C-Mn-Al	Sankar et al (1979)	308	5.1
C-Mn-Al	Ouchi and Okita (1982)	406	5.7
C-Mn-Al	Present Work	316	5.3
C-Mn-Nb-Al	Sankar et al (1979)	434	8.6
C-Mn-Nb-Al	Ouchi and Okita (1982)	401	6.1
C-Mn-Nb-Al	Present work	435	7.7

Table 10.2 Comparison of activation energy, Q, and stress exponent, n, of present work with previous studies.

Steel	Precipitate Type	Reduction in area (%)		Grain boundary Precipitate Size (nm)		Grain Boundary Precipitate Spacing (nm)		Matrix Precipitate Size (nm)	
		850°C	1050°C	850°C	1050°C	850°C	1050°C	850°C	1050°C
C-Mn	—	<b>99</b>	98	-	-	-	-	-	-
C-Mn-Ti-Al	Ti (C,N)	98	98	-	-	-	-	58	65
C-Mn-Al	AlN	<b>63</b>	98	<b>39</b>	51	32	84	-	-
C-Mn-Nb-Al	AlN, Nb(CN)	<b>53</b>	96	<b>45</b>	58	64	127	30	35
C-Mn-Al-Ca	AlN	<b>84</b>	98	40	50	35	90	-	-
C-Mn-V-Al	AlN, Nb(CN)	<b>66</b>	98	-	-	-	-	<b>40</b>	<b>70</b>

Table 10.3 Precipitate types and sizes present at test temperatures of 850°C and 1050°C  
( $\dot{\epsilon} = 3 \times 10^{-3} \text{ s}^{-1}$ )

Steel	Transformation Temperature (°C)			
	Ac <sub>1</sub>	Ac <sub>3</sub>	Ae <sub>1</sub>	Ae <sub>3</sub>
C-Mn	-	-	714	810
C-Mn-Al	-	-	716	826
C-Mn-V-Al	707	848	718	845
C-Mn-Nb-Al	-	-	714	840
C-Mn-Ti-Al	-	-	714	820
C-Mn-Al-Ca	-	-	720	858

Table 10.4 Transformation data, Ae temperature calculated using the equation of Andrews (1965), Ac temperatures determined by dilatometry (1% transformation).

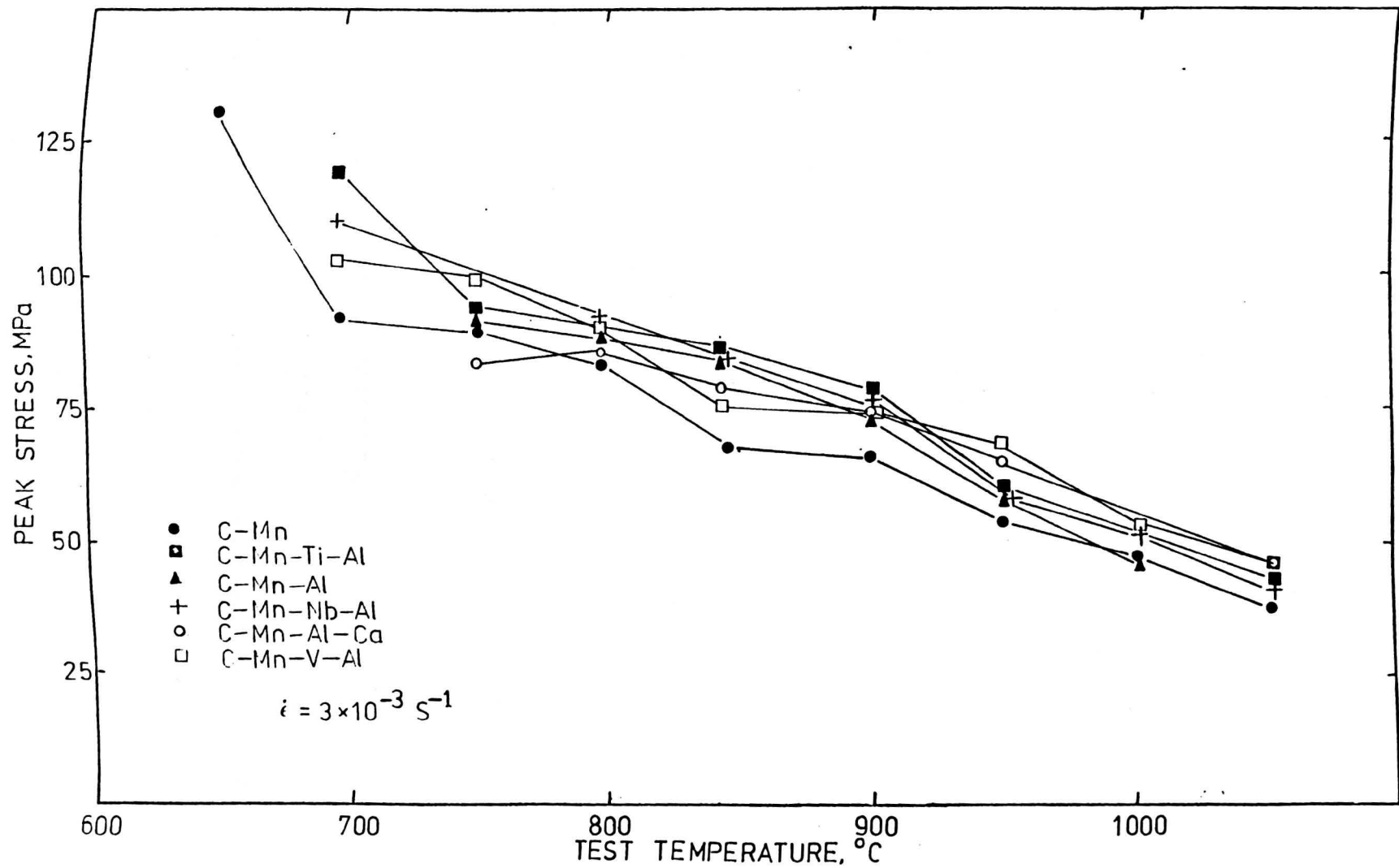
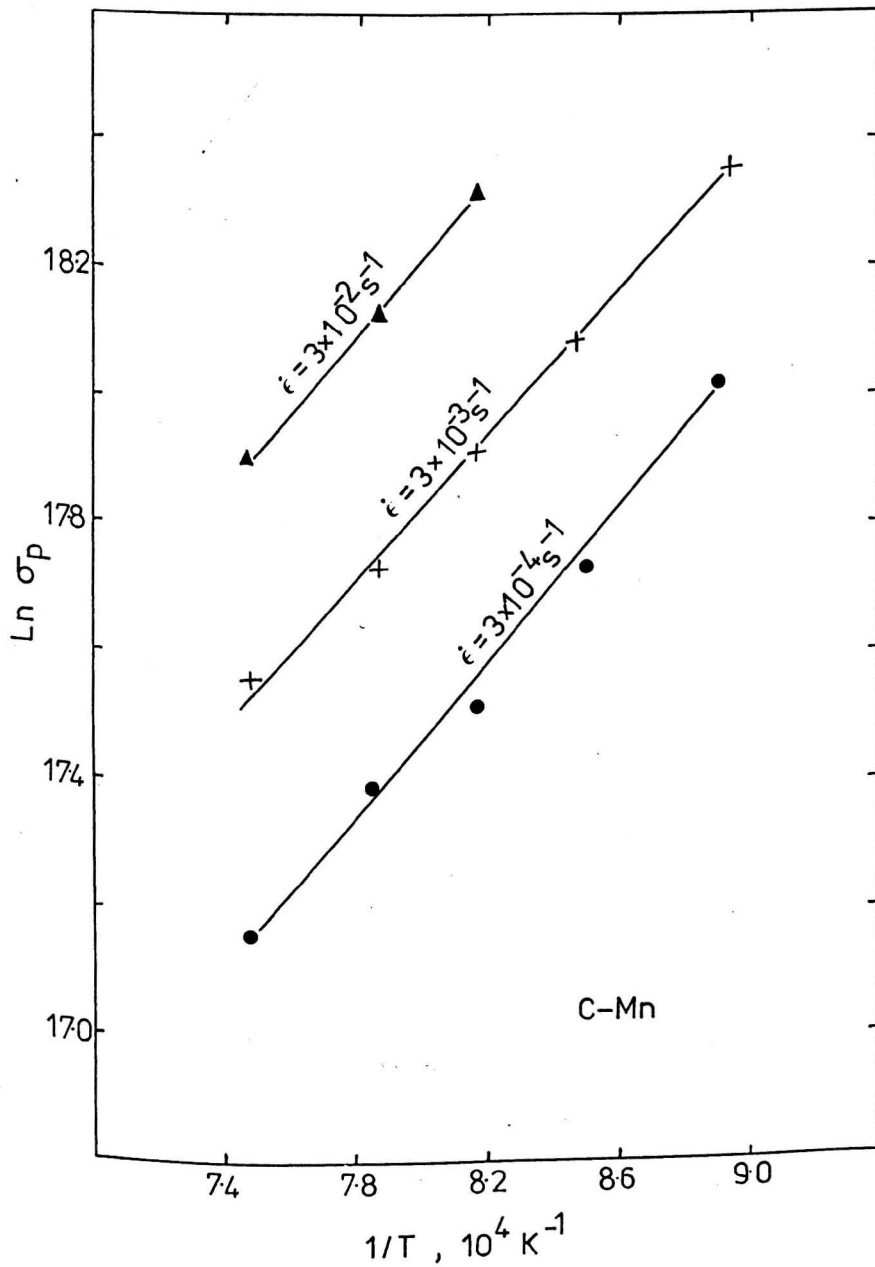
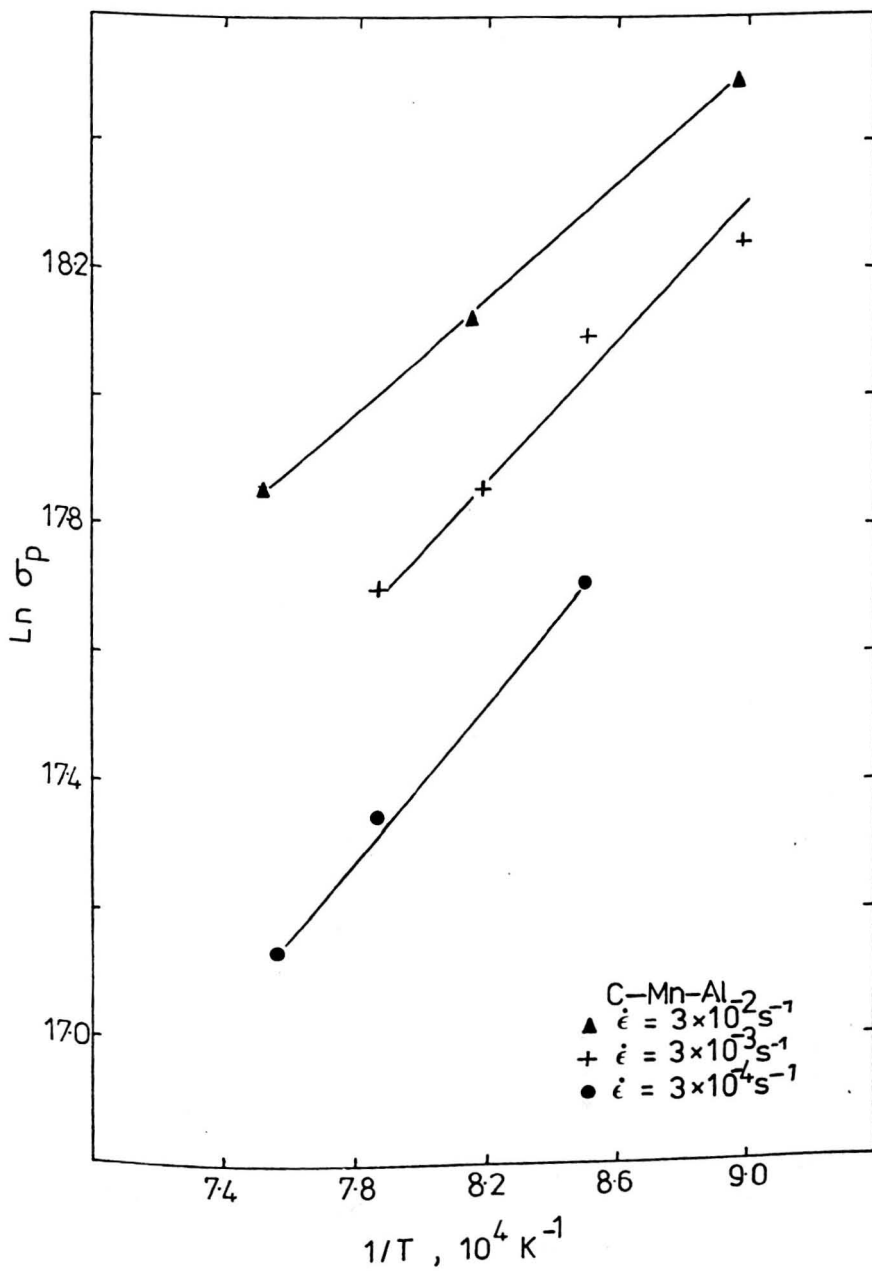


Fig. 19.1 Variation of peak stress with test temperature for six steels heated directly to test temperature



**Fig. 10.2** Variation of peak stress with temperature and strain rate for the C-Mn steel.



**Fig. 10.3** Plot of  $\ln$  peak stress versus  $1/T$ , where  $T$  is the absolute test temperature for the C-Mn-Al steel for strain rates in the range  $10^{-2} - 10^{-4} \text{ s}^{-1}$

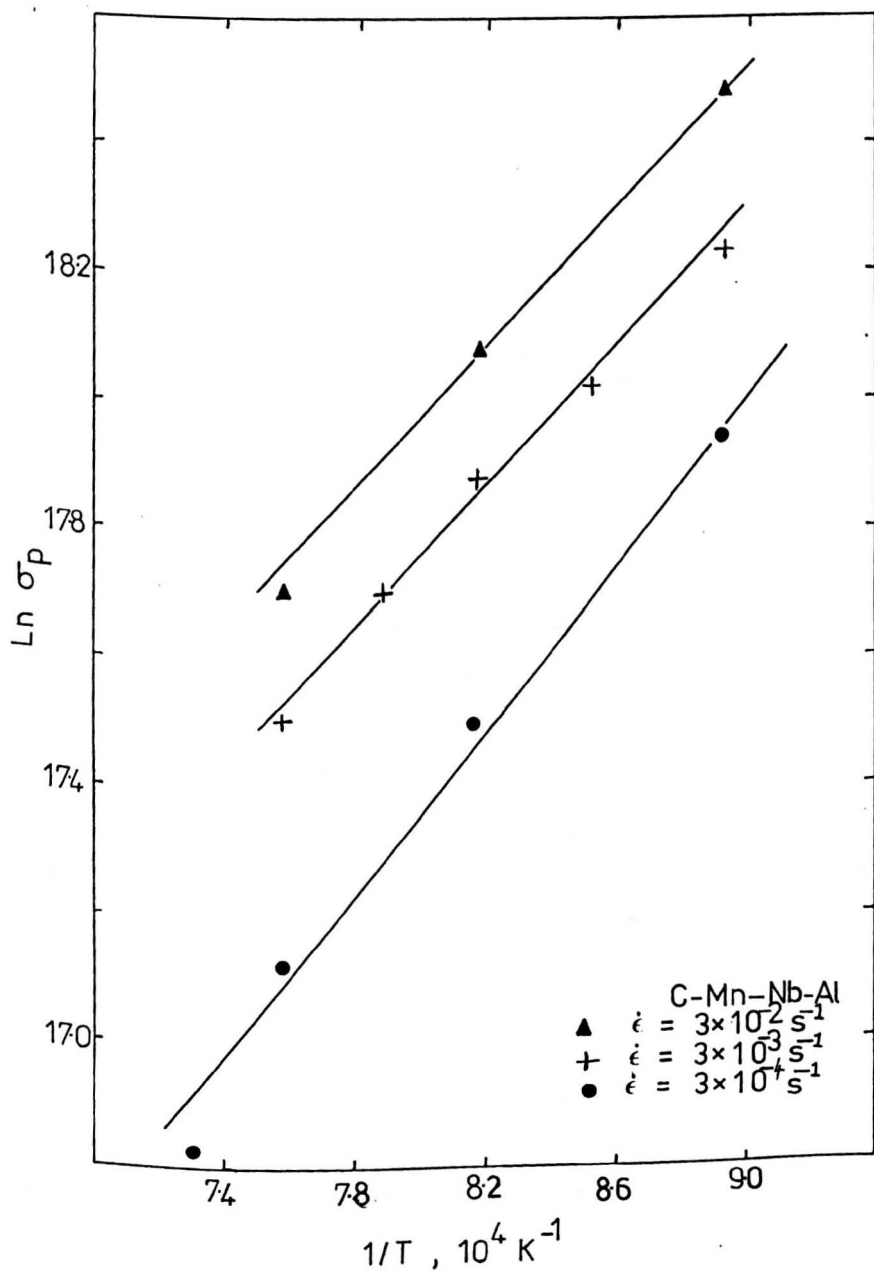


**Fig. 10.4** Plot of  $\ln$  peak stress versus  $1/T$ , where  $T$  is the absolute test temperature, for the C-Mn-Nb-Al steel for strain rates in the range  $3 \times 10^{-2} - 3 \times 10^{-4} \text{ s}^{-1}$

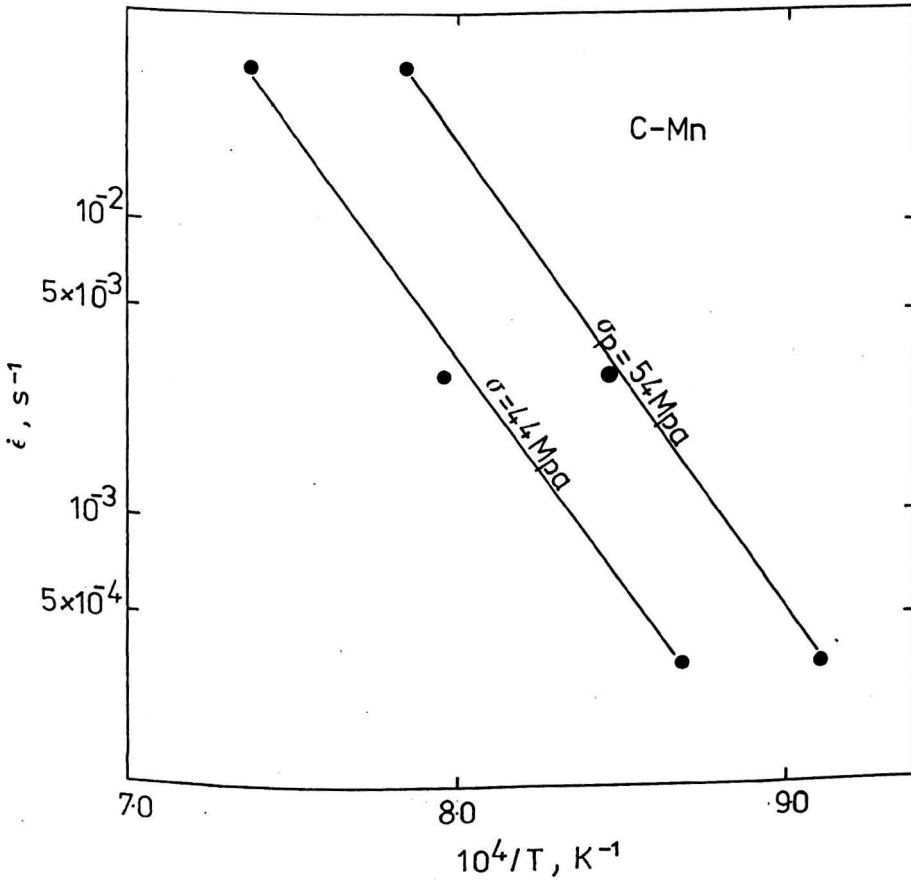


**Fig. 10.5** Plot of  $\ln \dot{\epsilon}$  against  $1/T$  at constant  $\sigma_p$  for the C-Mn steel.

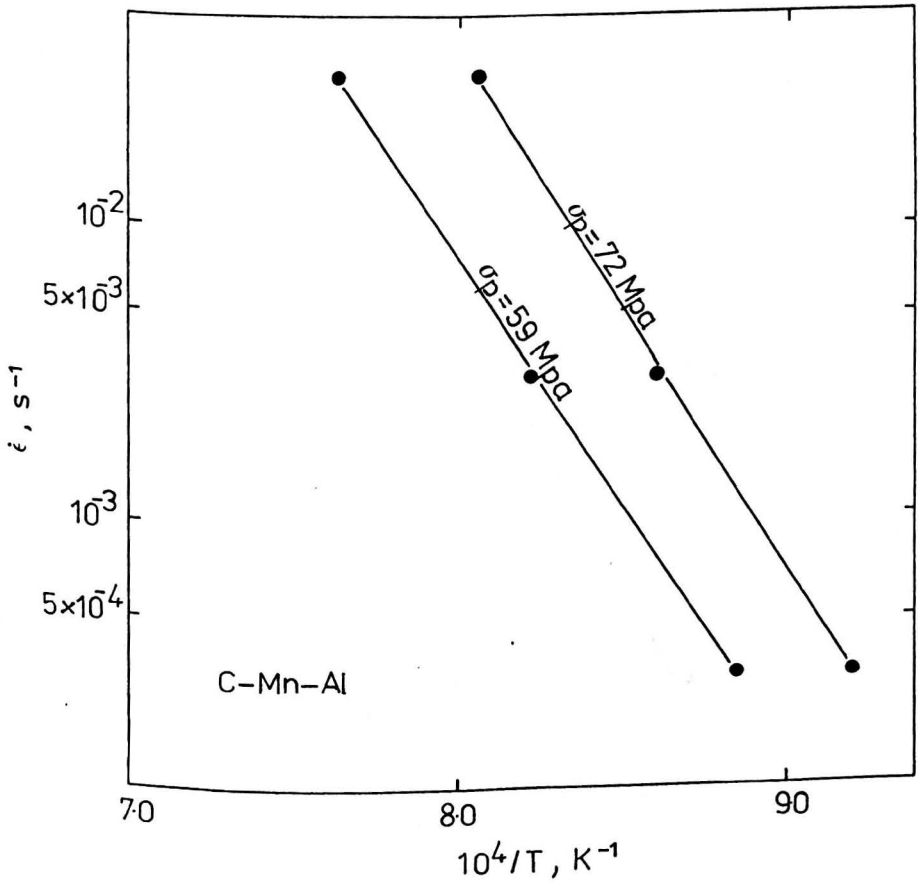
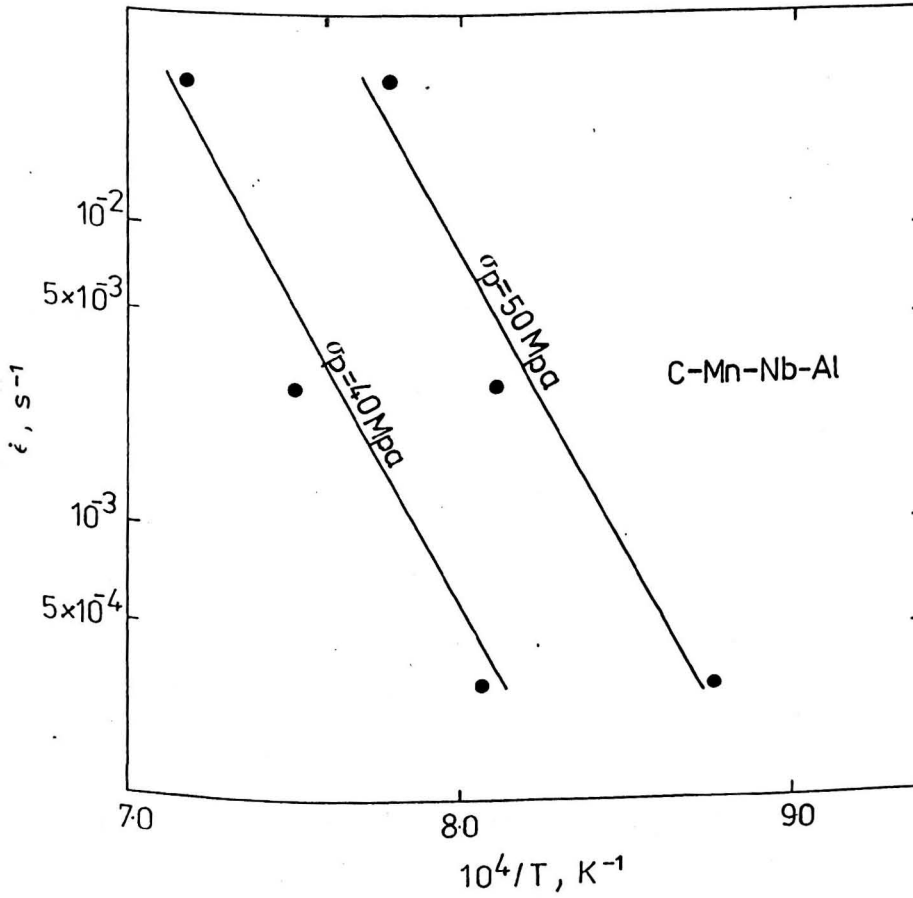
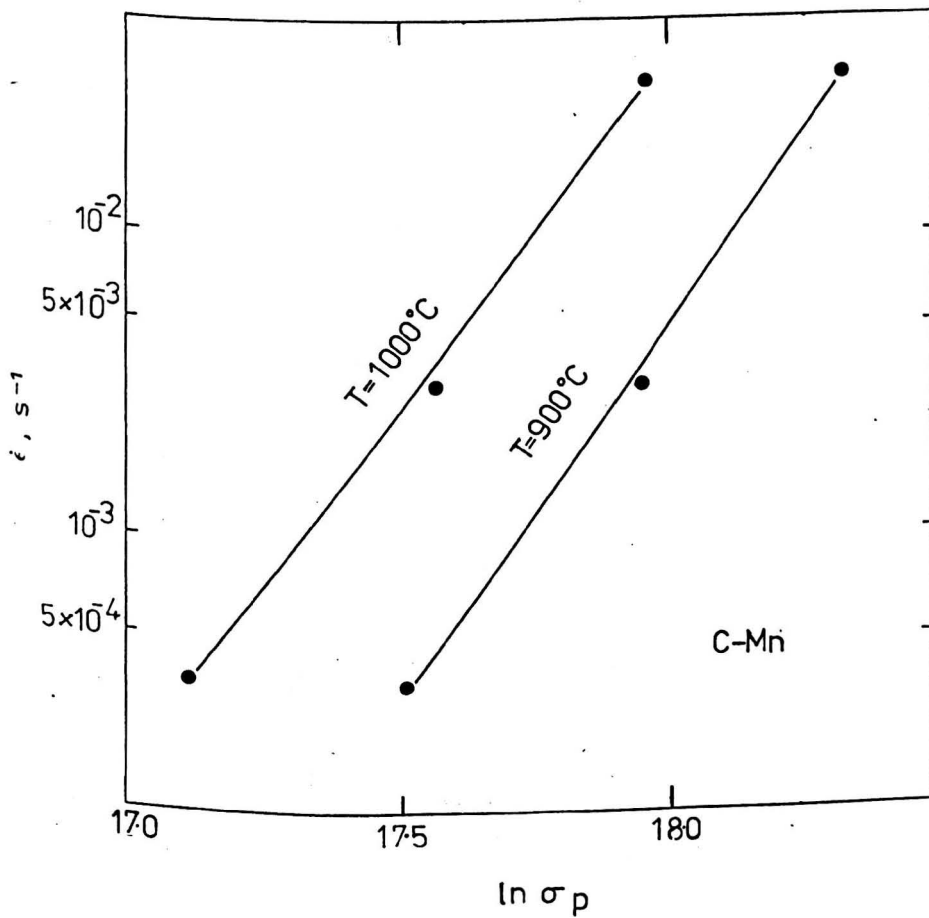


Fig. 10.6 Plot of  $\ln \dot{\epsilon}$  against  $1/T$  at constant  $\sigma_p$  for the C-Mn-Al steel.



**Fig.10.7**

Plot of  $\ln \dot{\epsilon}$  against  $1/T$  at constant  $\sigma_p$  for the C-Mn-Nb-Al steel.



**Fig.10.8**

Plot of  $\ln \dot{\epsilon}$  against  $\ln \sigma_p$  at constant temperatures for the C-Mn steel.

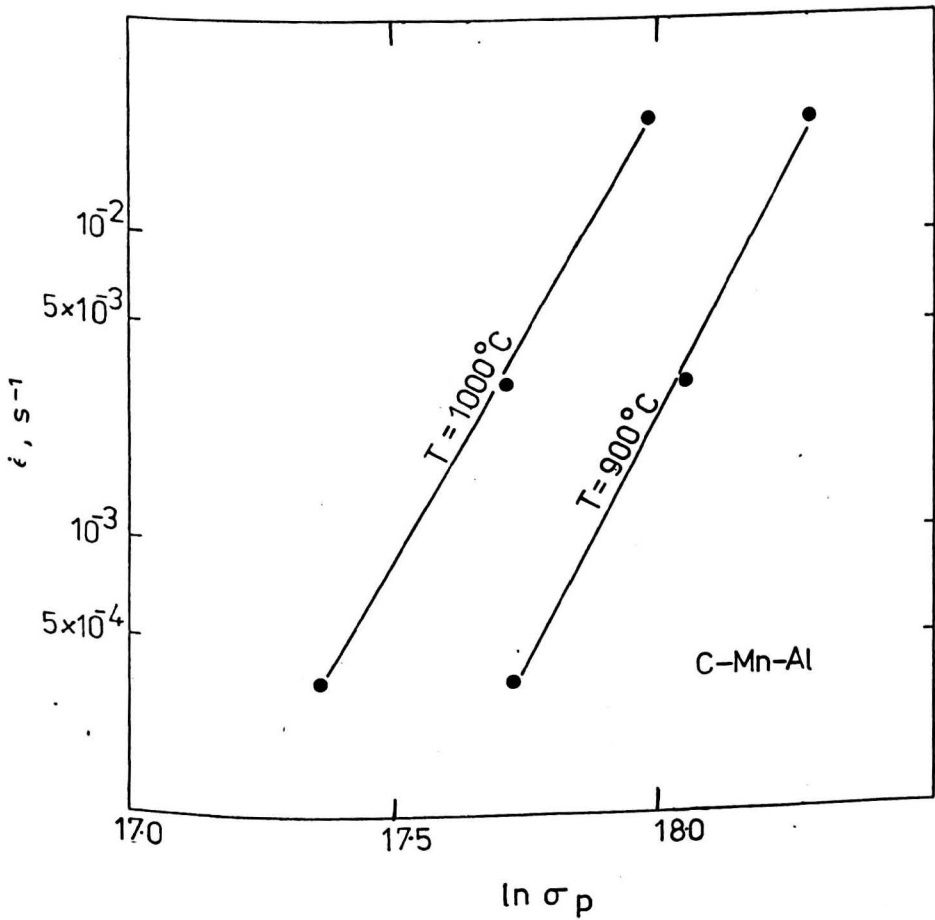


Fig. 10.9 Plot of  $\ln \dot{\epsilon}$  against  $\ln \sigma_p$  at constant temperatures for the C-Mn-Al steel.

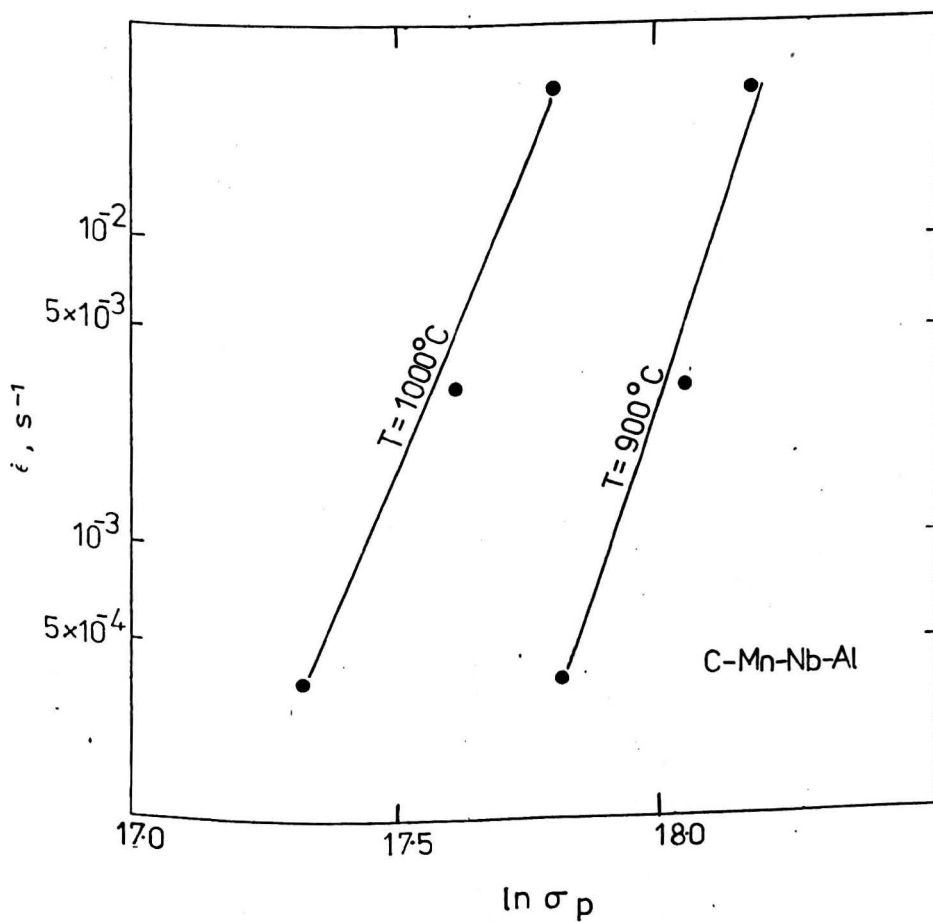


Fig. 10.10 Plot of  $\ln \dot{\epsilon}$  against  $\ln \sigma_p$  at constant temperatures for the C-Mn-Nb-Al steel.

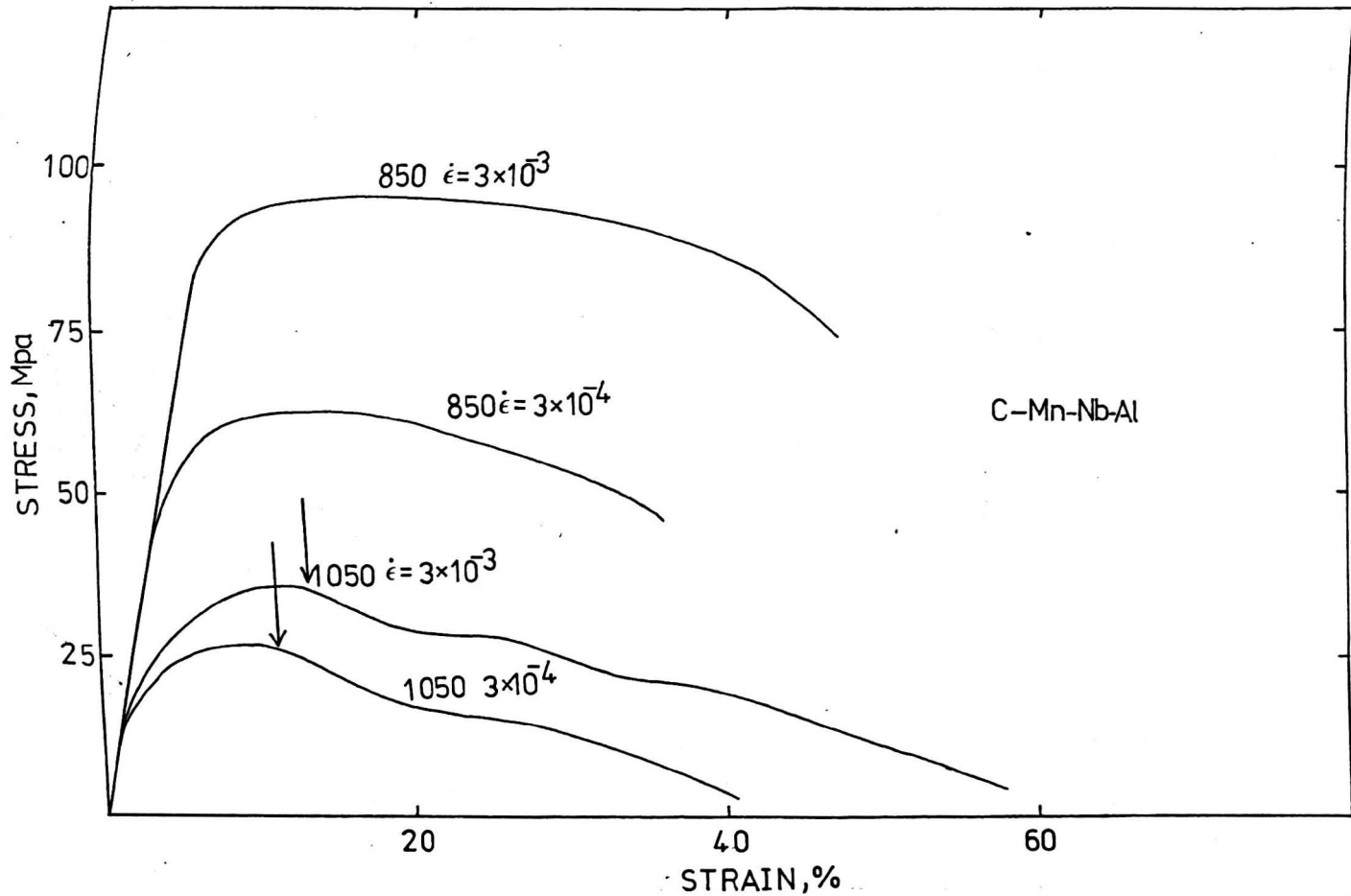


Fig. 10.11 Representative load-elongation curves at various temperatures and strain rates.

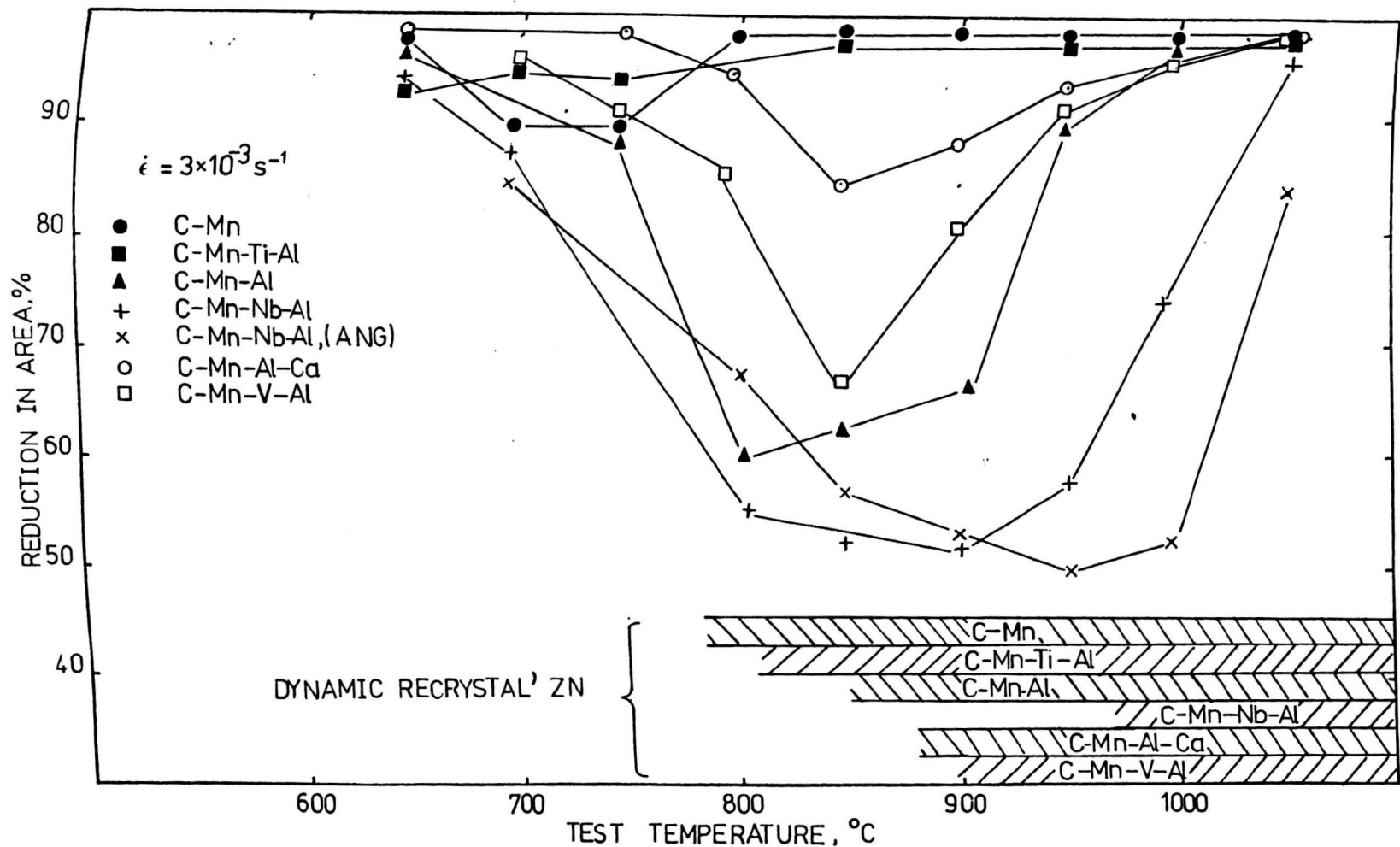


Fig. 10.12 Hot ductility curves for all six steels at  $\dot{\epsilon} = 3 \times 10^{-3} \text{ s}^{-1}$ , occurrence of dynamic recrystallization indicated by shaded regions.

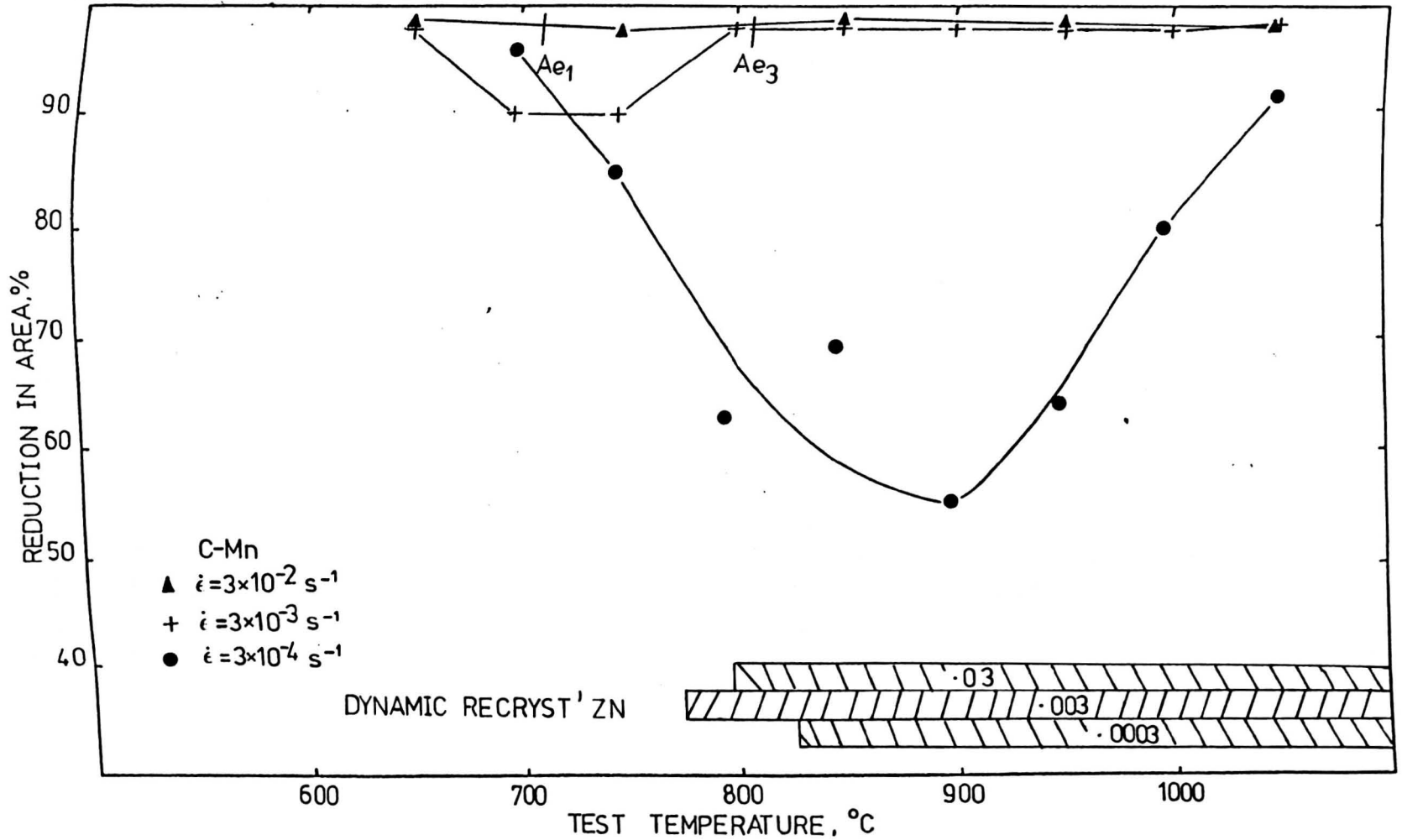


Fig. 10.13 Influence of strain rate on the hot ductility of C-Mn steel, occurrence of dynamic recrystallization indicated by shaded regions.

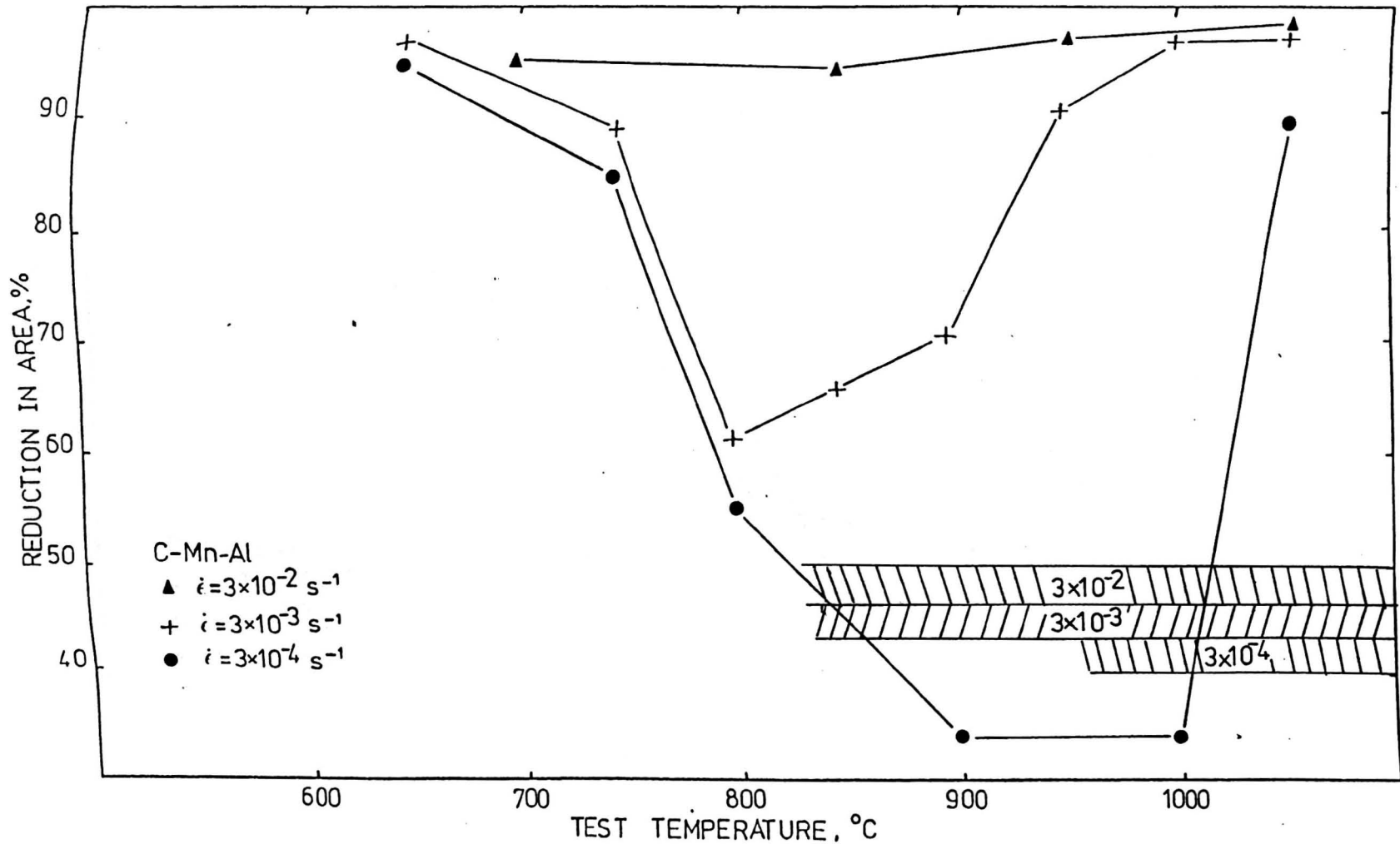


Fig. 10.14 Influence of strain rate on the hot ductility of C-Mn-Al steel, occurrence of dynamic recrystallization indicated by shaded regions.

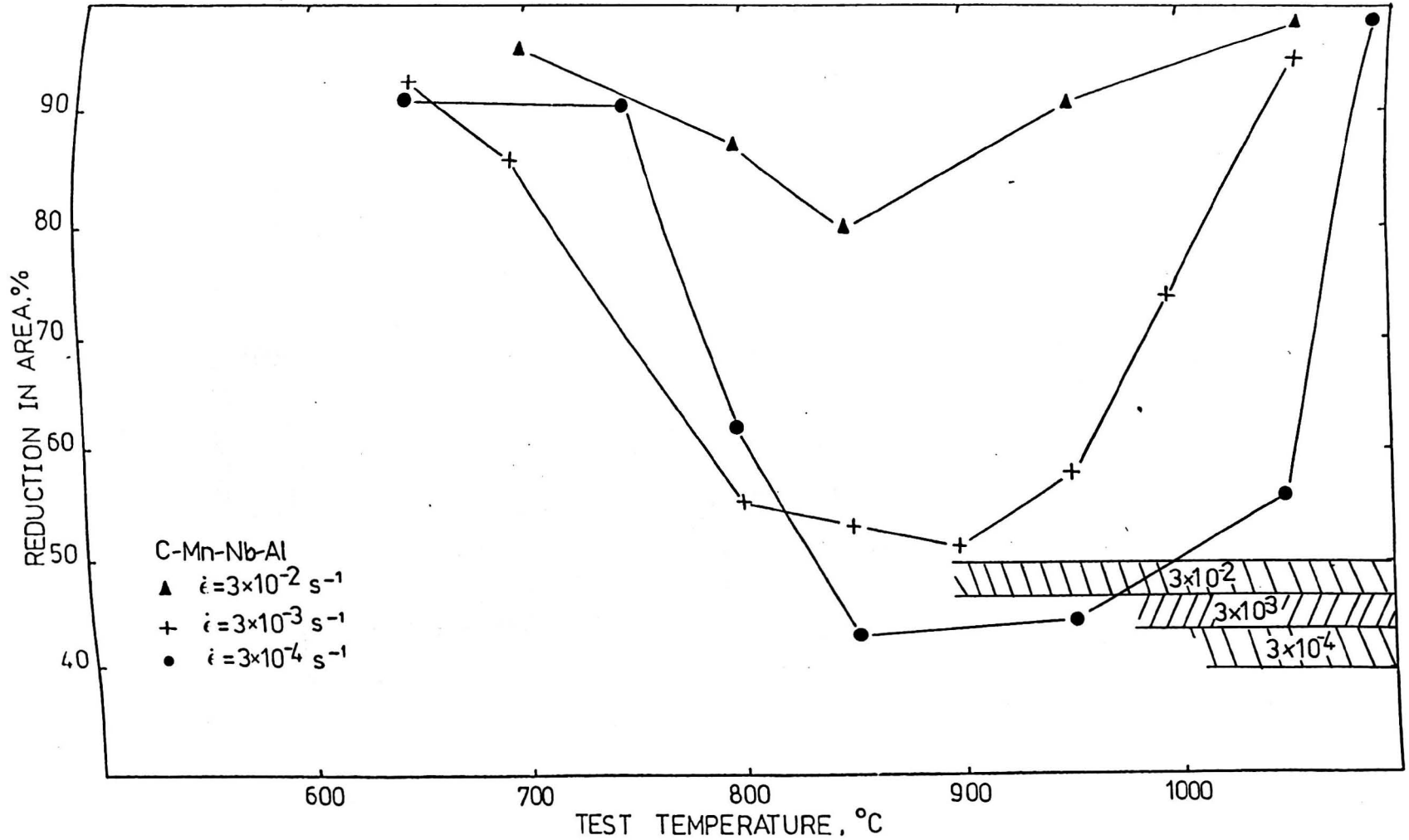


Fig. 10.15 Influence of strain rate on the hot ductility of C-Mn-Nb-Al steel, occurrence of dynamic recrystallization indicated by shaded regions.

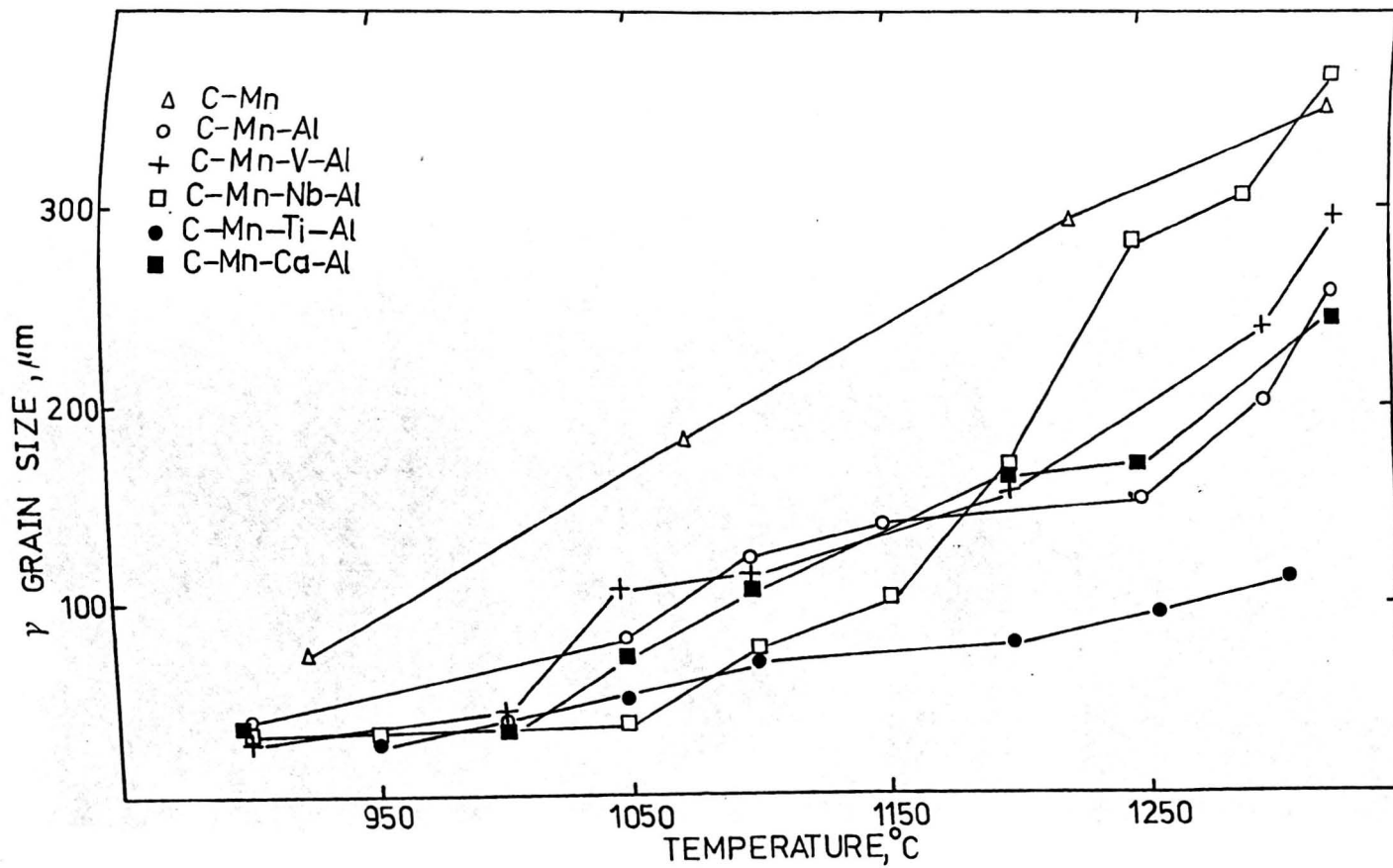
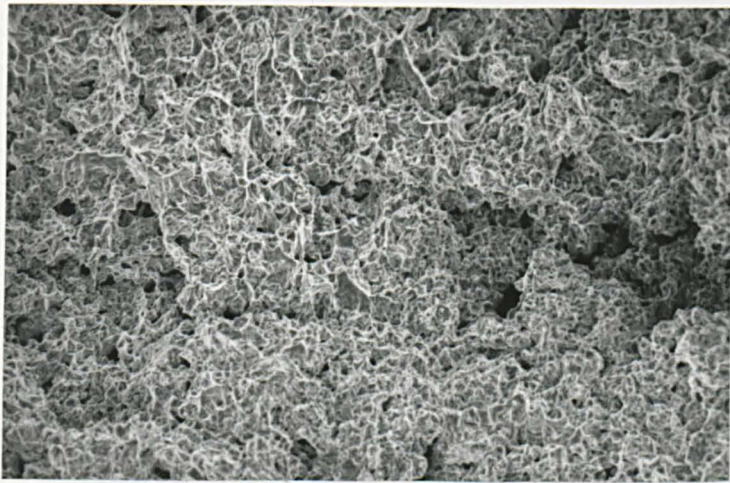
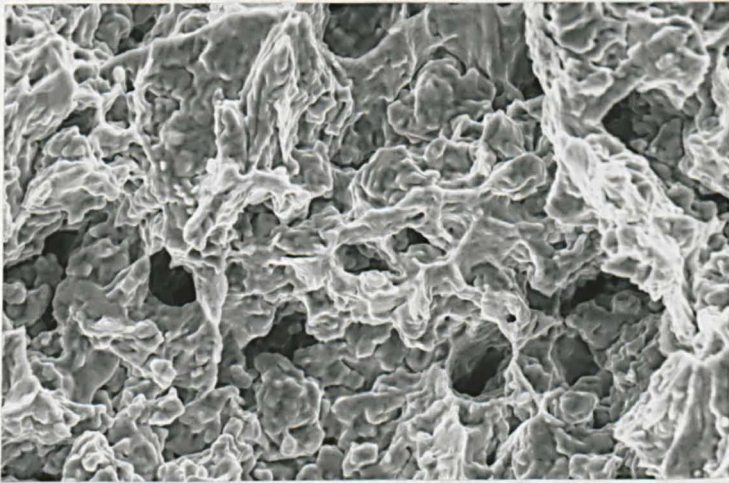


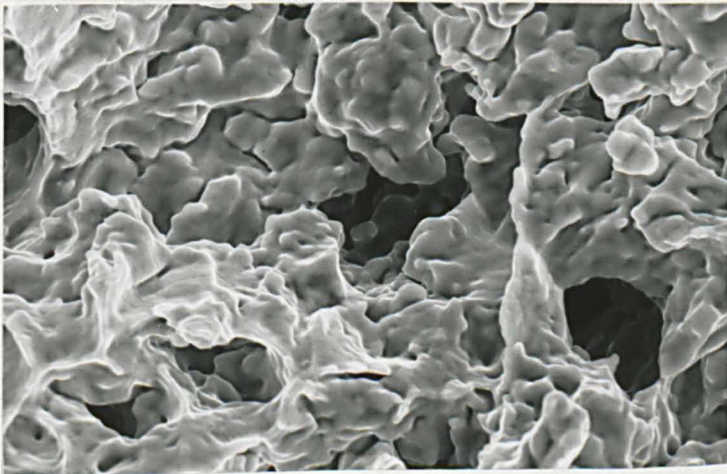
Fig. 10.16 Variation of austenite grain size with temperature.



100 μm



20 μm



10 μm

FIG. 10.17 Fracture surface of C-Mn-Nb-Al fractured at 850°C using a strain rate of  $3 \times 10^{-3} \text{ s}^{-1}$

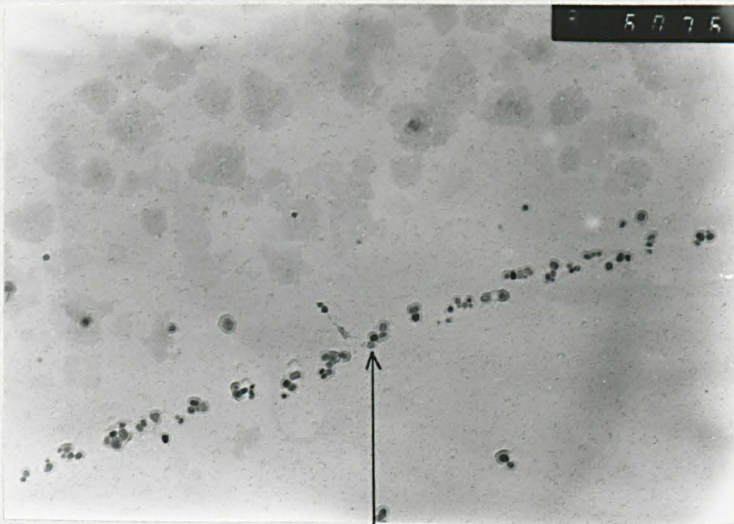


1.3 μm

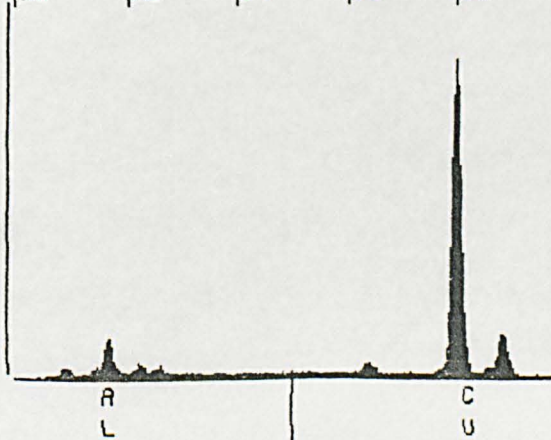


650 nm

Fig. 10.18 AlN precipitation in C-Mn-Al steel tested at 850°C using a strain rate of  $3 \times 10^{-3} \text{ s}^{-1}$



05-AUG-84 11:09:41 EDAX READY  
 RATE: 2981CPS TIME: 64LSEC  
 00-20KEY:10EV/CH PRST: 200LSEC  
 A: B:  
 FS= 3001 MEM: A FS= 200  
 |00 |02 |04 |06 |08



CURSOR (KEY)=05.000 EDAX

Fig.10.19 AlN precipitation in C-Mn-Al steel tested at 1050°C using a strain rate of  $3 \times 10^{-3} \text{ s}^{-1}$ , with associated X-ray spectrum.



Fig.10.20 AlN precipitation in C-Mn-Al-Ca steel tested at 850°C using a strain rate of  $3 \times 10^{-3} \text{ s}^{-1}$ .



Fig.10.21 AlN precipitation in C-Mn-Al-Ca steel tested at 1050°C using a strain rate of  $3 \times 10^{-3} \text{ s}^{-1}$ .

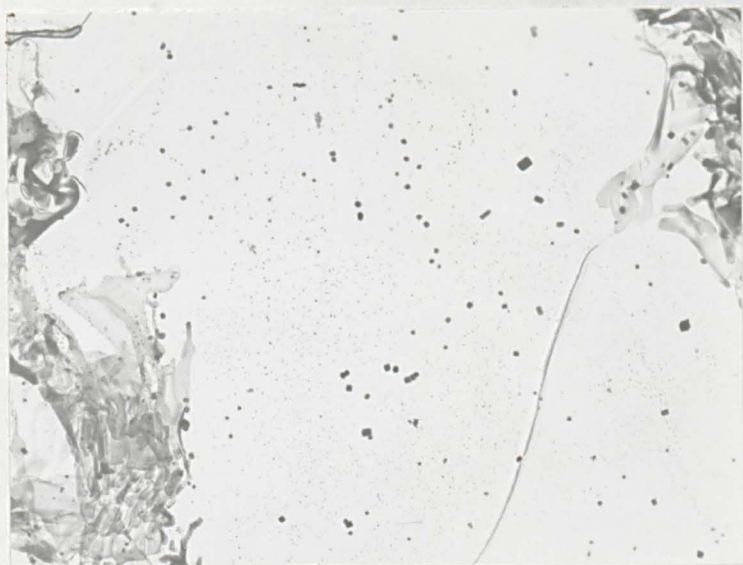
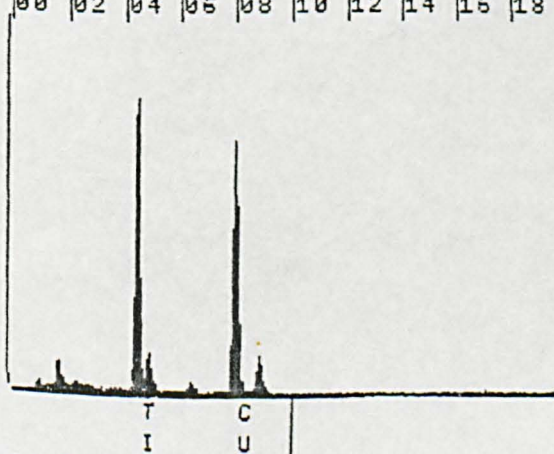


Fig.10.22 Precipitation in C-Mn-Ti-Al steel tested at 850°C using a strain rate of  $3 \times 10^{-3} \text{ s}^{-1}$



31-AUG-84 11:03:26 PEAK IDENT Y  
 RATE: 1703CPS TIME: 44LSEC  
 00-20KEV:10EV/CH PRST: 200LSEC  
 A: B:  
 FS= 2317 MEM: A FS= 2317  
 00 |02 |04 |06 |08 |10 |12 |14 |16 |18

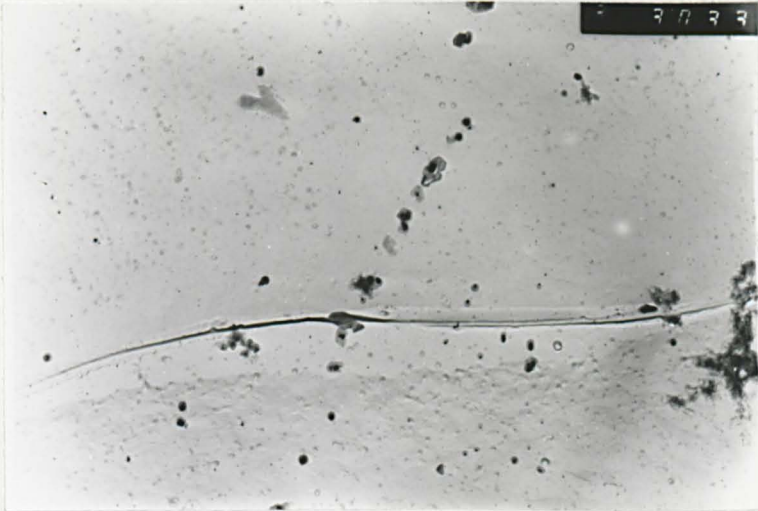


CURSOR (KEV)=10.080

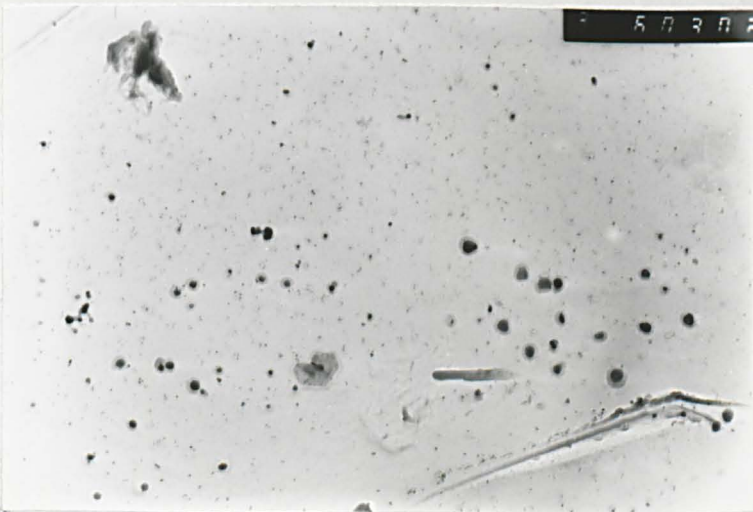
EDAX

FIG.10.23

Precipitation in C-Mn-Ti -Al steel tested at 1050°C using a strain rate of  $3 \times 10^{-3} \text{ s}^{-1}$ , and the associated X-ray spectrum.

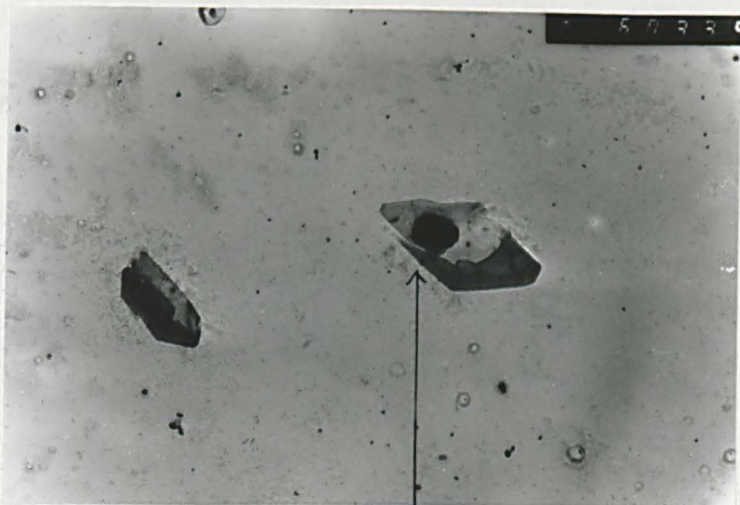


1.3 μm



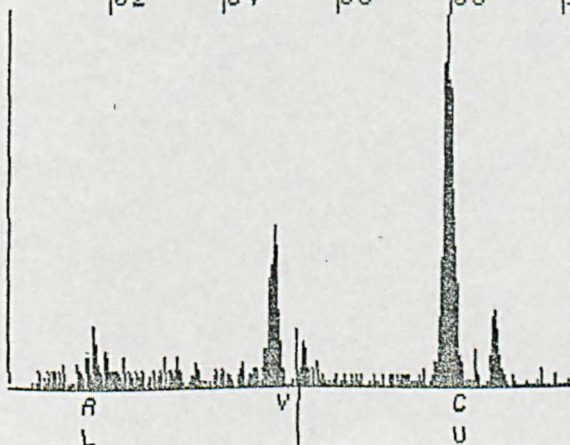
650nm

Fig.10.24 Precipitation in C-Mn-V-Al steel tested at 850°C using a strain rate of  $3 \times 10^{-3} \text{ s}^{-1}$



18-SEP-84 10:23:05 EDAX READY  
 RATE: 1090PS TIME: 23LSEC  
 00-20KEV:10EV/CH PRST: 200LSEC

A: B:  
 FS= 50 MEN: A FS= 50  
 |02 |04 |06 |08 |10



CURSOR (KEV)=05.400 EDAX

Fig.10.25

Precipitation in C-Mn-V-Al steel tested at 1050°C using a strain rate of  $3 \times 10^{-3} \text{ s}^{-1}$ , and associated X-ray spectra.

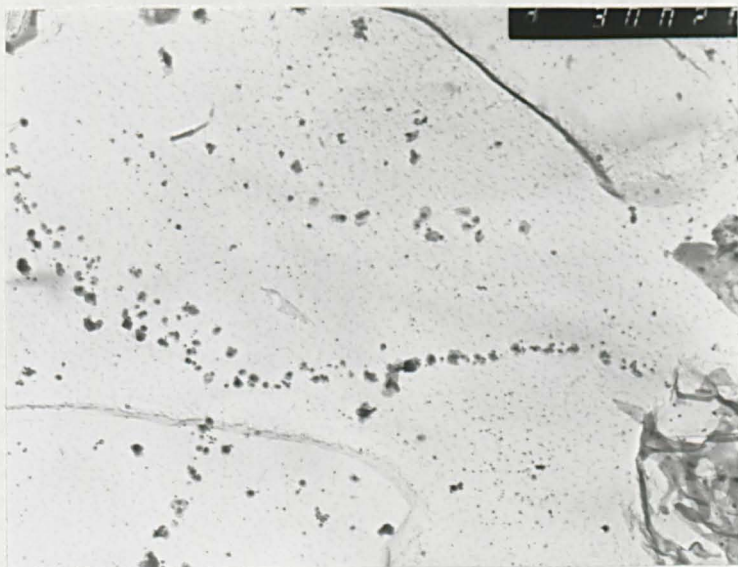
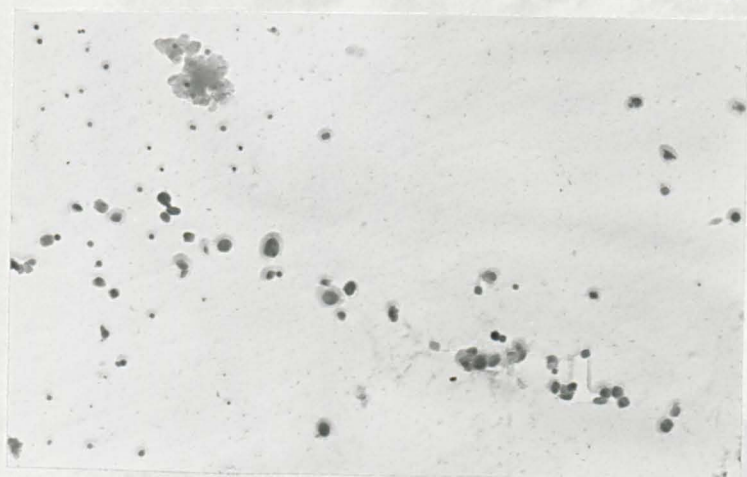


Fig.10.26 Precipitation in C-Mn-Nb-Al steel tested at 850°C using a strain rate of  $3 \times 10^{-3} \text{ s}^{-1}$

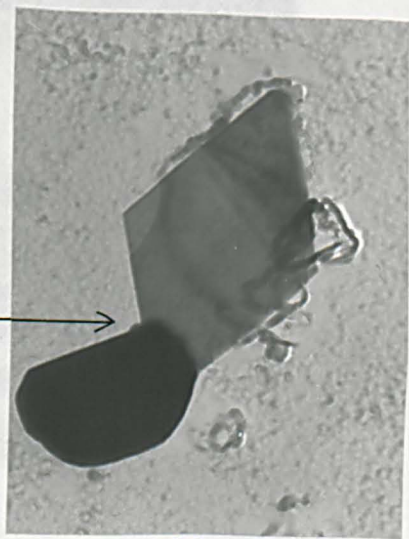
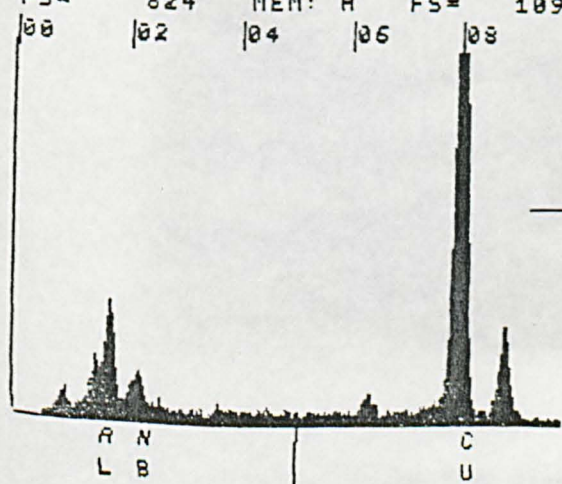


13 μm



650 nm

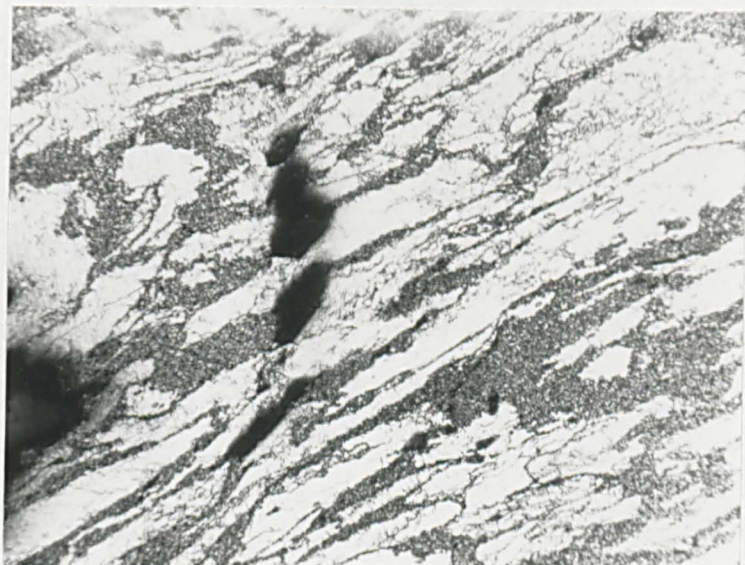
RATE: 3237CPS TIME: 56LSEC  
 00-20KEV: 10EV/CH PRST: 200LSEC  
 A: B:  
 FS= 824 MEM: A FS= 1096  
 00 |02 |04 |06 |08



400 nm

Fig.10.27

Precipitation in C-Mn-Nb-Al steel tested at 1050°C using a strain rate of  $3 \times 10^{-3} \text{ s}^{-1}$ , with associated X-ray.



400μm



200μm

Fig.10.28 Section through C-Mn steel fractured at 850°C using a strain rate of  $3 \times 10^{-3} \text{ s}^{-1}$  (A coarse ferrite/pearlite aggregate was produced prior to testing by heating to 1200°C and furnace cooling.)

## CHAPTER 11

Summary and Recommendations for Future Work

## 11.1 INTRODUCTION

In the previous chapters, some of the many factors which influence the hot ductility of steels have been discussed, and it is intended in this final chapter to draw together these various factors to form a coherent picture of the hot ductility behaviour of plain carbon, and micro-alloyed steels. Previous work and the present study, have generally shown that low ductility failures at temperatures in the range 600 - 1000°C, after testing using intermediate strain rates, are of two distinct types:- i) failure occurring due to strain concentration in the thin pro-eutectoid ferrite films formed at the  $\gamma$  grain boundaries after transformation and ii) crack formation at  $\gamma$  grain boundaries due to grain boundary sliding, followed by crack growth and coalescence in the austenitic state. These two distinct fracture modes will be discussed separately. From the conclusions reached in the present study, and those reached in previous studies, recommendations will be made to aid in the reduction of transverse cracking in continuously cast slab. Finally, recommendation for future work will be made, based on the results of the present study.

## 11.2 SUMMARY

### 11.2.1 Low Ductility Failure; $\alpha + \gamma$ region

A steel tested at a temperature within the two phase region may show brittle, intergranular failure, if a suitable ferrite distribution is present. The most deleterious form of ferrite with regards to hot ductility are the thin ferrite films formed along  $\gamma$  grain boundaries by deformation, as described in chapter 4. However, grain boundary ferrite produced under more equilibrium conditions is still capable of producing a significant ductility trough, as shown by the results of chapter 5.

In such two phase structures, as deformation proceeds, strain is concentrated in the ferrite films, and micro-voids nucleate at inclusions, chiefly MnS, within the ferrite films. These micro-voids grow and coalesce as deformation proceeds, and final failure appears intergranular in nature, the grain facets being covered with microvoids. Ductility begins to recover as the test temperature is lowered below the transformation temperature, and the ferrite films begin to thicken, hence reducing the strain concentration. An additional factor which may be responsible for the recovery of ductility is the reduction of the strength difference between austenite and ferrite as the temperature is lowered. (Wray, 1981)

The temperature range over which the ductility trough extends depends on composition, grain size and cooling rate from the solution temperature. For constant cooling rate and grain size, increasing C content lowers the transformation temperature, and hence lowers the temperature at which the ductility begins to fall, at least for C contents less than .35%. Above this value, the results of chapter 4 indicate that the ductility trough can

only be partially explained by the onset of transformation. For constant composition and cooling rate, increasing grain size prior to testing deepens and broadens the ductility trough. This occurs because in the coarse grained steels, thin films of deformation induced ferrite readily form at the grain boundaries, producing a marked loss of ductility. Cooling rate from the reheating temperature can influence the position of the ductility trough by altering the transformation temperature, faster cooling rates lowering the transformation temperature and hence shifting the ductility trough to lower temperatures.

The ductility trough occurring when samples are cooled into the two phase region is almost entirely absent when samples are heated into the two phase region, due to the fine, dispersed austenite/ferrite mixture produced, which provides no easy paths for crack propagation.

#### 11:2.2 Low Ductility failure; $\gamma$ region

Under suitable test conditions, both plain carbon and micro-alloyed steels can fail in this single phase austenite region with low ductilities. It appears that grain boundary cracks nucleate at triple points and propagate as deformation continues. Two types of grain boundary fracture were identified when failure had occurred in the single phase austenite region; intergranular decohesion (ID), which showed relatively flat facets, and intergranular micro void coalescence (IMC), which showed micro-voids on the grain facets. In the majority of cases, for either of these fracture modes to occur, it is necessary for the fracture strain,  $\epsilon_f$ , to be less than the critical strain for dynamic recrystallization,  $\epsilon_c$ . If this condition is not met, developing grain boundary cracks are prevented from propagating by the

onset of dynamic recrystallization. This idea is illustrated in Fig. 11.1, which shows the variations of  $\epsilon_f$  and  $\epsilon_c$  with temperature. It is well known that  $\epsilon_c$  decreases continually with increasing temperature (McQueen and Jonas, 1975). The variation of  $\epsilon_f$  with T is not so clearly understood, but some investigations have reported an increase in  $\epsilon_f$  with T, even though dynamic recrystallization had not occurred. (Wilcox and Honeycombe, 1984) However, Fig. 11.1 illustrates that as long as  $\epsilon_f$  is less than  $\epsilon_c$  at some temperature, a ductility trough will develop no matter what the precise variation of  $\epsilon_f$  with temperature. Fig. 11.1 also introduces the idea of the critical temperature,  $T_c$ , at which  $\epsilon_f = \epsilon_c$ . Above  $T_c$ , ductility is expected to increase rapidly as dynamic recrystallization proceeds, whilst below  $T_c$ , intergranular failure will occur. It is possible to explain the hot ductility behaviour of the plain C and micro-alloyed steels investigated in the previous chapters by the effects of precipitate, grain size and strain rate on  $\epsilon_c$  and  $\epsilon_f$ .

The influence of strain rate on  $\epsilon_c$  is well known,  $\epsilon_c$  decreasing as strain rate decreases, except possibly at very low strain rates (see section 2.3). The influence of strain rate on  $\epsilon_f$  is not so well documented, but in the majority of hot ductility studies the hot ductility decreases rapidly as strain rate decreases. (Mintz and Arrowsmith, 1979; Ouchi and Matsumoto, 1982). In some studies (Mintz and Arrowsmith 1979), and in the results of chapter 10, the temperature at which hot ductility first begins to fall increases as strain rate decreases. This behaviour is illustrated in Fig. 11.2 which shows the influence of varying strain rate over a range of temperatures on  $\epsilon_f$  and  $\epsilon_c$ . Fig. 11.2 shows that if it is

assumed that  $\epsilon_f$  is more sensitive to strain rate than  $\epsilon_c$ , and increase in the width of the ductility trough is expected. Precipitation is known to have a marked effect on both  $\epsilon_c$  and  $\epsilon_f$ .  $\epsilon_c$  is known to increase when fine nitride and/or carbide precipitates are present in sufficient volume fraction (Weiss and Jonas, 1979). The effect of precipitates on  $\epsilon_c$  is also expected to be temperature dependent, since at high temperatures precipitate size will be increased, and volume fraction decreased.  $\epsilon_f$  is also affected by precipitation, for a number of possible reasons; matrix precipitation will tend to concentrate strain at the grain boundaries when precipitate free zones develop, and grain boundary precipitates themselves may act as easy paths for crack propagation. The influence of precipitation on  $\epsilon_c$  and  $\epsilon_f$  is illustrated in Fig. 11.3, which shows that precipitation is expected to deepen and broaden the ductility trough. Thus thermal cycles such as those involving temperature oscillations during cooling from solution temperature, and those which produce many fine, dynamic precipitates, will produce a deepening and broadening of the ductility trough. Grain size prior to testing also influences both  $\epsilon_c$  and  $\epsilon_f$ .  $\epsilon_c$  is known to increase with increasing grain size, as discussed in section 2.6, creep studies, and the results of chapters 5 and 6, both indicate a decrease in  $\epsilon_f$  with increasing grain size. Fig. 11.4 illustrates the deepening and broadening effect on ductility trough of increasing grain size.

### 11.3 RECOMMENDATIONS FOR THE REDUCTION OF TRANSVERSE CRACKING

The results of chapter 8 have shown the importance of maintaining low amplitude temperature oscillations in the slab surface during continuous casting especially when a 'soft' cooling practice has been adopted, i.e. one which involves slab straightening at temperature above the ductility trough. Careful control and maintenance of cooling sprays to produce a more uniform cooling pattern would be expected to reduce transverse cracking by reducing NbCN precipitation before slab straightening.

Chapters 5 and 6 have shown that grain size prior to testing can have an influence on the hot ductility as measured in hot tensile tests, and hence a refinement in grain size prior to slab straightening might be expected to reduce transverse cracking.

Austenite grain size, following solidification, can be minimized by the choice of an appropriate C level, as described by Maehara et al, (1985), either below 0.10% or above 0.15%. These composition ranges limit the time spent by the solidification steel in the single phase austenite region of the phase diagram. Another possibility for refining austenite grain size is Ti treatment, which can lead to the formation of TiN or Ti-Nb compounds which are effective in restraining grain growth, if of a suitably fine size.

The results of chapter 7 indicate that dynamic precipitation of NbCN have a greater deleterious effect on hot ductility than static precipitates formed at the same temperature. Thus a reduction in cooling rate following solidification would reduce the supersaturation of Nb at the slab straightening temperature, and hence reduce the quantity of dynamically precipitated NbCN formed during straightening.

Strain rate is an important variable in controlling hot ductility as demonstrated by the results of chapter 10, and increases in strain

rate are effective in improving hot ductility. The strain rate during continuous casting is given by equations 2.1 and equation 2.2:-

$$\dot{\epsilon} = tV/2RL \dots\dots\dots 11.1$$

Thus it can be seen that increases in the casting velocity, V, and the slab thickness, t, and a decrease in the bending radius, R, or gauge length, L, will result in an increase in the strain rate,  $\dot{\epsilon}$ . However, to produce a significant improvement in ductility typically requires an increase in strain rate by a factor of 10. However, in commercial practise it is not feasible to produce such large variations in strain rate by altering V, t, R or L.

#### 11.4 RECOMMENDATIONS FOR FUTURE WORK

1. Chapter 5 and 6 dealt with the influence of grain size on hot ductility, but unfortunately only grain sizes less than 400  $\mu\text{m}$  were obtained. During continuous casting grain size in excess of 500  $\mu\text{m}$  are commonly obtained, and so there is a need to examine the influence of extremely coarse grain sizes on hot ductility.
2. In chapter 7, no conclusions could be drawn on the relative importance of the static and dynamic precipitation of AlN, due to the slow rate of AlN precipitation. Therefore, a further study should be carried out, using either slower cooling rates or longer holding times to encourage AlN precipitation, and using a steel with higher Al and N contents.
3. As discussed in chapter 9, a closer approximation of the cooling conditions experienced during continuous casting would be produced by the use of an increased cooling rate after solidification, and by the introduction of temperature oscillations during cooling.
4. In chapter 10, it was shown that both Ti and Ca are beneficial to the hot ductility of samples heated directly to test temperatures. Of more relevance to the continuous casting process is the hot ductility after high temperature solution treatments. Therefore it is recommended that the hot ductility of C-Mn-Nb-Al steels with Ti and Ca additions is examined after high temperature solution treatment.
5. It was suggested in chapter 10 that the improvement in hot ductility associated with Ca additions was due to the lower S levels present. To confirm this effect, it is recommended that C-Mn-Al and C-Mn-Nb-Al steels with different S levels are tested.
6. The results of chapter 7 indicate that dynamically precipitated

NbCN is more detrimental to hot ductility than the equivalent static precipitates. As well as holding time prior to testing, the proportions of static and dynamic NbCN is expected to be influenced by the cooling rate from solution treatment temperature. At present, only Mintz and Arrowsmith (1979) appear to have investigated the influence of cooling rate on the hot ductility of C-Mn-Nb-Al steels, so there is a need to extend their work over a wider range of cooling rates.

7. In the present study, the hot ductility of C-Mn steels has been investigated above and below the  $A_1$  temperature. However, the hot ductility of micro-alloyed steels after cooling from solution temperature was investigated only above the  $A_1$  temperature. Therefore, it is recommended that hot ductility tests are performed on micro-alloyed steels below the  $A_r3$  temperature to investigate the combined influence of precipitation and transformation.
8. The recovery of hot ductility as the test temperature is raised is often due to the onset of dynamic recrystallization. To date, there appears to have been little work done on the volume fraction of recrystallized material required to bring about this recovery in hot ductility. Measurement of these recrystallized volume fractions would be most easily made on fractured samples of an austenitic stainless steel, which had been quenched rapidly after fracture.

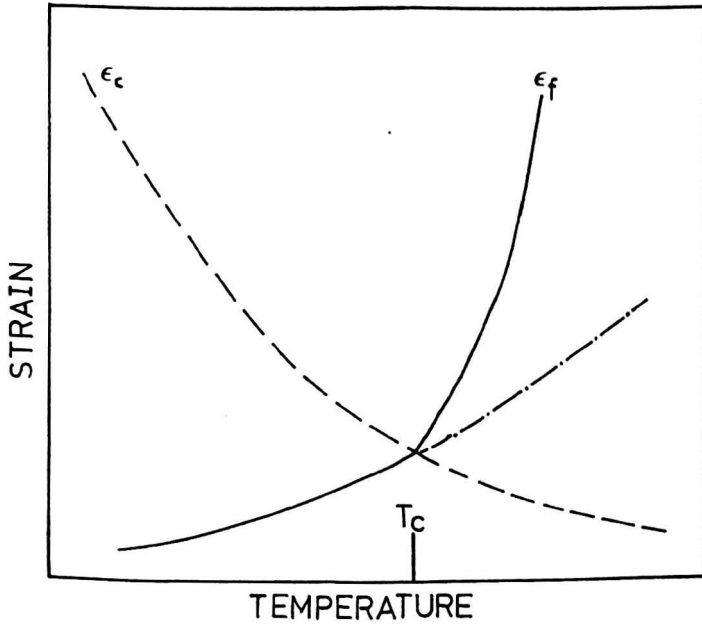


Fig. 11.1 Schematic illustration of variation of fracture strain ( $\epsilon_f$ ) and strain for the nucleation of dynamic recrystallization, ( $\epsilon_c$ ) with temperature.

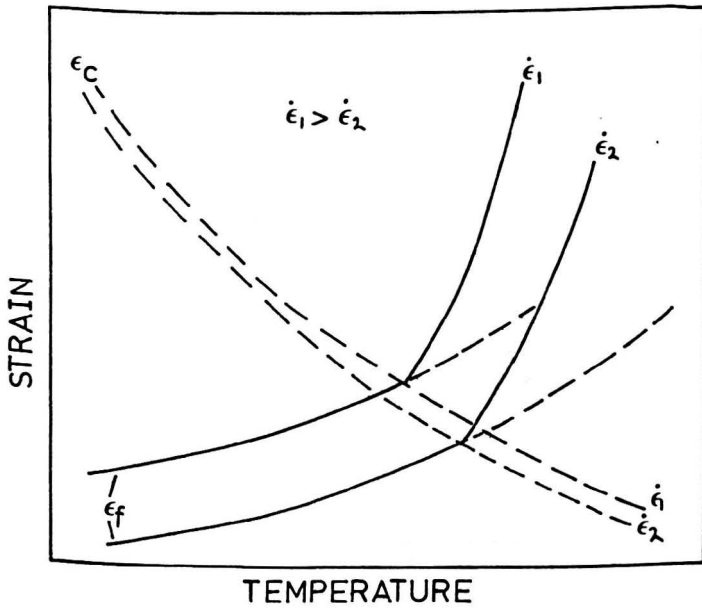


Fig. 11.2 Schematic illustration of variation of  $\epsilon_c$  and  $\epsilon_f$  with temperature and strain rate.

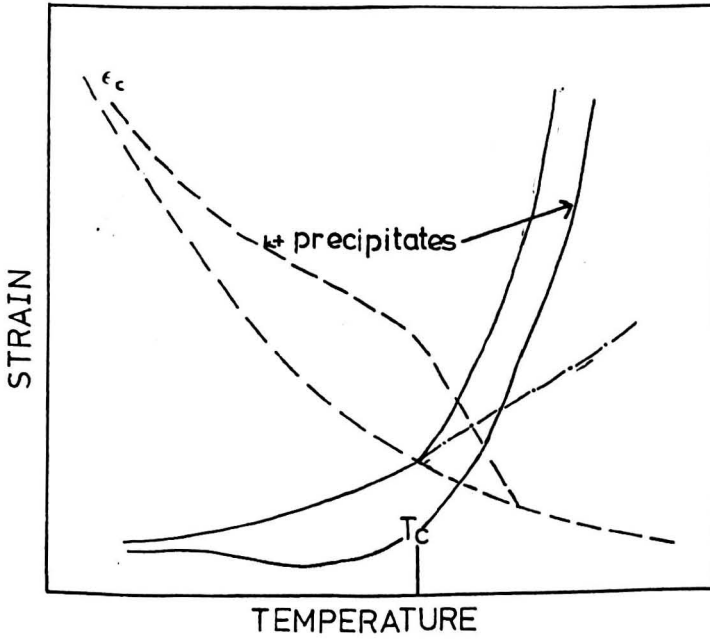


Fig. 11.3

Schematic illustration of variation of  $\epsilon_c$  and  $\epsilon_f$  with temperature and precipitation, assuming a sufficient volume fraction of 'fine' precipitates to increase  $\epsilon_c$ .

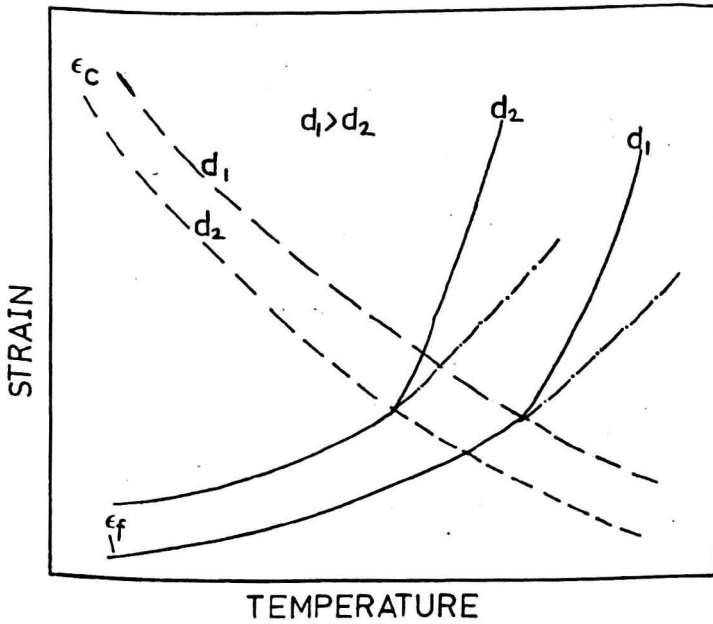


Fig. 11.4

Schematic illustration of variation of  $\epsilon_c$  and  $\epsilon_f$  with temperature and grain size.

APPENDIX 1

PROCEDURE FOR ELECTROPLATING (ANG, 1982)

(A) Preparation of all chloride solution.

Required electrolyte composition: Nickel Chloride ( $\text{NiCl}_2$ ) = 240 g/l

Boric Acid ( $\text{H}_3\text{BO}_3$ ) = 30 g/l

Exact amount of nickel chloride crystals (240g) and boric acid powder (30g) were each weighed in a Toppan machine. To each were added 1 litre of water. They were then mixed thoroughly in a glass container to obtain the required all chloride solution.

(B) Calculation of time and current required for a plating thickness of 100 $\mu\text{m}$ .

For dimensions of specimen please refer to Appendix

Density of nickel = 0.0089 g/mm<sup>3</sup>

Current density = 0.000538 amp/mm<sup>2</sup>

Z = 29.35 g

Weight deposited =  $\frac{ZIt}{96500}$  \_\_\_\_\_ (1)

Current required = current density x surface area of specimen \_\_\_\_ (2)

Weight of nickel deposited (in grams) = Density x Volume \_\_\_\_ (3)

Total surface area of specimen = 2{surface area (A)} +

2{surface area (B)} + surface area (C)

$$= 2\{\pi(6.3)^2 + 2\pi(6.3)(5.08)\} + \frac{\pi}{4}(12.6^2 - 7.6^2)$$

$$+ 2\{2\pi(3.8)(6.35) + \frac{\pi}{4}(7.6^2 - 5.04^2)\} + 2\pi(2.52)(25.4)$$

$$= 810.2 + 354 + 402.2$$

$$= 1566.4 \text{ mm}^2$$

From equation (2),

$$\text{Total current required} = 0.000538 \times 1566.4$$

$$= 0.843 \text{ Ampere}$$

∴ Current required  $\approx$  0.85A

$$\begin{aligned}\text{Volume of nickel deposited} &= \text{total surface area} \times \text{thickness of} \\ &\quad \text{plating} \\ &= 1566.4 \times 0.1 \\ &= 156.64 \text{ mm}^3\end{aligned}$$

From equation (3),

$$\begin{aligned}\text{Weight of nickel deposited} &= 0.0089 \times 156.64 \\ &= 1.3941 \text{ grams}\end{aligned}$$

From equation (1),

$$\begin{aligned}1.3941 &= \frac{ZIt}{96500} \\ \therefore t &= \frac{1.3941 \times 96500}{29.35 \times 0.843} \\ &= 5437.3 \text{ secs} \\ &= 1 \text{ hr } 30 \text{ mins } 37.2 \text{ secs}\end{aligned}$$

∴ Time required for plating  $\approx$  1 hr 31 mins.

(C) Procedure for Nickel Plating

Prior to plating, visual examination of the specimen is very important to ensure that no oxide is present on the specimen. It is necessary to abrade and then pickle the rolling oxides in hot 10%  $\text{H}_2\text{SO}_4$ .

The procedure for nickel plating was as follows:

- (i) Each specimen was ultrasonically cleaned for about 5 minutes
- (ii) The specimen was removed with the help of tongs and then washed in warm running water.
- (iii) 10% sodium hydroxide (NaOH) was heated in a beaker to  $50-70^\circ\text{C}$ . Anodic cleaning was carried out for 1 minute at 0.2A with half of the specimen immersed in the solution. The specimen (anode) was connected to the positive terminal of the supply and the nickel plate (cathode) to

the negative terminal.

- (iv) The specimen was then removed and washed with warm running water.
- (v) The same procedure was carried out on the other half of the specimen.
- (vi) The specimen was again removed and washed with warm running water.
- (vii) It was then immediately dipped in a 10% HCl solution for about 2 minutes.
- (viii) The cleaned specimen was then immersed in the plating solution. Both the current and plating solution were set at 0.8A and 60°C respectively. A magnetic stirrer was used.
- (ix) After about 1 hr the specimen was turned over to ensure even plating. Total plating time was about 2 hrs.
- (x) The specimen was then removed and blow dried.

## APPENDIX 2

### RECENT PUBLICATIONS

In the months between the completion of the Literature Survey of Chapter 2, and the final preparation of the thesis, a number of relevant papers have been published, and these will be discussed briefly.

Suzuki et al (1984) investigated the influence of strain rate and composition on the hot ductility of C-Mn-Al and C-Mn-Nb-Al steels using Gleeble and Instron testing machines, the temperature and strain rate ranges investigated being 600 - 1000°C and  $5 \times 5 \times 10^{-3} \text{ s}^{-1}$  respectively.

Decreasing the strain rate from 5 to  $5 \times 10^{-3} \text{ s}^{-1}$  led to the formation of a severe ductility trough for a C-Mn-Al steel, in general agreement with previous work discussed in section 2.5. C in the range 0.05 - 0.4% was shown to influence the depth and position of the ductility trough occurring in C-Al steels, increasing C contents leading to lower reduction in area values, and shifting the ductility trough to lower temperatures. This shift in position of the ductility trough was found to be consistent with the change in  $A_r$ , temperature associated with the varying C content. However, Maehara et al (1985) after testing a series of C-Mn-Nb-Al steels with C contents in the range 0.05 - 0.3 wt% under similar test conditions to those of Suzuki et al, showed no influence of C content on reduction in area values, in agreement with the results of Ouchi and Matsumoto (1982). Maehara et al (1985) did show that C content had a significant affect on reduction in area values of samples which had been cast 'in situ' immediately prior to testing. Hot ductility was reduced in the C range 0.10 - 0.15%, and this behaviour was explained in terms of the coarse austenite grains formed in this C range, due to the high temperature

of austenite formation for these compositions.

Further results on the influence of C content have been presented by Hannerz (1985), showing that in the temperature range 750 - 900°C, increasing C content from 0.07 to 0.28% C in a C-Mn-Al steel improved hot ductility, and this improvement was attributed to the associated increase in the  $A_1$  temperature.

Studies by both Suzuki et al (1984) and Hannerz (1985) indicated that increasing N contents in C-Mn steels reduced reduction in area values, and Hannerz also showed that increasing the product  $Al \times N$  broadened the ductility trough associated with the C-Mn-Al steels, in broad agreement with previous studies described in section 2.9. However, Suzuki et al reported that Al additions to a C-Mn steel with 0.009%N actually improved hot ductility.

The work of Hannerz on the influence of Nb and Ti on the hot ductility of C-Mn-Al and C-Mn-Nb-Al steels respectively confirmed previous findings discussed in section 2.9, indicating that increasing Nb decreases hot ductility, whilst Ti improved hot ductility.

The studies of both Hannerz and Suzuki confirmed the earlier reports by Mintz and Arrowsmith (1979) on the influence of P, by showing a slight improvement in hot ductility with increasing P in C-Mn and in C-Mn-Al steels.

Again, the results of Hannerz concerning the hot ductility of C-Mn-Al-V steels, confirmed earlier work discussed in section 2.9, and showed a slight deterioration in hot ductility with increasing V.

Both Hannerz and Suzuki et al investigated the influence of S on hot ductility. Suzuki et al reported a slightly detrimental effect of S in C-Mn-Al steels following solution treatment, but a very much larger detrimental effect when the samples were melted prior

to testing. However, Hannerz reported no influence of sulphur on hot ductility in Gleeble tests, although analysis of production data indicated that S tended to promote transverse cracking. The Gleeble results, however, were obtained from Al free steels, and as the work of Heritier et al (1981) indicates, the presence of both S and Al may be a pre-requisite for brittle failure. Hannerz also reported no influence of Ce or Mo on the hot ductility of C-Mn-Nb-Al steels.

### APPENDIX 3

Some of the results presented in this thesis have been accepted for publication in 'Materials Science and Technology'. These results include the work published in Chapter 4, and together with further work, the results of Chapter 9. The papers are to be entitled 'Influence of Carbon on the Hot Ductility of Steels' and the 'Hot Ductility of a Directly Cast C-Mn-Nb-Al Steel'. Letters of acceptance from the Institute of Metals are show over-leaf.

1 Carlton House Terrace London SW1Y 5DB  
Telephone: 01-839 4071 Telex: 8814813

28 November 1985

WB/KM/MST361

Dr B Mintz  
Dept of Mechanical Engineering  
The City University  
Northampton Square  
LONDON EC1V OHB

Dear Dr Mintz

THE HOT DUCTILITY OF DIRECT CAST  
C-Mn-Nb-Al STEELS

I acknowledge with thanks receipt of your letter of 1 November 1985 enclosing a revised version of the above paper for publication in Materials Science and Technology.

I am pleased to inform you that this is acceptable and I am now passing the paper over to our production department who will send you proofs for checking in due course.

Yours sincerely

1 Carlton House Terrace London SW1Y 5DB  
Telephone: 01-839 4071 Telex: 8814813

20 December 1985

TLH/CR/MST366

Dr B Mintz  
Dept of Mechanical Engineering  
The City University  
Northampton Square  
LONDON EC1V 0HB

Dear Dr Mintz

INFLUENCE OF CARBON ON THE HOT DUCTILITY OF STEELS

I acknowledge with thanks receipt of your letter of 21 November enclosing a revised version of the above paper for publication in Materials Science and Technology.

I am pleased to inform you that this is acceptable and I am now passing the paper over to our production department who will send you proofs for checking in due course.

Yours sincerely

## REFERENCES

- Ang, S.H. (1982) Final year project, Dept. of Mech. Eng., City University.
- Akben, M.G. Weiss, I., and Jonas, J.J. (1981). Acta. Met., 29, 111
- Andrews, K.W. (1965) JISI, 203, 721
- Badia, M. and Vignes, A., (1969). Acta. Met., 17, 177
- Bellot, J. and Gantois, M. (1978). Trans. ISIJ, 18, 536
- Bernard, G., Birat, J.P., Conseil, B. and Humbert, J.C. (1978). Rev. Met., 75 467.
- Biggs, B.L. (1959). JISI, 192 361
- Birat, J.P., Larrecq, M., Le Bon, A., Jeanneau, M., Poupon M., and Senaneuch, D. (1981) Steelmaking Procs., 64, 53.
- Brimacombe, J.K. and Sorimachi, K. (1977). Metall. Trans., 8B, 489.
- Bywater, K.A. and Gladman, T. (1976). Met. Technol., 3, 358
- Carlsson, C.G. (1964). Jernkont, Ann., 148 152
- Carlsson, J.E., Lehtinen, B., and Roberts, W. (1980), Swedish Institute for Metals Research Report No. 1505.
- Chang, H.C. and Grant, N.G. (1956). Trans. AIME, 206, 544
- Charles, J. (1980) In 'Hot Working and Forming Processes', Metals Soc. Book No. 264, 83.
- Cochrane, R.C. (1982) unpublished work.
- Coleman, T.H. and Wilcox, J.R. (1985). Mat. Sci. and Technol., 1, 80
- Cottingham, D.M. (1968). In 'Deformation under Hot Working Conditions', Special Report No. 108, London ISI, 145
- Coward, M.D., Richardson, G.J., and Sellars, C.M., (1977). Met. Technol. 4, 550.
- Decroix, J.H., Neveu, A.M. and Castro, R.J. (1968). In 'Deformation under Hot Working Conditions', Special Report No. 108, London ISI, 135.
- Desai, S.C. (1959) JISI, 191, 250
- Dieter, G.E., Mullin, J.V. and Shapiro, E. (1968). In 'Deformation under Hot Working Conditions', Special Report No. 108, London ISI, 7.
- Erasmus, L.A. (1964) JISI, 202, 32
- Ericson, L. (1977). Scand. J. Met., 6, 116
- Evans, H.E. (1969). Met. Sci. J., 3, 33
- Evans H.E. (1984). In 'Creep Fracture', Pergamon Press, 1984

- Evans, R.W. and Jones, F.L., (1976). *Met. Technol.*, 3, 494
- Evans, R.W. and Jones, F.L. (1978). *Met. Technol.*, 5, 1
- Fleck, R.G., Cocks, G.J., and Taplin, D.M.R., (1970). *Metall. Trans.*, 1A, 3415.
- Fujii, H., Ohashi, T., Hiromoto, K., and Oda, M. (1975) *Tetsu To Hagane*, 61, 5556
- Funnell, G.D. (1980). In 'Hot Working and Forming Processes' *Met. Soc. Book No. 264*, 104.
- Funnell, G.D. and Davies, R.D., (1978). *Met. Technol.* 5, 150.
- Garofalo, F. (1968). In 'Ductility' American Society for Metals, Metals Park, Ohio, 87.
- Gifkins, R.C., (1956). *Acta. Met.*, 4, 98
- Gittins, A. (1977). *Int. Met. Rev.*, 22, 212
- Gittins, A. and Moller, R. (1974). *MRL Report 53128*
- Gittins, A., Northway, L.G. and Freeman, J.P. (1971). *J. Aust. Inst. Met.*, 16, 225
- Gladman, T. and Pickering, F.B. (1967). *JISI*, 205, 653
- Gove, K.C. and Charles, J. (1974) *Met. Technol.* 1, 425
- Glover, G. and Sellars, C.M. (1973). *Metall. Trans.* 4, 765
- Hannerz, N.E. (1985). *Trans. ISIJ*, 25, 149
- Hannerz, N.E., Lindborg, U. and Lehtinen, B., (1968) *JISI*, 206, 68
- Harding, R.A., Sawle, R. and Sellars, C.M. (1977). *Met. Technol.*, 4, 142
- Harris, R., and Barnard, L. (1968). In: 'Deformation under Hot Working Conditions', Special Report No. 108, London ISI, 167.
- Hasebe, T. (1972). *Tetsu to Hagane*, 58, 227
- Heritier, P., Fourdex, A., and Kobylanski, A. (1981). *Scripta Met.*, 15, 753
- Irvine, K.J. Pickering, F.B. and Gladman, T. (1967) *JISI*, 205, 161
- Jonas, J.J. Sellars, C.M., and Tegart, W.J. McG. (1968). In 'Deformation under Hot Working Conditions', Special Report No. 108, London ISI, 21
- Kiessling, R. (1968). 'Non Metallic Inclusions in Steel' Pt. II, The Iron and Steel Institute.
- Klevebring, B.I. Borgren, E., and Mahrs, R. (1975). *Metall Trans.*, 6A, 319

- Kobayashi, H., Yamaguchi, S. and Endo, M., (1980). In 'Hot Working and Forming Processes', Met. Soc. Book No. 264, 133.
- Kozusu, I., Ouchi, C., Sampei, T. and Okita, T. (1976). In 'Microalloying '75', New York, United Carbide Corp., 120.
- Kutumba Rao, V., Taplin, D.M.R., Rama. Rao, P. (1975) Metall. Trans, 6A, 77
- Lankford, W.T. (1972). Metall. Trans., 3, 1331
- Le Bon, A., Rofes-Vernis, J. and Rossard, C. (1975). Met. Sci., 9, 36.
- Leslie, W.C. (1954). Trans ASM, 46, 1470
- Lucke, K., and Stuwe, H.P. (1963). In 'Recovery and Recrystallization of Metals' New York, ed. L. Himmel.
- Luton, M.J. and Sellars, C.M., (1969). Acta. Met., 17, 1033
- Maehara, Y. and Ohmori, Y. (1984). Mat. Sci. and Eng., 62, 109
- Maehara, Y., Yasumoto, K., Sugitani, Y. and Gunji, K. (1985) Trans. ISIJ, 25, 1045
- Malkiewicz, T., and Rudnik, S., (1963). JISI, 201, 33
- Matsubara, K. (1966). Trans. ISIJ, 6, 139
- Maunder, P.J.H. and Charles, J. (1968). JISI, 206, 979
- McQueen, H.J. and Bergerson, S. (1972). Met. Sci. J. 6, 25.
- McQueen, H.J. and Jonas, J.J. (1975). In 'Treatise on Materials Science and Technology', New York Academic Press, Vol. 6, 393.
- McQueen, H.J., Wong, W.A. and Jonas, J.J. (1967). Can. J. Phys., 45, 1225
- Mercer, R.E., and McPherson, N.A., (1980). Ironmaking and Steel-making, 7, 167
- Mintz, B. (1973) BSC report PROD. 370/2/73/D.
- Mintz, B. (1979) Unpublished work.
- Mintz, B., and Arrowsmith, J.M. (1979). Met. Technol., 6, 24
- Mintz, B., and Arrowsmith, J.M. (1980). In 'Hot Working and Forming Processes', Met. Soc. Book No. 264, 99.
- Mintz, B., Wilcox, J.R. and Arrowsmith, J.M. (1980). In 'Recrystallization and Grain Growth of Multi-Phase and Particle Containing Materials', Ris Ø National Laboratory, Denmark.
- Moore, P.G. (1968). In 'Deformation under Hot Working Conditions', Special Report No. 108, London ISI, 68.
- Mori, H. (1974). Tetsu To Hagane, 60, 784

- Morozenskii, L.I., Mitenev, O.A., and Krutikov, V.K., (1965). Stahl, 4, 272.
- Morrison, W.B. (1975). Met. Technol, 2, 33
- Muller, T.L.F. (1967). PhD. Thesis, University of Sheffield.
- Nicholson, A., Smith, D. and Shaw, P. (1968). In 'Deformation under Hot Working Conditions' Special Report No. 108, London ISI, 161.
- Norstrom, L.A. (1977). Scan. J. Met., 6, 269.
- Nozaki, T., Matsuno, J. Murata, K., Ooi, H. and Kodama, M., (1978) Trans. ISIJ, 1978, 18, 330
- Offerman, C., Dacker, C.A. and Enstrom, C. Scan. J. Met., (1981), 10, 115
- Ohmori, Y. and Maehara, Y., (1984). Trans. J. Inst. Met., 25, 160
- Osinkolu, G.A., Tacikowski, M., and Kobylanski, A., (1985). Mat. Sci. and Technol. 1, 520
- Ouchi, C., and Matsumoto, K., (1982). Trans. ISIJ, 22, 181
- Ouchi, C., and Okita, T., (1982). Trans. ISIJ, 22, 543
- Reynolds, J.H. and Gladman, T. (1980). In 'Hot Working and Forming Processes', Metals Soc. Book No. 246, 171.
- Reynolds R.A. and Tegart, W.J. McG. (1962) JISI, 200, 1044
- Robbins J.L., Sherby, O.D. and Shepard, O.C. (1961) JISI, 199, 175
- Robbins, J.L., Shepard, O.G., and Sherby, O.D., (1967) Trans. ASM, 60, 205
- Roberts, W. (1982) In: 'Deformation Processing and Structure' ASM Metals Park Ohio, 109.
- Roberts, W., Boden, H., and Ahblom, B. (1979) Met. Sci., 13, 195
- Roberts, W., Liddefelt, H. and Sandberg, A. (1980). In 'Hot Working and Forming Processes' Metals Soc. Book No. 264, 38
- Rogberg, B. (1983) Scan. J. Met., 12, 175
- Rossard, C. (1973) In 'Proceedings of 3rd ICSMA'
- Ruibal, E., Urcola, E.E. and Fuentes, M. (1984). Met. Technol, 11 189.
- Rundell, G.R. and Raudebough, R.J., (1961). Trans. ASM, 53, 233
- Salmon Cox, P.H. and Charles, J.A. (1965). JISI, 203, 493
- Sankar, J., Hawkins, D.N., and McQueen, H.J. (1979). Met. Technol, 6, 325.
- Schmidt, L. and Josefsson, A. (1974). Scan. J. Met., 3, 193

- Schnable, E., and Schwaab, P., (1976). Arch. Eisenhüttenwesen, 47, 577
- Sekine, H. and Maruyama, T. (1976). Trans. ISIJ, 16, 427
- Segal, A. and Charles, J., (1977). Met. Technol., 4, 177
- Sellars, C.M. (1980). In: 'Hot Working and Forming Processes' Metals Soc. Book No. 264, 3.
- Sellars, C.M. and Tegart, W.J. McG., (1966) Mem. Sci. Rev. Met., 63, 731
- Sellars C.M. and Tegart, W.J. McG., (1972) Int. met. Rev., 17, 1
- Shahinian, P. and Lane, J.R., (1953). Trans. ASM, 45, 177
- Smith, D., Nicholson, A. and Murray, J.D. (1972) JISI, 210, 412
- Sopher, R.P., (1958). Welding Journal, 37, 481S
- Stone, P.G. and Murray, J.D., (1965). JISI, 203, 1094
- Stroh, A.N., (1955). Proc. Roy. Soc. London, A232, 548
- Suzuki, H.G., Nishimura, S., Imamura, J. and Nakamura, Y. (1984) Trans. ISIJ 24, 169
- Suzuki, H.G., Nishimura, S., and Nakamura, Y. (1984) Trans. ISIJ, 24, 54.
- Suzuki, H.G. Nishimura, S., and Yamaguchi, S., (1982). Trans ISIJ, 22, 48
- Taplin, D.M.R. and Whittakers, V.N., J. Ins. Met., 92, 426
- Tegart, W.J. McG., (1968) In: 'Ductility', Metals Park, Ohio, 133.
- Tegart, W.J. McG., and Gittins, A. (1977) In+ 'The Hot Deformation of Austenite' Met. Soc. AIME, New York 1.
- Tomono, H. (1977) In; CONAST Slab Seminar, Zurich.
- Turkdogan, E.T., Ignatawics, I., and Pearson, J. (1955) JISI, 180, 34
- Uvira, J.L., and Jonas, J.J. (1968) Trans. Met. Soc. AIME, 242, 1619
- Vodopivec, F., (1973) JISI, 211, 664
- Vodopivec, F., (1978) Met. Technol., 5, 118
- Vodopivec, F., Gabrovsek, M., Ralic, B., (1975) Met. Sci., 9, 324
- Wagenaar, H.W. (1968) In: 'Deformation Under Hot Working Conditions' Special Report No. 108, London ISI, 38.
- Watanabe, H., Smith, Y.E. and Pewke, R.D. (1977) In: 'The Hot Deformation of Austenite', Met. Soc. AIME, New York, 140.
- Waudby, P.E. (1979) In: 'Inclusions' Inst. of Metall., London, 94
- Weinberg, F., (1979) Metall. Trans., 10B, 219

- Weiss, I. and Jonas, J.J., (1979) Metall. Trans., 10A, 831
- Weiss, I. and Jonas, J.J., (1980) Metall. Trans., 11A, 403
- White, F.E. and Rossard, C. (1968) In: 'Deformation under Hot Working Conditions' Special Report No. 108, London ISI, 14.
- Wilber, G.A., Batra, R., Savage, W.F., Childs, W.J. (1975). Metall. Trans., 6A, 1727
- Wilcox, J.R., (1982) PhD Thesis, University of Cambridge.
- Wilcox, J.R. and Honeycombe, R.W.K. (1984) Met. Technol., 11, 217
- Woodfine, B.C. and Quarrell, A.G., (1960), JISI, 19S, 409
- Wray, P.J. (1975) Metall. Trans., 6A, 1379
- Wray, P.J. (1981) Met. Technol, 8, 466
- Wray, P.J. (1984) Metall. Trans. 15A
- Wray, P.J. and Holmes, M.F. (1975). Metall. Trans., GA, 1189
- Wright, J.A. and Quarrell, A.G. (1962) JISI, 200, 299
- Yamanaka, K., Terasaki, H., Ohtani, H., Oda, M., Yoshihara, M., (1980) Trans. ISIJ, 20, 810
- Yasumoto, K., Maehara, Y., Ura, S., and Ohmori, Y., (1985) Mat. Sci. and Technol. 1, 111